U.PORTO

Universidade do Porto
FEUP Faculdade de Engenharia

BOSCH

Printed Circuit Boards Experimental and Numerical Characterization:

Mechanical, Thermal and Vibration Analysis

Carlos Manuel Pinto Castro

Dissertation submitted to
Faculdade de Engenharia da Universidade do Porto
for the degree of:

Master in Mechanical Engineering

Advisor:
Eng. Pedro Bastardo
(Bosch Security Systems – Ovar)

Co-Advisors:
Prof. Paulo Tavares de Castro
(Full Professor)

Prof. Sérgio Tavares
(Invited Professor)

Departamento de Engenharia Mecânica
Faculdade de Engenharia da Universidade do Porto

Porto, June 2017

The work presented in this dissertation was performed at the
Laboratory of Technological Tests,
Laboratory of Optics and Experimental Mechanics,
Laboratory of Vibrations of Mechanical Systems
Department of Mechanical Engineering
Faculty of Engineering
University of Porto
Porto, Portugal
and at
Bosch Security Systems
Ovar, Portugal.

Carlos Manuel Pinto Castro
E-mail: em12042@fe.up.pt

Faculdade de Engenharia da Universidade do Porto
Departamento de Engenharia Mecânica
Rua Dr. Roberto Frias s/n
4200-465 Porto
Portugal

Abstract

Quality and durability of electronic systems require high and increasing levels of reliability assurance. The complexity of printed circuit boards morphology explains the little information available about their mechanical, thermal and vibration characterization.

In attempt to develop this area of study, a population of printed circuit board specimens was subjected to experimental tests – mechanical, thermal and vibration. Numerical simulation was performed to model the mechanical tests' results and a parametric evaluation was carried out. The thermal tests provided useful information for gap pad dimensioning and knowledge of the gradient displacements fields caused by thermal loads. The vibration tests confirmed the performance reliability of a printed circuit board assembly under normal and severe vibration conditions.

It was concluded that accurate knowledge of the material properties is crucial for generating reliable material models. Further, no linear relation was found between the selected printed circuit boards material properties and geometric parameters, suggesting that each printed circuit board model should be individually characterized.

Keywords: PCBs characterization, Solder Joints Reliability, Numerical Modelling, Mechanical Testing, Thermography, Digital Shearography, Vibration Analysis

Resumo

A qualidade e durabilidade de sistemas electrónicos requerem elevados e crescentes níveis de fiabilidade. A morfologia complexa de placas de circuito impresso explica a escassa informação disponível sobre a sua caracterização mecânica, térmica e vibratória.

Na tentativa de desenvolver esta área de estudo, uma população de amostras de placas de circuito impresso foi submetida a testes experimentais – mecânicos, térmicos e vibratórios. Simulações numéricas para modelar os resultados dos testes mecânicos e uma avaliação paramétrica foram realizadas. Os testes térmicos forneceram informação útil para o dimensionamento de "gap pads" e conhecimento dos gradientes de deslocamento provocados pelas cargas térmicas. Os testes de vibração confirmaram a fiabilidade de uma placa de circuito impresso com componentes electrónicos sob condições de vibração normais e severas.

Concluiu-se que o conhecimento preciso das propriedades dos materiais é crucial para gerar modelos numéricos fiáveis. Além disso, não foi encontrada uma relação linear entre as propriedades do material e os parâmetros geométricos das placas de circuito impresso seleccionadas, sugerindo que cada modelo destas deve ser individualmente caracterizado.

Palavras-Chave: Caracterização de PCBs, Fiabilidade de Juntas Soldadas, Modelação Numérica, Testes Mecânicos, Termografia, Xerografia, Análise de Vibração

Zusammenfassung

Qualität und Langlebigkeit bzw. Strapazierfähigkeit von elektronischen Systemen fordern ein hohes und stetig steigendes Niveau von Zuverlässigkeit. Da die Leiterplatten Morphologie sehr komplex ist, ist nur wenig über ihre mechanischen und thermischen Eigenschaften sowie deren Erschütterungsverhalten bekannt.

Bei dem Versuch weitere Erkenntnisse in diesem Studienbereich zu erlangen, wurde eine bestimmte Anzahl an Leiterplatten experimentellen Tests im Bereich der Mechanik, Thermik sowie Erschütterung unterzogen. Numerische Simulationen zur Modellierung der mechanischen Testresultate wurden realisiert und im Anschluss eine parametrische Bewertung durchgeführt. Die thermischen Versuche ergaben nützlichen Informationen für die "Gap Pad" Dimensionierung. Zusätzlich konnte Klarheit über den Verformungsgrad gewonnen werden, welcher durch wärmebedingte Belastungen verursacht wird. Die Erschütterungstests bestätigten die Abhängigkeit der Leistung von Leiterplattenbauweisen unter normalen Bedingungen sowie bei starker Erschütterung.

Zusammenfassend kann gesagt werden, dass genaues Wissen über die Eigenschaften des Materials ausschlaggebend ist um verlässliche Modelle zu generieren. Des Weiteren konnte kein linearer Zusammenhang zwischen den Materialeigenschaften der ausgewählten Leiterplatten und den geometrischen Parametern hergestellt werden. Aus dieser Kenntnis ist vorzuschlagen, dass jede Leiterplatte individuell zu charakterisieren ist.

Schlüsselwörter: PCBs Charakterisierung, Zuverlässigkeit von Lötverbindungen, Numerische Modellierung, Mechanische Test, Thermografie, Digital-Shearografie, Schwingungsanalyse

To my Family
You know your Worth to me

To Sofia Araújo
My second Mother

To Goldpot
As Always

"Whenever you find yourself on the side of the majority, it is time to pause and reflect."

–Mark Twain

"Where's your will to be weird?"

–Jim Morrison

"Life is pretty simple: You do some stuff. Most fails. Some works. You do more of what works. If it works big, others quickly copy it. Then you do something else. The trick is doing something else."

–Leonardo da Vinci

Acknowledgements

Great achievements are only possible with the guidance of great mentors. Thus, I was never self-made, as I had their help.

From the Faculty of Engineering of the University of Porto:

To my co-supervisors, Professor Paulo Tavares de Castro and Professor Sérgio Tavares, for the tireless support, guidance, ideas and suggestions throughout this entire work. Your words of encouragement always made me try one more time.

To Professor Mário Vaz, for also accompanying part of the work, and for providing the conditions for some experimental tests realization.

To Engineer Nuno Viriato, for the help in preparing the experimental set-ups and to perform the experimental tests in the Laboratory of Optics and Experimental Mechanics.

To Professor José Dias Rodrigues, for the help in preparing the vibration tests set-up and advice on their realization.

To Investigator Albertino Arteiro, for the initial ideas for preparing the numerical models and for the insights on the experimental data results.

To Professor Hernâni Lopes, for the help in preparing and executing the digital shearography tests.

From Bosch Security Systems Ovar:

To my supervisor, Engineer Pedro Bastardo, whose guidance and ideas have helped me to explore better solutions to the problems I encountered, to enrich my work.

To Engineer Rui Guimarães, for sharing his knowledge of PCBs and for helping with the selection of specimens for the experimental tests.

To Engineer Francisco Moreira, for welcoming me to the ENI section from Bosch Security Systems Ovar.

To Engineers Bruno Arcipreste and Pedro Sampaio, from Bosch Car Multimedia – Braga, for clarifying some questions regarding PCBs strain measurement and for preparing an experimental workshop on this issue.

Last, but not least:

To my colleague and friend José Rodrigues, for all the discussions about this work, good conversations and words of support when times were tough.

Contents

Abstract i

Resumo iii

Zusammenfassung v

Acknowledgements ix

List of Figures xv

List of Tables xix

Nomenclature xxi

1 Introduction 1
- 1.1 The Bosch Group . . . 1
  - 1.1.1 Strategy . . . 2
  - 1.1.2 History . . . 2
  - 1.1.3 Bosch in Portugal . . . 3
- 1.2 Bosch Security Systems . . . 4
  - 1.2.1 Products . . . 6
- 1.3 Bosch Security Systems – Ovar . . . 7
  - 1.3.1 Internal Organization . . . 7
- 1.4 Project Background . . . 10
- 1.5 Aim and Objectives . . . 10
- 1.6 Outline . . . 11

2 State-of-the-art 13
- 2.1 Definition & Morphology . . . 13
- 2.2 Manufacturing Process . . . 15
  - 2.2.1 Single-Sided Boards . . . 16
  - 2.2.2 Double-Sided Plated Through-holes . . . 19
  - 2.2.3 Multi-Layer Boards . . . 20
- 2.3 Design for Reliability in Electronic Packaging . . . 21
  - 2.3.1 Lead-Free Solders . . . 22
  - 2.3.2 Surface Mount Technology . . . 24
  - 2.3.3 Solder Joints . . . 25
  - 2.3.4 PCBs Cratering . . . 26
  - 2.3.5 Mechanical Testing . . . 27
  - 2.3.6 Numerical Modelling and Simulation . . . 28

2.4 Thermal Imaging . . . 30
2.4.1 Thermal Cameras . . . 30
2.5 Summary . . . 32

3 Gap Pads **33**
3.1 Thermal Interface Materials . . . 33
3.2 Thermal Gap Pads . . . 34
3.2.1 Parameters . . . 35
3.2.2 Review . . . 36
3.2.3 Companies . . . 37
3.3 Data Analysis . . . 38
3.3.1 Bergquist . . . 38
3.3.2 T-Global . . . 39
3.4 Summary . . . 40

4 Problem Statement **41**
4.1 Issue . . . 41
4.1.1 Approaches . . . 42
4.1.2 Guideline . . . 44
4.2 Selected Printed Circuit Board Models . . . 45
4.3 Bosch Car Multimedia – Braga . . . 46
4.3.1 PCB Strain Measurement Q&A . . . 46
4.3.2 PCB Strain Measurement Training . . . 48
4.4 Summary . . . 50

5 Mechanical Testing **51**
5.1 Overview . . . 51
5.2 Methodology . . . 51
5.2.1 Three-point bending test . . . 52
5.2.2 Four-point bending test . . . 53
5.2.3 Experimental Approach . . . 53
5.3 Organization . . . 56
5.4 Three-point bending tests . . . 56
5.4.1 Experimental Set-up . . . 56
5.4.2 Experimental Procedure . . . 58
5.4.3 Results . . . 60
5.4.4 Discussion . . . 69
5.5 Four-point bending tests . . . 70
5.5.1 Experimental Set-up . . . 70
5.5.2 Experimental Procedure . . . 71
5.5.3 Results . . . 74
5.5.4 Discussion . . . 93
5.6 Global Remarks . . . 93
5.7 Summary . . . 96

6 Numerical Modelling **97**
6.1 Overview . . . 97
6.2 Three-point bending tests . . . 98
6.2.1 Set-up . . . 98
6.2.2 Results . . . 102

6.2.3 Discussion . . . 106
6.3 Four-point bending tests . . . 107
6.3.1 Set-up . . . 107
6.3.2 Results . . . 107
6.3.3 Discussion . . . 114
6.4 Parametric Evaluation . . . 115
6.4.1 Scenarios . . . 116
6.4.2 Discussion . . . 117
6.5 Summary . . . 120

7 Thermal & Vibration Testing **121**
7.1 Thermography . . . 121
7.1.1 Overview . . . 121
7.1.2 Experimental Set-up . . . 122
7.1.3 Analysis & Discussion . . . 124
7.2 Digital Shearography . . . 129
7.2.1 Review . . . 129
7.2.2 Experimental Set-up & Procedure . . . 131
7.2.3 Results & Discussion . . . 132
7.3 Thermo-Vibration . . . 137
7.3.1 Experimental Set-Up . . . 137
7.3.2 Experimental Procedure . . . 139
7.3.3 Discussion . . . 140
7.4 Summary . . . 141

8 Conclusions & Further Work **143**
8.1 Conclusions . . . 143
8.2 Further Work . . . 144

References **147**

A 4PB CAD Drawings **155**

B Numerical Scenarios Comparison **161**

C Matlab Codes **163**
C.1 Gap Pads Data Analysis . . . 164
C.2 3PB & 4PB Tests Data Import . . . 169
C.3 3PB & 4PB Tests Distances . . . 171

D Software Algorithm **173**

List of Figures

1.1 Bosch headquarters, in Stuttgart, Germany [1] 2
1.2 Bosch Termotecnologia S.A., in Aveiro [1] 3
1.3 Bosch Car Multimedia S.A., in Braga [1] 3
1.4 Bosch Security Systems Timeline [1] 4
1.5 Bosch Security Systems Business Units [1] 4
1.6 Bosch Security Systems reference cameras [1] 6

2.1 Examples of printed circuit boards [6; 7] 14
2.2 Multi-layer printed circuit boards stack-up details [2] 14
2.3 Example of a printed circuit board assembly [10] 15
2.4 Major steps of the manufacturing process of a single-sided printed circuit board [2] 18
2.5 Major steps of the manufacturing process of a double-sided, plated through-hole board [2] 20
2.6 Different failure modes on a printed circuit board solder joint [26] 22
2.7 Schematic figures of THT and SMT [32] 24
2.8 Cracking of a capacitor [34] 25
2.9 Structure of a solder joint [19] 25
2.10 Pad cratering [33] 26
2.11 Common location for brittle solder joint fracture of a BGA [37] 26
2.12 3D material model of a printed circuit board with solder joints [19] 29
2.13 Black body radiation as a function of wavelength for various absolute temperatures [51] 31
2.14 Examples of thermal images [52; 53] 31

3.1 Illustration of a thermal gap filler and gap pad [56] 34
3.2 Gap pad 1000HD graph relating the thermal resistance with resultant thickness, provided by Henkel's Bergquist Company [56] 36
3.3 Pressure versus deflection graph obtained from continuous strain test method for a range of gap pad products, provided by Bergquist Company 38
3.4 Pressure versus deflection graph obtained from step strain test method for a range of gap pad products, provided by Bergquist Company 39
3.5 T-Global gap pad L37-3 39
3.6 T-Global gap pad L37-3S 40
3.7 T-Global gap pad TGX 40

4.1 PCBA direct mounting approach 43
4.2 PCBA indirect mounting approach 43
4.3 Three and six-sigma areas of the Gaussian bell curve 44
4.4 Experimental procedure of the PCB strain measurement workshop 49

5.1 Three-point bending test schematic drawing 52
5.2 Three-point bending test shear and moment diagrams 52
5.3 Four-point bending test schematic drawing 53
5.4 Four-point bending test shear and moment diagrams 53
5.5 Schematic drawing of a printed circuit board geometric parameters 54
5.6 Measurement devices 55
5.7 Thickness mean and deviation values for the different PCB models 55
5.8 3PB tests experimental set-up 57
5.9 Schematic drawing of the 3PB tests 57
5.10 PCB model 3 specimen 59
5.11 PCB model 7 specimen 59
5.12 PCB model 9 specimen 59
5.13 PCB model 3 load-displacement curves, in direction 1 61
5.14 PCB model 3 load-displacement curves, in direction 2 62
5.15 PCB model 3 slope comparison, in directions 1 and 2 63
5.16 PCB model 7 load-displacement curves, in direction 1 64
5.17 PCB model 7 load-displacement curves, in direction 2 65
5.18 PCB model 7 slope comparison, in directions 1 and 2 66
5.19 PCB model 9 load-displacement curves, in direction 1 67
5.20 PCB model 9 slope comparison, in direction 1. 68
5.21 Four-point bending tests experimental set-up 70
5.22 Schematic drawing of the 4PB tests 71
5.23 PCB model 1 specimen 72
5.24 PCB model 2 specimen 72
5.25 PCB model 5 specimen 73
5.26 PCB model 6 specimen 73
5.27 PCB model 12 specimen 73
5.28 PCB model 14 specimen 73
5.29 PCB model 1 load-displacement curves, in direction 1 75
5.30 PCB model 1 load-displacement curves, in direction 2 76
5.31 PCB model 1 slope comparison, in directions 1 and 2 77
5.32 PCB model 2 load-displacement curves, in direction 1 78
5.33 PCB model 2 load-displacement curves, in direction 2 79
5.34 PCB model 2 slope comparison, in directions 1 and 2 80
5.35 PCB model 5 load-displacement curves, in direction 1 81
5.36 PCB model 5 load-displacement curves, in direction 2 82
5.37 PCB model 5 slope comparison, in directions 1 and 2 83
5.38 PCB model 6 load-displacement curves, in direction 1 84
5.39 PCB model 6 load-displacement curves, in direction 2 85
5.40 PCB model 6 slope comparison, in directions 1 and 2 86
5.41 PCB model 12 load-displacement curves, in direction 1 87
5.42 PCB model 12 load-displacement curves, in direction 2 88
5.43 PCB model 12 slope comparison, in directions 1 and 2 89
5.44 PCB model 14 load-displacement curves, in direction 1 90
5.45 PCB model 14 load-displacement curves, in direction 2 91
5.46 PCB model 14 slope comparison, in directions 1 and 2 92
5.47 Flexural Young modulus in function of the number of copper layers of the selected PCB models, in longitudinal and transversal directions 94

5.48 Flexural Young modulus in function of the copper percentage of the selected PCB models, in longitudinal and transversal directions 95

6.1 Three-point bending material model parts 99
6.2 Material properties window 100
6.3 Assembly module interface, in Abaqus 2017 100
6.4 Interaction module interface, in Abaqus 2017 101
6.5 Meshing of the plate and cylinder parts, in Abaqus 2017 101
6.6 Comparison of the cylinders' mesh influence on the load-displacement curve 102
6.7 Deformed shape with a magnification of U_3 displacement distributions along PCB model 3 103
6.8 Numerical and experimental load-displacement curves comparison, for PCB model 3 103
6.9 Deformed shape with a magnification of U_3 displacement distributions along PCB model 7 104
6.10 Numerical and experimental load-displacement curves comparison, for PCB model 7 104
6.11 Deformed shape with a magnification of U_3 displacement distributions along PCB model 9 105
6.12 Numerical and experimental load-displacement curves comparison, for PCB model 9 105
6.13 Deformed shape with a magnification of U_3 displacement distributions along PCB model 1 108
6.14 Numerical and experimental load-displacement curves comparison, for PCB model 1 108
6.15 Deformed shape with a magnification of U_3 displacement distributions along PCB model 2 109
6.16 Numerical and experimental load-displacement curves comparison, for PCB model 2 109
6.17 Deformed shape with a magnification of U_3 displacement distributions along PCB model 5 110
6.18 Numerical and experimental load-displacement curves comparison, for PCB model 5 110
6.19 Deformed shape with a magnification of U_3 displacement distributions along PCB model 6 111
6.20 Numerical and experimental load-displacement curves comparison, for PCB model 6 111
6.21 Deformed shape with a magnification of U_3 displacement distributions along PCB model 12 112
6.22 Numerical and experimental load-displacement curves comparison, for PCB model 12 112
6.23 Deformed shape with a magnification of U_3 displacement distributions along PCB model 14 113
6.24 Numerical and experimental load-displacement curves comparison, for PCB model 14 113
6.25 PCB model 6 stack-up 115
6.26 Global comparison of numerical model's scenarios 117
6.27 Load-displacement curves comparison between the default and # 5 scenarios 118
6.28 Von Mises stress distribution in scenario # 6 detailed geometry material model 119

7.1 Bosch DCN-WAP [1] . . . 121
7.2 PCB model 13 . . . 122
7.3 PCBA of the DCN-WAP product . . . 122
7.4 Experimental set-up for the thermography tests . . . 123
7.5 Temperature profile along the sketched lines on PCBA model 13 top surface, at room temperature . . . 124
7.6 Temperature profile along the sketched lines on PCBA model 13 top surface, at the maximum temperature time instant . . . 125
7.7 Temperature profile along the sketched lines on PCBA model 13 top surface, during cooling . . . 125
7.8 Temperature evolution with time along the sketched lines of the top surface of PCBA model 13 . . . 126
7.9 Temperature profile along the sketched lines on PCBA model 13 bottom surface, at room temperature . . . 127
7.10 Temperature profile along the sketched lines on PCBA model 13 bottom surface, at the maximum temperature time instant . . . 127
7.11 Temperature profile along the sketched lines on PCB model 13 bottom surface, during cooling . . . 128
7.12 Temperature evolution with time along the sketched lines of the bottom surface of PCBA model 13 . . . 128
7.13 Schematic diagram of digital shearography [82] . . . 129
7.14 Reference image of PCBA model 13 for the digital shearography measurements 130
7.15 Experimental set-up of the digital shearography tests . . . 131
7.16 Shearographic patterns obtained for the different measurements . . . 133
7.17 Rotation values obtained for the 1^{st} measurement in digital shearography . 134
7.18 Rotation values obtained for the 2^{nd} measurement in digital shearography . 135
7.19 Rotation values obtained for the 3^{rd} measurement in digital shearography . 136
7.20 Setting of the PCBA and housing on the electromagnetic shaker . . . 138
7.21 Experimental set-up of the vibration tests . . . 138
7.22 Schematic diagram of the vibration tests experimental set-up . . . 138
7.23 Harmonic excitation, defined by a sine wave . . . 139

List of Tables

2.1 Specified requirements for the Sn-Pb solder substitute [29] 23
2.2 Comparison between the properties of SAC 305 and Sn-Pb eutectic solder [31] 24
2.3 Infrared sub-regions [50] 30

4.1 Summary of the selected printed circuit boards and the correspondent experimental test performed 45

5.1 Geometric parameters of the PCB model ssubmitted to the the 3PB tests . 58
5.2 Support span values defined for the PCB models submitted to the 3PB tests 59
5.3 PCB model 3 slope and flexural properties 63
5.4 PCB model 7 slope and flexural properties 66
5.5 PCB model 9 slope and flexural properties 68
5.6 Geometric parameters of the PCB models submitted to the 4PB tests . . . 71
5.7 Support and loading span values defined for the PCB models submitted to the 4PB tests 72
5.8 PCB model 1 slope and flexural properties 77
5.9 PCB model 2 slope and flexural properties 80
5.10 PCB model 5 slope and flexural properties 83
5.11 PCB model 6 slope and flexural properties 86
5.12 PCB model 12 slope and flexural properties 89
5.13 PCB model 14 slope and flexural properties 92

6.1 Experimental and numerical slopes comparison of the PCB models subjected to the three-point bending tests 106
6.2 Experimental and numerical slopes comparison of the PCB models subjected to the four-point bending tests 114
6.3 Copper properties [74] 115
6.4 FR-4 properties [75] 115
6.5 Slope values for the different scenarios, and relative error calculation 117
6.6 Flexural Young Moduli values for the different scenarios 119

7.1 Values of the parameters for the vibration measurements 140

Nomenclature

Latin Letters

a	Acceleration	$\mathrm{m{\cdot}s^{-2}}$
A	Area	$\mathrm{mm^2}$
b	Width	mm
c	Wien's displacement constant	$\mathrm{nm{\cdot}K^{-1}}$
E	Young modulus	MPa, GPa
E_f	Flexural Young modulus	MPa, GPa
f	Frequency	Hz
G	Shear modulus	GPa
h	Thickness	mm
I	Moment of inertia	$\mathrm{mm^4}$
k	Thermal conductivity	$\mathrm{W{\cdot}(mK)^{-1}}$
L	Length	mm
LS	Load span	mm
m	Load-displacement curve slope	$\mathrm{N{\cdot}mm^{-1}}$
n	Number of copper layers	–
P	Load	N
P_D	Heat flux	W
R_θ	Thermal resistance	$\mathrm{m^2{\cdot}K{\cdot}W^{-1}}$
SS	Support span	mm
T	Temperature	K, °C
ΔT	Temperature difference	K, °C
$x(t)$	Amplitude	m
Z_θ	Thermal impedance	$\mathrm{K{\cdot}W^{-1}}$

Greek Letters

δ	Displacement	mm
ε	Strain	–
λ	Wavelength	nm
ν	Poisson Ratio	–
σ	Stress	MPa

Acronyms

3PB	Three-Point Bending
4PB	Four-Point Bending
BGA	Ball Grid Array
BHS	Bosch Human Resources System
BOM	Bill Of Materials
BPS	Bosch Production System
BU	Business Units
CAD	Computer-Aided Design
CCD	Charge-Coupled Device
CCU	Central Control Unit
CM	Car Multimedia
CoC	Centre of Competences
CTE	Coefficient of Thermal Expansion
CTG	Controlling Finance
EFQM	European Foundation for Quality Management
ENI	Engineering Network International
ESPI	Electronic Speckle Pattern Interferometry
FCM	Facility Management
FEUP	Faculty of Engineering of the University of Porto
FRP	Fibre Reinforced Polymers
HRL	Human Resources
HSE	Health Safety Environment

I/O	Input/Output
IoT	Internet of Things
IP	Internet Protocol
ISEP	Polytechnic of Porto – School of Engineering
IT	Information Technology
LET	Laboratory of Technological Tests
LOME	Laboratory of Optics and Experimental Mechanics
LVMS	Laboratory of Vibrations of Mechanical Systems
MAT	Materials Management
MBI	Manufacturing Business Interface
MOE	Manufacturing Operations and Engineering
MEMS	Micro Electro-Mechanical Systems
NEMI	National Electronics Manufacturing Initiative
NCMS	National Centre for Manufacturing Science
OSP	Organic Surface Protectant
OvrP	Ovar Plant
PCB	Printed Circuit Board
PCBA	Printed Circuit Board Assembly
PDM	Project Data Manager
PM	Project Manager
PQA	Philips Quality Award
PWB	Printed Wiring Board
QMM	Quality Management
RoHS	Restriction of Hazardous Substances
ROI	Return On Investment
SMT	Surface Mount Technology
SPM	Spatial Phase Modulation
ST	Security Systems
TEF	Technical Functions
TER	Support Services

THT	Through Hole Technology
TIM	Thermal Interface Material
TPM	Temporal Phase Modulation
TT	Thermotechnology
VS	Value Streams
WEEE	Waste Electrical and Electronic Equipment

Chapter 1

Introduction

This work results of the symbiosis between an industrial and academic environment. Hence, a partnership between the student, the teaching institution, Faculty of Engineering of the University of Porto (FEUP), and the company, Bosch Security Systems (ST) – Ovar, was agreed, allowing the sharing, creation and discussion of knowledge gathered for this master thesis.

The realization of this work involved the split of tasks between FEUP and Bosch ST – Ovar, depending on their nature, and included gathering of scientific and business/industrial information, execution of experimental tests, numerical simulations and both academic and industrial advice collection.

1.1 The Bosch Group

"It has always been an unbearable thought to me that someone could inspect one of my products and find it inferior in any way. For that reason, I have constantly striven to produce products which withstand the closest scrutiny – products which prove themselves superior in every respect."

–Robert Bosch, 1918
Founder

The Bosch Group is a leading global supplier of technology and services. It employs roughly 390000 associates worldwide (as of 31^{st} December 2016). The company generated sales of 73.1 billion Euro in 2016. Its operations are divided into four business sectors:

- **Mobility Solutions** – being one of the world's largest suppliers of cutting-edge automotive technology.
- **Industrial Technology** – leading in drive and control technology, packaging and process technology.
- **Consumer Goods** – as the world's largest power tool manufacturer and leading manufacturer in household appliances.
- **Energy and Building Technology** – as the leading manufacturer of security, safety and communications solutions and thermotechnology.

1.1.1 Strategy

Being a leading Internet of Things (IoT) company, Bosch offers innovative solutions for smart homes, smart cities, connected mobility and connected industry. It uses its expertise in sensor technology, software, and services, as well as its own IoT cloud, to offer its customers connected, cross-domain solutions from a single source. The Bosch Group's strategic objective is to create solutions for a connected life and to improve the quality of life worldwide with products and services which are innovative and exciting. In short, Bosch creates technology that is *Invented for life*. The Bosch Group comprises Robert Bosch GmbH and its roughly 450 subsidiaries and regional companies in some 60 countries. Including sales and service partners, Bosch's global manufacturing, engineering, and sales network covers nearly every country in the world. The basis for the company's future growth is its innovative strength. At 120 locations across the globe, Bosch employs 59000 associates in research and development [1].

"Our new mission statement "We are Bosch" explains what drives us, what we have in common, and what we stand for. We want to leave a lasting trace in the world – achieved by a unique outstanding team."

–Volkmar Denner
Chairman, Board of Management

1.1.2 History

The company was set up in Stuttgart, in 1886, by Robert Bosch (1861−1942) as "Workshop for Precision Mechanics and Electrical Engineering". The special ownership structure of Robert Bosch GmbH assures the entrepreneurial freedom of the Bosch Group, making it possible for the company to plan over the long term and to undertake significant up-front investments in the safeguarding of its future. 92 % of the share capital of Robert Bosch GmbH is held by Robert Bosch Stiftung GmbH, a charitable foundation. The majority of voting rights are held by Robert Bosch Industrietreuhand KG, an industrial trust. The entrepreneurial ownership functions are carried out by the trust. The remaining shares are held by the Bosch family and by Robert Bosch GmbH [1].



Figure 1.1. Bosch headquarters, in Stuttgart, Germany [1]

1.1.3 Bosch in Portugal

Established in Portugal since 1911, Robert Bosch, S.A. is a subsidiary of Robert Bosch GmbH, leading global supplier of technology and services, and one of the largest and oldest private industrial corporations. In 2014, Bosch in Portugal generated 811 million Euro in sales. Around 90 % of its production is distributed globally to over 60 countries, which makes Bosch one of the top 10 exporters in Portugal, having exported an equivalent to 0.4 % of the national GDP in 2014. In addition, Bosch is one of the largest industrial employers in the country, currently with some 3.800 associates. Bosch is represented in Portugal by Bosch Termotecnologia, S.A., in Aveiro, Bosch Car Multimedia Portugal, S.A, in Braga, and Bosch Security Systems — Sistemas de Segurança, S.A., in Ovar, developing and producing a wide range of products for hot water solutions, car multimedia, and security and communications systems, respectively. Most of them are exported to international markets. The group also has a sales office and a BSH Appliances division, both located in Lisbon.



Figure 1.2. Bosch Termotecnologia S.A., in Aveiro [1]



Figure 1.3. Bosch Car Multimedia S.A., in Braga [1]

1.2 Bosch Security Systems

Bosch Security Systems is known for being the preferred partner for security, safety and communication needs. It operates all over the world, delivering solutions according to customers' needs and providing services to manage their business. The product portfolio includes video surveillance, intrusion detection, fire detection and voice evacuation systems as well as access control and management systems (**Fig. 1.5**). Professional audio and conference systems for communication of voice, sound and music complete the range.

This Bosch activity branch is inserted in the Energy and Building Technology business sector, and it provides and guarantees energy services, building security and automation. The company's history has nearly a hundred years of continuous growth, since 1920 (**Fig. 1.4**).

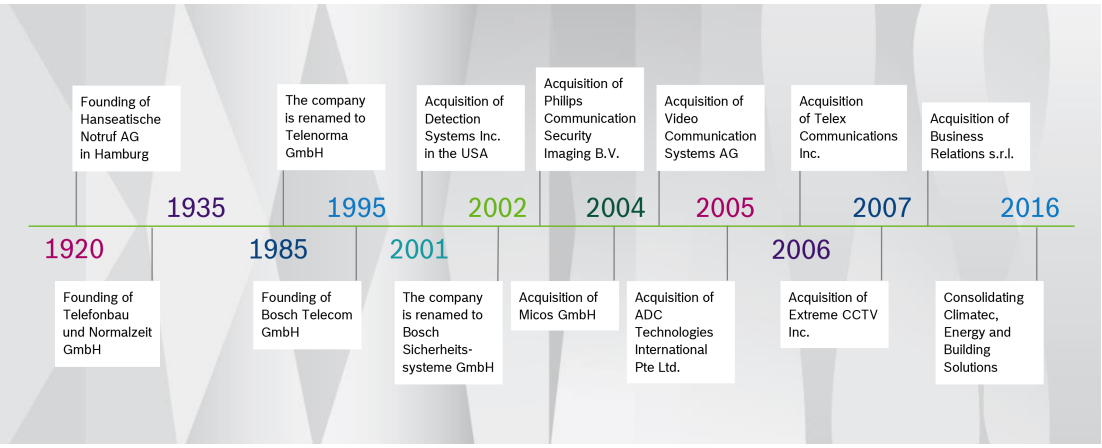


Figure 1.4. Bosch Security Systems Timeline [1]

Bosch ST is very centred in its customers, with its constant demand in delivering better products and services. Thanks to technical excellence, it empowers its partners with interoperable products that make individual solutions possible. The company's main directive is making the world a safer and a more secure place.

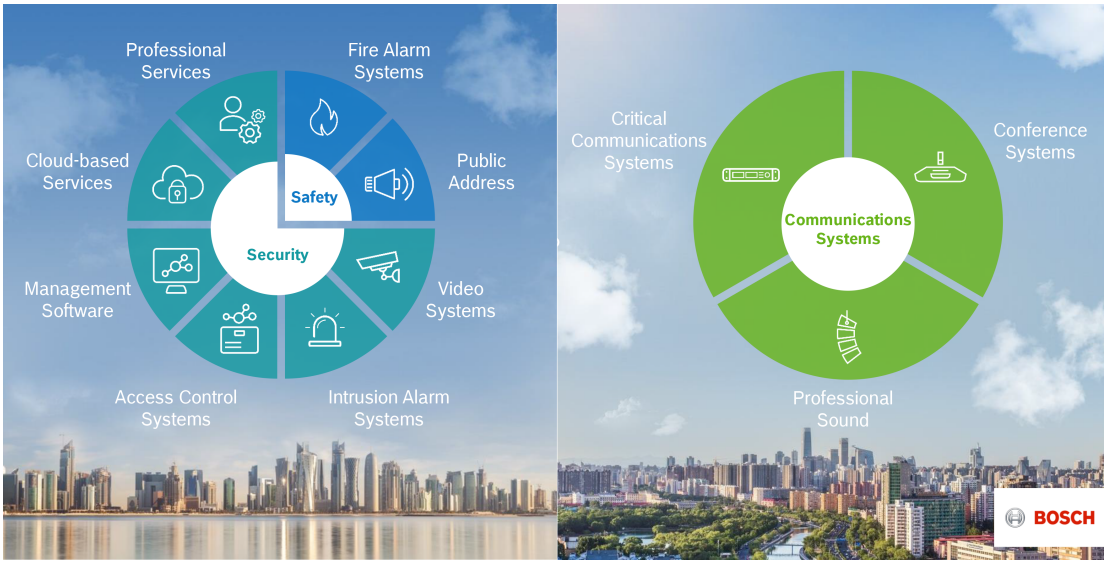


Figure 1.5. Bosch Security Systems Business Units [1]

Besides this solution portfolio, Bosch ST also integrates additional units, namely:

- **Business Development** – responsible for keeping contact with major end-users, consultants and other influencers. The latest technology is combined with extensive global expertise to create individually tailored solutions which answer their specific needs.
- **Training and Certification** – responsible for offering extensive training in all security systems. Makes use of classroom trainings, virtual classrooms and web-based trainings to expand employee's knowledge and expertise. Their achievements can be documented with structured certifications.
- **Tech Support** – provides companies with decisive advantage in global competition.
- **After-sales Services** – provide continued assistance from experienced experts, offering a superior return on investment (ROI) of their products.

Bosch ST encourages its employees to generate innovative ideas and execute them, despite the complexity of the technical requirements, how specific the application or how big or small the project may be. Customers demand solutions which integrate components from different providers. The company's extensive portfolio and key technologies guarantee that those solutions are created. This stands out the company's common values and selling proposition, aiming for market profitably. For the moment, there are numerous references of Bosch ST products spread worldwide, divided in the portfolio categories previously introduced.

For solutions in safety and security, those include towers (Shanghai Tower, China), hotels (Hilton Complex Bursa, Turkey), airports (Antalya Airport, Turkey, Dubai International Airport, United Arab Emirates), water supply stations (Panta Rhei South-North Water Transfer Project, China), shopping centres (Marmara Park, Turkey), banks (VTB Group, Russia), museums (Polin Museum of Polish Jews, Poland).

For solutions in communication systems, those include conference systems (2014 G20 Conference, Australia), professional sound (Allianz Riviera, Nice, France) and critical communication systems (NBC Olympics, Rio de Janeiro, Brazil).

In its global product business, Bosch offers not only an innovative product range, but also a business partner program for planners, system integrators, installers, wholesalers, and original equipment manufacturers. With its international and local presence Bosch is always close to where its customers are, and guarantees a high level of service worldwide.

In Germany and the Netherlands, the Bosch "Building Security" unit provides customized security solutions. Apart from classic building technology services, the "Building Security" unit offers services such as planning, financing, assembly, and maintenance, as well as the operation of security systems.

For other selected countries, Bosch offers customized solutions for large scale projects, from the planning to the preparation of the tender. The implementation is executed by experienced system integrator [1].

1.2.1 Products

Bosch ST provides a wide range of products within each of the business units. For Video Systems, Bosch produces an extensive IP range of innovative and relevant video products with an open architecture and interoperability for easy access to unique features.

The video products can be divided in IP Cameras, IP Recording, Analog Cameras and Analog Recording. By its turn, they can be fixed, panoramic, moving and even speciality cameras. Other features include range, resolution, outdoor ready, thermal detection, built-in microphone, face detection, video motion detection, etc. Some of the reference products are the Dinion, Autodome IP and MIC 7000 cameras (**Fig. 1.6**).



(a) Dinion **(b)** Autodome IP **(c)** MIC 7000

Figure 1.6. Bosch Security Systems reference cameras [1]

Besides Video Systems, Bosch ST provides another numerous spectrum of products and services, specifically:

- **Intrusion Alarm Systems** – intelligent intrusion detection with a delicate balance between quick response to real security breaches and ignoring costly false alarm triggers.
- **Access Control Systems** – turn-key solutions with security management applications, access control products and Bosch or 3^{rd} party security devices.
- **Fire Alarm Systems** – from intelligent fire detection to advanced voice evacuation for safe and future-proof investments.
- **Public Address** – sound reinforcement, digital networked audio, intercom and conferencing for applications ranging from concert sound to aviation and dispatch.
- **Conference Systems** – optimal communication of voice and sound – from intimate informal meetings to major multi-lingual conferences with thousands of delegates.
- **Management Software** – namely Access Control, Video and Alarm Management for complex enterprise solutions such as airports, metro systems and large commercial applications.
- **Professional Services** – managing large scale and highly complex projects with professional security services from Bosch.
- **Cloud-based Services** – a software as a service solution, easily enabling remote video monitoring services over the internet, based on the Bosch IP video camera portfolio.

1.3 Bosch Security Systems – Ovar

Bosch Security Systems – Ovar is part of the Security Systems Business Unit solutions, and it is focused on the production of video cameras, monitors, digital recorders and accessories for security systems.

Throughout the late years, the organization has been engaged in a continuous development process, whose impact enhanced its competitiveness. The company's main achieved goals include:

1996 Certification according to the ISO 9002: 1995 standard.

2000 Certification according to the ISO 14001 standard.
Distinguished with the Philips Quality Award (PQA).

2003 Establishment and monitoring of targets/goals, according to the Business Balanced Scorecard concept.
Introduction of the Bosch Production System (BPS).

2004 First evaluation according to the European Foundation for Quality Management (EFQM).
Participation in the European Quality Award, organized by the EFQM.

2005 Certification according to the ISO 9001: 2000 standard.
Introduction of the six-sigma methodology.

1.3.1 Internal Organization

At Bosch ST – Ovar, each department is responsible for a certain number of tasks which are interconnected with all the others, and reports to the Ovar plant (OvrP) manager. A summary of the main departments is presented below.

Human Resources

The Human Resources (HRL) department is involved in implementing Bosch's strategies and satisfying customers expectations, thanks to the proactive solutions, instruments and processes of excellence it generates. Economy and innovation are the hallmarks of this department.

In both strategic and operational affairs, Human Resources are seen as the partners to the board of management of Ovar. They ensure the company is seen as an attractive employer, striving to be at the cutting-edge of the market, built on the motivation and competence of its managers and associates. Moreover, all operating units are continuously supported in the further development of their organization. Those aims are achieved by guaranteeing clear structures, efficient processes and high-performance human resources tools, standardized in the Bosch Human Resources System (BHS). Every of these elements is subjected to further development on an ongoing basis.

Controlling Finance

The Controlling Finance (CTG) department is responsible for controlling, reporting, accounting, fiscal and legal issues. Besides, it provides financial shared services for National Sales Organization and Service Operations, both located in Lisbon. The main goal is to ensure the reliability of the financial information and support OvrP and its customers, so that the right business decisions are made.

Manufacturing Operations and Engineering

The Manufacturing Operations and Engineering (MOE) department has Quality, Flexibility, Reliability and Speed as the core elements of the production processes. It manufactures products for the Video Systems, Communication Systems and Fire Business Units (BUs) and also products for others divisions, namely Thermotechnology (TT). The BPS methodologies provide the framework to engage every associate of the organization in a continuous development/improvement process, following a step-by-step approach.

The department is organized by Value Streams (VS), being *Source-Make-Delivery* the value chain under focus. Employees teams are led by a VS manager, responsible for the operational management and process improvement of a value chain, since the delivery of the product to the customer up to purchase to suppliers (dock to dock).

The MOE group supports OvrP in the following areas:

- MOE1 – SMT with the assembly of electronics boards
- MOE2 – Value Stream Video
- MOE3 – Value Stream Extreme Video
- MOE4 – Value Stream Communication
- MOE5 – Through Hole Technology (THT)
- MOE6 – Industrial Engineering
- MOE7 – Value Stream Fire and TT

Quality Management

The Quality Management (QMM) department is responsible for the implementation, maintenance and continuous improvement of the Quality Management System. It promotes quality awareness and customer orientation within the OvrP. The core competences include:

- Monitoring of the processes quality performance, from the industrialization phase to mass production.
- Executing products audits and reliability tests.
- Reporting the Quality performance of the organization.
- Promoting the identification and satisfaction of customer's requirements, as well as legal, regulatory and statutory ones.

Moreover, this department supports the continuous improvement of the organization – its processes, product quality, environmental and safety performance – promoting and supporting the implementation of Quality methods and tools. Operational excellence and high level of customer satisfaction are the main elements of the department's vision. Preventive quality is a key aspect to achieve the "zero defects" vision.

Technical Functions

The Technical Functions (TEF) group responsibility lies in the industrialization process within the OvrP, and supports it in the following divisions:

- TEF1 – responsible for the development and maintenance of test equipment.
- Centre of Competences (CoC) – divided into two groups: the first one, Process Engineering, composed by automatic insertion machines and optical blocks, related to processes inside the cleanroom.
- Electronics Engineering – development of production test equipment and maintenance.
- Manufacturing Business Interface (MBI) – consists of a group of project leaders who ensure the industrialization process.
- ITM — Information Technology (IT) dedicated to manufacture.
- Engineering Network International (ENI) – responsible for the product development and support of the development centres.

The latest division, ENI, is composed by a team of nine mechanical engineers, two component engineers, two project data manager (PDM) and one project manager (PM).

The mechanical engineers are responsible for providing support for products during the production phase and developing 2D and 3D CAD design for simulations testing. The PDMs are responsible for the creation and maintenance of bill of materials (BOM), product documents and processing of engineering revisions, whilst the component engineers are responsible for the technical analysis, support and approval and follow up of these product changes. Lastly, the PM does the products' life-cycle analysis (LCA).

These areas ensure the production and industrialization processes support, so that the OvrP is always prepared for the introduction of newly developed products, coming from the R&D centres, with which the department works within and outside its division.

Support Services

The Support Services (TER) department is responsible for ensuring the maximum satisfaction of the internal and external clients by contributing in the following areas:

- Process Engineering
- Maintenance (Equipment and Tools)
- IT
- Facility Management (FCM)

Other Departments

- Materials Management (MAT) – divided in Logistics Warehouse operations (LOG1) and In/outbound and MP Order Desk (LOG2).
- HSE (Health Safety Environment) – responsible for guaranteeing the health and safety of all the employees.

1.4 Project Background

The following pages comprehend a deeper understanding of printed circuit boards (PCBs) behaviour and morphology, initially based upon the many years of research in the Micro Electro-Mechanical Systems (MEMS) field. The rapid evolution of electronic systems has been leading to incredible developments among scientific and technological areas, mainly influenced by the fast processing and manipulation of information. Along with these developments, the need for better portability and reduced dimensions of circuits has been a battle against geometric constraints and physical limits of electronic packages. These packages, throughout their relatively short lifetime span, suffer from mechanical, thermal and vibrational effects. Such combination of effects results in fragility and, consequently, fracture and failure of the printed circuit board or of its components. In most of the cases, these flaws are only detected during the use-phase of a product. The urge to control this issue has to reconsider the product's manufacturing process, by fixing the flaws during the production-phase.

In order to evaluate and understand the reasons behind these failures, the availability of mechanical properties and material models is required. Although experimental tests can provide more precise data, they become very time consuming and severely expensive. The considerable number of specimens to be tested intend to average the variation of geometric parameters, which account for severe changes in the obtained results (deviations of $30 - 40$ %), while compared to the experimental ones. This is due to the micro scale dimensions of the layers, foils and paths of the PCBs interconnections. The challenge of creating simplified material models, compared to the accuracy of more detailed ones, aims to provide quick-fix solutions, while still assuring a reliable quality of results. Therefore, the play between efficiency and accuracy of the outputs is something to account for.

In addition to mechanical characterization of PCBs, insight about the service temperatures is useful when a thermal interface material is to be dimensioned (in this case, gap pads). Reciprocally, notions of vibrational behaviour can indicate if these conditions are a source of printed circuit boards' electrical connection failure.

1.5 Aim and Objectives

Given this, the main goal of this work – to understand the causes of PCB failures – is to be achieved through the following steps:

- **Selection of a group of PCB specimens** to be analysed.
- **Perform experimental tests** to obtain information about their material properties.
- **Creation of material models**, validated with the experimental data collected, capable of simulating the working conditions of a given PCB model.
- Insertion of the outputs (*e.g.* stress and strain values) in an **artificial neural network** to read and recognize patterns among the obtained results.
- **Creation of a GUI software** capable of relating PCBs geometric parameters with boundary conditions of any kind, which would provide the upper limits under which that PCB would perform perfectly, without suffering critical damage.

The aforementioned steps represent a volume of work not entirely predictable. Therefore, it was agreed, at the start of the preparation of this dissertation, that decisions to drop one or more of the steps could eventually be taken, as a result of the evolution of the work.

The contribution of this knowledge for Bosch ST – Ovar would optimize its production yield and, consequently, increase sales and customer satisfaction.

1.6 Outline

The thesis resumes with the state-of-the-art in **Chapter 2**, including a more detailed description of printed circuit boards, referring to their materials, manufacturing process, reliability issues, experimental tests and numerical modelling. A brief notion about thermal imaging, with useful insight for the thermography tests, is also reviewed.

In **Chapter 3**, the topic of thermal interface materials is detailed, and a gap pads' review is highlighted, since clear knowledge about their dimensioning is valuable for later implementation in printed circuit board assemblies, for efficient heat dissipation of the electronic components.

Chapter 4 states the issues Bosch ST – Ovar addresses to be solved, and defines a strategy for approaching them, which gives birth to the next two chapters.

Thus, **Chapter 5** covers the mechanical tests carried out in order to obtain the mechanical properties of the selected printed circuit board specimens, while **Chapter 6** is dedicated to numerical validation of the mechanical tests and to a study of printed circuit boards parameters, whose influence on the outputs is quantified.

As additional tasks for printed circuit boards' characterization, **Chapter 7** describes the realization of thermography, digital shearography and vibration tests, respectively.

Lastly, the main conclusions on printed circuit boards characterization gathered from this work, as well as suggested future works, are presented in **Chapter 8**.

Chapter 2

State-of-the-art

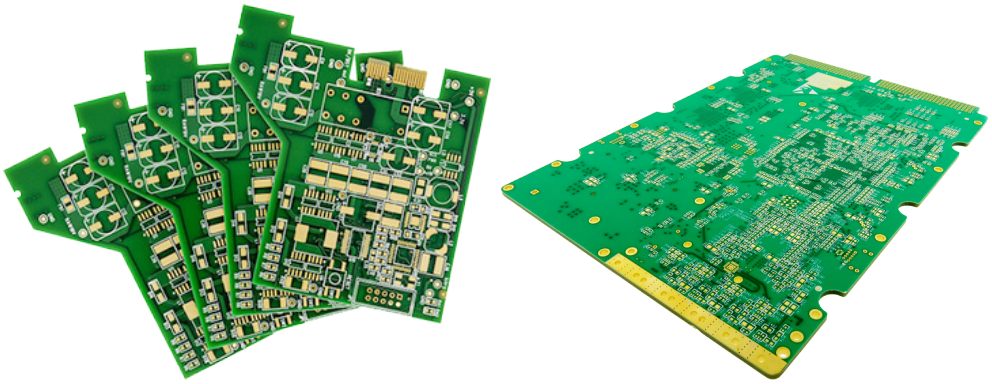
This state-of-the-art review identifies the main issues concerning printed circuit boards use. It resumes with their manufacturing process, followed by design for reliability topics, exploring the lead-free solders, surface mount technology, solder joints, cratering, mechanical testing and numerical modelling. Moreover, a summary of thermal imaging is documented and the gap pads' topic is stated, being explored in-depth in the subsequent chapter.

2.1 Definition & Morphology

Printed Circuit Board (PCB) is a module of a bare board – *i.e.* with conductors but no electronic components – which assures the mechanical support and electrical connection of electronic components (**Fig. 2.1**). These are disposed in a certain layout, using conductive pathways, tracks or signal traces etched (or "printed") from copper paths, laminated onto a non-conductive substrate (**Fig. 2.2**). Copper is chosen because of its excellent properties as a conductor of heat and electricity. However, it quickly oxidises in the presence of air and water. If the copper surface on the printed circuit board is not coated or treated with a protective agent, the exposed area would rapidly become unsolderable. Therefore, all printed circuit boards necessarily use some form of surface finish on the exposed pads, to which the electronic components are to be soldered. The purpose of the surface finish is normally to protect a copper pad and exposed traces between the time the board is manufactured and when it is subsequently assembled. This would ensure that the board can later be soldered successfully during the assembly process [2].

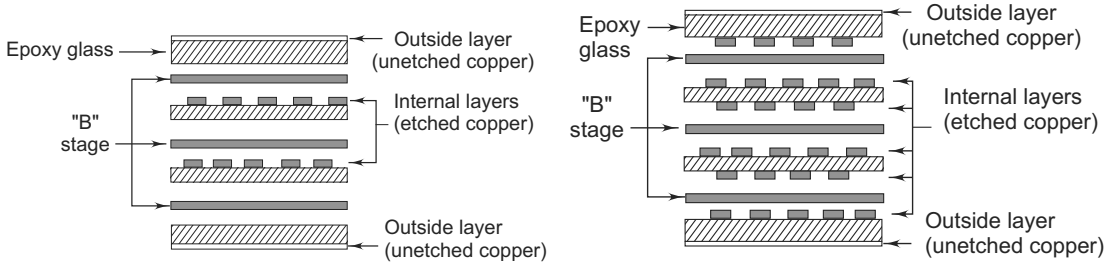
Electronic components – *e.g.* capacitors, transistors, resistors or active devices – are generally soldered on the PCB, although advanced PCBs may contain components embedded in the substrate. This substrate layers are made of fibre reinforced polymers (FRP), which guarantee the structural and insulation functions, and these can be prefabricated or come in a prepreg form. Typically, FR-4 – woven glass fibre and an epoxy resin – is the common substrate material [2–4]. Laminates commonly used for general purpose applications are normally paper base type, whereas epoxy glass laminates are preferred for superior mechanical and electrical properties. The mechanical properties include punching and drilling qualities, flexural strength, flame resistance and water absorption. The important electrical properties include dielectric strength, dielectric constant, dissipation factor, insulation resistance, and surface and volume resistivity [2; 4; 5].

PCBs can be conceived in a rectangular shape (the more common solution), in rounded shapes or a combination of both cases, so that they can meet the geometrical and other requirements.



(a) Set of four printed circuit boards **(b)** Multi-layer printed circuit board

Figure 2.1. Examples of printed circuit boards [6; 7]



(a) Four-layer board **(b)** Eight-layer board

Figure 2.2. Multi-layer printed circuit boards stack-up details [2]

Alternatives to PCBs include wire wrap and point-to-point construction. PCBs require the additional design effort to lay out the circuit, but manufacturing and assembly can be automated. Manufacturing circuits with PCBs is cheaper and faster than with other wiring methods, as components are mounted and wired with one single part [2; 8].

PCBs can be found in desktop and laptop computers. They serve as the foundation for many internal computer components, such as video cards, controller cards, network interface cards, and expansion cards. These components all connect to the motherboard, which is also an example of a printed circuit board. However, their range of application is extended to many other electronic devices, which include one or more incorporated PCBs – *e.g.* televisions, radios, beepers, digital cameras, mobile devices and tablets. The PCBs found in mobile devices may look similar to those found in desktop computers and large electronics, but they are typically thinner and contain finer circuitry [2; 3; 9].

When the board has only copper tracks and features, and no embedded components have been manufactured into the actual substrate of the board, it is more correctly referred to as printed wiring board (PWB) or etched wiring board. Although more accurate and distinct from what would be known as a true printed circuit board, the term "printed wiring board" has generally fallen into disuse, as the distinction between circuit and wiring has become blurred. On the other hand, a PCB populated with electronic components is called a printed circuit assembly (PCA), printed circuit board assembly or PCB assembly (PCBA) (**Fig. 2.3**). In informal use, the term "PCB" is used both for bare and assembled boards, the context clarifying the meaning [2; 9].

For simple electronic devices, PCBs can be single-layer. For complex hardware – *e.g.* computer graphics cards and motherboards – they may have up to twelve layers. They are

most often coloured in green, but they can come in any colour. PCBs can be single sided (one copper layer), double sided (two copper layers) or multi-layer (outer and inner layers). The latter allow for much higher component density [2; 3; 9]. Conductors on different layers are connected with vias. Bosch ST – Ovar works intensively with multi-layer PCBs, so this category is the most relevant for this work.

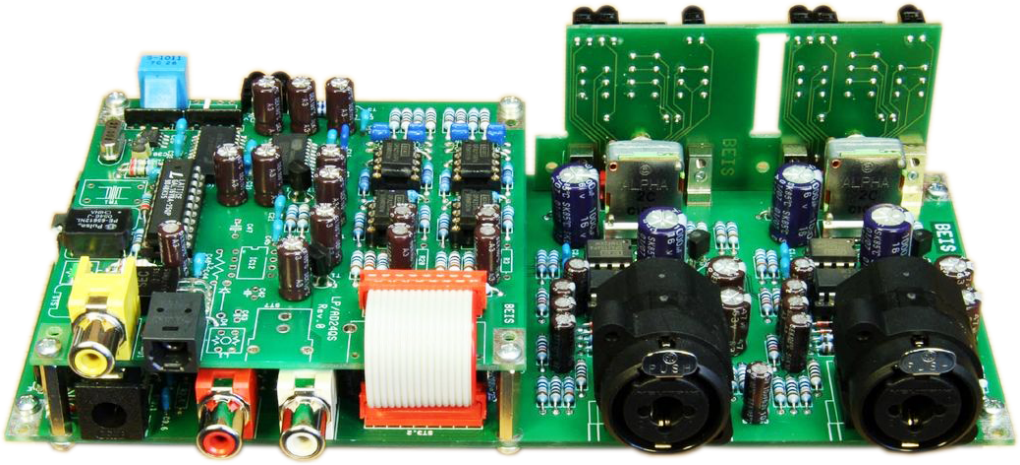


Figure 2.3. Example of a printed circuit board assembly [10]

2.2 Manufacturing Process

The manufacturing process of printed circuit boards is rather complex. Although there is a variety of manufacturing processes, most of them have identical steps. Variations in these basic steps are usually made by manufacturers, to improve quality and specific yield.

The better-known process is the "print and etch" method. In this purely subtractive method, the used base material is copper – to which all the electronic components are soldered – with one or more layers of etched metal tracks, so that the connection is made. The etching process involves achieving a conductive pattern formed on one or both sides of the laminate.

There are four specific phases of PCBs manufacturing process:

- Design
- Fabrication
- Assembly
- Test

These different phases, previously individual activities isolated from each other, are nowadays aggregated in a holistic approach, which considers design for manufacturability, assembly and testability, due to the increasing complexity of PCBs, coupled with the current trends – software based design and test procedure development.

According to the classification of printed circuit boards, the manufacturing process steps are as follows:

2.2.1 Single-Sided Boards

- **Schematic Diagram** – represents the electronic components and connections in the most readable form. It is developed taking into account the components specifications, interactions and physical packages. The circuit diagram normally starts on paper, and then it is transferred and finished in computer-aided design (CAD), the main reference document for design.

- **Artwork Generation** – the components and connections in the PCB layout derived from the circuit diagram are physically placed and routed by the designer. The artwork is usually enlarged two to four times to improve accuracy.

- **Panel Preparation** – the base material for PCBs is a copper clad laminate, with copper on one side only, facing up. The sheets of the laminate are sheared to provide panels of the required size, keeping it slightly longer than the master pattern of the PCB. The preferred size is 350x508 mm. Usually, the base material is FR-4, with 1.6 mm of thickness, with copper foil cladding 305 g/m^2, with 35 μm. The board must be previously cleaned to get rid of contaminants, which may be in the form of organic material (oils and greases), particulate (dust and machining particles), oxides or sulphides.

- **Image Transfer** – transfer of the original artwork pattern to the copper surface on the card. This artwork may be in the form of a photographic negative or positive.

- **Etching** – removal of copper from undesirable areas, in order to achieve the desired circuit patterns. Several chemical processes have been developed and used for etching, using either ferric chloride, ammonium persulphate, chromic acid, cupric chloride and alkaline ammonia, with each of them having its own advantages and disadvantages. Etching is usually done by the immersion, bubble, splash or spray method. The spray etching method is the most current. Undoubtedly, the etching process is the core of the PCB manufacturing process.

- **Board Drilling** – for small scale production, boards are drilled by using single head manually controlled machines. Jigs are used to ensure that correct drill sizes are used and that no holes are missed. Boards can be stacked so that many of them can be drilled simultaneously. Mass production usually utilizes numerically controlled drilling machines with several heads. The vias and pads have copper etched from the centre to facilitate centring of the drill. With the increasing miniaturization of electronic components, the need for smaller hole diameters has gone up. Also, a proper drill must be selected for each type of laminate. Tungsten carbide or diamond tipped drills are preferred for fibreglass boards. For small scale production, boards are drilled by using single head manually controlled machines.

- **Coatings** – the circuit traces are protected with a masking material, known as soldermask. The soldermask is only removed if electrical access to the circuitry is required for soldering the electrical components. All the other areas must be protected with other form of surface finish. The most commonly used surface finish processes are:

  - Hot Air Solder Level – application of tin/lead solder to exposed copper. The solder and exposed copper form an inter metalic chemical bond that protects the copper from oxidation.
  - Immersion Precious Metal Plating – based on the plating of the circuit board surface with electroless nickel/immersion gold, silver or tin which provide immunity to corrosion from environmental exposure. Although the solderability of each of the coatings is different, they provide a flat attachment surface which is essential for achieving a reliable solder joint with fine-pitch parts.
  - Organic Surface Protectant (OSP) Coating – the circuit board is coated by submersion in a chemical bath containing a nitrogen-bearing organic compound with adhesion to the exposed metal surfaces and not absorbed by the laminate or soldermask. These coatings have a limitation: they break down during a thermal cycle in assembly and are not usually recommended for double-sided circuit boards.
  - Conformal coatings – conformal coatings enhance the performance and reliability of printed circuit assemblies that are likely to be subjected to a hostile environment. They are plastic film envelopes which seal out dirt and environmental contaminants. These coatings, which come in the form of acrylics, polyurethanes, epoxies and silicones, are usually applied by spraying, manually or with computer-controlled machines.

- **Testing** – There are two types of PCB tests: bare board test and loaded board tests. The bare board test checks for shorts, opens and net list connectivity, whereas the loaded board tests include analysis of manufacturing defects and in-circuit, functional and combinational tests. With an increase in the track density and the number of through-holes, it has become necessary to test the printed circuit board before assembly. It has been observed that the failure rate in highly populated printed circuits may be as high as twenty per cent. If the boards are not tested at the pre-assembly stage, the failures at a later stage may prove to be extremely expensive in the case of high density and multi-layer boards. Before populating a board with expensive devices such as application specific ICs and microprocessors, it is cost-effective to first check whether the bare board meets expected quality standards. Bare board testing is thus becoming mandatory for the PCB manufacturers. It may be noted that at each stage of the manufacturing process, it is necessary to undertake cleaning and it is desirable to carry-out inspection. However, for simplicity, these stages are not included in the design and description [2].

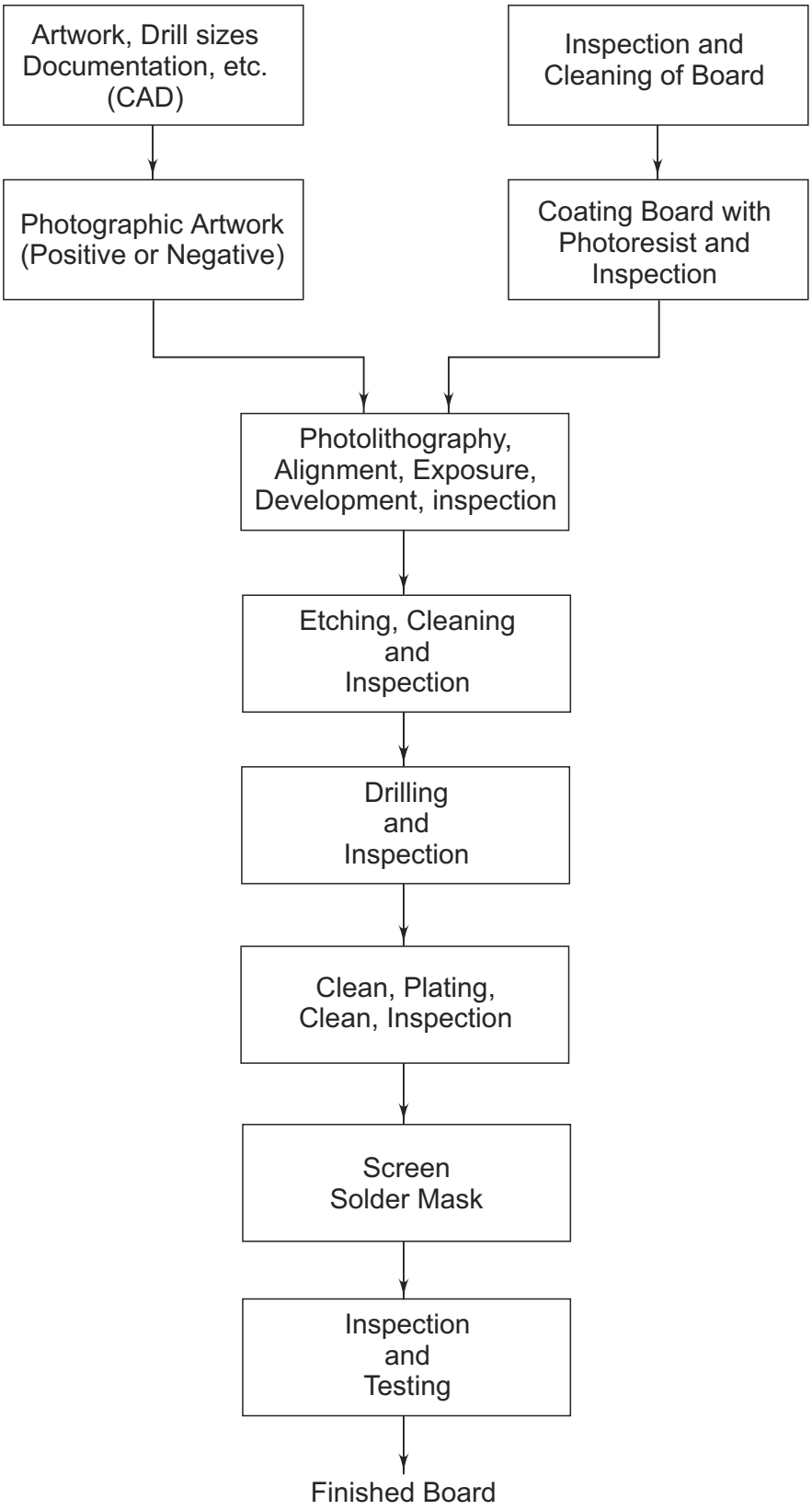


Figure 2.4. Major steps of the manufacturing process of a single-sided printed circuit board [2]

2.2.2 Double-Sided Plated Through-holes

The "print and etch" method used for single-sided boards is applicable to most board processing. However, the process for producing double-sided plated through-holes boards is more complex. Hence, although there are several possible similarities, the steps differ from the single-sided ones. The following description explains the differences between the aforementioned steps for the single-sided boards.

- **Panel Preparation** – laminate sheets with copper cladding on both sides are cut to size as per requirement. Although the size of the panel depends upon the capacity of the plating equipment, the preferred size for many manufacturers is 305x406 mm.
- **Hole Drilling** – the double-sided board is first drilled, which is followed by the removal of any burs by manual or automatic means. The board is then thoroughly cleaned to remove chips of glass fibre and resin. Cleaning is usually done by using a jet of water under high pressure, of the order of $20 - 60$ atmosphere.
- **Electroless Copper Plating** – the board is first sensitized by immersing it in a solution of stannous chloride. The stannous ions are absorbed on the board surface, particularly onto the exposed resin of the hole walls. This is followed by immersion of the board in an acidified solution of palladium chloride. The palladium ions are reduced to the colloidal state and form a thin layer which catalyses electroless copper deposition. Electroless copper deposition takes place in a bath with solution containing copper sulphate, sodium hydroxide, formaldehyde, a reducing agent and other special additives. Here, the copper ions are reduced to metallic copper. This results in deposition of copper, whose thickness is determined by the duration of the board in the solution. Usually, a thickness of about 40 microns of copper is built-up on the base copper and on the hole walls.
- **Image Transfer (Photolithography)** – both sides of the board are covered with a thin layer of a photoresist, which may be solid or a liquid, and either positive or negative. A solid negative working resist is mostly used. The image transfer process occurs with the resist removed from the area where the tracks are to be kept. This is the reverse of the print and etch process. The copper areas, which will remain on the finished PCB and the hole walls, are unprotected. All other areas are covered by the hardened photoresist. Developing of both sides is usually done in an automatic spray machine.
- **Tin-Lead Plating** – the exposed track areas are electroplated with tin-lead alloy by immersing the board in an electroplating bath. All conductive areas, *i.e.* all the conductors required on the PCB and within the holes, get plated to a thickness of about $20 - 25$ microns. The minimum thickness should not be less than 10 microns. This metal is used as a resist in the etching process. Etching: The etching process is similar to the one described in the previous section except that the etchant used must not attack the tin-lead alloy. After etching, the selective areas of the board can be plated with precious metals such as gold or nickel, followed by the application of surface finish coatings such as: hot-air levelling, soldermasking and organic surface protectant.

The board is then finally inspected and tested as per the user's specifications. It is quite possible that some repairs or rework may be required on the finished boards [2].

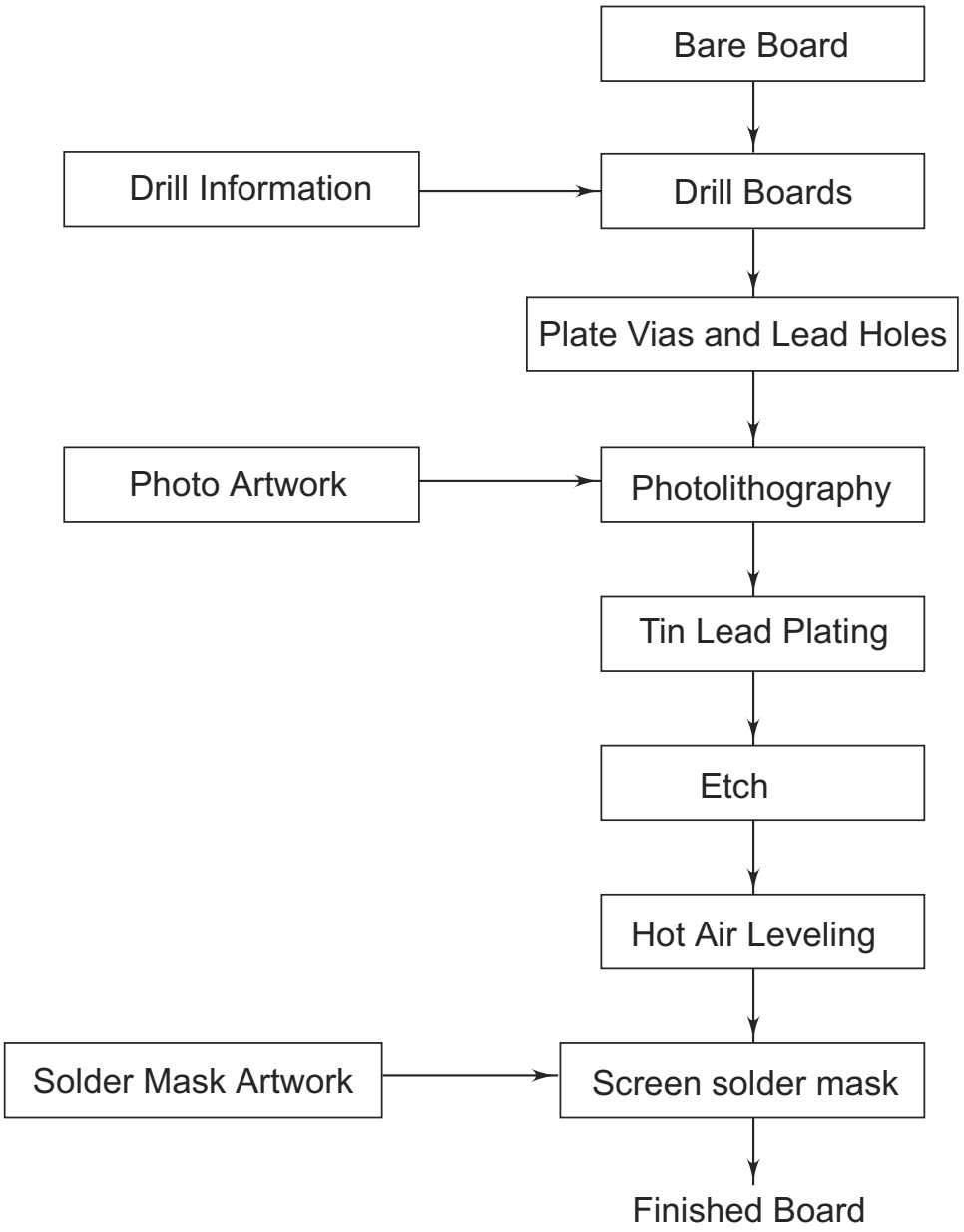


Figure 2.5. Major steps of the manufacturing process of a double-sided, plated through-hole board [2]

2.2.3 Multi-Layer Boards

Multi-layer boards are manufactured by laminating or bonding layers of patterned, pre-etched, undrilled copper clad laminates together. Essentially, the multi-layer boards are produced by bonding together inner layers and outer layers with prepreg. The layers are bounded together with unetched copper top and bottom layers. The individual layers must be arranged in a pressing tool to prevent misalignment of the layers. The stack is laminated to form a single multi-layer board, which can then be processed as double-sided plated through-hole circuit board. Bonding is performed in a hydraulic press or in an autoclave [2].

2.3 Design for Reliability in Electronic Packaging

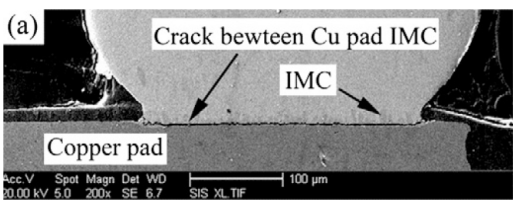
Reliability engineering and management grew up largely in response to the problems of the low reliability of early electronic equipment. Many of the developed techniques emerged from electronic applications. The design and construction of an electronic system, more than any other branch of engineering, involves the use of numerous components which are similar, but over which the designer and production engineer have relatively little control [11]. Quality control is the major determinant of reliability in electronic components. An electronic system unreliability cannot only be measured by the number of flawed components, but also by the interconnections – solder joints and wire bonds. In harsh environment applications (automotive, avionics, military...), these interconnections are more prone to fail. Additionally, the load applied to the components must be monitored, so that it stays within the allowable boundaries, during the product operating conditions [11]. The most common cause of failure of solder joints on surface mounted components and on connections is fatigue. This type of fatigue is mainly mechanical and thermal. The latter has a bigger influence on the life expectancy of solder joints.

The demands on printed circuit boards are continuously increasing. Although the increase of the number of layers provides more signal planes [12], the current trend of miniaturization in electronics industries has preferably led to a necessary increase of density of interconnections. Innovative solutions propose to incorporate passive and/or active components onto inner layers of PCBs and connect them through laser microvias, with the advantage of increasing the connections, reducing the number of solder joints – which are the sources of failure – and improving the electrical performance as well [13]. Due to customer requirements, the size of the boards has to be reduced or, at least, the number of input/output (I/O) has to be greater [13; 14]. Thus, the build-up design and the interaction of the different integrated materials has to be optimised [15]. Every PCB must be reliable for a long period. Typically, for military and aeronautic industries, the service duration of the component must be larger than a decade [13; 16].

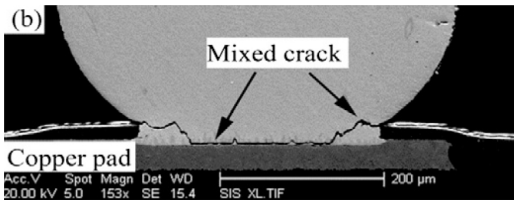
To improve the reliability of PCBs, mechanical (static and modal) tests, numerical validation, fatigue analysis and knowledge of failure modes provide information that enhances the understanding and promote better solutions for many of the PCB's industry problems [15; 17]. Some of these problems concern:

- **High local stresses** – cause fracture of circuit paths and, thus, malfunction of the components based on the PCB [15].
- **Mechanical impact** – the main failure mechanism of solder joints under dynamic impact [18; 19].
- **Cyclic thermal loading** – leads to a degradation of the electrical properties and, subsequently, to circuit failure. There are industry-wide standards to test the reliability of PCBs under these conditions [20].
- **Warpage** [21].
- **Cratering** [22–24].
- **Solder joint fracture** [12; 13; 18; 19; 25–27].

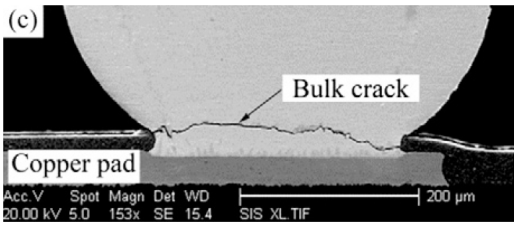
The latter point is the main cause of failure of printed circuit boards (**Fig. 2.6**). The crack is typically found in the solder joints located at the edge of the Ball Grid Arrays (BGAs), the circuit most critical components [18; 27]. At Bosch ST – Ovar, this same phenomenon occurs for most of the rejected or flawed PCB models. Therefore, its study would contribute to lower the rejection and flaw rates on the different PCB models, during the production-phase, so that this issue can be mitigated during the use-phase.



(a) Crack between IMC and copper pad



(b) Mixed crack



(c) Crack within bulk solder

Figure 2.6. Different failure modes on a printed circuit board solder joint [26]

2.3.1 Lead-Free Solders

The Restriction of Hazardous Substances (RoHS) directive [28] forced the industry to meet the 2006 deadline to completely remove lead, as other banned substances, from most of their consumer products and respective manufacturing processes.

Perhaps the most affected item were the solders, whose standard composition was made of Sn-Pb eutectic. Exhausting research and experimental work was performed by industries and academic institutions, so that a reliable solution could be found for replacing the standard solders [29]. This replacement would require a similar performance of the Sn-Pb eutectic, widely used since more than fifty years ago, when it was first implemented. The first criteria for a solder which could replace the standard Sn-Pb eutectic were quantified and set the requirements to be met, created by the National Centre for Manufacturing Science (NCMS) Pb-Free Solder Project, in 1997 [29], presented in **Tab. 2.1**.

Nevertheless, in 1999, the Waste Electrical and Electronic Equipment (WEEE) and RoHS Directives [28; 30] led the National Electronics Manufacturing Initiative (NEMI) to establish an even more quantitative set of criteria.

The requirements to be met are the following:

- Have a melting point as close to that of the Sn-Pb as possible.
- Be eutectic or as close to eutectic as possible.
- Contain no more than three elements.
- Make no use of existing patents if possible, to facilitate implementation.
- Have a potential reliability equal to or better than Sn-Pb eutectic.

Table 2.1. Specified requirements for the Sn-Pb solder substitute [29]

Solder Property	Definition	Acceptable Levels
Liquidus Temperature	Temperature at which solder alloy is completely molten.	< 225 °C
Pasty Range	Temperature differences between solidus and liquidus temperatures; temperature range where the alloy is part solid and part liquid.	< 30 °C
Wettability	A wetting balance test assesses the force resulting when a copper wire is immersed in and wetted by a molten solder bath. A large force indicates good wetting, as does a short time to attain a wetting force of zero and a short time to attain a value of two thirds of the maximum wetting force.	$F_{Max} > 300$ μN $t_0 < 0.6$ s $t_{2/3} < 1$ s
Area of Coverage	Assesses the coverage of the solder on Cu after a typical dip test.	< 225 % coverage
Drossing	Assesses the amount of oxide formed in air on the surface of molten solder after a fixed time at the soldering temperature.	Qualitative scale
Thermo-mechanical Fatigue	Cycles-to-failure for a given percent failed of a test population based on a specific solder-joint and board configuration, compared to Sn-Pb eutectic.	Some percentage, usually > 50 %
Coefficient of Thermal Expansion (CTE)	Thermal expansion coefficient of the solder alloy is the fraction change of length per °C temperature change. Value used for comparison was CTE of solder alloy at room temperature.	$< 2.9e^{-5}$ /°C
Creep	Stress required at room temperature to cause failure in 10000 minutes.	> 3.4 MPa
Elongation	Total percent elongation of material under uni-axial tension at room temperature.	$>> 10$ %

Although no clear consensus was reached, the most promising family of alloy to replace the Sn-Pb eutectic was the Sn-Ag-Cu (SAC) ternary alloy system.

Bosch ST uses the SAC 305 (Sn-3.0Ag-0.5Cu) solder alloy. Lead free solders are replacing lead rich solders, thanks to their higher rigidity and lower ductility [18]. A comparison between the mechanical properties of SAC 305 and the standard Sn-Pb solders is presented in **Tab. 2.2**.

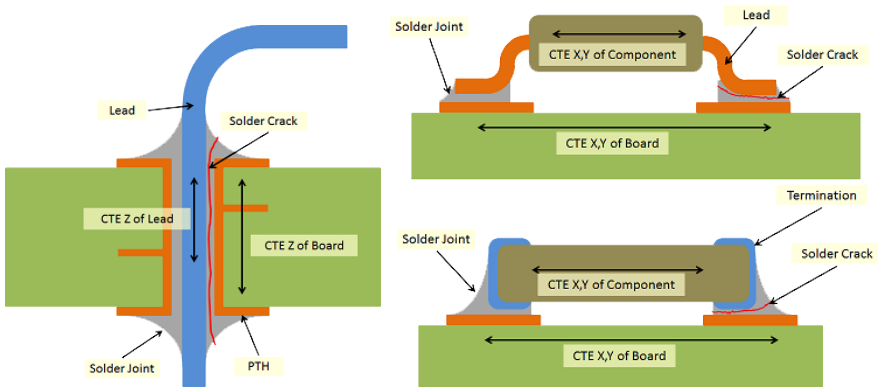
Table 2.2. Comparison between the properties of SAC 305 and Sn-Pb eutectic solder [31]

Solder Property	63Sn-37Pb	SAC 305
Liquidus Temperature /°C	183	220
Solidus Temperature /°C	183	217
Tensile Strength /MPa	34.7	41.1
Yield Point /MPa	28.4	34.2
Elongation /%	91.2	41.0
Coefficient of Work Hardening	0.032	0.040
Young Modulus /GPa	40	50
Poisson Ratio /−	0.37	0.36
Specific Gravity /−	8.4	7.4
Specific Heat /J·(gK)$^{-1}$	0.18	0.23
Thermal Conductivity, at 25 °C /%	52.8	63.2
CTE /10^{-6}·K^{-1}	21.6	21.6

2.3.2 Surface Mount Technology

For printed circuit board assemblies, mechanical fixation and electrical connection between the electronic components and their terminals is made by means of soldering. There are two types of technology for this purpose, shown in **Fig. 2.7**:

1. **Through hole technology** (THT)
2. **Surface mount technology** (SMT)



(a) Through hole technology **(b)** Surface mount technology

Figure 2.7. Schematic figures of THT and SMT [32]

In the early days, PCBA connections were made using only THT, and a single component would occupy space on both sides of the board and should have leads to go through the board's holes. During the 1960s, the demand for using more components per board, without increasing its size, gave birth to the SMT, broadly spread in the 1980s [33]. Thanks to this technology, components as smaller leads, pre-attached solder balls or pads could

be soldered to PCB's surface, which would be on the same one they would be placed. For more efficient use of the board's size, components started to be smaller, allowing both sides of the board to be used. However, these solders were more susceptible to crack under mechanically or thermally induced stresses, since the rigid connection does not deform and, thus, all the stresses are transfered to the solder and to the component itself. The most common case of component cracking is that of the small SMT ceramic capacitors (**Fig. 2.8**) which, being ceramic, have very low ductility, thus they fracture easily [33].

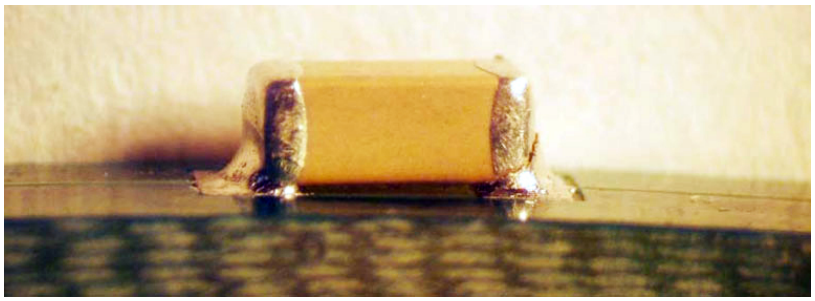


Figure 2.8. Cracking of a capacitor [34]

2.3.3 Solder Joints

Solder joints serve as mechanical, thermal and electric interconnections between the components and the PCB, being its most vulnerable part (**Fig. 2.9**). Reliability of solder joints under drop impact loading is very important, specially in mobile electronic products [19]. The stresses in solder joints are due to a combination of bending moments in the PCB and the inertia forces, due to component mass and acceleration. In worst case scenarios, these stresses may cause one of the following failure modes: PCB delamination, solder joint fracture, lead fracture or component package fracture [25]. Design analysis has suggested that the robustness of the interconnections subjected to mechanical bending can be increased by increasing the diameter of the solder joints [35].

To investigate the mechanical behaviour of solder joints, mechanical tests have to be performed. The most current tests found in literature include three and four-point bending tests and vibration tests.

Although out of the scope of this work – more focused in PCB's characterization – there are also approximate solutions for solder joint failure prediction of PCB assemblies, subjected to mechanical bending, detailed in [35; 36]. The same solutions have been validated against finite element analysis, and there was good matching of results.

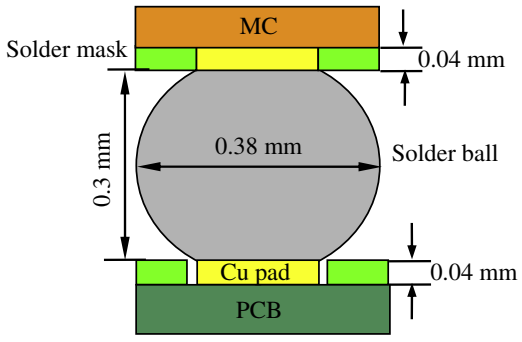


Figure 2.9. Structure of a solder joint [19]

2.3.4 PCBs Cratering

A pad crater is the mechanical cracking of the PCB laminate under a component connecting pad (**Fig. 2.10**). Some cracks do not cause immediate electrical failure, and are only detected in the use-phase of the product, going undetected during the production-phase, specifically during the functional tests. In fact, small cracks under the pad may be initiated during manufacturing and test. Hence, long term reliability risks are more critical for partial cracks that are not detectable [22].

Also, pad crater could actually occur in the BGAs edge solder joints (**Fig. 2.11**), under thermal stress or thermo-mechanical stress, as previously stated [23].

Based on numerical simulations, the maximum von Mises stress in these critical solder joints occurs at the interface of PCB side, and it increases with the increase of the PCB deflection [19].

For thermo-mechanical analysis, the standard practices in electronic industry consist of a set of combined tests of temperature and vibration, designed to evaluate solder interconnections' reliability at different temperatures. Temperature dominates crack propagation path of solder joint during vibration test [26]. Other standard practice consists in evaluating the number of cycles to failure of the PCB solder joints. This prediction is based on using empirical relations, such as the Coffin-Manson approach [12; 13; 17; 24].

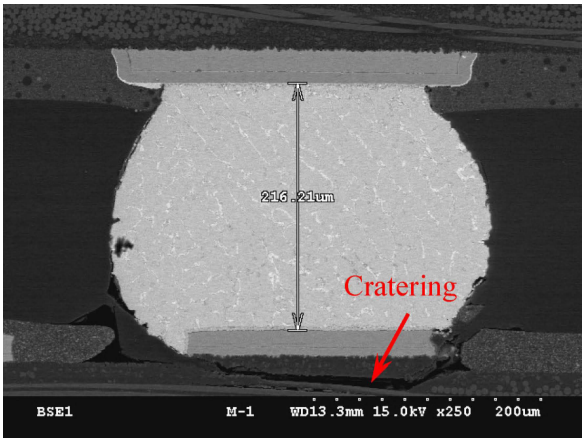


Figure 2.10. Pad cratering [33]

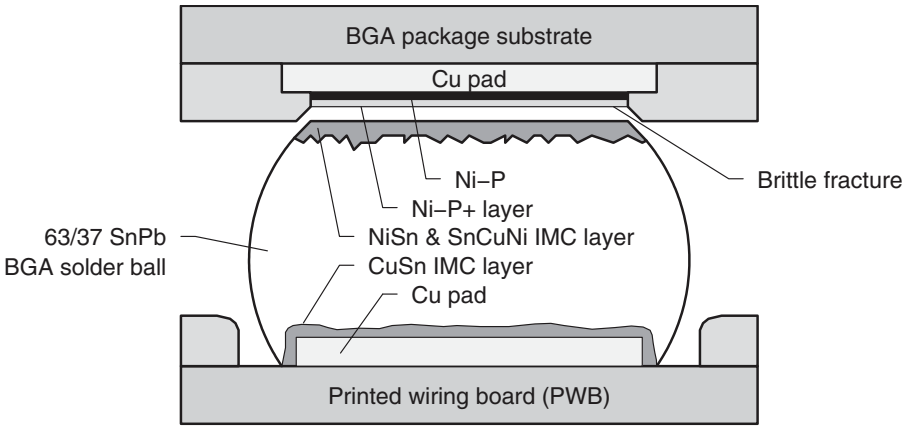


Figure 2.11. Common location for brittle solder joint fracture of a BGA [37]

2.3.5 Mechanical Testing

As previously stated, mechanical testing is crucial for a detailed characterization of any printed circuit board. A disadvantage of these board level tests is that they are quite expensive and time-consuming. Moreover, the reasons for the different board performances are not always comprehensible, as only global failure effects (and not the local failure initiation and propagation) can be monitored [15].

Mechanical testing can be divided in static and modal tests, as discussed below.

Static Tests

The static tests used in industry to obtain the mechanical properties of printed circuit boards are:

- **Tensile tests**
- **Three-point bending (3PB) tests**
- **Four-point bending (4PB) tests**

As PCBs have only very thin layers – about 1.6 ± 10 % – no experimental mechanical out-of-plane characterisation can be performed [15]. The importance of the knowledge of the direction dependent material properties is crucial in the material characterization, specially for numerical validation of the experimental results [15]. The mechanical properties of multi-layer PCBs can be basically represented by their bending stiffness [38].

As it will be discussed in **Chapter 5**, the right tests for this analysis are the three and four-point bending ones. According to [39], a three-point bending scheme is an ideal choice for generating reliability models because multiple packages can be tested under multiple loads in a single test. On the other hand, the four-point bending test is an ideal method for testing a larger sample size of packages under a particular predefined stress level. Although the selected PCB models were restricted to small sizes, both tests were performed.

Modal Tests

Modal tests are also used to obtain material properties and assist in the design of PCB for drop reliability [27]. The most usual ones carried out used in industry are:

- **High speed bending tests** – designed to investigate fatigue failure of interconnections [27].
- **Drop impact tests** [18].
- **Vibration tests** [16; 25–27; 40; 41].

The probability of solder joints failure to occur is strongly influenced by the local PCB vibration response [40]. For these modal tests, the excitation frequency is one of the key factors for evaluating board level package reliability under vibration loading. One curious experimental approach used in [16] consists in applying Miner's rule and random vibration theory – generally used to predict the fatigue life of mechanical structures – to assess the fatigue life of BGA packages, benefiting the design optimization of PCB assemblies.

2.3.6 Numerical Modelling and Simulation

Numerical modelling stands as the main contributor to printed circuit boards behaviour prediction under a given set of external conditions. A feasible and robust numerical model (also referred as "material model") cuts out the need for additional experimental tests, which are expensive and time-consuming. However, for certain applications, a discrete approach leads towards a complete characterization of a PCB model, from its initial idea to the final product in hand. In this case, numerical modelling is taken as a step to follow, and not as a general approach. In fact, for a complete numerical characterization, an individual material model has to be developed and experimently validated for each new printed circuit board that is produced. Numerical simulation based on test validation can provide more detailed data to reliability design fast and cheaply [19]. On the other hand, a general approach would use the same material model for any PCB characterization by modifying the layout, number of layers, material properties and boundary conditions, assuming every of the aforementioned variables are known. Another onward approach would consist in gathering a great number of outputs – *e.g.* stress, strain and displacement values for certain regions of the model – from numerical simulations of different PCB models (differing in number of layers, stack-up profile, material properties, size and boundary conditions) and merge them in an artificial neural network [42; 43], which later used could provide the outputs for every other PCB model, based on the previous parametric values injected on the neural network.[1]

Based on the references, PCBs numerical modelling has been covered in warpage analysis [21], solder joints performance [12; 13; 18; 19; 25–27], thermo-mechanical analysis [13; 44–46] and vibration analysis [16; 25–27; 40; 41]. For every of the previous references, a detailed material model, with proper settings of geometry, boundary and loading conditions and material data is required for accurate behaviour prediction [15; 21; 47].

For solder joints analysis, [19] states that, in order to obtain a more realistic behaviour of solder joints under drop impact loading, it is necessary to use a material model that is able to describe the strain rate effect of the solder in the numerical simulation. The linear elastic or rate independent models neglect the strain rate effect completely and, consequently, lead to inaccurate prediction of stress and strain in solder joints. If all the solder joints are modeled by fine solid finite elements, the material nonlinearity and transient dynamic nature of the problem make the computation expensive. Therefore, it is important to reduce the number of solder joints whenever possible – which are the main sources of failure – by replacing them with epoxy adhesives with given properties [13; 48].

For thermo-mechanical analysis, cyclic thermal loading is a frequent loading case to be simulated, which occurs in many PCB cases. As cyclic thermal loading is a fatigue issue, material models reproducing the constitutive behavior under cyclic loading, as well as a description for damage evolution, are needed [20].

For vibration analysis, the first major difficulty in creating good PCB finite element models is in specifying the input parameters, namely the stiffness, density, damping and boundary conditions. A secondary difficulty is due to variation that may occur in each of the input parameters, where the variation will cause supposedly identically manufactured and assembled PCBs to have different responses [40]. It is important to accurately model the mass and boundary conditions if accurate results are required [25]. Although not just in vibration analysis, factors of safety are useful when local properties smearing is not possible [25]. In other way, factors of safety are used when a constant error between the numerical and experimental results is obtained.

[1] To the author's best knowledge, no study about this topic has been carried out so far.

Overall mechanical properties of printed circuit boards can vary according to the different number of (copper and FR-4) layers, layout of circuits and polymeric and composite reinforcing materials used in their fabrication. Tiny circuits and their complex layouts inside the PCB also limit the possibility of comprehensive modelling of the PCB [47].

According to [12; 16; 19; 20; 24; 27; 41], PCBs' material models are normally created in software Abaqus, as an orthotropic elastic material model [19] or as a viscoplastic one [20]. The conducting layers can be regarded as epoxy-copper composites [15] and they do not consider solder/intermetallic interfacial failure and solder plasticity [18]. Furthermore, a composite shell is commonly used to model the composite layup [15; 38], and a 3D model is considered (**Fig. 2.12**), for this makes a more precise comparison with experimental data [13; 18]. However, there are numerous existing works about PCB isotropic material models [15], which are easier to conceive and faster to run. Although these approaches may often not be sufficient to meet the accuracy criteria, a field-proven 3-steps concept for modelling PCBs is covered in [49]. The accuracy of simplified finite element models is mainly dependant on various sources of error, including inaccuracy in the model input parameters, errors in the solution process (linear versus non linear situations).

When modeling solder joints, it is possible to greatly simplify the creation of these models by using lead spring constants in place of detailed lead models [40]. When components are soldered to a PCB, they will locally increase its mass and stiffness [25; 40]. For good accuracy, especially when large numbers of components are present, the material model should include this added mass and stiffness effect. Yet, this increases the complexity of the model. One solution that avoids excessively complicated models is to assume that the additional mass and stiffness of the component can be included by artificially increasing the Young modulus (and density, if a modal analysis is carried out).

Additional simplifications can still be made. As a general rule, small components (discrete resistors and capacitors) may usually be ignored, whilst larger and heavier components (heat-sinks, power transformers, large capacitors...) should always be modelled [40]. If more detail is intended, building a detailed material model of the PCB and components has to be created. However, this approach is rarely used, as it requires a long time to build and solve the model [25], but it is the appropriate choice for damage assessment [20]. At the end, it is important to gather proper material data, especially when the local stress and deformation fields are important [15].

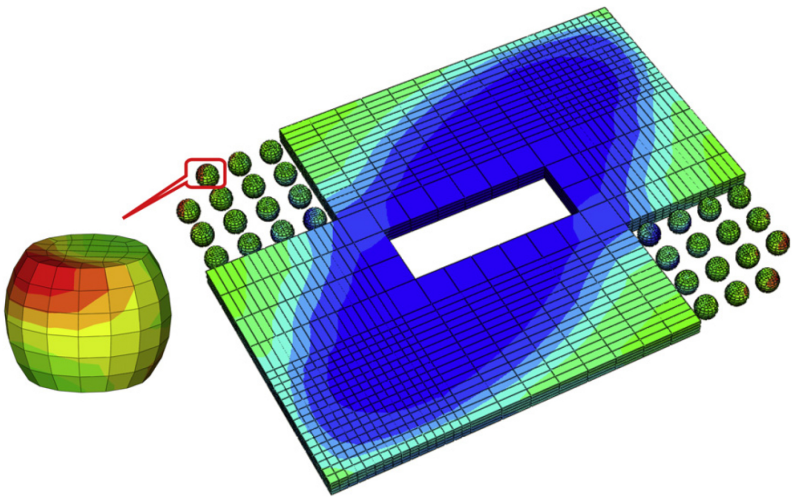


Figure 2.12. 3D material model of a printed circuit board with solder joints [19]

2.4 Thermal Imaging

As previously emphasized, printed circuit boards' characterization could really benefit from thermal analysis, since the temperature influences are pointed as a main source of failure, although clear understanding of its effects is still lacking [26]. In this direction, thermal imaging technology allows the creation of thermograms. These differ from regular photographs, since they represent not the visible light spectrum colours the human eye can perceive, but a colour or brightness distribution related to the registered object's surface temperature. Although it started within scientific research and military applications, thermography became a very valuable analysis and diagnosis tool for a wide range of industries through its development and cost reduction over the years. It is a non-invasive full-field analysis technology, allowing the detection of cracks, inclusions and other defects or malfunctions, as well as the thermal behaviour characterization of products [50].

The most relevant type of radiation for thermal imaging is the infra-red one. However, this type of radiation can also be classified within wavelength ranges, as it is usually arbitrarily grouped (**Tab. 2.3**).

Table 2.3. Infrared sub-regions [50]

Sub-region	Wavelength /μm
Near infrared	$0.75 - 3$
Middle infrared	$3 - 6$
Far infrared	$6 - 15$
Extreme	$15 - 100$

2.4.1 Thermal Cameras

For thermal cameras, it is important to distinguish wavelength ranges within the infra-red region, since there are different types with more sensible wavelengths, and each one is more suitable for certain applications. Regarding Wien's law [51]:

$$\lambda_{Max} = \frac{c}{T} \tag{2.1}$$

where λ_{Max} is the wavelength /nm, c the Wien's displacement constant[2] and T the absolute temperature /K, one easily concludes that the higher the temperature of the body one wants to capture, the shorter the wavelength at which its radiation peaks (**Fig. 2.13**).

[2] Equal to $2.898e^{-3}$ /nm·K^{-1}.

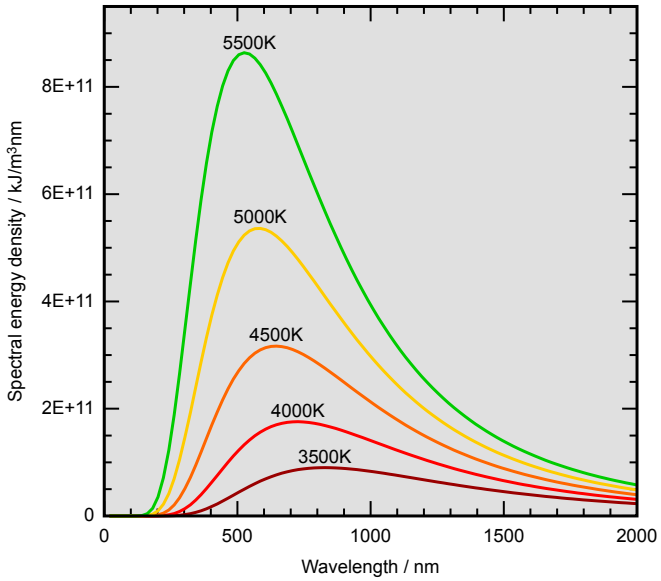
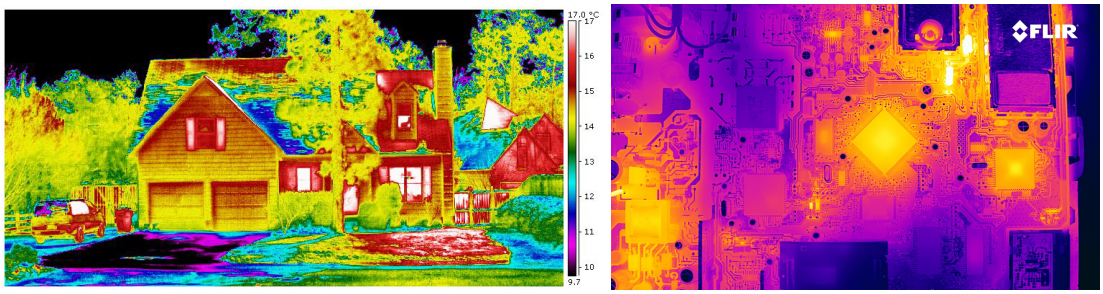


Figure 2.13. Black body radiation as a function of wavelength for various absolute temperatures [51]

Therefore, for relatively low temperature and temperature difference measurements, such as building or pavement monitoring at mild atmospheric temperature, one should use a long wave camera. On the other end, if the object under measure exhibits large temperature gradients or higher temperatures, a short wave camera is more appropriate. **Figs. 2.14a** and **2.14b** illustrate examples of a house and PCBA thermal images, respectively.



(a) Thermal image of a house **(b)** Thermal image of a PCBA

Figure 2.14. Examples of thermal images [52; 53]

Besides the camera's spectral range, each equipment's parameters differs from one another, such as in resolution, frame-rate, field of view, noise-equivalent temperature (NET)[3], etc. It is also possible to separate thermal cameras, regarding their constructive and operating solution, into cooled and uncooled cameras.

The former were the first ones to appear and the need for cooling comes from the fact that they use narrow gap semiconductor photo-detectors as sensors, and if they were to operate at room temperature, they would be flooded from their own radiation and, thus, being incapable of performing. Though these cameras have a higher resolution than their uncooled counterparts, the complex, bulky, power and time consuming cooling systems make them expensive. Therefore, it's not usual to find them within civil applications [50].

[3] It is a measure of the sensitivity of the sensor and many others.

Uncooled thermal cameras either use pyroelectric materials or microbolometers as sensors. The difference between these two types of sensors lies in the way a change in temperature is measured, while with pyroelectric material a change in temperature induces a change in the crystalline structure's polarization and thus the appearance of a measurable voltage, microbolometers consist on an array of pixels each made up from several layers and, simply put, the top layer receives radiation from the object to measure and, by increasing its temperature changes its resistance, the change in resistance is then read and processed with the use of a readout circuit and computed as a temperature reading [50].

Undoubtedly, thermal imaging provides valuable full-field temperature measurement, whose application in printed circuit boards' analysis can improve the perception of the thermal effects. In **Chapter 7**, this topic is explored more in-depth. On the flip side, electronic speckle pattern interferometry (ESPI) also proves to be a very high sensitivity measurement technique, which may be used in the study of deformations produced by convective heating and by vibration [44]. The fusion of these two technologies would, in further works, greatly improve the data quality obtained from any PCB's thermo-mechanical behaviour, mirroring real life operating conditions.

2.5 Summary

This chapter went through a great variety of topics, from the definition until the statement of the main problems concerning printed circuit boards (stresses, thermal effects, cratering and solder joint fracture) and methodologies required to tackle them, which start from the accurate characterization of each individual board in terms of mechanical, thermal and vibration behaviour, achieved through experimental tests and numerical modelling. Hence, the following chapters seek to clarify the previous issues.

Although printed circuit boards' failure depends on many factors, the temperature is the parameter which has a bigger impact on their reliability. Therefore, and since the thermal effects lead to fracture of the components, efficient heat dissipation is required during every PCBA operating conditions. To serve this purpose, thermal interface materials are potential candidates for the task – specifically gap pads – discussed in the following **Chapter 3**.

Chapter 3

Gap Pads

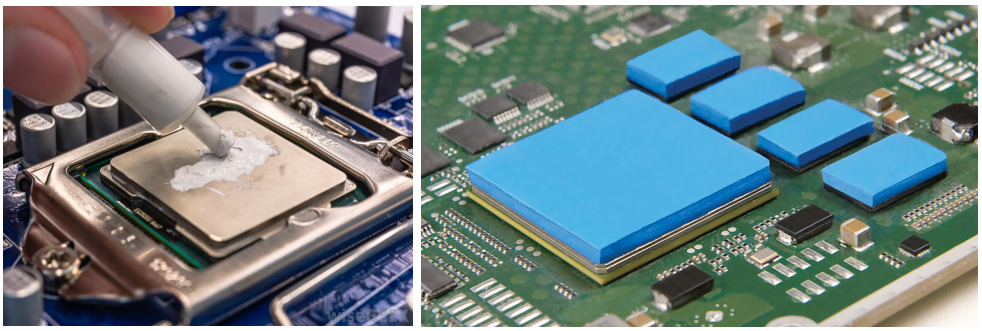
This chapter explores the essential information about thermal gap pads use and their benefits in providing heat transfer pathways through electronic assemblies. An overview of other heat dissipation materials introduces the topic, followed by the comparison to each other, highlighting both benefits and limitations. The required parameters for thermal analysis and gap pad dimensioning are stated, followed by a review of the most recent studies conducted and reference to the main companies which commercialize gap pads. Lastly, a brief data analysis from Bosch ST suppliers Henkel's Bergquist Company and T-Global is carried out.

3.1 Thermal Interface Materials

A thermal interface material (TIM) is any material that can be placed between two contact surfaces, so that thermal coupling – mainly heat dissipation – can be enhanced [54]. Therefore, a TIM is inserted between a heat generating device and the heat dissipation device (also known as 'heat sinks", "heat spreader" or "housing") in order to prevent failure due to excessively high temperatures during products' use (in this case, printed circuit board assemblies) [55].

Depending on the type of application, different TIMs can be used, namely:

- **Thermal grease** – allows using a very thin bond line of grease, thus creating a small thermal resistance. However, the bond has no mechanical strength, thus an external fixation mechanism is needed. It is only recommended when the grease content can be contained or when its viscosity allows it to remain in position during the operating life of the product.
- **Thermal glue** – also allows a very thin bond line, yet providing some mechanical strength to the bond after curing. Although it is still a very thin bond line, it is thicker than the thermal grease one, as it cures.
- **Thermal gap filler** – allows thicker bond lines than the previous two. Additionally, it enables an easier disassembly of the components, thanks to its low adhesiveness.
- **Thermal gap pad** – it is a viscoelastic material, and it does not come in liquid state or paste, as the previous ones, but in solid state. It is typically made of silicone or a silicone-based material.
- **Thermal adhesive** – it is essentially a thermal gap pad with adhesive properties [54].



(a) Gap filler **(b)** Gap pad

Figure 3.1. Illustration of a thermal gap filler and gap pad [56]

The two most common TIMs are thermal gap pads and gap fillers. The use of thermal gap pads implies a greater amount of waste, due to material yield issues in the cutting process, since they come in rectangular shapes (**Fig. 3.1b**). Obviously, the less material waste, the lower cost for the solution [57]. The limitations of using gap fillers are mainly related to higher aquisition costs. Additionally, gap fillers generally tend to provide a better thermal performance than gap pads with equal thermal conductivity. As they are dispensed in a liquid state, wet adjoining between surfaces is very efficient, therefore reducing the thermal resistance [57]. Still, another major limitation of gap fillers is related to surface cleansing. Expensive equipments are required to control the surface quality – related to the applied quantity – specially in printed circuit boards dispensers points, where high waste amounts are accumulated. Hence, this issue makes the process not lean.

In regard to printed circuit boards, gap pads and gap fillers can be used wherever air can be replaced between any heat-generating device and the housing. This can be done using one sheet of gap pad or individual pieces of appropriate thicknesses, or by using a gap filler, if stack-up tolerances and height variations are significant. However, either gap pads and gap fillers conduct heat less effectively than a minimal amount of thermal grease.

At this moment, Bosch ST aims to better investigate the application of gap pads and include them in their products assembly, so that heat dissipation efficiency can be improved during a given product service [56]. The main reason is to eliminate the limitations described above, in order to optimize the process, making it leaner.

3.2 Thermal Gap Pads

Thermal gap pads (or simply "gap pads") are viscoelastic materials which are currently electronics industry's reference TIM. Their use guarantees greater conformability, higher thermal performance and easier application in electronic components/products [56]. In other words, gap pads offer electrically insulating and thermally conductive properties, optimizing the thermal management of electronic devices [58].

Gap pads provide an effective thermal interface between heat sinks and electronic devices where uneven surface topography, air gaps and rough surface textures are present.[1] They are a quick-fix thermal solution, replacing all the other available TIMs [59].

If correctly applied, the main benefits of gap pads use are:

[1] Nevertheless, air bubbles imprisonment can be a problem to deal with, since they lead to thermal resistance increase, *i.e.* an inefficient heat dissipation.

- Elimination of air gaps to reduce thermal resistance
- High conformability to reduce interfacial resistance
- Low-stress vibration damping
- Easier material handling
- Better portability and cleansing
- Electrical insulation
- Simplified application
- Puncture, shear and tear resistance
- Improved performance for high-heat assemblies
- Compatibility with automated dispensing equipment

As a limitation, currently, gap pads are still very expensive. However, in specific cases, its price is competitive with the other thermal interface materials. Their range of application is extensive, comprising a great variety of electronics, automotive, medical, aerospace and military applications [56], *e.g.*:

- Between an IC and a heat sink or chassis[2]
- Between a semiconductor and heat sink
- CD-ROM/DVD cooling
- Heat pipe assemblies
- RDRAM memory modules
- DDR SDRAM
- Hard drive cooling
- Power supply
- Signal amplifiers
- Between other heat-generating devices and chassis

3.2.1 Parameters

The scenario that best illustrates the real problem of heat dissipation through a gap pad can be described by heat conduction. Hence, admitting one dimensional, steady-state heat conduction, neglecting the convection and radiation effects on the analysis, the heat flux is defined by the Fourier Law:

$$P_D = k \cdot A \cdot \frac{\Delta T}{h} \tag{3.1}$$

[2] Typical packages include BGAs, QFP, SMT power components and magnetics.

where P_D is the heat flux /W, k the thermal conductivity /W·(mK)$^{-1}$, A the contact surface area /mm^2, ΔT the temperature difference between surfaces /K and h the resultant gap pad thickness of the application /mm.

The heat flux is inversely proportional to the gap pad resultant thickness. Therefore, the bigger the compression of the material, the more heat dissipation one obtains. Other two parameters necessary to define the thermal behaviour of this analysis are the thermal impedance and thermal resistance. Thermal impedance /K·W^{-1} is defined by:

$$Z_\theta = \frac{h}{k \cdot A} + R_i \tag{3.2}$$

where R_i is the initial impedance. It can also be defined by the following equation:

$$Z_\theta = \frac{\Delta T}{P_D} \tag{3.3}$$

by knowing the value of the temperature difference ΔT and heat flux P_D. Another important parameter to define is the thermal resistance /m^2·K·W^{-1}:

$$R_\theta = \frac{h}{k} \tag{3.4}$$

Usually, the companies that commercialize gap pads provide, in their products' datasheets, the thermal resistance variation with the resultant gap pad thickness.

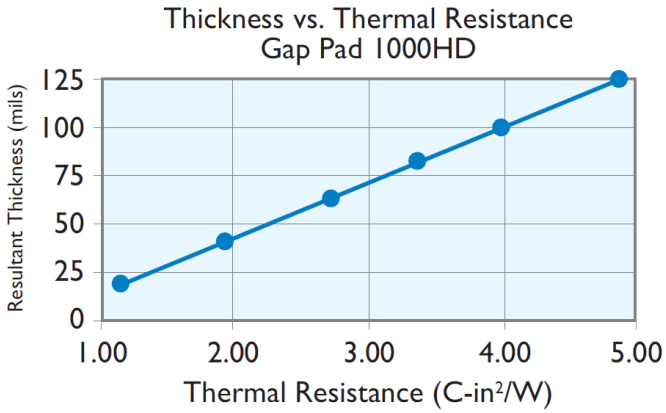


Figure 3.2. Gap pad 1000HD graph relating the thermal resistance with resultant thickness, provided by Henkel's Bergquist Company [56]

A practical case consists in fixing an intended heat flux P_D value, given by the PCBA components which dissipate its higher amount, and a temperature difference between surfaces ΔT. With these two parameters, the thermal impedance can be obtained using Eq. (3.3). Choosing a gap pad model with certain thermal properties, its thermal conductivity k value is obtained. The contact surface area A depends on the size of the component against which the gap pad will be compressed, depending on the type of application. Using Eq. (3.2), the resultant gap pad thickness is derived.

3.2.2 Review

So far, a small amount of studies has been conducted on gap pads performance analysis. The few available label important remarks about the importance of the involved parameters defined in the previous **Section 3.2.1**.

Gap pads are designed to fill gaps caused by imperfectly flat or smooth surfaces which should be in thermal contact. Young modulus is a measure of the hardness (or softness) of the gap pad's material. They are relatively firm at room temperature, but become soft and well able to fill gaps at higher temperatures [60], although there is no significant variance in hardness for silicone gap pads (or gap fillers too) [56]. Therefore, good surface contact (also called "wetting") is also important, since softer interface materials tend to lower thermal impedance. Better wetting results in lower contact resistance but thinner gap pads are preferred to maximize the thermal conductivity. Poor surface contact – *e.g.* due to high friction component surface – between a gap pad and its neighbouring substrates usually occur over time after repeated temperature cycles as devices are turned on and off [46]. Hence, a gap pad with a very high thermal conductivity does not automatically deliver the best thermal management performance.

Other critical aspects are related to the components stress minimization while compressing the gap pad, air gaps elimination – as they inhibit efficient heat transfer – and heat flux improvement [46; 61]. According to [56], high mounting pressures, applied using screws or clips, should be avoided, because they cause the component (in this case, any from a printed circuit board) and the gap pad to deflect, as the distance between the components decreases. Stress can be controlled by proper optimization of the physical characteristics of the pad, the assembly, and the conditions under which the gap pad is deflected during the assembly process.[3] This deflection allows the thermal pad to effectively fill both micro and macro voids between the components, which in turn maximizes the rate of thermal transfer through the system. However, it also causes stress to occur due to the pads inherent resistance to deflection. Therefore, the minimization of peak stress is a parameter to be kept under control [55].

In short, the following guidelines allow stress minimization during deflection of gap pads:

- Reduce strain rate of deflection.
- Apply the deflection force in steps.
- Use individual gap pads equally sized to the components.
- Provide open relief areas, preferably in three dimensions around each gap pad.
- Avoid high friction surfaces against the gap pad.
- Use the thinnest gap pad possible [55].

3.2.3 Companies

The reference companies in the market which commercialize gap pads are Henkel's Bergquist Company, Laird and Parker Chromerics. Bosch ST works with the former two and also with T-Global. The clearest and best quality gap pads' information is obtained from Bergquist Company.

Bergquist Company is world leader in thermal management through Technology, Innovation and Service. It serves as a multitude of industries worldwide, including automotive, computer, consumer electronics, military, motor control, power conversion, telecommunications, etc. Every test methods performed for gap pads characterization follow the ASTM D5470 standard [56; 63; 64].

[3] Additionally, the application of a lubricant along the gap pad surface generally reduces the compressive force necessary to achieve 50 % of its compression [62].

3.3 Data Analysis

Relying on gap pads data provided by Bergquist Company and T-Global, a set of curves relating various parameters – pressure, deflection and thermal resistance – were plotted. This allows for better understanding of the data provided by these two suppliers and, additionally, serves as a database for future analyses regarding the use of their gap pad products.

3.3.1 Bergquist

Being the most reliable supplier, Bergquist Company provided data relating pressure and deflection. Pressure is equal to stress. Deflection is equal to the ratio of the change in thickness to the original thickness of the gap pad material. As stated in **Section 3.2.2**, a soft gap filling material is desired to minimize the pressure exerted on printed circuit boards, component leads and solder joints. Knowing the evolution of the deflection of each gap pad model with the applied pressure, the Young modulus can be obtained. As seen in **Figs. 3.3** and **3.4**, Young modulus does not have a linear behaviour, since gap pads are viscoelastic materials. Additionally, according to their test method, continuous strain and step strain tests were performed.

The former clarify the design engineer about the constant rate of strain relaxation modulus of a gap pad to calculate the stress exerted on PCBs, components and solder joints, while the product is being assembled (**Fig. 3.3**). The latter allow to know the step strain relaxation modulus of a gap pad to determine the stress over time, as the material stress relieves itself from the assembly process (**Fig. 3.4**). For both cases, depending on the strain rate applied, the stress induced in the application can be reduced. Information regarding the resultant thickness and correspondent thermal impedance is available on their products' datasheets.

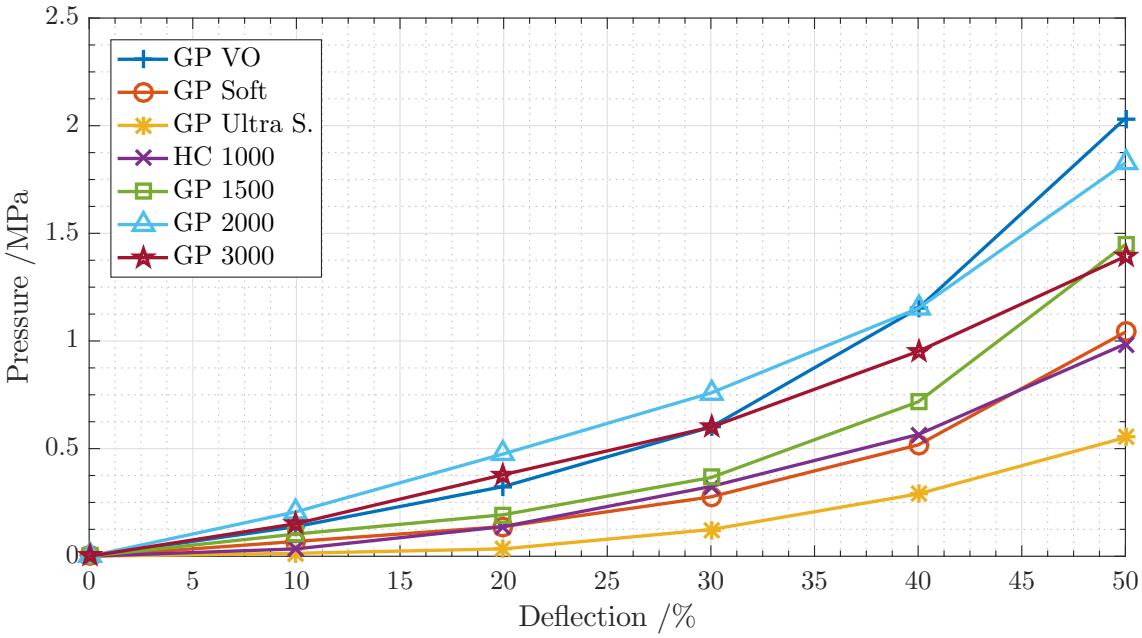


Figure 3.3. Pressure versus deflection graph obtained from continuous strain test method for a range of gap pad products, provided by Bergquist Company

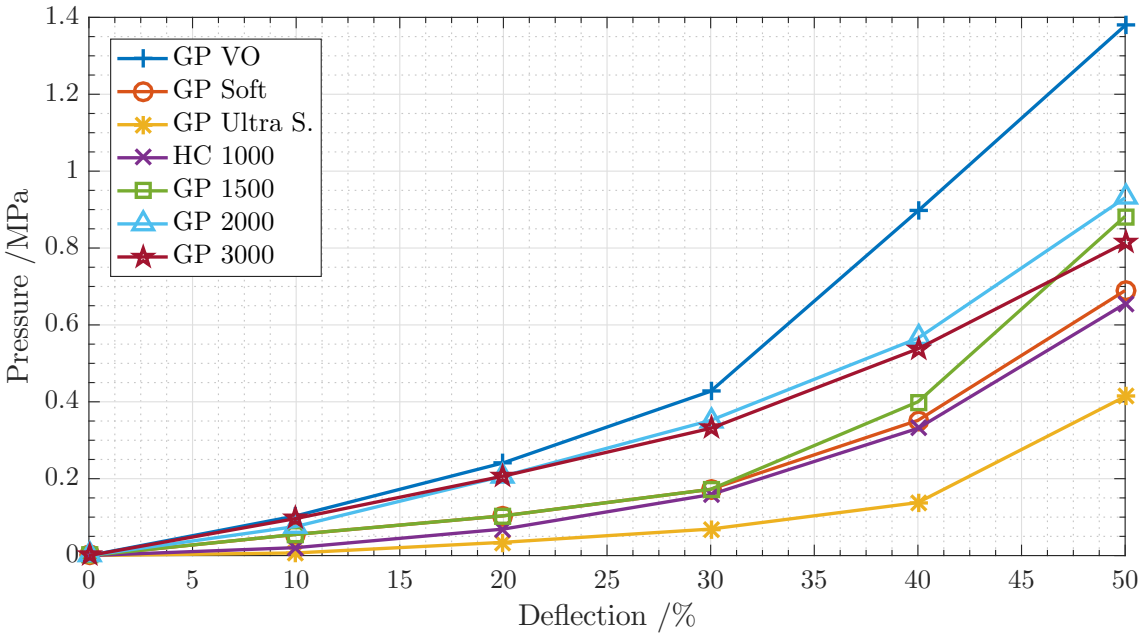
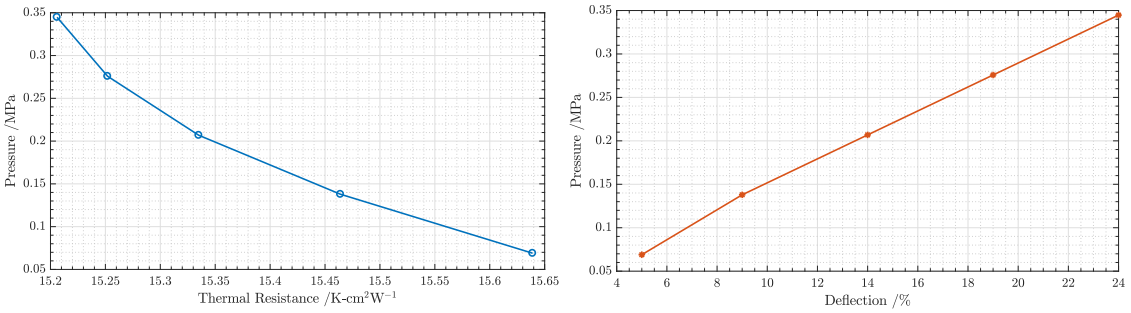


Figure 3.4. Pressure versus deflection graph obtained from step strain test method for a range of gap pad products, provided by Bergquist Company

3.3.2 T-Global

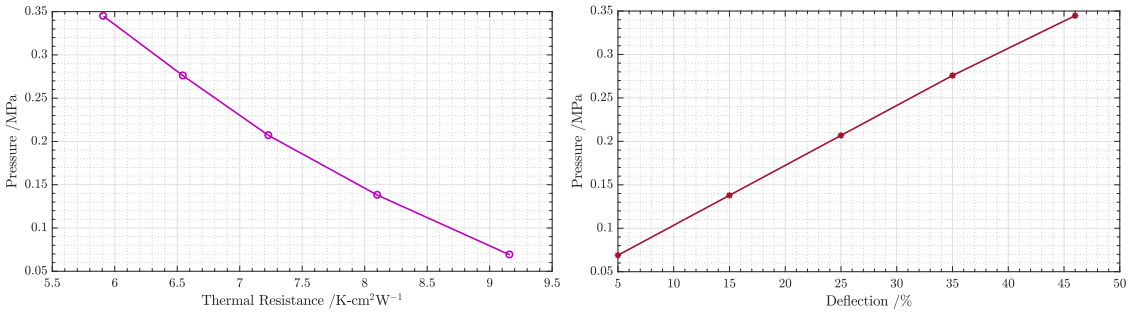
The T-Global company provided information only from three selected gap pad products (**Figs. 3.5**, **3.6** and **3.7**). Similarly, if any of these gap pad models would be used in future applications, the values for the input parameters would be obtained from these curves.



(a) Pressure versus thermal impedance

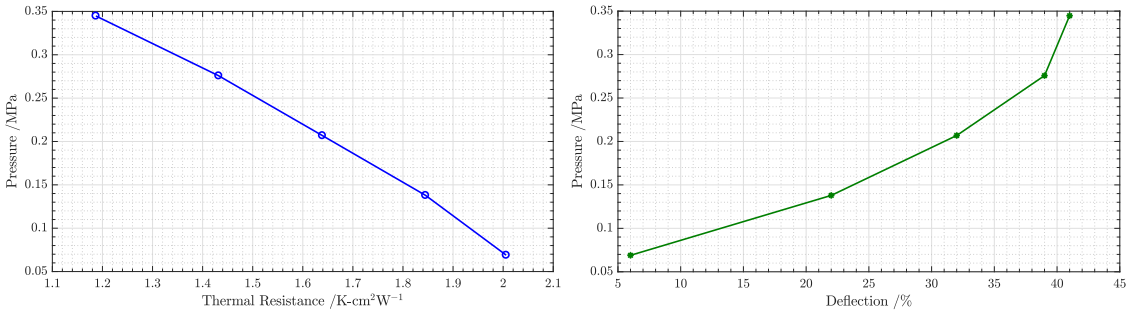
(b) Pressure versus deflection

Figure 3.5. T-Global gap pad L37-3



(a) Pressure versus thermal impedance **(b)** Pressure versus deflection

Figure 3.6. T-Global gap pad L37-3S



(a) Pressure versus thermal impedance **(b)** Pressure versus deflection

Figure 3.7. T-Global gap pad TGX

3.4 Summary

This chapter covered the essential information about the implementation of gap pads in electronic assemblies, stating their benefits, thermal parameters, literature review, involved companies and data analysis from two Bosch ST gap pad suppliers. Although this information is valuable for PCB characterization, it one of the final steps of the aim of this study.

Therefore, it is necessary to state the issue in hands and outline a strategy for approaching it, covered in the next **Chapter 4**.

Afterwards, the next step is to characterize the material properties of a selected population of printed circuit board models' specimens, by submitting them to a series of three and four-point bending tests, as discussed in **Chapter 5**.

Chapter 4

Problem Statement

This chapter states and clarifies the problems of Bosch ST – Ovar to be addressed. For this, the background of this issue is stated and a guideline for approaching it is delineated, going through the printed circuit board models' selection and ending with insights collected from Bosch CM – Braga to enrich this study.

4.1 Issue

A direct and simple strategy is desired for assessing PCB models' behaviour under external conditions, and it resumes with the knowledge of their material properties. So far, Bosch ST – Ovar has not conducted experimental tests in order to obtain the mechanical properties of their printed circuit board models, with or without embedded electronic components. For reliability improvement, and based on internal reports, the relation between printed circuit boards' number of copper layers, size and thickness, copper distribution and stack-up profile would provide massive value to their characterization. Still, these are yet to be known. Quantifying and understanding the impact of the aforementioned parameters in printed circuit boards' stiffness is a task to be handled. Hence, experimental tests realization and their numerical validation is a starting point for the characterization of printed circuit boards.

As stated in **Chapter 2**, the critical components of PCBs are the BGAs, for being the components with bigger dimensions, whose solder joints, upon bending loading, are more prone to crack. As they have no associated damping, this leads to circuit failure. The search for industry standards – found on [65] – to characterize printed circuit boards' behaviour was carried out, but none could meet the needs of this study.

For both experimental and numerical procedures, this study would evaluate the influence of printed circuit board's:

- **Size**
- **Number of copper and FR-4 layers**
- **Number of components**
- **Layout of the components on the board**

Several assumptions were made, considering that, initially, every PCB model is defect-free, ready to be tested in perfect conditions and that the soldering process had been well executed.

Early meetings at Bosch ST – Ovar aimed to elucidate about this issue in hand. Summing up every debated idea to decide the right approach to tackle this problem, the initial guidelines were set:

- **Realization of experimental tests**. For mechanical testing, these should be 3PB and 4PB tests[1], and for thermal and fatigue analysis, thermography, digital shearography and vibration tests.

- **Numerical validation of the experimental tests**. The material models would be the basis of future PCB models' behaviour prediction, upon a given set of boundary and loading conditions. The existence of a CAD drawing for every model, whose geometry would be imported, would dispense the need to conceive it from scratch, with no knowledge about how much detail should be considered.[2] Unfortunately, there are no CAD drawings of any PCB model existing in Bosch ST's database. The only reachable file format is Gerber, from which it is not feasible to export a 3D CAD drawing of any printed circuit board. The Gerber file format only contains information regarding the layers profile, paths, size (width, length and hole dimensions), copper percentage in each layer, etc.

- **Implementation of an Artificial Neural Network**. Once validated, the material models would be used to perform a parametric study, in which the number of layers, thickness, mechanical properties, boundary conditions and location of the components on the PCB (namely, the BGAs) would vary. Once a considerable amount of cases was gathered, the outputs (*e.g.* stress and strain values) would be injected in an artifitial neural network [42; 43; 66; 67], created in software Matlab.

- **Creation of a Matlab GUI software**. This software would use the created artificial neural network, by providing her a set of inputs and, based on its learning data collected from the numerical simulations, a pattern would be recognized and the outputs would be generated for a desired specific case. An initially outlined algorithm to be followed is presented in **Appx. D**.

4.1.1 Approaches

Initially, for numerical modelling, it was predicted that the detailed geometry of every PCB model could be approximated to a rectangular plate, with given length, width and thickness.[3]

As discussed in the previous **Chapter 3**, the use of gap pads requires a thermal analysis of PCBAs beforehand, while they are powered on. From it, the value of the maximum temperature difference, needed for gap-pad dimensioning, as well as information about the temperature evolution on the board, would be extracted. Further, the influence of the thermal gradients on PCBAs' bending would be tracked (covered in **Chapter 7**).

Also referred during early meetings at Bosch ST – Ovar, two practical cases were highlighted, regarding PCBAs' housing mounting configuration. Depending on it, the board's behaviour would be different:

[1] Ambitiously, a notch test would be performed in the PCB specimens, since, based on feedback analysis, there is a probability of formation of these in the copper layers, when soldering is executed.

[2] Namely, the inclination of the different FR-4 layers, whose values are not provided by the suppliers, and the type of prepreg used.

[3] A parametric study evaluating this simplification is discussed in **Chapter 6.4**.

- **Direct Mounting** – this approach considers a PCBA mounted directly on the support surface, under which the gap pad lies, being compressed against the BGA. The board is fixated with four screws on the corners. The tightening torque is a function of the height of compression of the gap pad.[4]

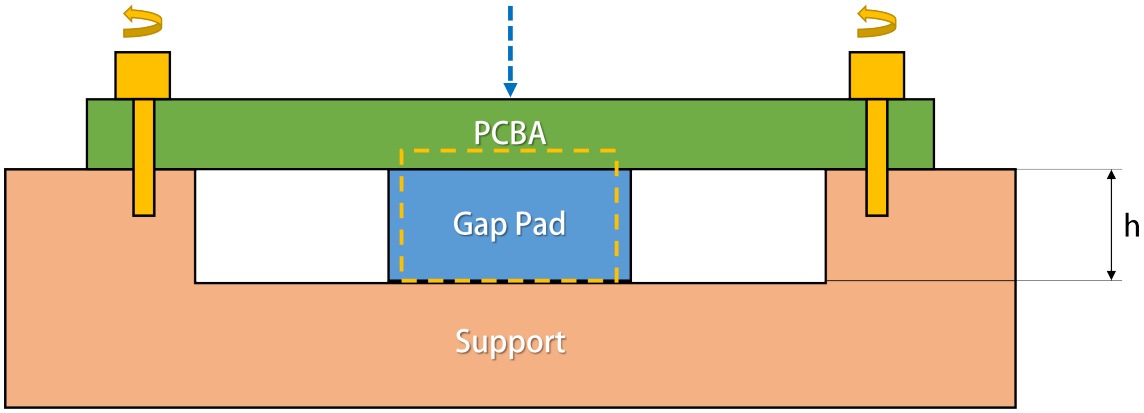


Figure 4.1. PCBA direct mounting approach

- **Indirect Mounting** – this approach adds one extra block (or more), which is placed between the board and the support surface. This time, the tightening torque is function of the height of compression h of the gap-pad and of the extra block's height Δ, and geometric tolerances play an important role. According to the three-sigma methodology[5], tolerances allowance is bounded between upper and lower limits (**Fig. 4.3**). In this case, they are related to the compression of the gap pad. The challenge lies in combining the heights of the PCBA, blocks and gap pad, so that the final tolerance lies within this allowance interval.

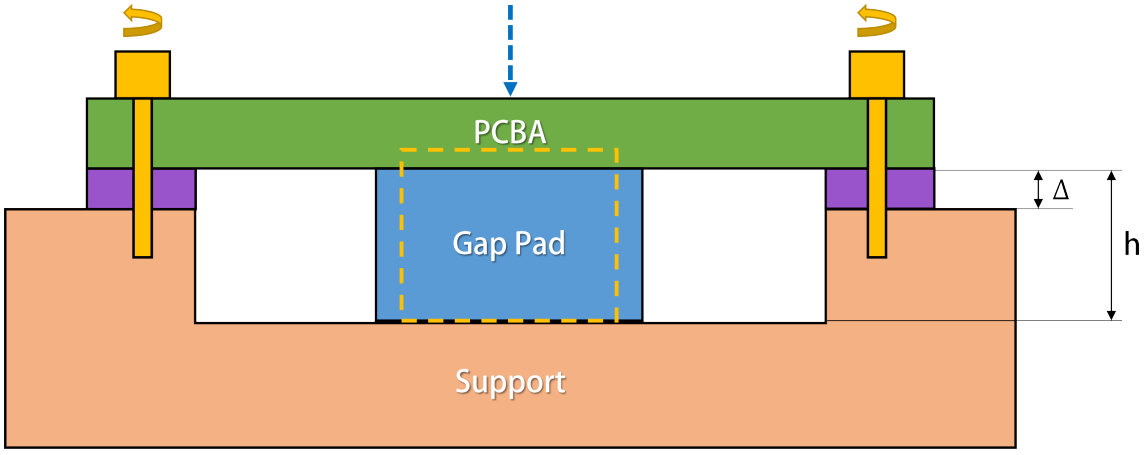


Figure 4.2. PCBA indirect mounting approach

[4] The relation between the applied force and the tighening torque can be found on [68].
[5] The one used by Bosch ST. On the other hand, Bosch CM, directed to automotive industry, follows the six-sigma methodology (with tighter specifications) for their products.

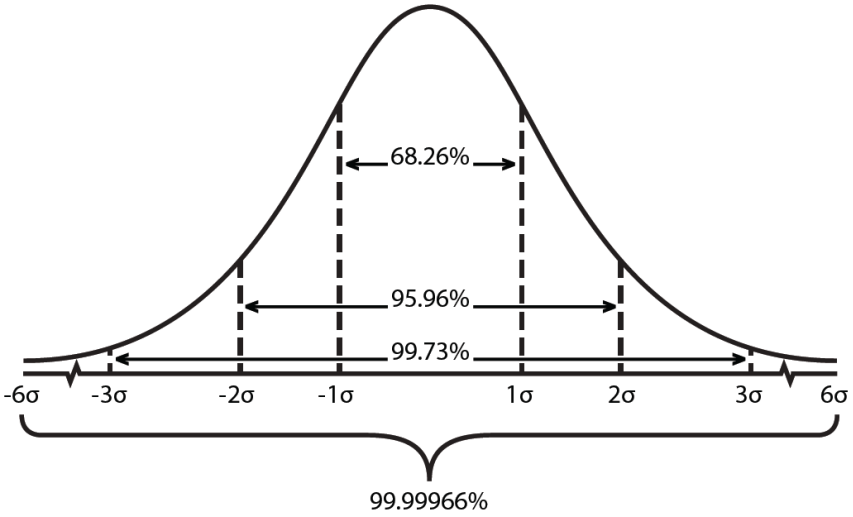


Figure 4.3. Three and six-sigma areas of the Gaussian bell curve

For gap pad dimensioning, as seen in the previous **Chapter 3**, the thermal resistance is the parameter which dictates how much compression the gap pad can be subjected to. The more heat dissipation one desires, the bigger the final compression of the gap pad has to be. Therefore, the upper limit is defined by the need of guaranteeing low thermal resistance, whilst the lower one by the applied pressure on the PCBA's surface.

In order to further explore these parametric relations, whose knowledge would provide a solution to these problems, a feasible characterization of every printed circuit board model is required first-hand.

One of the first steps was searching in the for literature analytical models for printed circuit boards' characterization, namely on [69–71], by considering it as a rectangular plate. Unfortunately, no information that could accurately characterize them was found. Also, in a conversation with a professor from FEUP[6] on this issue, his feedback confirmed the previous statement. Therefore, alternative approaches had to be created.

As an alternative, a group of engineers from Bosch CM – Braga was contacted, hoping they could provide more insight about PCBs' characterization, since it is a transversal area between these Bosch divisions. The collection of insights is treated in **Section 4.3**.

4.1.2 Guideline

Building upon the previous strategies on how to tackle this issue, for the work in hand and for further works in printed circuit boards' characterization, the following guideline was prescribed:

- **Mechanical, thermal and vibration analysis execution**, for the selected PCB models.
- **Creation of material models**, which would combine the mechanical and thermal (thermo-mechanical) analyses, later integrated in an artificial neural network.

[6] Pedro Ribeiro (Associate Professor).

The thermal analysis would provide valuable information for gap pad dimensioning and its implementation on Bosch ST's products, aiming to increase heat dissipation efficiency, and detection of critical areas affected by thermal loads. The vibration analysis, combined with the thermal one, would specify the number of cycles until a given PCBA model would fail. This analysis would contribute to increase the reliability of the products operating under vibration conditions.[7]

Therefore, to kick-off this characterization, a population of printed circuit board models had to be selected.

4.2 Selected Printed Circuit Board Models

A population of multi-layer printed circuit board models was gathered from Bosch ST – Ovar database. **Tab. 4.1** presents every PCB models' number[8], the respective internal reference and the correspondent experimental test under which they were submitted.

Table 4.1. Summary of the selected printed circuit boards and the correspondent experimental test performed

PCB Model	Bosch ST Reference	Experimental Test
1	F.01U.292.030	Four-point bending
2	F.01U.254.222	Four-point bending
3	F.01U.215.662	Three-point bending
5	F.01U.269.978	Four-point bending
6	F.01U.127.336	Four-point bending
7	F.01U.134.622	Three-point bending
8	F.01U.283.626	X
9	F.01U.320.900	Three-point bending
11	F.01U.276.917	X
12	F.01U.275.156	Four-point bending
13	F.01U.312.078	Thermography, Digital Shearography & Vibration
14	F.01U.330.849	Four-point bending

As perceived from the previous table, PCB models 8 and 11, in the end, were not subjected to any analysis, given that their size and shape could not fit in the category of the other models. Still, their thickness was measured, whose results are discussed in the next **Chapter 5**.

However, to further understand this issue, and to confirm if the defined strategy was the right choice, a collaboration with Bosch Car Multimedia – Braga was made, which brought more insight to this work.

[7] In the project phase, Bosch ST's products are subjected to the HALT test, which includes both thermal and vibration analysis. This test specifies the limits for the products usage, based on standards and certifications applied to them, as well as on reference experiences of past products' projects.

[8] Chosen arbitrarily, based on the order of selection during this work.

4.3 Bosch Car Multimedia – Braga

Two meetings to Bosch Car Multimedia – Braga were arranged in order to obtain some information regarding PCBs' experimental testing and for training in strain measurement.

Although it is a different Bosch division, the production of PCBs is a common service. As stated before, Bosch CM – Braga has more rigorous standards for their final products and, at the same time, they have more detailed methods to predict their PCB models performance. This richer knowledge would provide value to this study, by combining the efforts for understanding this same issue.

4.3.1 PCB Strain Measurement Q&A

Based on literature revision and previous discussion meetings, a list of questions was prepared, mainly for strain measurement purposes[9], but meanwhile branched to every topic related with printed circuit board analysis performed at their plant. It follows the main subjects examined during the first meetings.

Controlled Strain Gauges Localizations

Regarding the experimental tests, the electrical components placed in critical areas submitted to strain measurement – whose strain is measured with strain gauges – are the BGAs of bigger dimensions and the ceramic components.[10] The critical areas are defined by performing numerical simulations and extracting the maximum displacement, strain and stress values and/or by empirical form.

According to Bosch CM's internal standard, strain rosettes are used for controlling the BGAs strain in, at least, three corners. These are defined, again, with finite element analysis and/or empirical forms. For the soldered components, uni-axial strain gauges are used, which are glued between the board and the component. This means that, beforehand, the component has to be unsoldered.

Strain Limits

The specified strain limits are based on experimental tests performed by Bosch in the past, which concluded that flaws – *i.e.* generation of cracks and their propagation – started emerging from 1100 microstrains.

Thus, three cases were specified:

- < 500 microstrains – the PCB is within the safe limits, and ready to work perfectly.
- $500 - 800$ microstrains – the line production still continues, but corrective measures are applied.
- > 800 microstrains – the line production is interrupted and corrective measures are applied.

The CoC defines the process rules for strain measurement and control. The responsible engineer[11] defines the localization for strain gauges placement (which differs from each PCB model) and confirms the equipments validation.

[9] Given that, simultaneously, strain measurements studies were also being carried out.
[10] Given that certain PCB models do not have embedded BGAs.
[11] Engineer Pedro Sampaio (TEF8 section).

Strain Rate Values

The strain rate values are indifferent, since its validity for high strain rates is already included within the defined strain limits. The rate of acquisition is 600 Hz, in order to guarantee that the biggest strain event is identified.

Relation between number of copper layers and mechanical behaviour

It was stated that, from experience, there is no direct relation between the number of copper layers and the mechanical properties of a PCB model. On top of that, the orientation of the stacked-up FR-4 fibres can vary within the same PCB model. In order to determine the mechanical properties, the relation between the copper percentage and FR-4 is used. For the copper percentage, the established values are 30%, 40% and 60%.

Numerical Modelling

There are no internal material models created and executed, since this service is requested to Bosch CM's development centre. Nevertheless, it is known they consider the PCB as a rigid rectangular plate. Similarly to the initial attempts, one auxiliary step which could simplify the preparation of the PCB geometry is its extraction from the Gerber file of each model. This attempt was already endeavoured by the ENG section, yet still with no success.

Strain Gauges Temperature Compensation

For any type of PCB model, that is already considered on the data analysis.

Stiffness increment with embedded components

The added stiffness due to the embedded components is disregarded/neglected, since the PCB stiffness raises with the addition of them. In other words, by not considering the electronic components, one is working within a safety range, given that a stiffness rise/increment results in smaller strain values.

Specimens Limit of use

Unless a destructive process is being performed, the same PCB specimen can be used more than once. For clinching processes, it can be used up to five times. For every other cases, up to one hundred times.

Experimental Machine Noise

During strain measurement tests, the normal machine noise oscillates between -3 and 3 micro-strains, which is a low value that can be disregarded.

Equipment Check Periods

The experimental equipment is checked every six months or when 120000 cycles are reached. Previously, a check-list is made and all the equipments are classified in accordance with a risk analysis.[12] Whenever any sporadic equipment replacement occurs, sometimes this means also changing the equipment's placement location.

[12] Which can be either 0, 1 or 2.

4.3.2 PCB Strain Measurement Training

On a second meeting to Bosch CM – Braga, a workshop on PCB strain tests preparation was conducted, directed to the parallel work on PCBs' strain measurement. Three PCB model specimens were selected, being the three for functional tests evaluation purposes.

The procedure consisted in placing strain gauges in specific areas of the specimens – following the procedure stated in Bosch CM's internal standard – so that, afterwards, one could measure the strain values when each specimen would be subjected to the functional tests.

Instrumentation

- Linear and rosette strain gauges (**Figs. 4.4a** and **4.4b**)
- Gloves[13]
- Solder sucker de-soldering pump
- Soldering iron
- Sandpaper (**Fig. 4.4d**)
- Solvents – conditioner, neutraliser and catalyst (**Fig. 4.4e**)
- Alcohol
- Adhesive tape
- Elastic glue

Procedure

The experimental procedure is quite lengthy and requires demanding precision skills, specially when handling the strain gauges. Its steps are presented below:

1. Removal of the components close to the area where the strain gauges would be placed, using the soldering iron (**Fig. 4.4c**).
2. With the solder sucker de-soldering pump, remove the solder in excess, so that the surface does not become irregular.
3. With the sandpaper and one drop of conditioner, remove the remaining debris[14], until only the copper tracks are observed.[15]
4. With the neutraliser, clean the sanded areas.
5. Prepare the strain gauges collage, by using a glass as a plane surface, and adhesive tape, to fix them to the surface (**Fig. 4.4f**). Previously, the glass surface should be cleaned with alcohol.

[13] Though not used on the undertaken workshop.

[14] Use a linear movement of removal, since a rotational one introduces initial deformations on the surface. Additionally, constant switch of the sandpaper makes the debris removal more efficient.

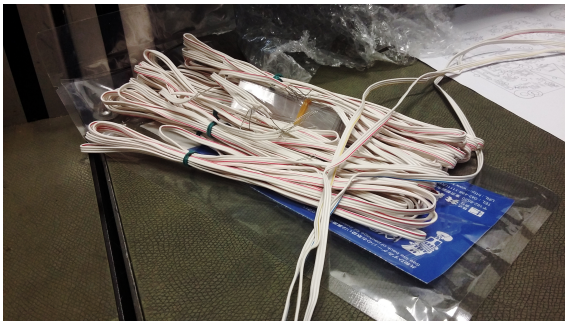
[15] Although all the green colour of the specimen surface should disappear, exaggerated surface sanding can lead to copper removal, which latter would affect the strain measurement quality, once the surface would initially be deformed.

6. Glue the strain gauges, with the bright part facing upwards, corresponding to the welded wires zone, without any irregularity.

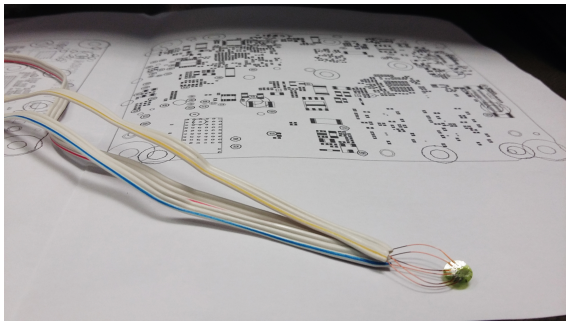
7. Create a rectangular frame for each of the strain gauges, and cut them individually.

8. Before collage, apply indirectly the catalyst on the specimen's surface with a cotton swab, in order to avoid contaminations.

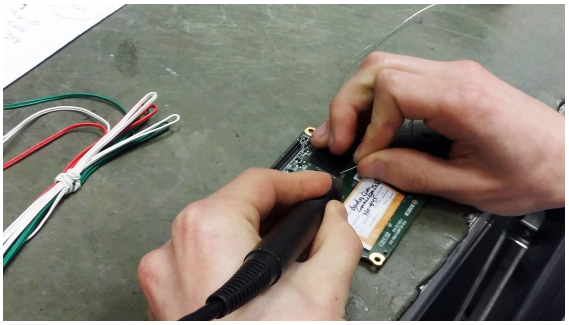
9. Apply one drop of elastic glue[16] on each strain gauge, glue it on the prepared surface area and carefully apply some pressure – with the tip of the finger or a cotton swab tip – to the strain gauge for ten to twenty seconds, so that an effective collage is assured.



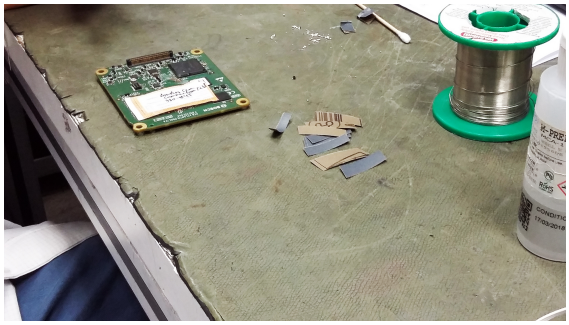
(a) Linear strain gauges



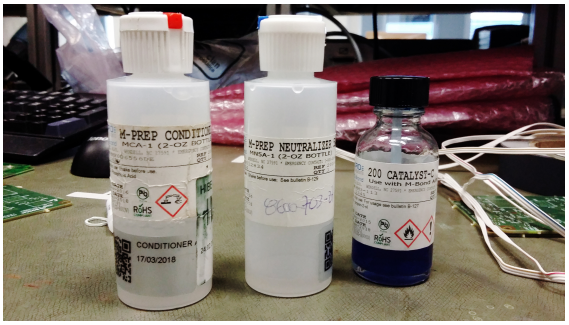
(b) Rosette strain gauges



(c) Components removal



(d) Strips of sandpaper



(e) Conditioner, neutraliser and catalyst



(f) Strain gauges collage on the glass

Figure 4.4. Experimental procedure of the PCB strain measurement workshop

[16] An elastic glue is more flexible when deformations are introduced on the specimen, and its influence on strain measurement quality is minimal.

4.4 Summary

Due to time constrains and complexity of this issue, the initial approach was concentrated on mechanical testing and numerical validation. Only the static component of the PCB models' behaviour was considered, since the thermal considerations account for an extensive and exhausting data processing, since the material model would be much more detailed.[17]

Hence, 3PB and 4PB tests were performed in order to obtain the mechanical (flexural) properties of the selected PCB models, discussed in the next **Chapter 5**.

[17] Namely, the knowledge of the coefficients of thermal expansion in the three directions.

Chapter 5

Mechanical Testing

This chapter is dedicated to describe the course of the conducted mechanical tests – three and four-point bending tests. It starts with an overview and methodology of both tests, followed by their set-up, procedure and results presentation. These tests are crucial, to the extent that the flexural properties of the selected printed circuit board models are obtained, so that a behaviour tendency – relating the flexural stiffness with the number of copper layers and/or copper percentage in each layer – can be inferred. Therefore, the discovery of a common parameter or pattern among every PCB model that could allow to predict their mechanical behaviour would be the ideal.

5.1 Overview

In order to obtain the flexural properties (flexural stiffness and strength) of the selected PCB specimens, three-point and four-point bending tests were performed.

The ASTM D7264/7264M – 15 standard [72] was consulted as a guideline for preparing the experimental set-up. This standard presents a test method for flexural properties of polymer matrix composite materials, in which two procedures, A and B, are distinguished. The procedure A is intended for three-point bending tests, whilst the procedure B is for four-point bending tests. However, this standard methodology is suitable for beam applications, and with its extension to printed circuit boards tests – assuming it behaves like a plate – the induced errors may overestimate (or even underestimate) the real mechanical properties of the PCB models. The standard states that those differences may be significant, particularly for laminates with a large number of plies in the $\pm$ 45° direction. Unfortunately, as previously stated in **Chapter 4**, the PCBs' suppliers do not provide the different plies orientations. Thus, there is no guarantee of how accurate (or erroneous) the derived results will be. There is also no specific information about what is meant with "large amount of plies".

Additionally, the ASTM D7264/7264M – 15 standard [72] refers that the wider the specimen, the higher the deviations from the beam theory will be. Among the selected specimens, only PCB model 9 could perhaps be treated as a beam. For every other PCB model, this simplification cannot be made.

5.2 Methodology

As previously stated, three and four-point bending tests were carried out, based on the ASTM D7264/7264M – 15 standard. A description of both tests is now presented.

5.2.1 Three-point bending test

This experimental test consists in resting the selected PCB models' specimens on two supports, while a loading nose is applied midway between them. In this configuration, the maximum flexural stress is located under the direction of the center force member. Also, in this configuration there is the presence of a vertical shear force along the beam except right under the mid-point force application member.

A schematic diagram of the test is presented in **Fig. 5.1** and the correspondent shear and moment ones are illustrated in **Fig. 5.2**.

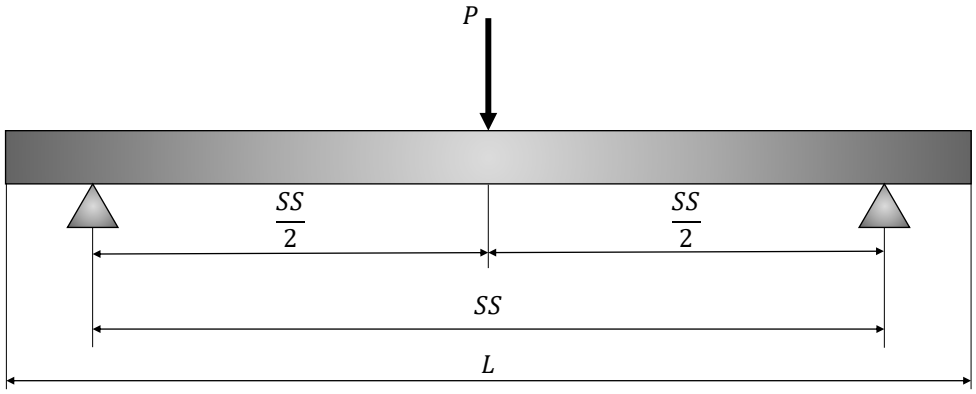


Figure 5.1. Three-point bending test schematic drawing

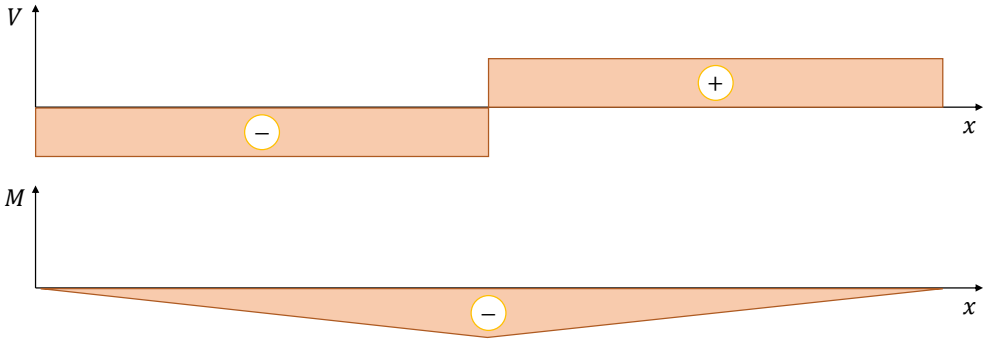


Figure 5.2. Three-point bending test shear and moment diagrams

where P is the load /N, SS the support span /mm and L the specimen length /mm. The calculated parameters are the maximum flexural stress σ /MPa, maximum strain ε /− and flexural Young modulus E_f /MPa, stated in Eqs. (5.1), (5.2) and (5.3), respectively.

$$\sigma = \frac{3 \cdot P \cdot SS}{4 \cdot b \cdot h^2} \tag{5.1}$$

$$\varepsilon = \frac{6 \cdot \delta \cdot h}{SS^2} \tag{5.2}$$

$$E_f = \frac{SS^3 \cdot m}{4 \cdot b \cdot h^3} \tag{5.3}$$

where b is the width of the specimen /mm, h the specimen's thickness /mm, δ the measured displacement /mm and m the slope of the secant of the load-displacement curve /N·mm^{-1}.

5.2.2 Four-point bending test

This experimental test adds one more loading nose to the previous configuration. The support span distances are kept constant, and a loading span is defined (**Fig. 5.3**). In this configuration, the bending moment is constant between the central force application members (**Fig. 5.4**). Consequently, the maximum flexural stress is uniform between these two members. Moreover, the area between the central force application members has no resultant vertical shear forces.

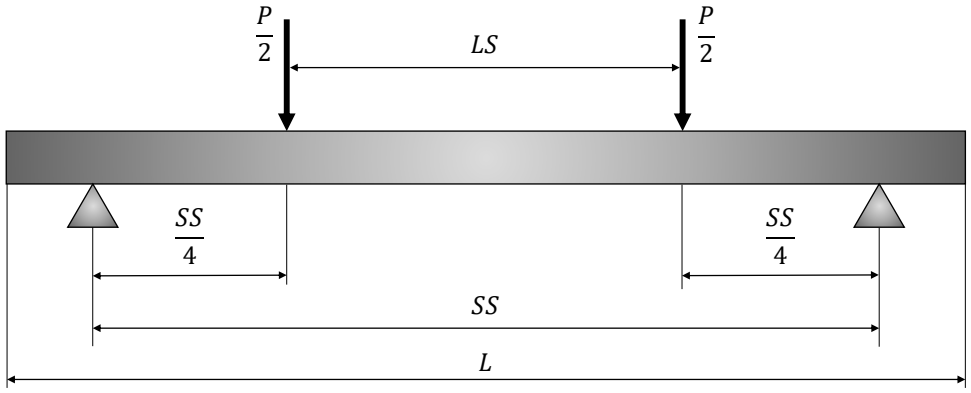


Figure 5.3. Four-point bending test schematic drawing

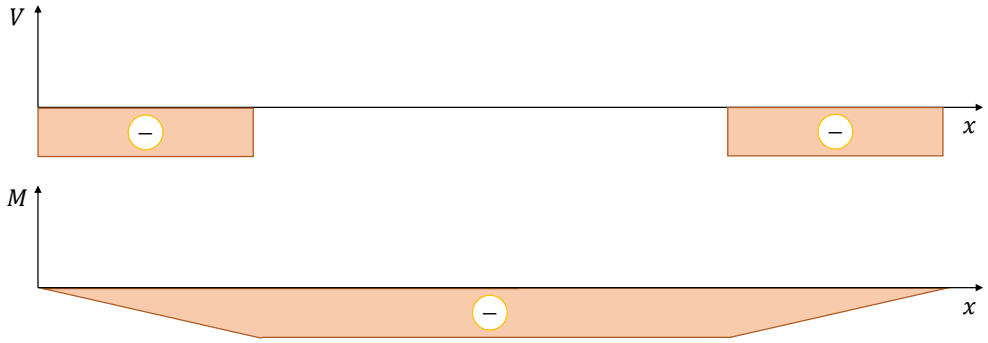


Figure 5.4. Four-point bending test shear and moment diagrams

The previously stated parameters, with the exception of the maximum flexural stress σ – which is obtained likewise – are now calculated according to the following equations:

$$\varepsilon = \frac{4.36 \cdot \delta \cdot h}{SS^2} \tag{5.4}$$

$$E_f = \frac{0.17 \cdot SS^3 \cdot m}{b \cdot h^3} \tag{5.5}$$

5.2.3 Experimental Approach

Inspired by the previous two procedures, two experimental approaches were defined, depending on each specimen's size:

- **Small specimens approach**
- **Lengthier specimens approach**

For this study, only the former was considered, once great part of the specimens' size was considered small.

Small Specimens Approach

This approach is used for specimens whose minimum length is up to the support span defined for the experimental set-up – in this case, for PCB model 6, with 51 mm of width. It considers testing every specimen in the 0° and 90° directions – hereafter referred as directions 1 and 2, respectively – *i.e.* along their length and width (**Fig. 5.5**). This step is crucial to evaluate if the flexural properties remain relatively constant in the two directions, so that one may consider the specimens as a quasi-isotropic material, for numerical modelling discussed in **Chapter 6**. Additionally, this proper determination of the direction dependent material properties is crucial for the accurate evaluation of the critical local stresses [15; 40]. In case the differences are significant, although this simplification can still be made, the numerical simulations will not accurately model the real behaviour of the PCB.

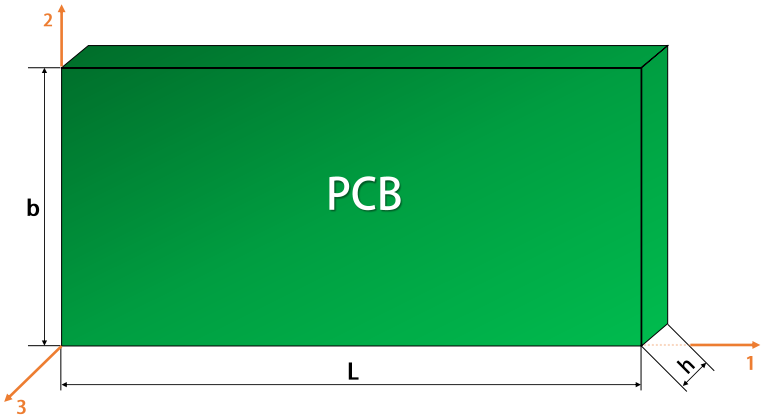


Figure 5.5. Schematic drawing of a printed circuit board geometric parameters

During the experimental tests, a displacement control was made, fixing it to a maximum value of 1 mm. This limit was set based on a previous test of a PCB model, conducted by Bosch ST – Ovar, documented in an internal report [73]. During those operating conditions, the maximum verified PCB displacement was of 0.573 mm. By setting it at 1 mm, one is already testing the specimens up to higher displacements, just to ensure that, even at superior displacement values, the plasticity effects – which are undesirable – are not present. However, for the three-point bending tests – the first ones to be conducted – this upper limit for the displacements was not set. Therefore, it was arbitrarily chosen, yet around $1.5 - 2$ mm.

Three measurements for each specimen in each direction were made for the three-point bending configuration, and two measurements for the four-point bending configuration. The reason behind removing one extra measurement in the latter tests is explained based on the results from the former. Therefore, the results showed little deviation from the second to the third measurement, meaning that performing two measurements is more than enough to obtain precise results, even though the standard recommends testing at least with five specimens of the same model.

The specimens length and width were measured using a Vernier calliper (**Fig. 5.6a**). Being a more sensitive parameter, the thickness was measured using a micrometer (**Fig. 5.6b**).



(a) Vernier calliper **(b)** Micrometer

Figure 5.6. Measurement devices

After the geometrical measurement of the different PCB specimens, no thickness tendency was found between the lengthier and smaller ones. Nevertheless, for both cases, the measured values were within the specified tolerance of ± 10 % – corresponding to a maximum of 1.76 mm and a minimum of 1.44 mm – with the exception of the maximum measured value for PCB model 2 and for PCB model 14[1], as perceived in **Fig. 5.7**. However, the thickness values were not verified for more specimens of these two PCB models, as specimen variability can justify if these values remain constant for every thickness measurement.

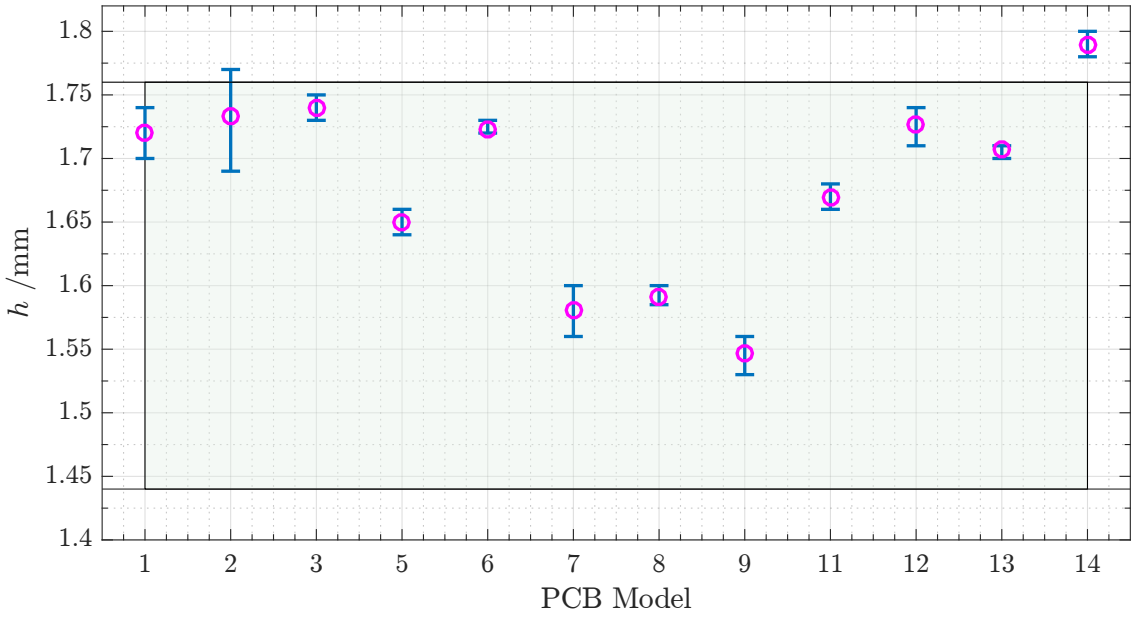


Figure 5.7. Thickness mean and deviation values for the different PCB models

Lengthier Specimens Approach

This approach would be used for specimens whose length exceeds the maximum adjustable support span. In conversation with a professor from FEUP[2] about obtaining the mechanical properties of lengthier PCBs, an useful suggestion was given.

Instead of considering the entire PCB specimen, only a portion of it would be tested, *i.e.* it would be cut in different strips, so that smaller specimens would be obtained. By submitting these smaller specimens to tensile tests, the load-displacement curve would be

[1] This model corresponds to the Atlantis project which, at the moment, is still under development.
[2] Marcelo Moura (Associate Professor).

obtained. This approach is more valid than considering the specimens as plates, because now these could be treated as beams, since their width is considerably smaller. Therefore, the beam theory could easily be applied to these ones. Moreover, although the copper distribution along the specimens' thickness is heterogeneous, it is expected that its influence in the mechanical behaviour would be minimal. In other words, the fact of considering different slices with different copper patterns would not lead to considerable result deviations between PCB models, as explored in the next **Section 6.4**.

In order to obtain the Young modulus, the load value would be divided by the specimens' surface area, and the strain would be obtained by continuously subtracting the final length by the initial length, both divided by itself. Thus, a stress-strain curve would be obtained, whose slope is equal to the Young modulus of the specimen. To measure the Poisson ratio, two strain gauges would be placed on top of the PCB, displaced by 90° between them, to measure the strains along the length and width of the specimen. The division of strain in transversal direction (ε_2) by the strain in longitudinal direction (ε_1) is equal to the Poisson ratio. Although this procedure is similar for isotropic materials, its extension to this application may generate satisfying values for the specimens' mechanical properties.

5.3 Organization

Due to time constrains, the first experimental tests run where the three-point bending ones, although it was initially intended to resume with the four-point bending configuration. Hence, the three-point bending tests were carried out, followed by the four-point bending ones later on. As stated in **Section 4.2**, three specimens – one for each of three PCB models – were selected for the former, and six others – also one for each of the six PCB models – were selected for the latter test.

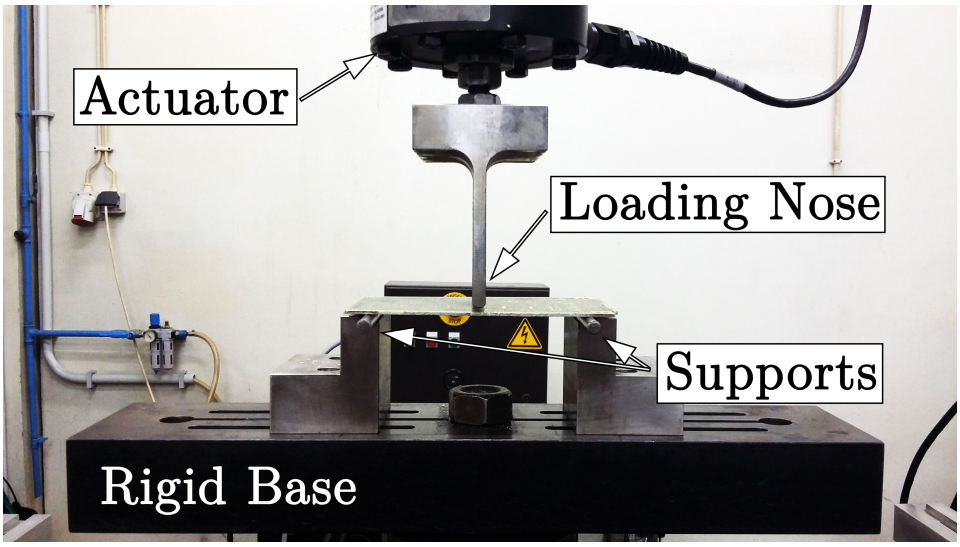
For both tests, the same specimen of each PCB model was tested thrice, for the 3PB ones, and twice, for the 4PB ones. Hence, by not considering any other specimen of the same PCB model, the processing history of the other specimens – which could have influenced the flexural properties – remains unknown in this analysis. In fact, the manufacturing and assembly variability can produce significant differences in the response of supposedly identical PCB assemblies, highlighting the importance in measuring variability [40].

5.4 Three-point bending tests

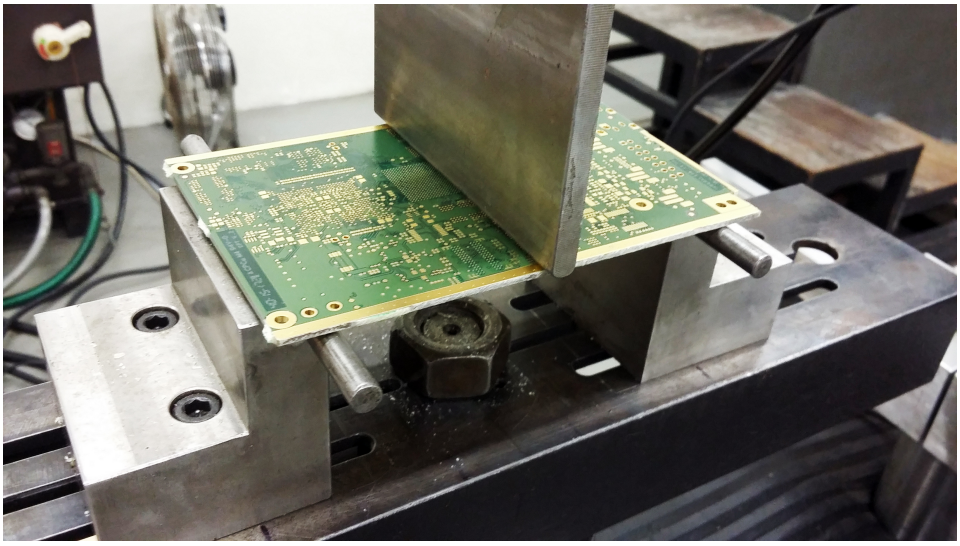
Before proceeding to a more rigorous and feasible approach, the first PCB models' characterization followed a series of coarser trials for testing. The obtained flexural properties would be used to create and validate the material models, which later would replace the need to perform these experimental tests, improving the efficiency of the PCB models' behaviour analysis.

5.4.1 Experimental Set-up

The experimental tests were performed at the Laboratory of Technological Tests (LET). The test machine used was a MTS 810, with a capacity of 250 kN (**Fig. 5.8a**). Each specimen was simply supported by two needle bearings with 8 mm of diameter, and loaded by a rigid cylindrical nose, also with 8 mm of diameter (**Fig. 5.8b**). A control in displacement was used for every test.



(a) MTS 810 machine



(b) PCB model 7 specimen setting

Figure 5.8. 3PB tests experimental set-up

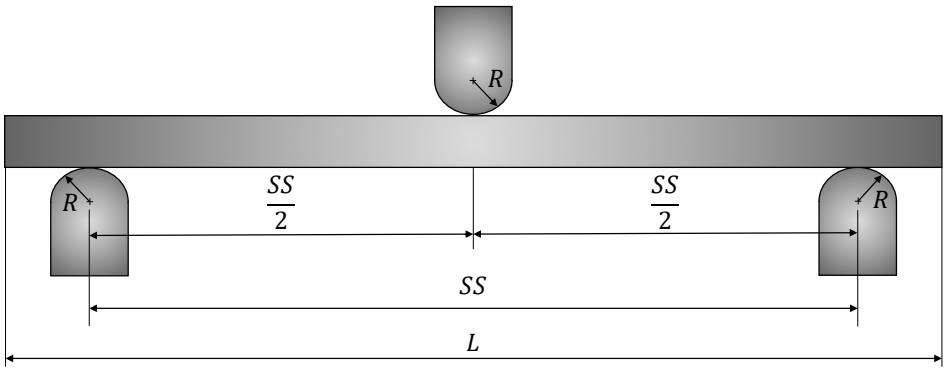


Figure 5.9. Schematic drawing of the 3PB tests

Note that the support span could be regulated, depending on the value chosen for each PCB model specimen, as seen in **Fig. 5.8b**.

By this time, the displacement limits for the different PCB model's were not yet known. Therefore, based on the beam theory, an approximation for this maximum displacement was made, following the formula for simply supported beams:

$$\delta = \frac{P \cdot SS^3}{48 \cdot E \cdot I} \tag{5.6}$$

where E is the Young modulus /MPa and I the moment of inertia /mm^4. By fixing an arbitrary load value (within the range of $0-40$ N), the support span (defined for preferable settling of the specimens, and not according to the ASTM D7264/7264M – 15 standard), the Young modulus (within $14-28$ GPa for FR-4, according to [5]) and the moment of inertia I for rectangular plates, determined using the following Eq. (5.7):

$$I = \frac{b \cdot h^3}{12} \tag{5.7}$$

the maximum displacements, under which the specimen would behave in the elastic regime, were calculated. This maximum displacement establishes the boundaries of the specimens' elastic behaviour, so that the same specimen could still be tested again afterwards, as engineers at Bosch CM – Braga do, as referred in **Section 4.3.1**.

Although with no scientific rigour, these coarse approximations did not deviate much from the observed specimens' behaviour.

5.4.2 Experimental Procedure

Each specimen's support position was controlled with the Vernier calliper, by measuring the support span. As previously mentioned, alternatively to the followed standard, the support span for every PCB model specimens was defined just for simplicity of setting them on the supports.

The measured displacements corresponded to the displacements of the actuator, and not to the specimens' suffered displacement when loaded. By comparison with the test machine and loading devices' stiffness, the specimens' stiffness values are insignificant, thence the displacements of the actuator correspond to the real displacements of the specimens.

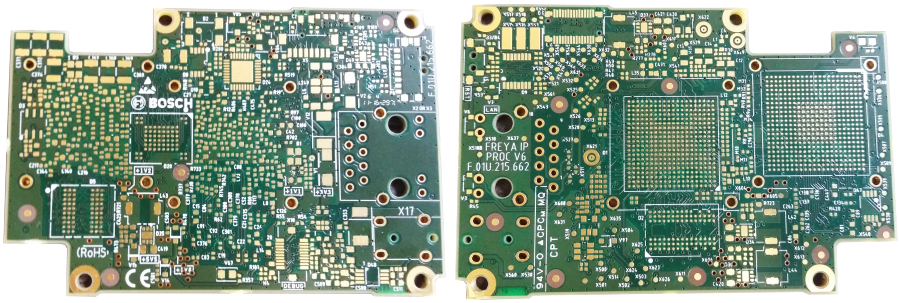
A summary of each PCB model's geometric parameters and support span values for each direction is presented in **Tabs. 5.1** and **5.2**, respectively. The parameter n corresponds to the number of copper layers. In addition, the PCB models 3, 7 and 9 specimens are illustrated in **Figs. 5.10**, **5.11** and **5.12**, respectively.

Table 5.1. Geometric parameters of the PCB model ssubmitted to the the 3PB tests

PCB model	L /mm	b /mm	h /mm	n
3	77.4	51.4	1.73; 1.74; 1.75	8
7	125	79	1.56; 1.58; 1.60	10
9	355	70	1.53; 1.55; 1.56	12

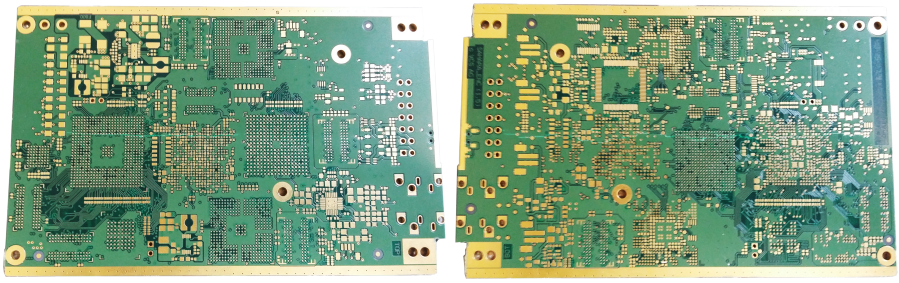
Table 5.2. Support span values defined for the PCB models submitted to the 3PB tests

PCB model	Direction	SS /mm
3	1	60
	2	45
7	1	100
	2	55
9	1	220



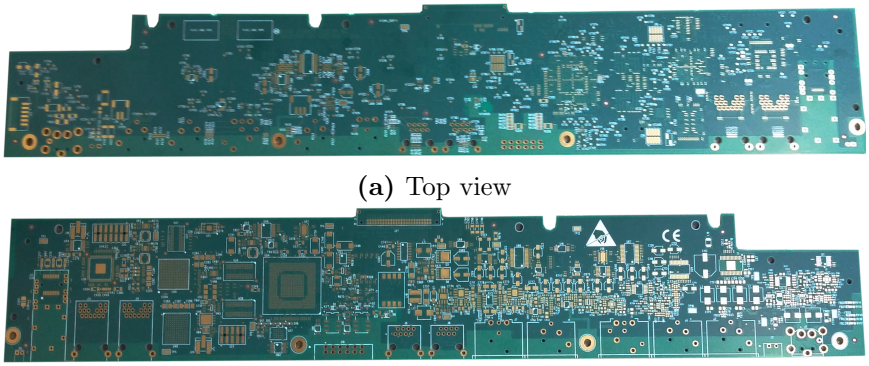
(a) Top view **(b)** Bottom view

Figure 5.10. PCB model 3 specimen



(a) Top view **(b)** Bottom view

Figure 5.11. PCB model 7 specimen



(a) Top view

(b) Bottom view

Figure 5.12. PCB model 9 specimen

These specimens were selected because of their difference in terms of size and number of copper layers. As previously mentioned, for these specimens, the measured thickness values revealed to be within the ± 10 % tolerance.

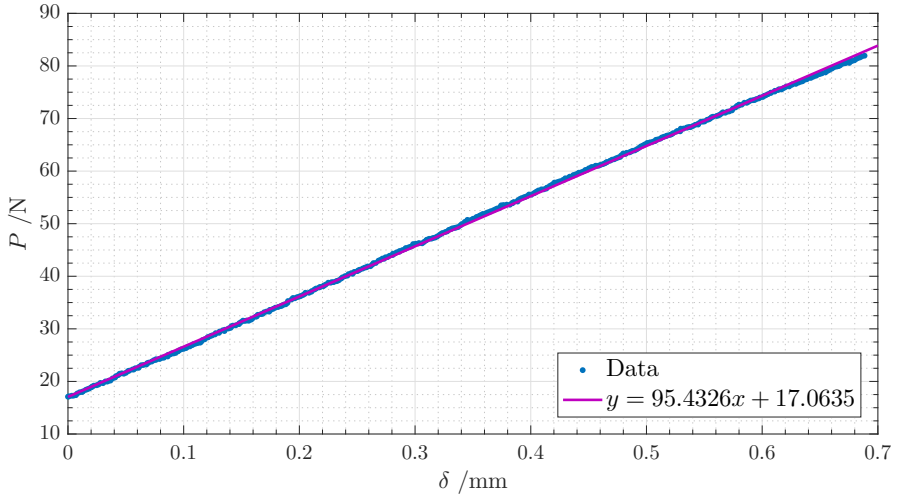
PCB model 7 specimen was the one with closer resemblance to a rectangular shape, which favoured its mounting on the experimental set-up. The same can be verified for PCB model 9, although it is too lengthy. For this reason, only a certain portion of it was considered, ignoring the surface area from the left side until the first rounded corner (**Fig. 5.12**). Lastly, PCB model 3 shape cannot be approximated to a rectangular one, due to the removed portions on the upper and lower left corners (**Fig. 5.10a**).

In order to obtain the flexural properties, the input parameters were the support span, the width and the thickness of the specimens, as stated in Eq. (5.3). A Matlab algorithm was created to obtain the slope of the load-displacement curve, by performing a linear fitting, as well as to calculate the maximum flexural stress and maximum strain values. Although three different thickness values were measured for each PCB model specimen, the bigger one was considered, which results in a lower flexural Young modulus. This way, a safety margin was being applied.

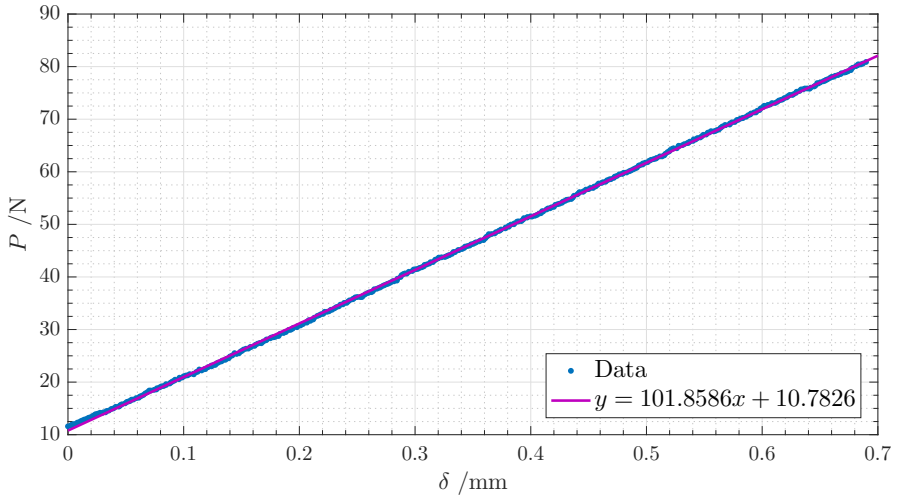
5.4.3 Results

The load-displacement curves were plotted for each of the three measurements, with the exception of PCB model 3 in direction 2, where only two measurements were made.

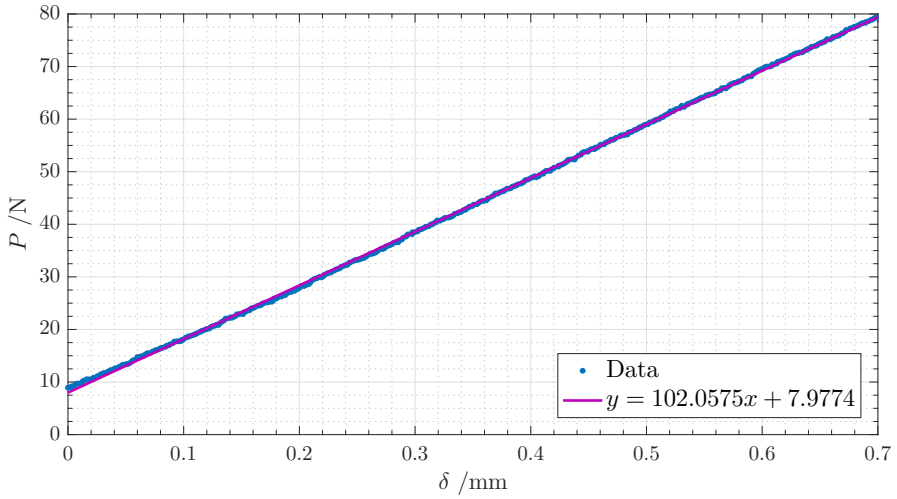
PCB model 3



(a) 1^{st} measurement

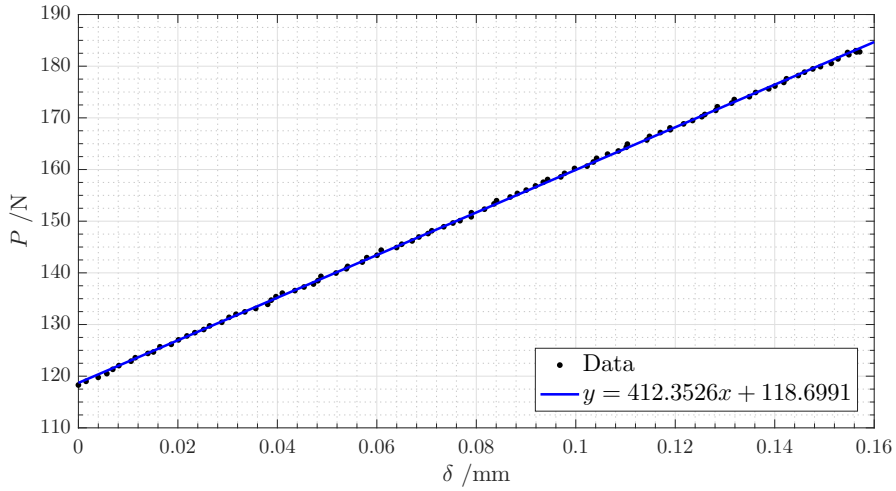


(b) 2^{nd} measurement

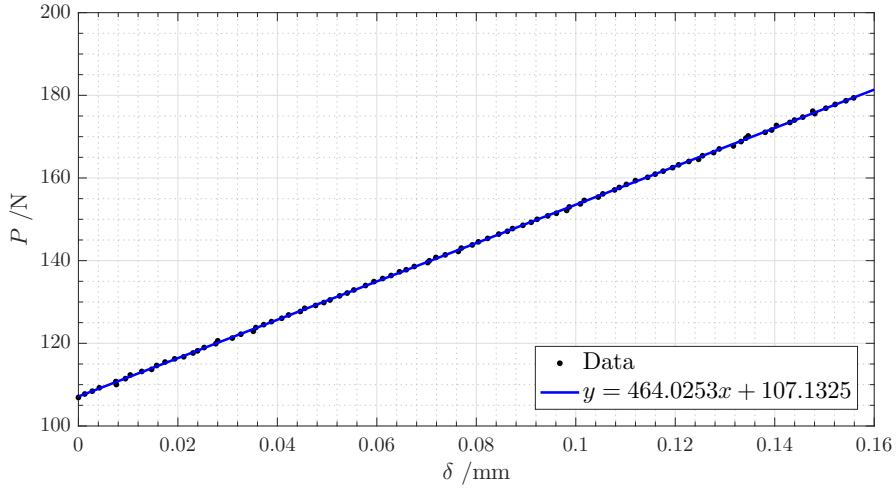


(c) 3^{rd} measurement

Figure 5.13. PCB model 3 load-displacement curves, in direction 1

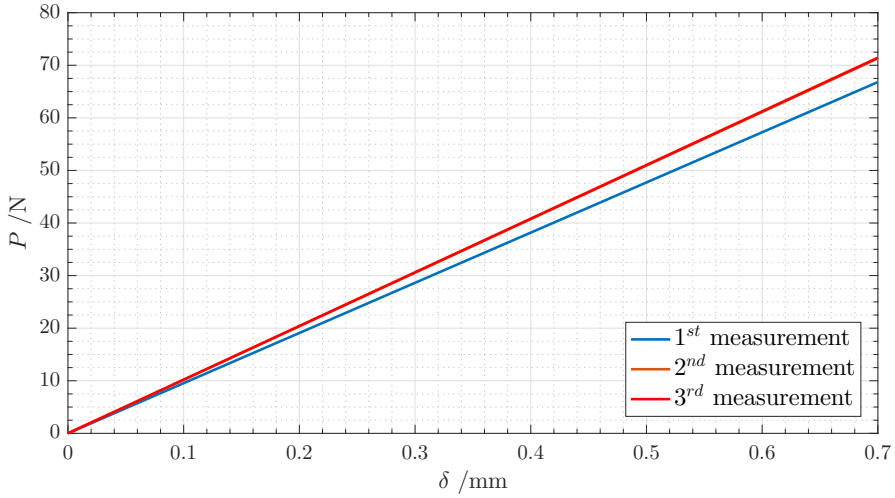


(a) 1^{st} measurement

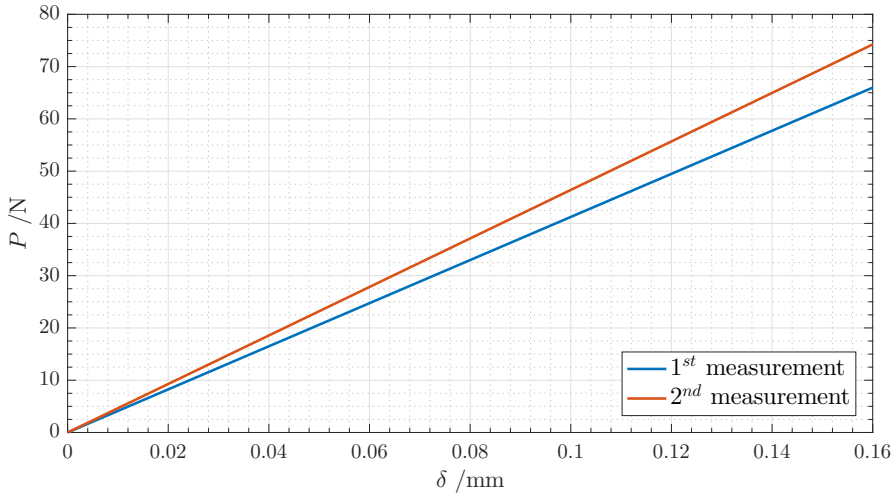


(b) 2^{nd} measurement

Figure 5.14. PCB model 3 load-displacement curves, in direction 2



(a) Measurements in direction 1.



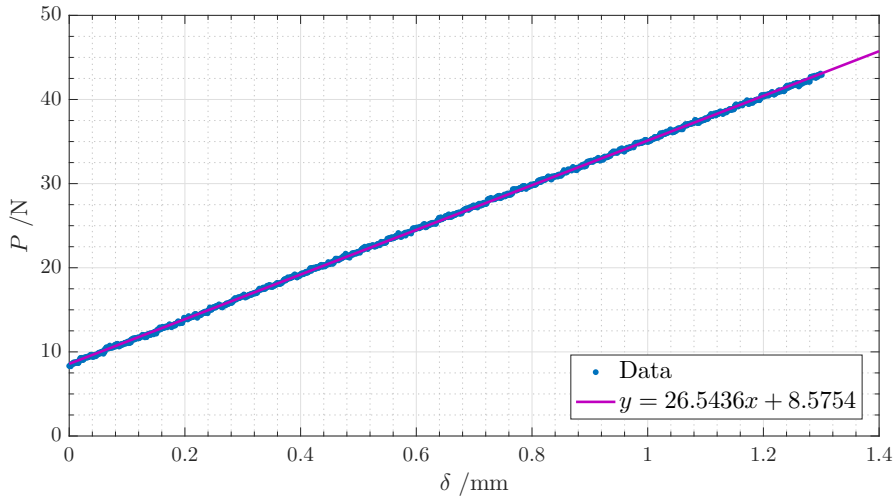
(b) Measurements in direction 2.

Figure 5.15. PCB model 3 slope comparison, in directions 1 and 2

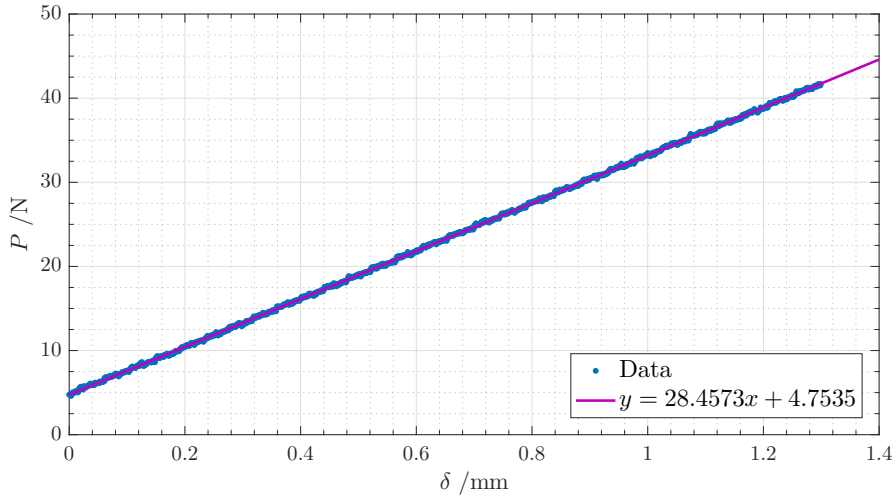
Table 5.3. PCB model 3 slope and flexural properties

PCB model 3	m /N·mm^{-1}	σ_{max} /MPa	ε_{max} /−	E_f /GPa
Direction 1	95.4326	23.4265	0.0166	18.707
	101.8586	23.1231		19.967
	102.0575	22.6753		20.006
Direction 2	412.3526	26.0556	0.0275	22.646
	464.0253	25.5412		25.484

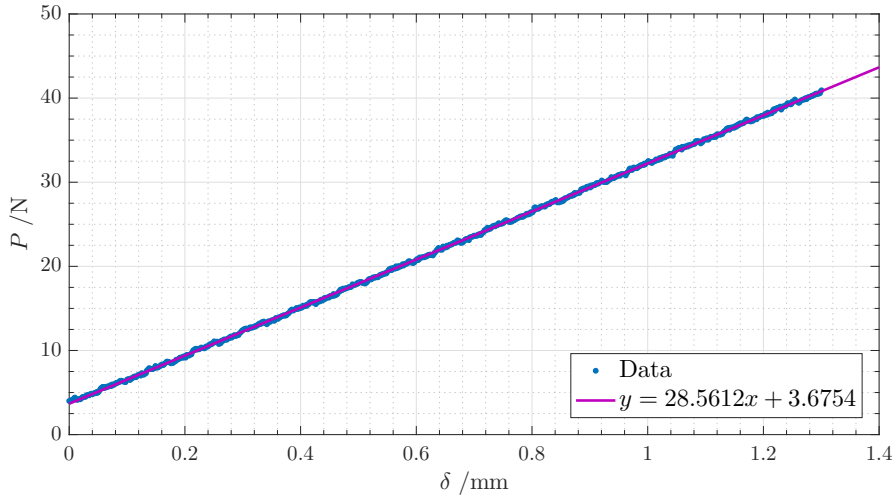
PCB model 7



(a) 1^{st} measurement

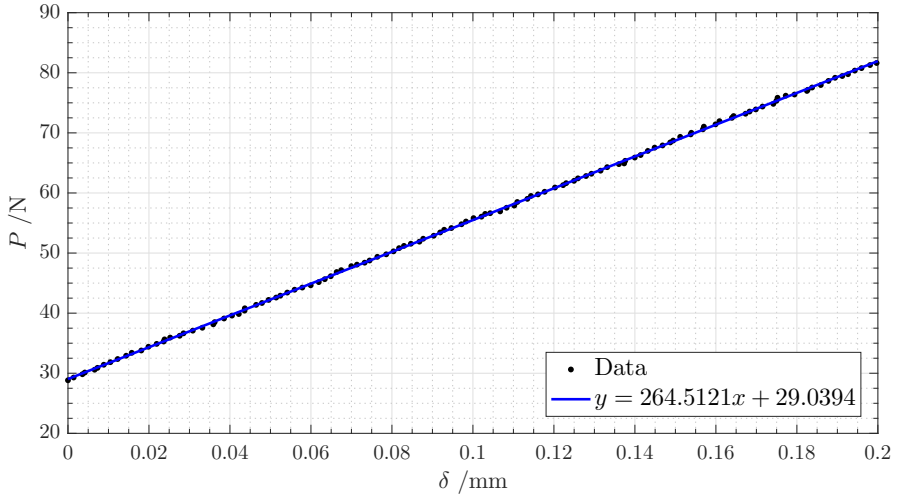


(b) 2^{nd} measurement

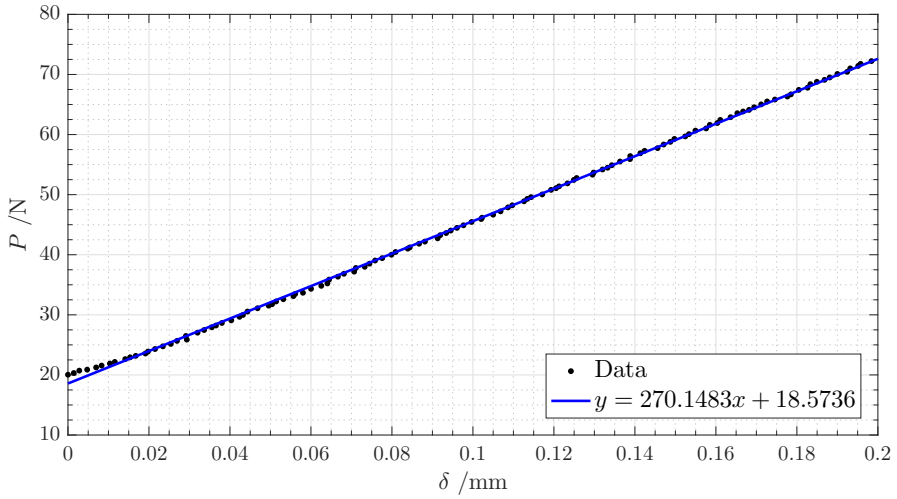


(c) 3^{rd} measurement

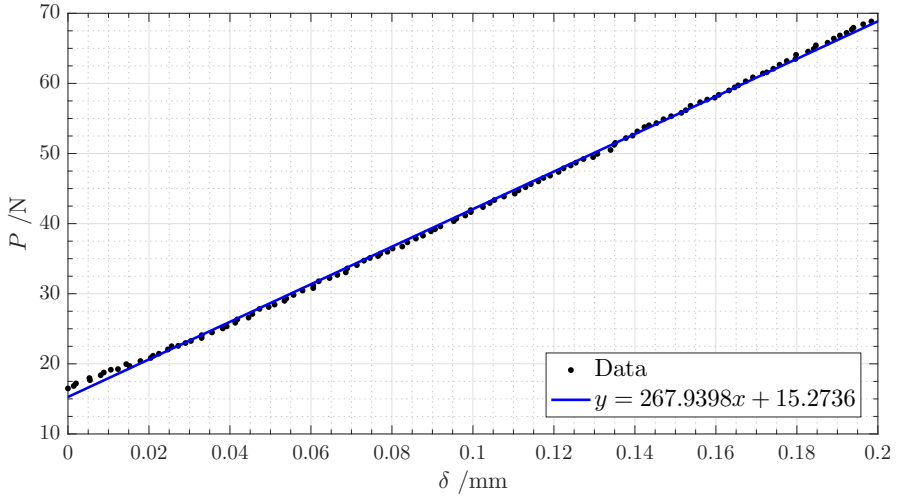
Figure 5.16. PCB model 7 load-displacement curves, in direction 1



(a) 1^{st} measurement

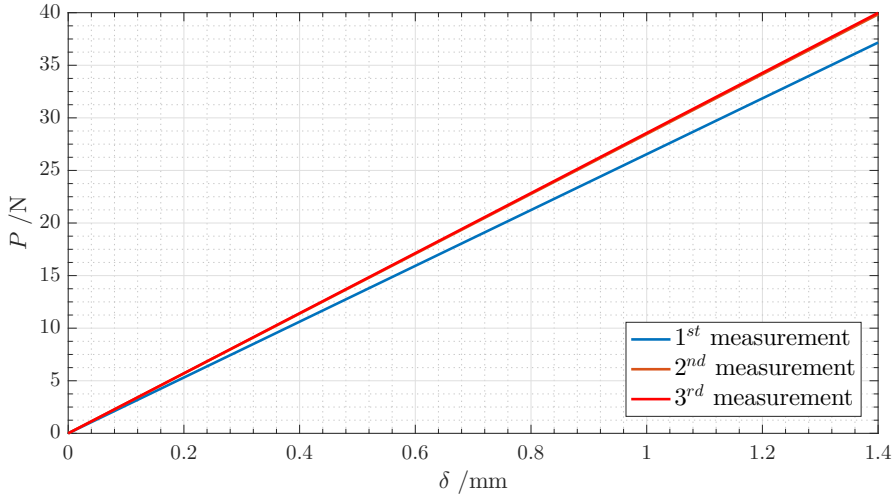


(b) 2^{nd} measurement

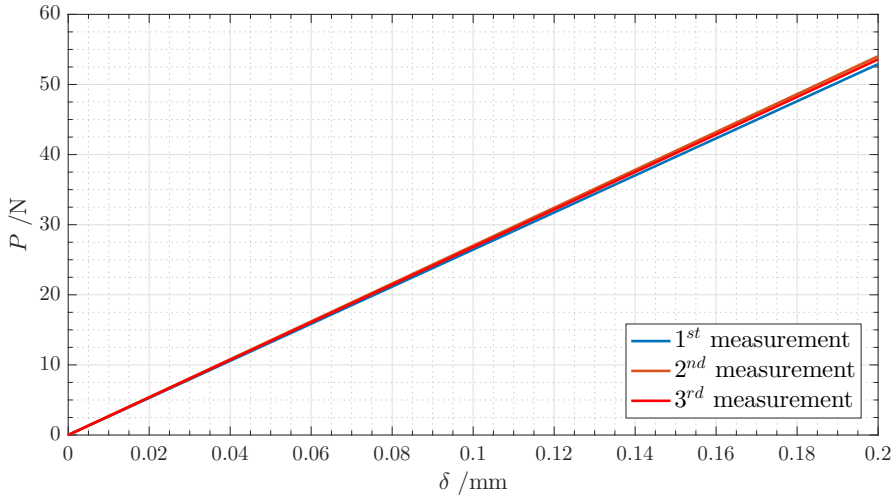


(c) 3^{rd} measurement

Figure 5.17. PCB model 7 load-displacement curves, in direction 2



(a) Measurements in direction 1.



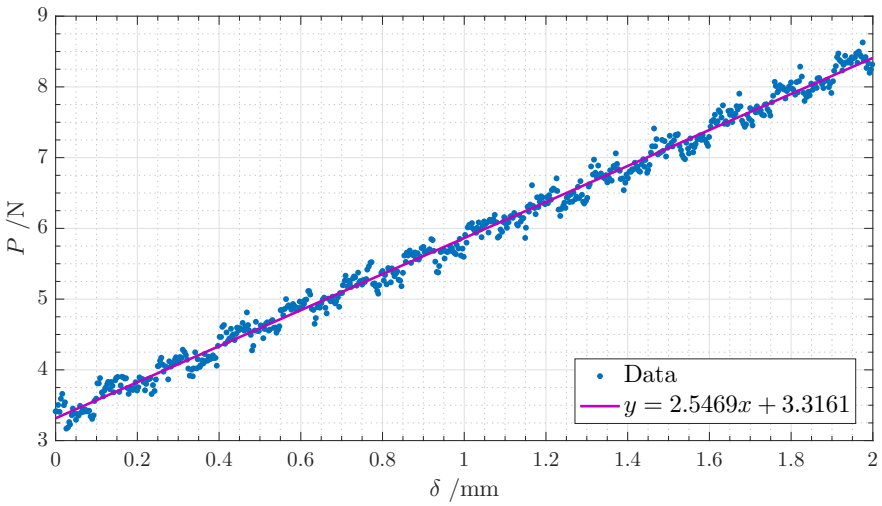
(b) Measurements in direction 2.

Figure 5.18. PCB model 7 slope comparison, in directions 1 and 2

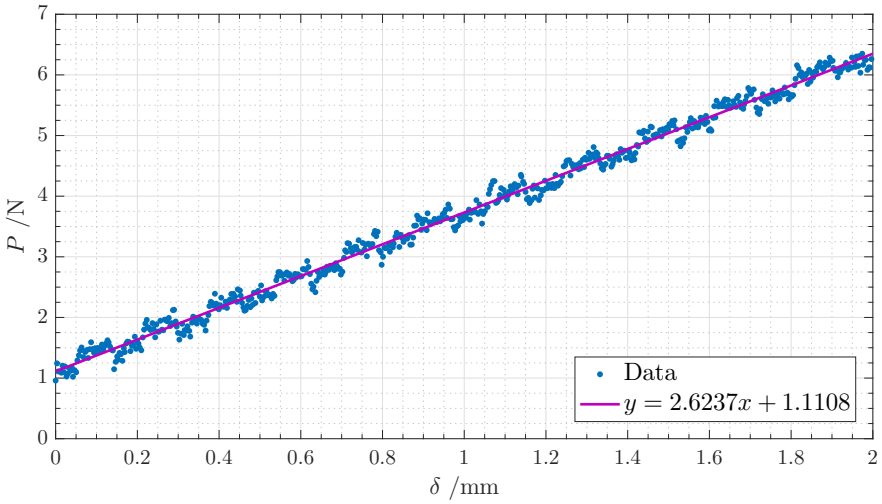
Table 5.4. PCB model 7 slope and flexural properties

PCB model 7	m /N·mm^{-1}	σ_{max} /MPa	ε_{max} /−	E_f /GPa
Direction 1	26.5436	15.9761	0.0062	20.507
	28.4573	15.4596		21.986
	28.5612	15.1787		22.066
Direction 2	264.5121	10.5224	0.0168	21.488
	270.1483	9.3964		21.946
	267.9398	8.9233		21.773

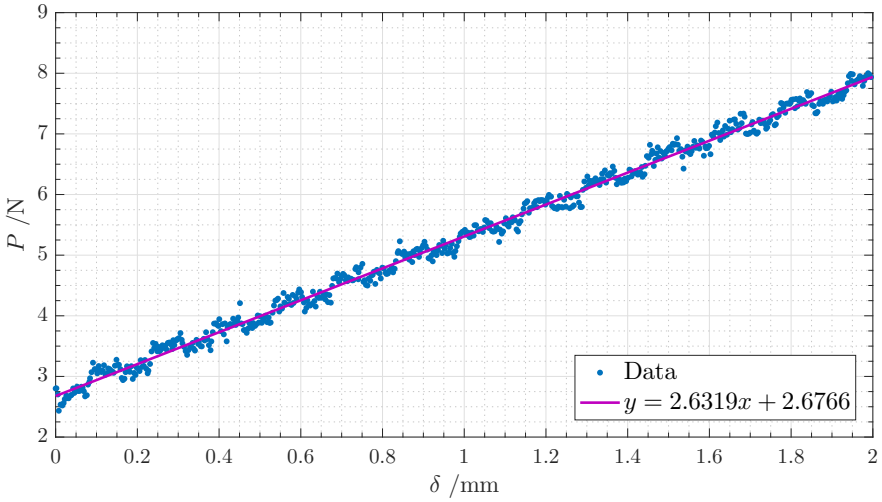
PCB model 9



(a) 1^{st} measurement



(b) 2^{nd} measurement



(c) 3^{rd} measurement

Figure 5.19. PCB model 9 load-displacement curves, in direction 1

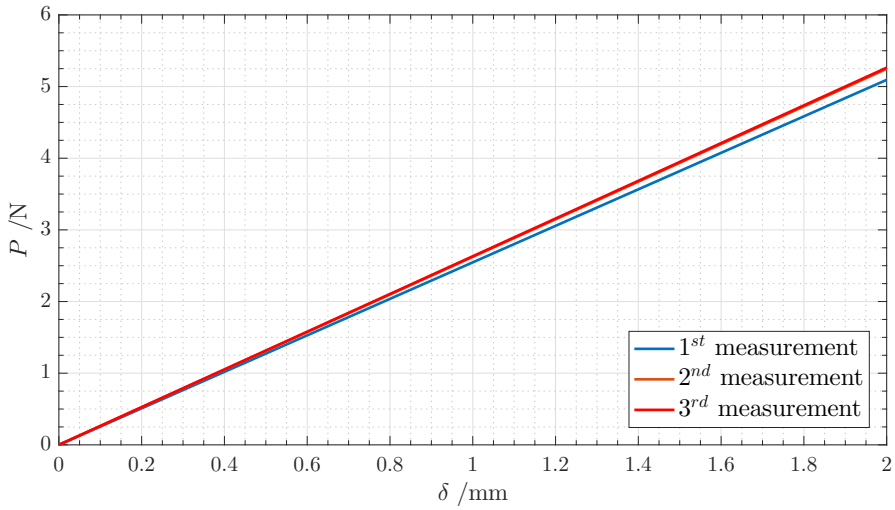


Figure 5.20. PCB model 9 slope comparison, in direction 1.

Table 5.5. PCB model 9 slope and flexural properties

PCB model 9	m /N·mm^{-1}	σ_{max} /MPa	ε_{max} /−	E_f /GPa
	2.5469	8.3574		25.512
Direction 1	2.6237	6.1496	0.0015	26.232
	2.6319	7.7492		26.363

5.4.4 Discussion

Judging by the previous curves for all the tested specimens, there is a linear relationship between the load and displacement values. However, only the elastic regime was included, being the initial points removed, as they corresponded to the setting of the specimen. The slope difference between the measurements should be discussed, since the relative error between the first and second measurements is higher than the one between the second and third measurements. One possible reason can be related to the specimens material hysteresis, meaning that there is a grain reorganization after the material is deformed, making it stiffer than before – hardening. Another explanation, which best captures this phenomenon, refers to the specimens setting. Initially, small clearances exist between the specimen and the supports. It is obvious that when a next measurement is executed, the clearances will be smaller than before, and one is closer to directly calculate the real stiffness value of the material. Based on the results, at the moment of the second measurement, the material is already being completely loaded, since great part of the clearances (or even totally) have been removed. Therefore, as a tip for future measurements, it is reasonable to initially apply a reduced pre-load to the every specimen, without damaging it, and then the following measurement would reproduce the material's real response. In this way, by only performing one unloading step, the tests execution is more productive and less time-consuming.

The slope rise is in accordance with the decrease of the maximum flexural strength. Exceptionally, the fact that the slope decreases between the second and third measurements of PCB model 7 in direction 2 is residual. The same cannot be concluded for PCB model 3 specimens in direction 2, where the slope difference is considerable.

For the PCB models 3 and 7 specimens, the points' deviations are small, while compared to the PCB model 9 specimen, which indicates the presence of a considerable amount of load noise. This behaviour was already expected, since this PCB model 9 specimen is lengthier than the former two, thus more susceptible to higher oscillations during the loading phase.

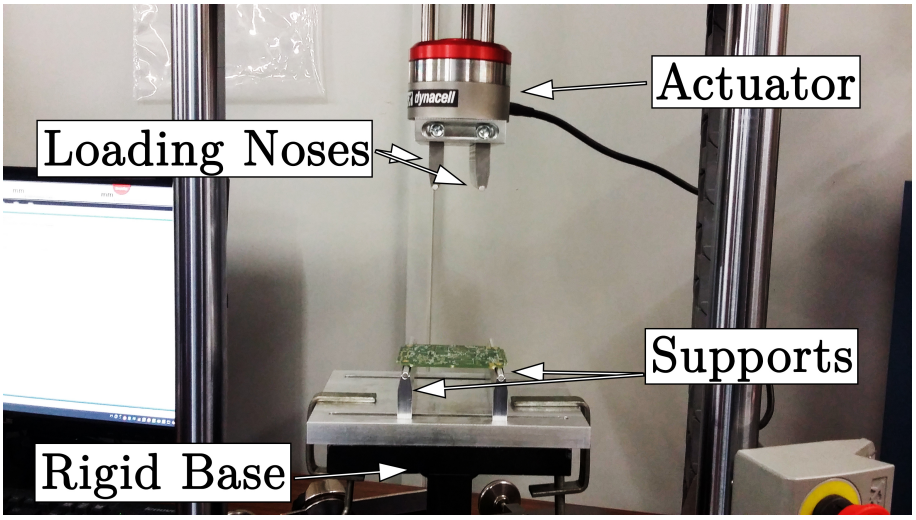
It is concluded that the derived flexural stiffness for every PCB model specimens is within the expected range stated in [5], *i.e.* from $14 - 28$ GPa. The specimens' maximum displacement was overestimated, and the maximum strain calculated revealed to surpass the allowable limit set by Bosch ST – Ovar internal report – 0.573 mm – in the two directions. The most important aspect to highlight is the quasi-isotropic behaviour of PCB model 7, which differs from some of the statements referred in **Chapter 2**, whose conclusions stated how anisotropic printed circuit boards mechanical properties are. In fact, from all of the three tested specimens, its shape is the closest to a rectangle. This indicates that the closer every specimen's shape is to a rectangle, the more the material can be treated as quasi-isotropic. This unveils the possibility of simplifying the approach for many of the PCBs' numerical models, as long as their shape is rectangular. However, there are no guarantees of how accurately this material model would predict their mechanical behaviour.

5.5 Four-point bending tests

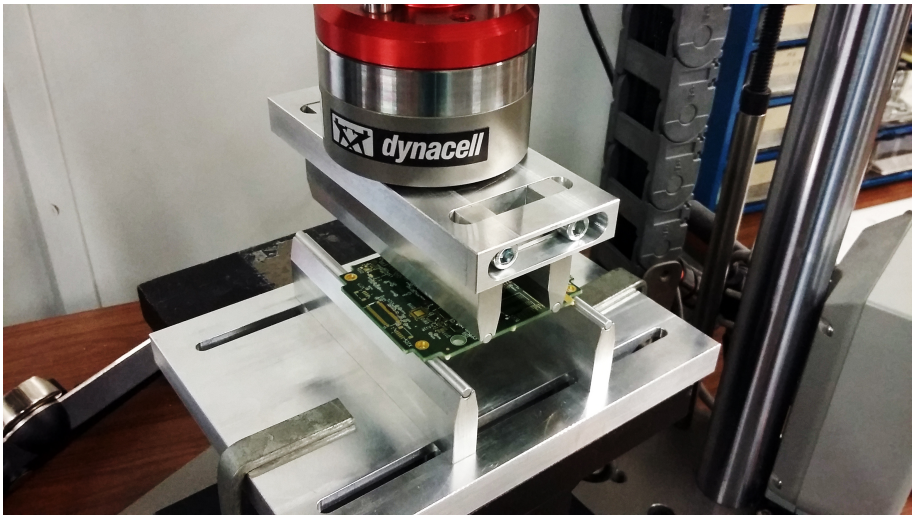
Based on the feedback given from the previous tests, the four-point bending ones aimed to be more rigorous in both measurement and data collecting. Unlike the 3PB tests, where the experimental set-up was already built, for these ones a CAD model had to be conceived, using software Solidworks 2017, whose drawings are attached in **Appx. A**.

5.5.1 Experimental Set-up

The experimental tests were performed at the Laboratory of Optics and Experimental Mechanics (LOME). The test machine used was a Instron ElectroPuls E1000, with a capacity of 1 kN (**Fig. 5.21a**). Each specimen was simply supported by two needle bearings with 4 mm of diameter, and loaded by two rigid cylindrical noses, also with 4 mm of diameter (**Fig. 5.21b**). Similarly, a control in displacement was used for every test, and the support span, as well as the load span, could be regulated, depending on the value chosen for each PCB model's specimen (**Fig. 5.21b**).



(a) Instron ElectroPuls E1000 machine



(b) PCB model 1 specimen setting

Figure 5.21. Four-point bending tests experimental set-up

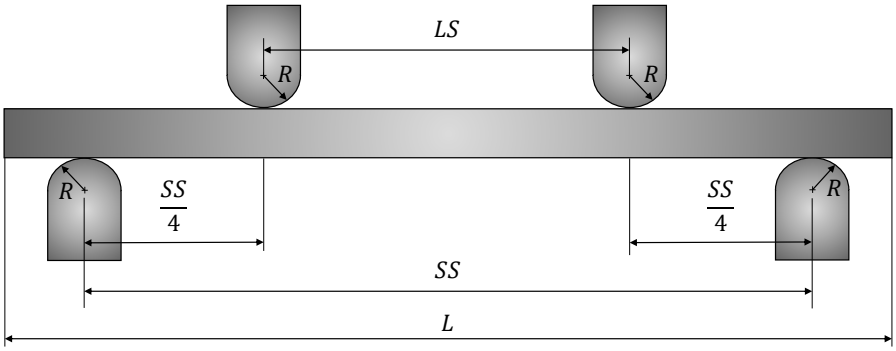


Figure 5.22. Schematic drawing of the 4PB tests

5.5.2 Experimental Procedure

Again, each specimen's support and load position was controlled with the Vernier calliper, by measuring the support and loading spans, respectively. However, this time, the support and loading spans for every PCB model specimens were defined as:

$$SS = \frac{4}{5} \cdot L \tag{5.8}$$

$$LS = \frac{SS}{2} \tag{5.9}$$

following the precautions stated in the ASTM D7264/7264M – 15 standard [72]. The measured displacements corresponded to the displacements of the actuator, and not to the specimens suffered displacement when loaded. Also based on the aforementioned reasons for the 3PB tests, one could consider that the displacements of the actuator correspond to the real displacements of the specimens.

For each measurement, a pre-load of 20 N – intended to favour the setting of every specimen on the supports – was initially applied, followed by a displacement of 1 mm. As verified in the 3PB tests, by doing only two measurements this time, the derived results would reproduce the material's real response, while simultaneously making the entire procedure more productive and less time-consuming.

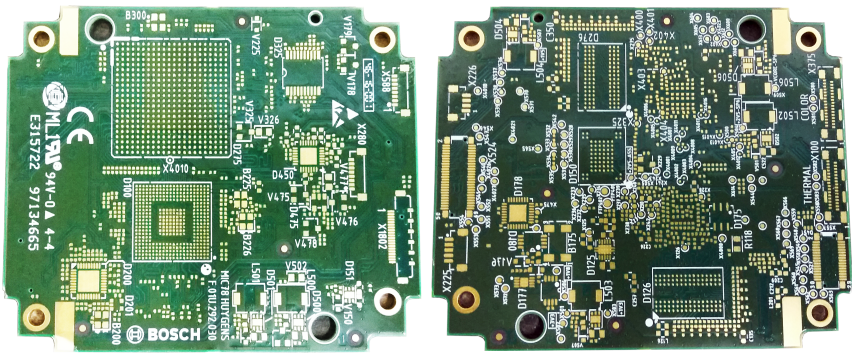
A summary of each PCB model's geometric parameters and support and loading span values for each direction is presented in **Tabs. 5.6** and **5.7**, respectively. The PCB models 1, 2, 5, 6, 12 and 14 specimens are illustrated in **Figs. 5.23**, **5.24**, **5.25**, **5.26**, **5.27** and **5.28**, respectively.

Table 5.6. Geometric parameters of the PCB models submitted to the 4PB tests

PCB model	L /mm	b /mm	h /mm	n
1	78.55	65.8	1.70; 1.72; 1.74	8
2	65.9	58.8	1.69; 1.74; 1.77	8
5	66	59	1.64; 1.65; 1.66	4
6	75.4	51.9	1.72; 1.73; 1.73	6
12	77.8	51	1.71; 1.73; 1.74	2
14	80	70	1.78; 1.79; 1.80	8

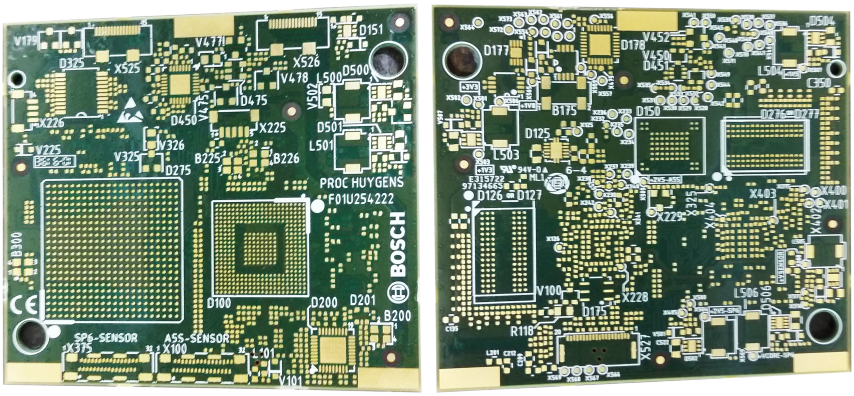
Table 5.7. Support and loading span values defined for the PCB models submitted to the 4PB tests

PCB model	Direction	SS /mm	LS /mm
1	1	62.84	31.42
	2	52.64	26.32
2	1	52.72	26.36
	2	47.04	23.52
5	1	52.8	26.40
	2	47.2	23.60
6	1	60.32	30.16
	2	41.52	20.76
12	1	62.24	31.12
	2	40.8	20.40
14	1	56	28
	2	56	28



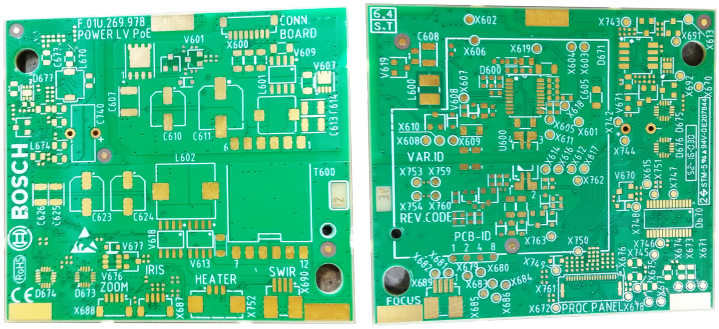
(a) Top view **(b)** Bottom view

Figure 5.23. PCB model 1 specimen



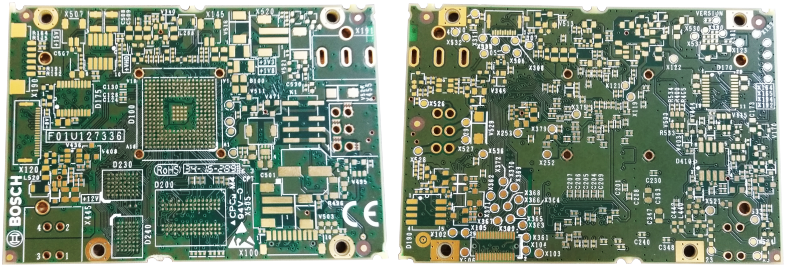
(a) Top view **(b)** Bottom view

Figure 5.24. PCB model 2 specimen



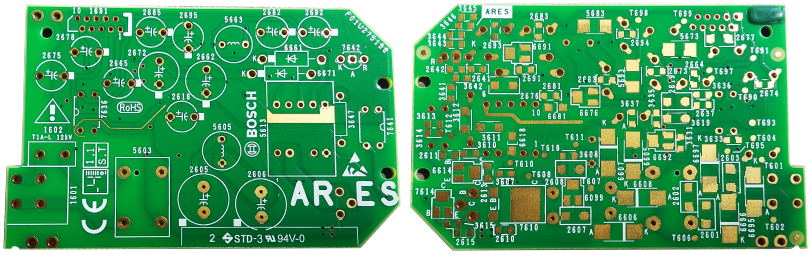
(a) Top view **(b)** Bottom view

Figure 5.25. PCB model 5 specimen



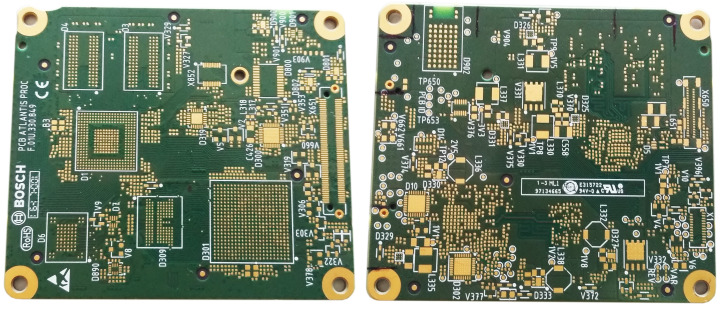
(a) Top view **(b)** Bottom view

Figure 5.26. PCB model 6 specimen



(a) Top view **(b)** Bottom view

Figure 5.27. PCB model 12 specimen



(a) Top view **(b)** Bottom view

Figure 5.28. PCB model 14 specimen

The selected specimens have very similar sizes[3] and also very close resemblances to a rectangular shape, which made their setting easier. Equally, a linear fitting of the load-displacement results was made and the chosen thickness corresponded to the bigger measured value.

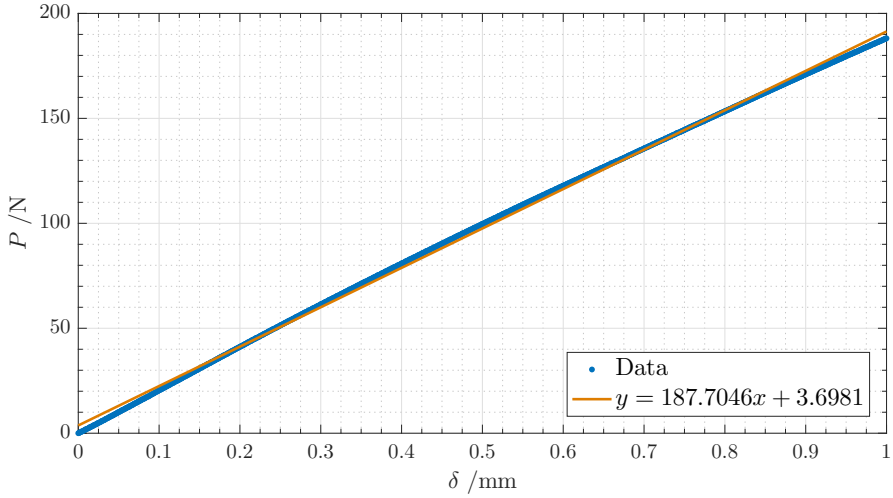
However, the maximum flexural stress and maximum strain were not calculated this time, since the applied displacement of 1 mm was set for the loading noses, and it does not correspond to the displacement at the center of each specimen – as in the 3PB tests configuration – where the maximum stress and strain values would be obtained. However, if a LVDT had been used at the center of every specimen, the maximum displacement could have been measured.

5.5.3 Results

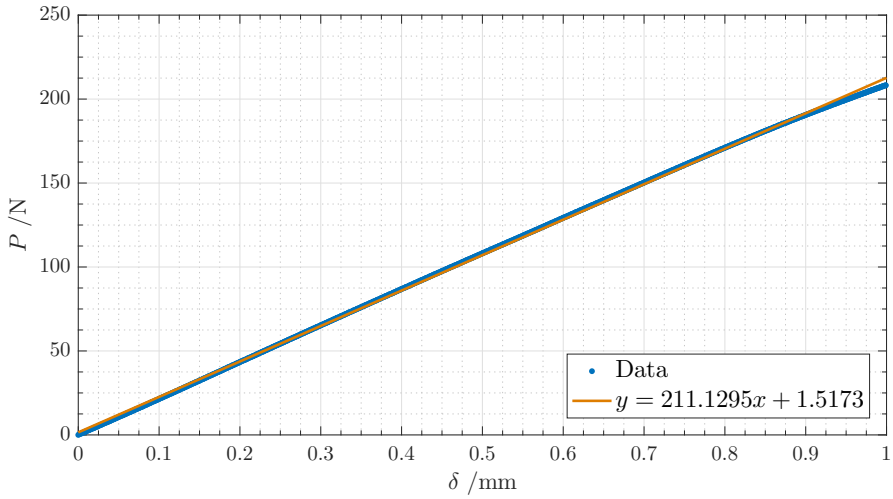
The load-displacement curves were plotted for each of the two measurements for every PCB model specimen.

[3] PCB models 2 and 5 have slightly the same size.

PCB model 1

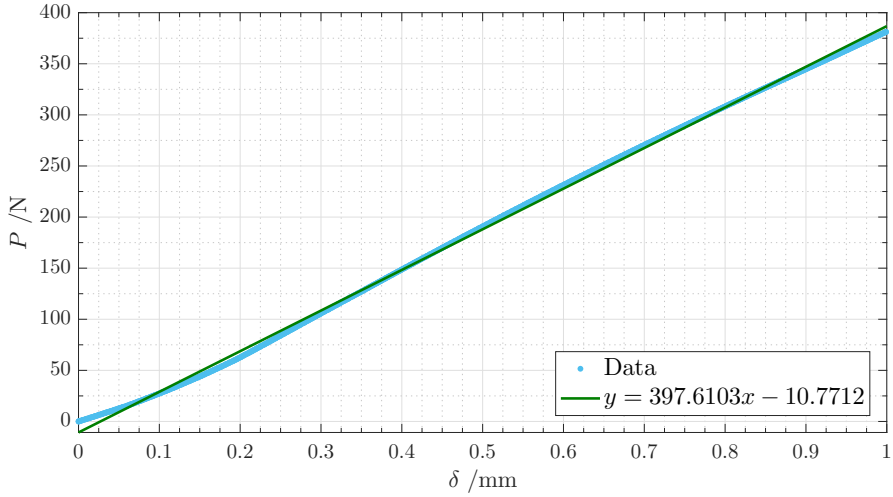


(a) 1^{st} measurement

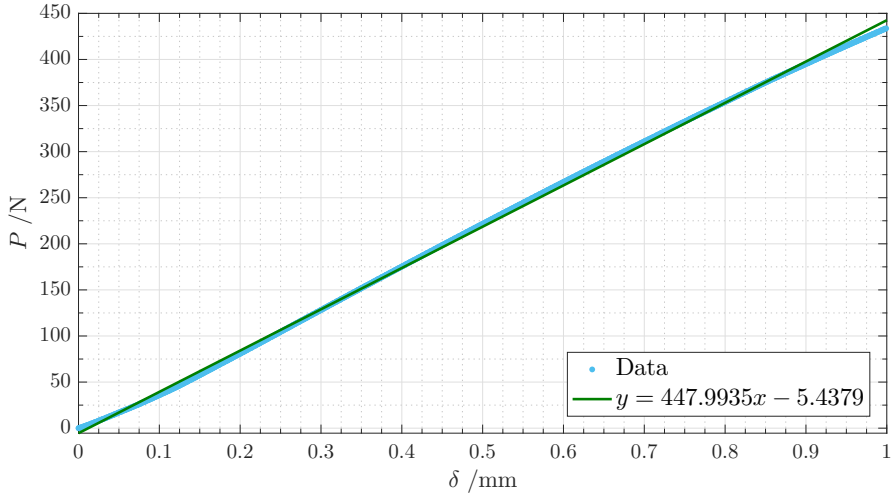


(b) 2^{nd} measurement

Figure 5.29. PCB model 1 load-displacement curves, in direction 1

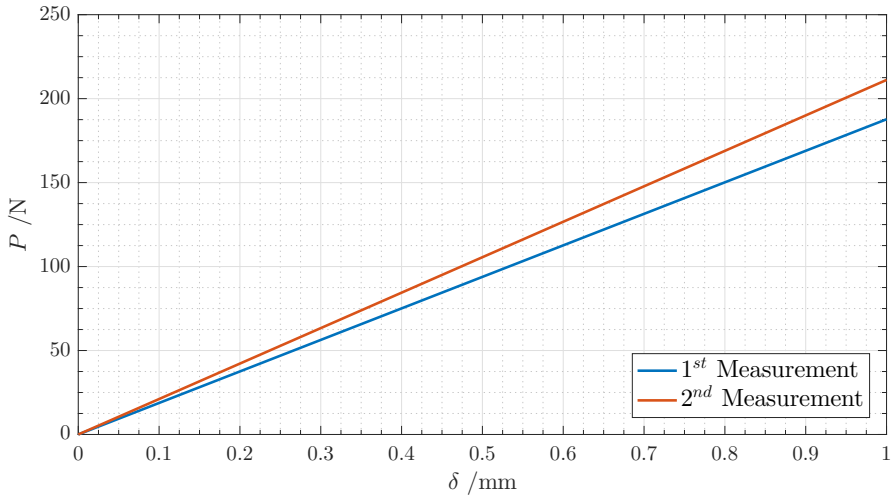


(a) 1^{st} measurement

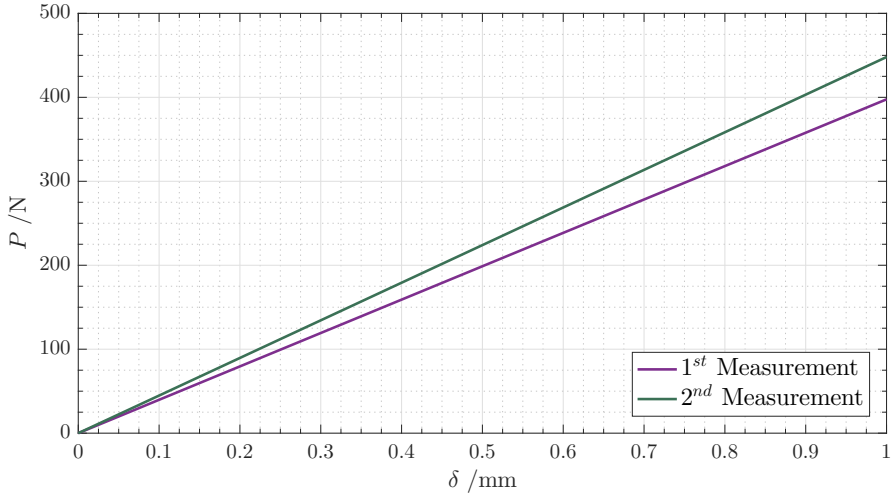


(b) 2^{nd} measurement

Figure 5.30. PCB model 1 load-displacement curves, in direction 2



(a) Measurements in direction 1



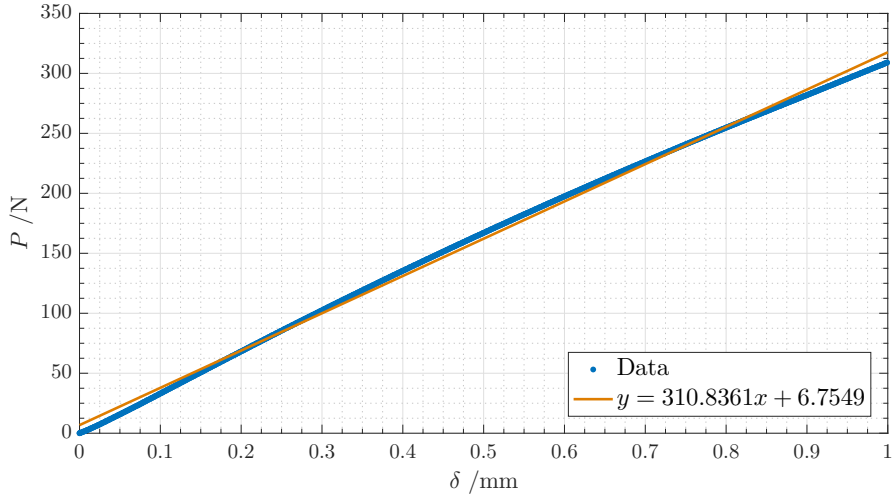
(b) Measurements in direction 2

Figure 5.31. PCB model 1 slope comparison, in directions 1 and 2

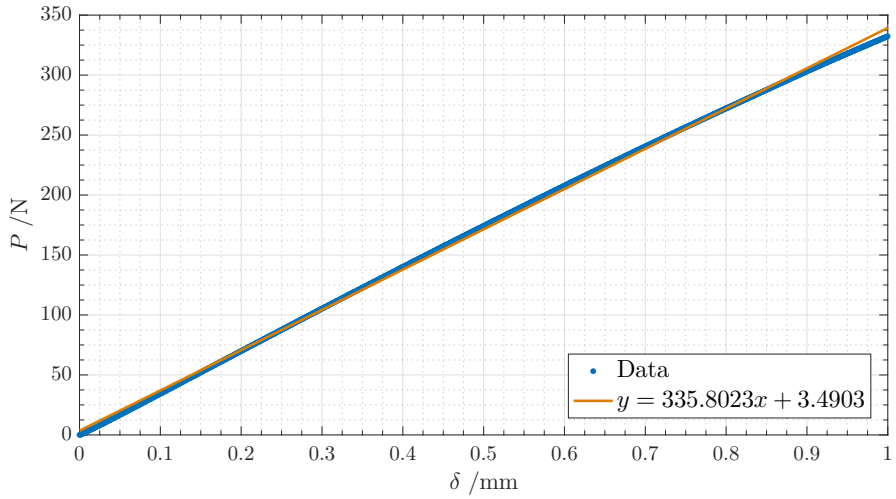
Table 5.8. PCB model 1 slope and flexural properties

PCB model 1	m /N·mm^{-1}	E_f /GPa
Direction 1	187.7046	22.843
	211.1295	25.694
Direction 2	397.6103	23.827
	447.9935	26.846

PCB model 2

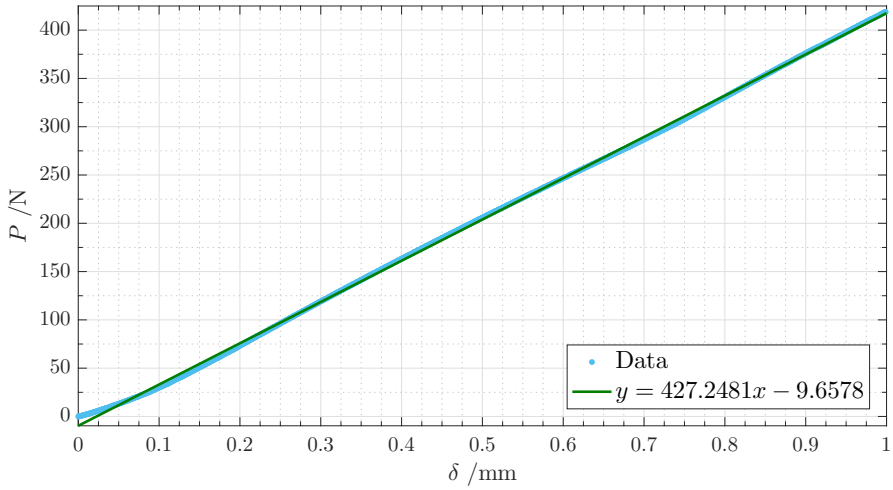


(a) 1^{st} measurement

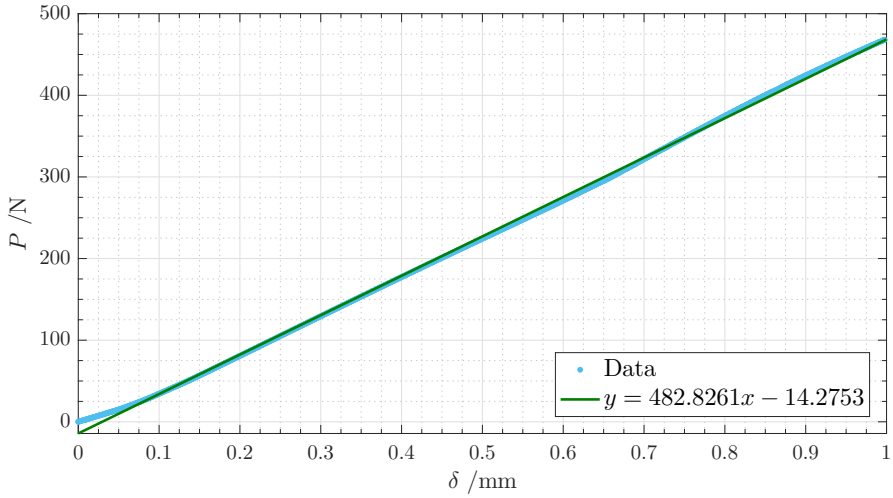


(b) 2^{nd} measurement

Figure 5.32. PCB model 2 load-displacement curves, in direction 1

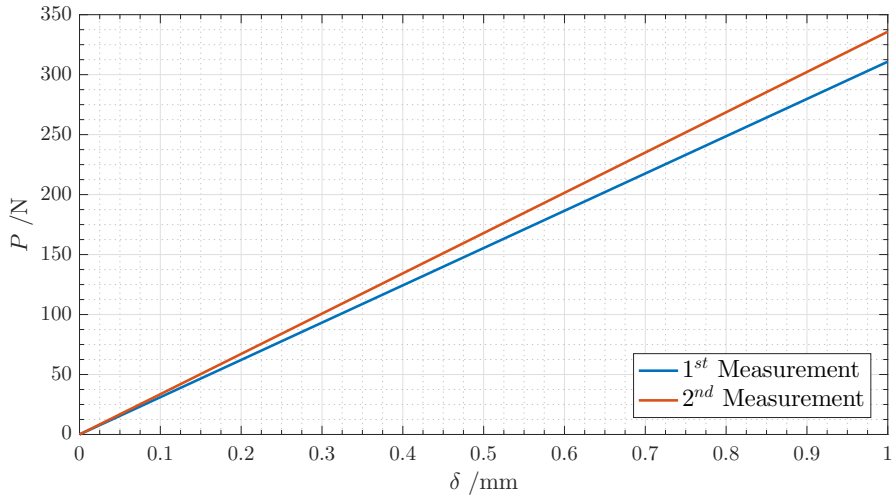


(a) 1^{st} measurement

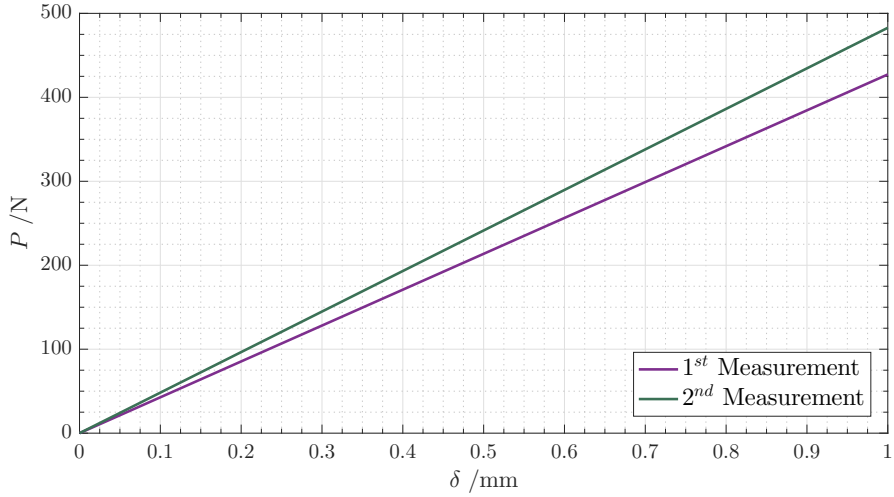


(b) 2^{nd} measurement

Figure 5.33. PCB model 2 load-displacement curves, in direction 2



(a) Measurements in direction 1



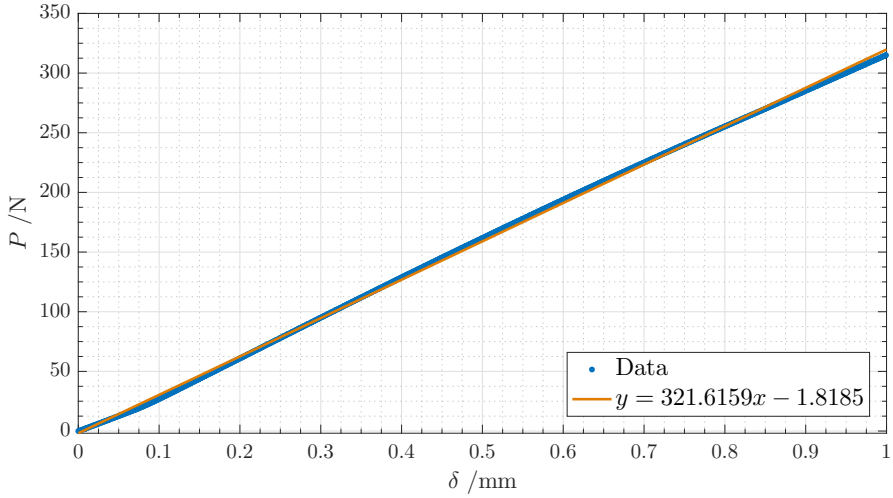
(b) Measurements in direction 2

Figure 5.34. PCB model 2 slope comparison, in directions 1 and 2

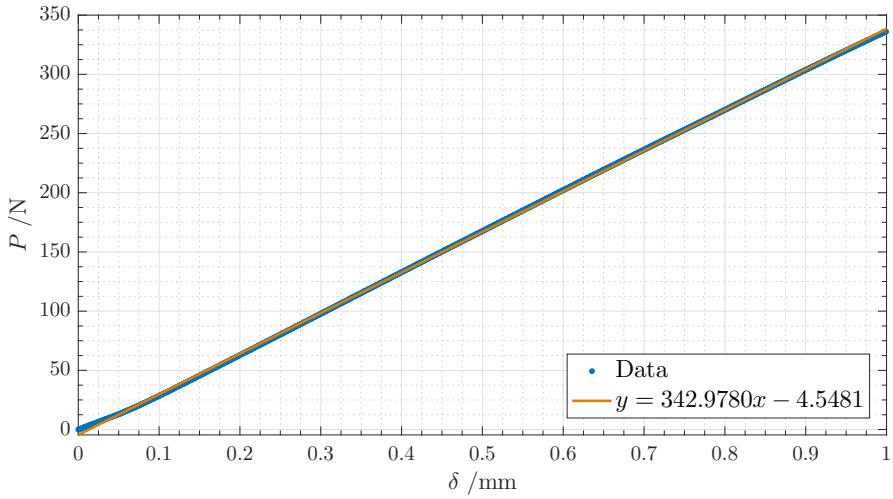
Table 5.9. PCB model 2 slope and flexural properties

PCB model 2	m /N·mm^{-1}	E_f /GPa
Direction 1	310.8361	23.747
	335.8023	25.654
Direction 2	427.2481	20.688
	482.8261	23.380

PCB model 5

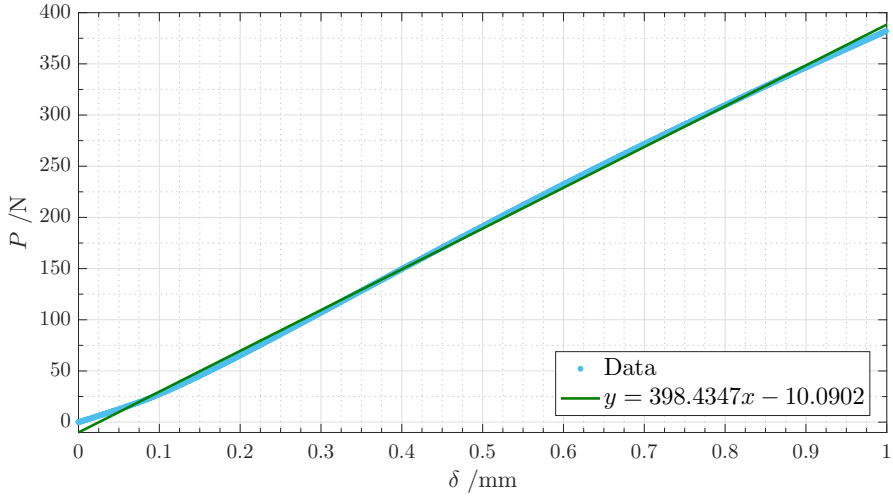


(a) 1^{st} measurement

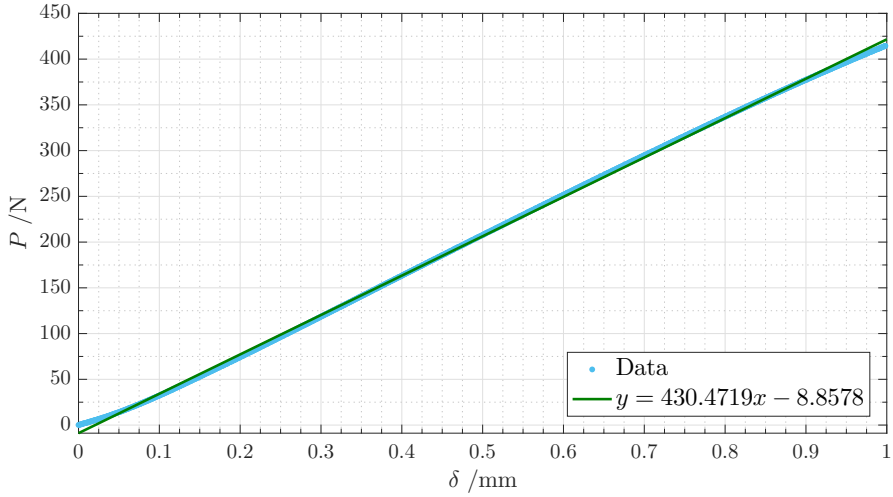


(b) 2^{nd} measurement

Figure 5.35. PCB model 5 load-displacement curves, in direction 1

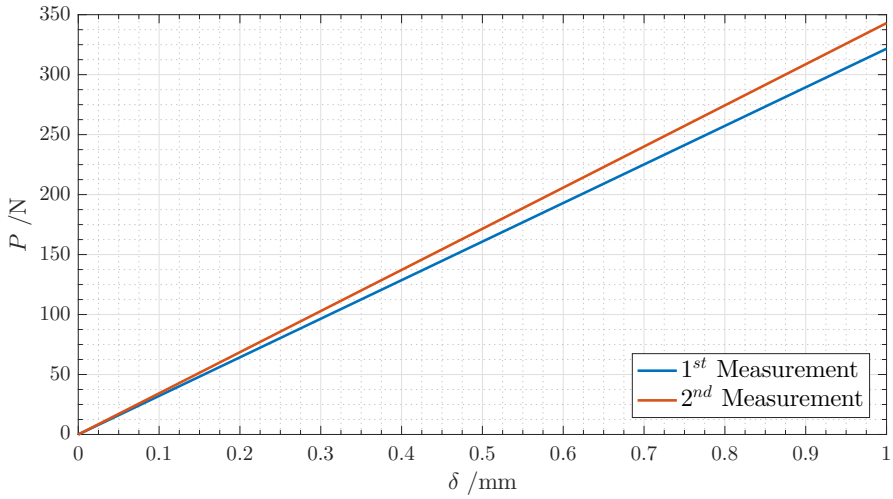


(a) 1^{st} measurement

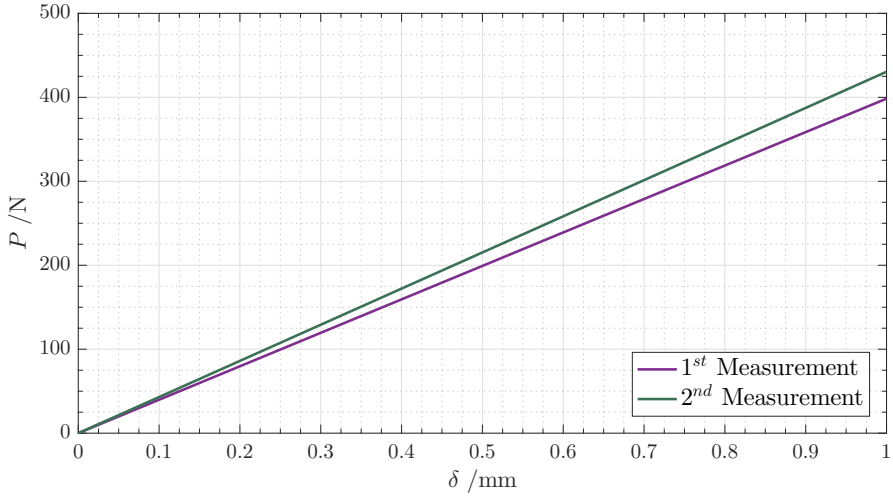


(b) 2^{nd} measurement

Figure 5.36. PCB model 5 load-displacement curves, in direction 2



(a) Measurements in direction 1



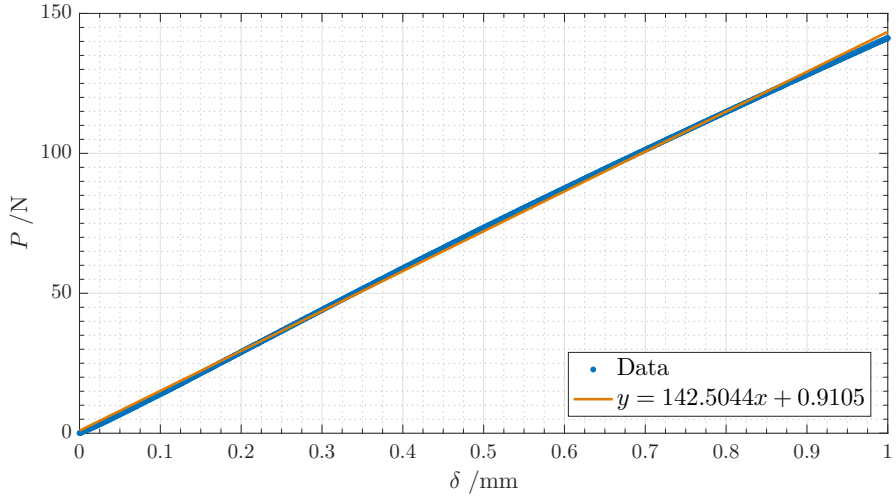
(b) Measurements in direction 2

Figure 5.37. PCB model 5 slope comparison, in directions 1 and 2

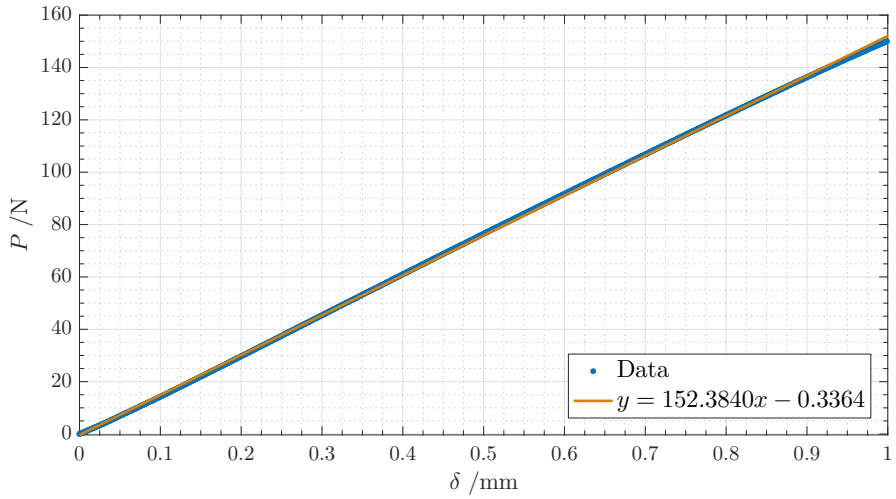
Table 5.10. PCB model 5 slope and flexural properties

PCB model 5	m /N·mm^{-1}	E_f /GPa
Direction 1	321.6159	29.820
	342.9780	31.801
Direction 2	398.4347	23.592
	430.4719	25.489

PCB model 6

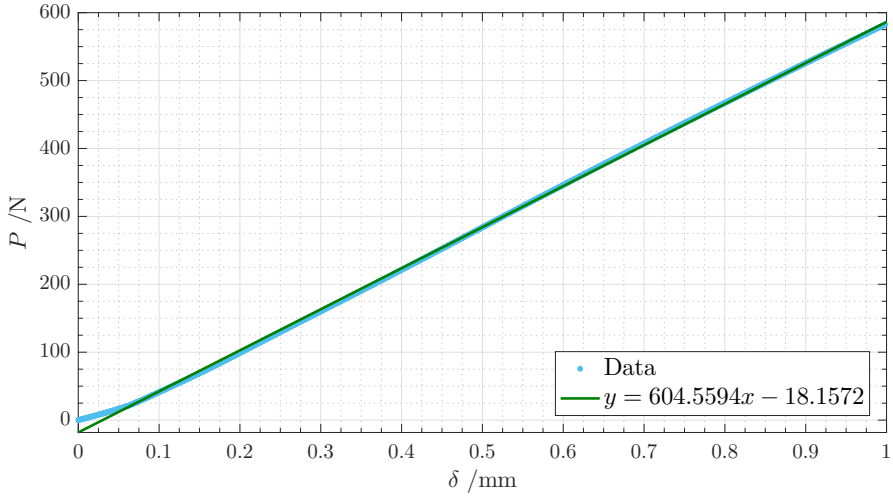


(a) 1^{st} measurement

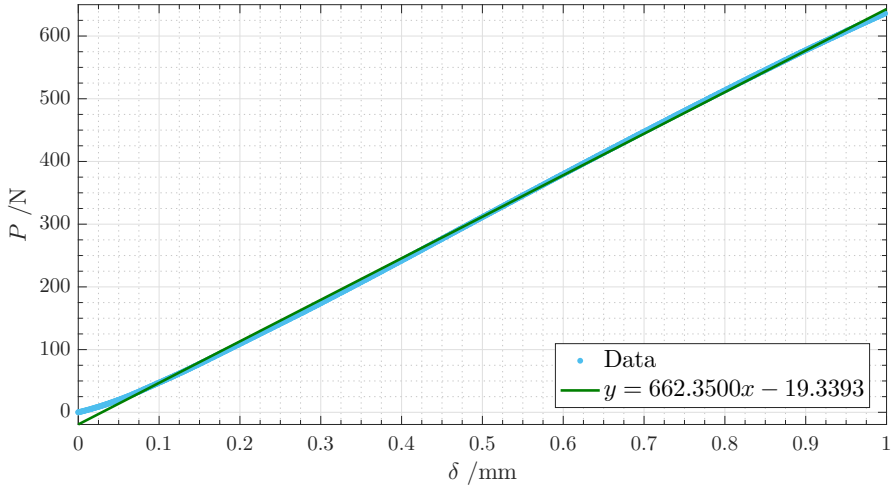


(b) 2^{nd} measurement

Figure 5.38. PCB model 6 load-displacement curves, in direction 1

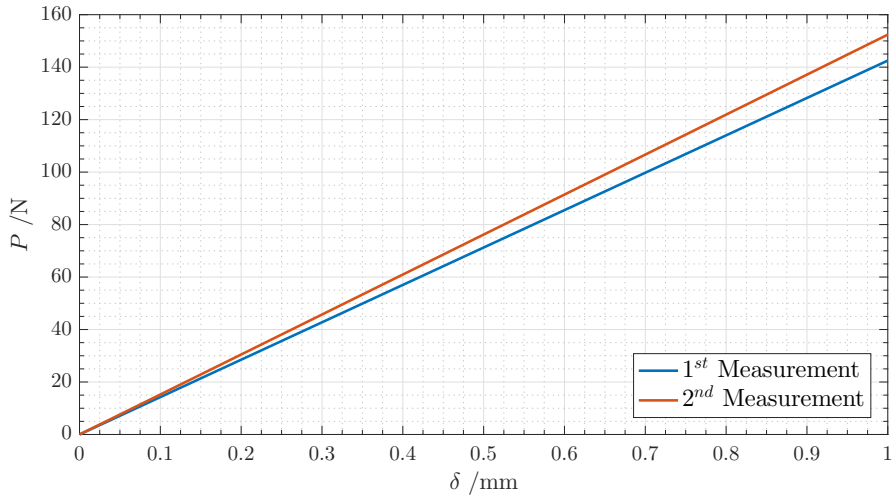


(a) 1^{st} measurement

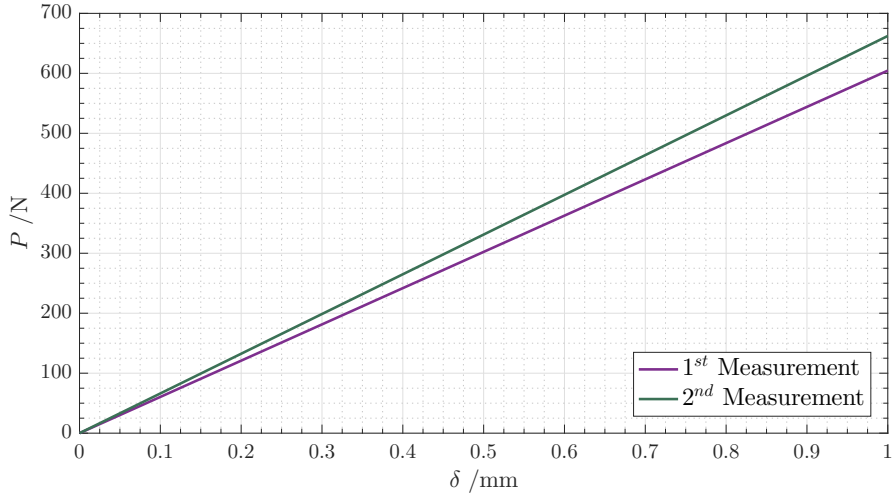


(b) 2^{nd} measurement

Figure 5.39. PCB model 6 load-displacement curves, in direction 2



(a) Measurements in direction 1



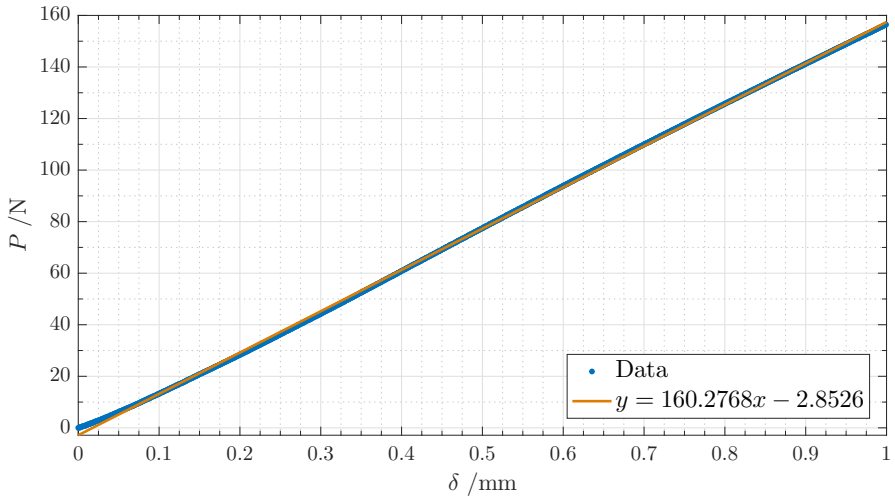
(b) Measurements in direction 2

Figure 5.40. PCB model 6 slope comparison, in directions 1 and 2

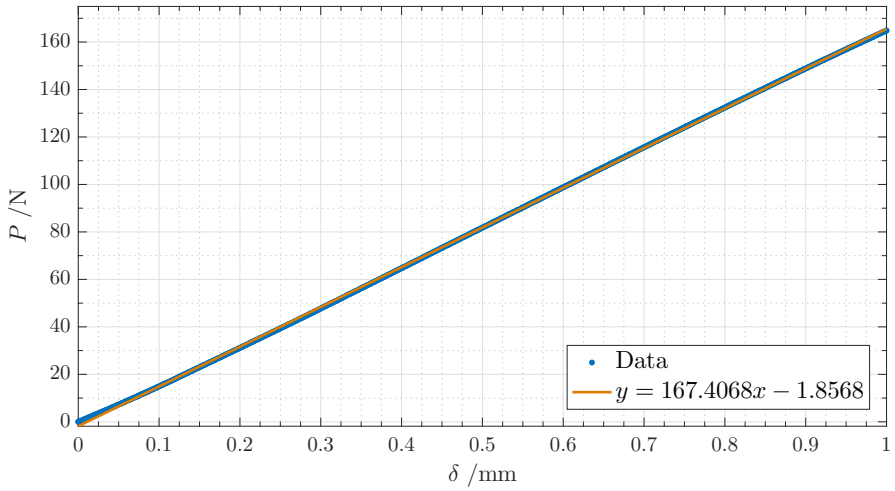
Table 5.11. PCB model 6 slope and flexural properties

PCB model 6	m /N·mm^{-1}	E_f /GPa
Direction 1	142.5044	19.786
	152.3840	21.158
Direction 2	604.5594	18.843
	662.3500	20.644

PCB model 12

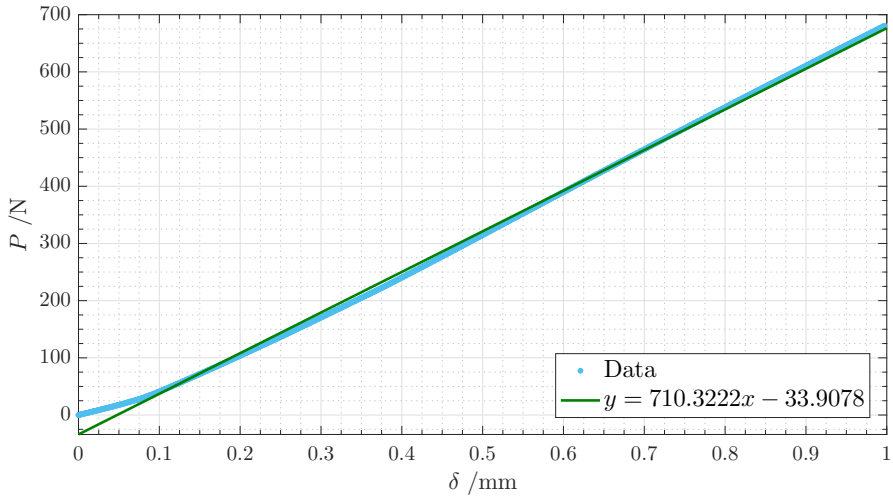


(a) 1^{st} measurement

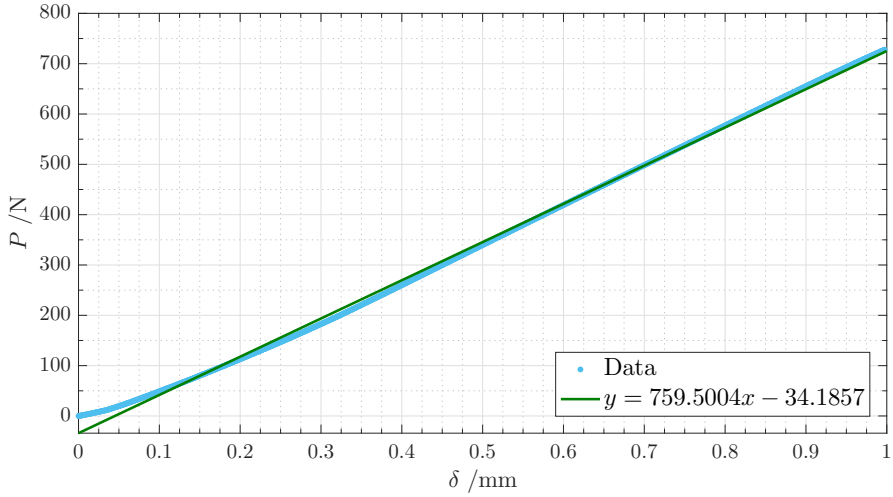


(b) 2^{nd} measurement

Figure 5.41. PCB model 12 load-displacement curves, in direction 1

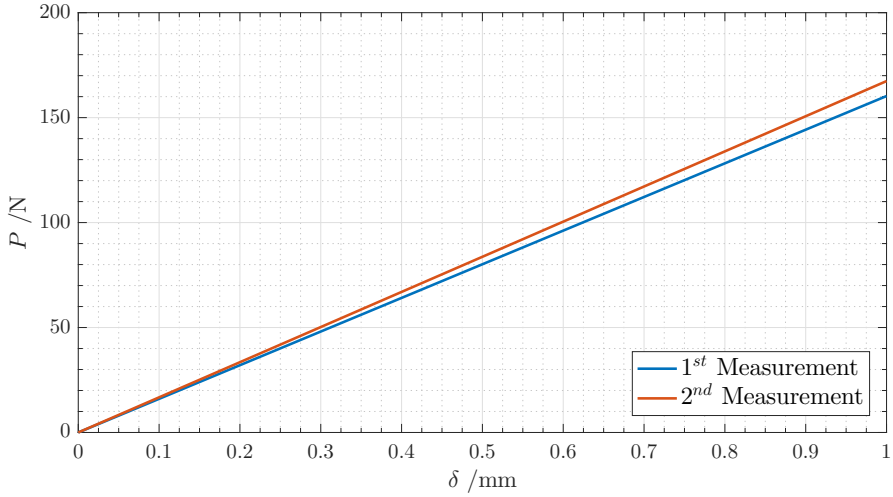


(a) 1^{st} measurement

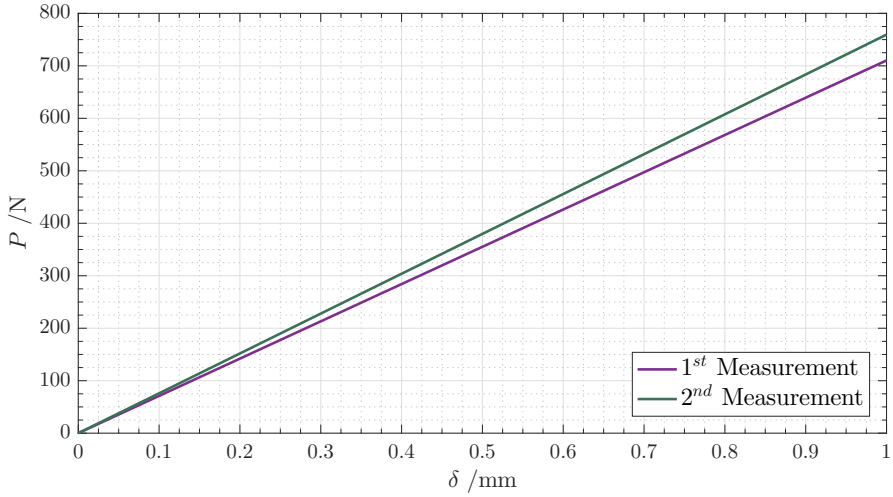


(b) 2^{nd} measurement

Figure 5.42. PCB model 12 load-displacement curves, in direction 2



(a) Measurements in direction 1



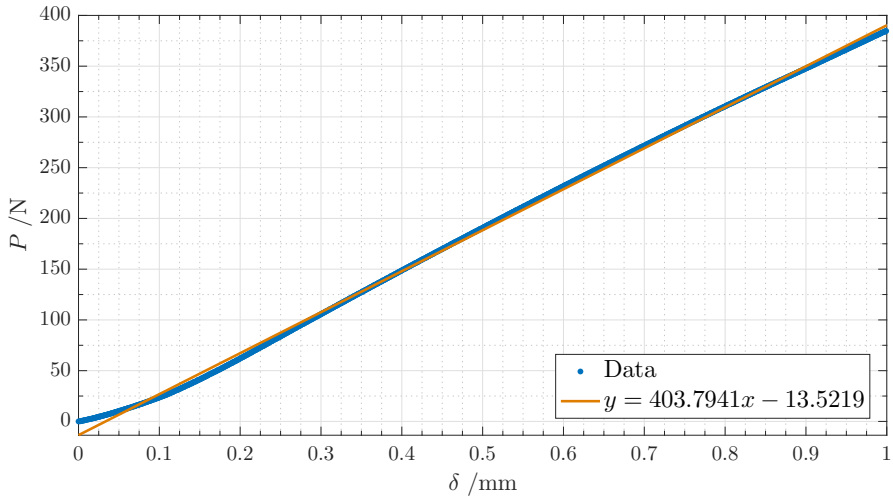
(b) Measurements in direction 2

Figure 5.43. PCB model 12 slope comparison, in directions 1 and 2

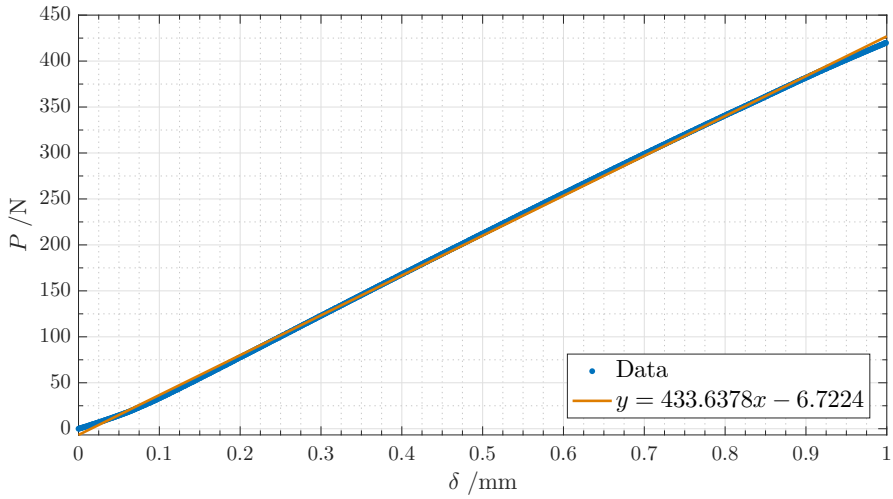
Table 5.12. PCB model 12 slope and flexural properties

PCB model 12	m /N·mm^{-1}	E_f /GPa
Direction 1	160.2768	24.452
	167.4068	25.540
Direction 2	710.3222	20.010
	759.5004	21.396

PCB model 14

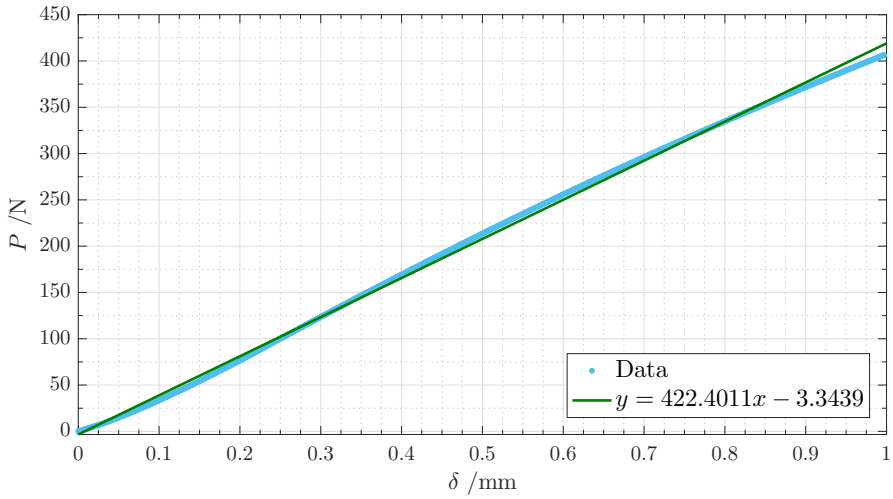


(a) 1^{st} measurement

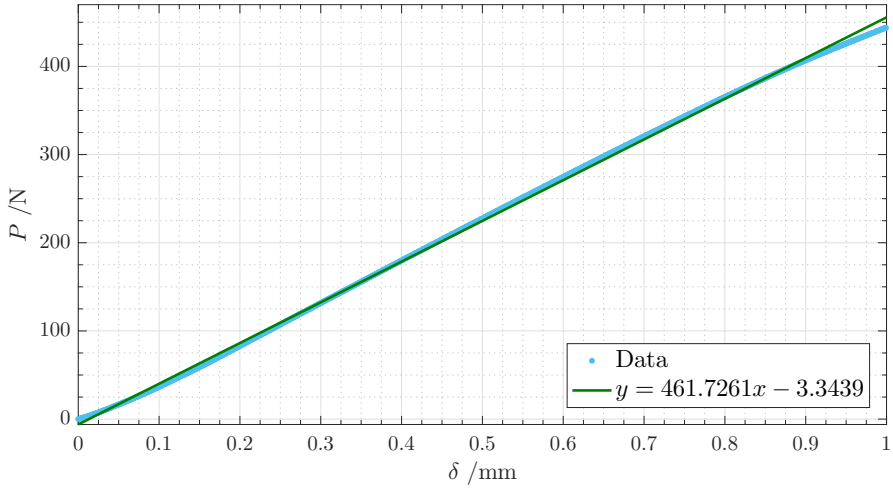


(b) 2^{nd} measurement

Figure 5.44. PCB model 14 load-displacement curves, in direction 1

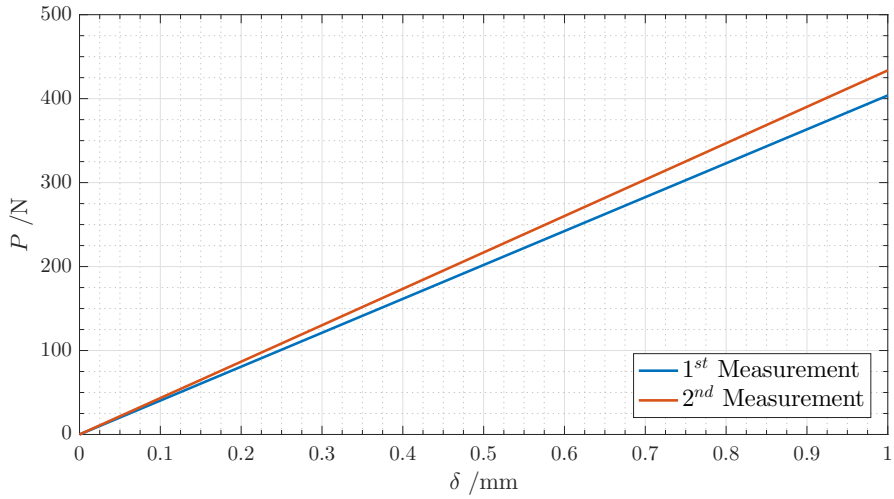


(a) 1^{st} measurement

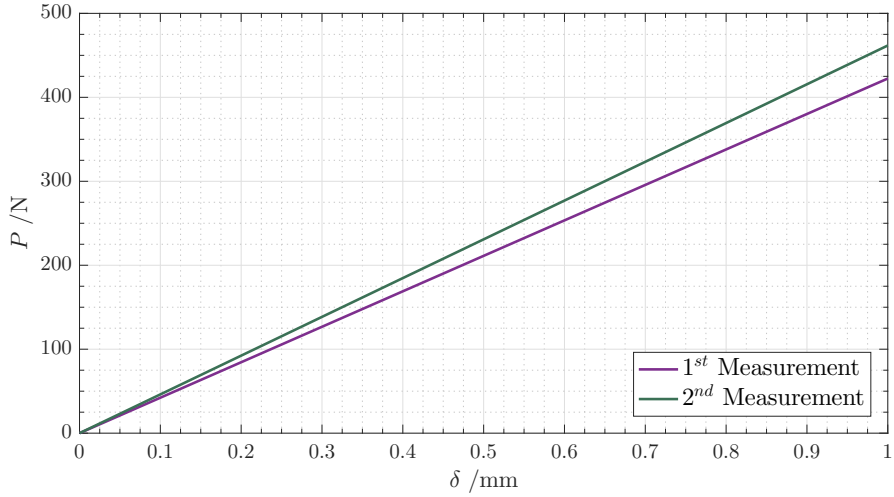


(b) 2^{nd} measurement

Figure 5.45. PCB model 14 load-displacement curves, in direction 2



(a) Measurements in direction 1



(b) Measurements in direction 2

Figure 5.46. PCB model 14 slope comparison, in directions 1 and 2

Table 5.13. PCB model 14 slope and flexural properties

PCB model 14	m /N·mm^{-1}	E_f /GPa
Direction 1	403.7941	29.530
	433.6378	31.712
Direction 2	422.4011	27.029
	461.7261	29.545

5.5.4 Discussion

Based on the obtained curves for the different PCB models' specimens, the derived flexural stiffness values obtained are equally contained in the window of $14 - 28$ GPa [5], with the exception of models 5 (in longitudinal direction) and 14 (in both directions). For the former model, the fact of not having specimen variability does not clarify if the 31.801 GPa value is the real one or if the material has internal flaws, originated during the manufacturing process. On the other hand, and as stated in **Chapter 4**, the former model is still under development. Therefore, this reason can explain why the derived values are out of the window range. In further developments, with geometric and material changes in the model, the new flexural stiffness values could be decreased, being then contained within the defined stiffness interval.

Contrary to what was previously supposed, the fact that the closer every specimen's shape is to a rectangle does not necessarily imply that the material can be treated as quasi-isotropic. In fact, PCB models 5 and 12 have a considerable difference between the flexural stiffness values in direction 1 and 2, as seen in **Tabs. 5.10** and **5.12**, respectively.

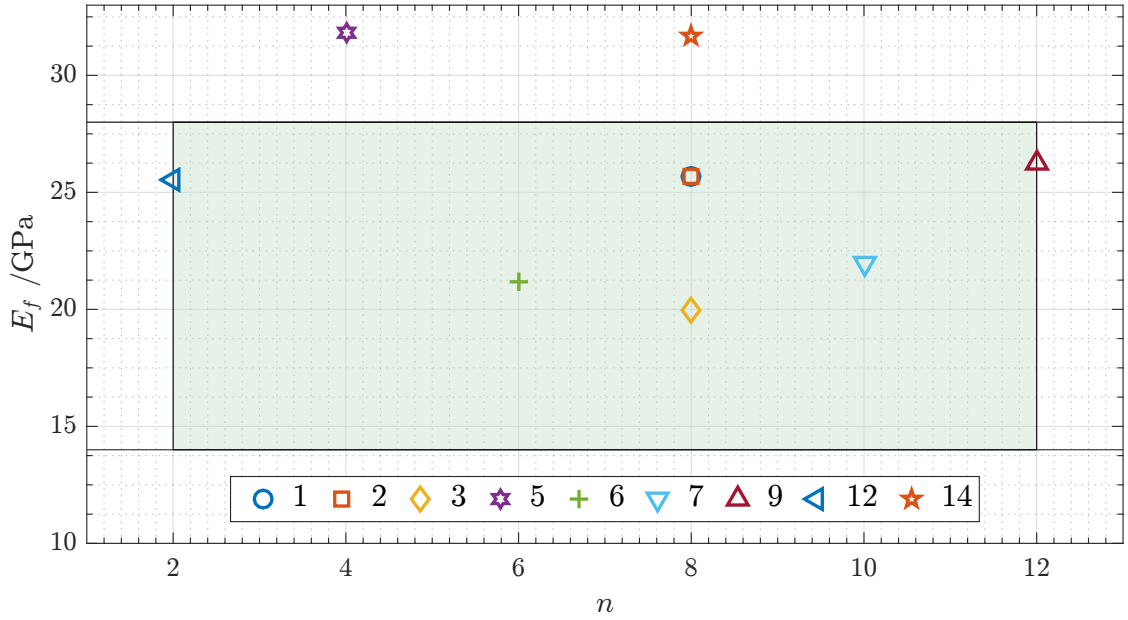
Although the four-point bending tests are more appropriate to lengthier specimens[4] [39], the intention behind performing them on the selected specimens lied on the absence of vertical shear forces. However, a less desired convergence between the numerical and experimental results was verified, whose potential reasons are explained in the next **Chapter 6**.

5.6 Global Remarks

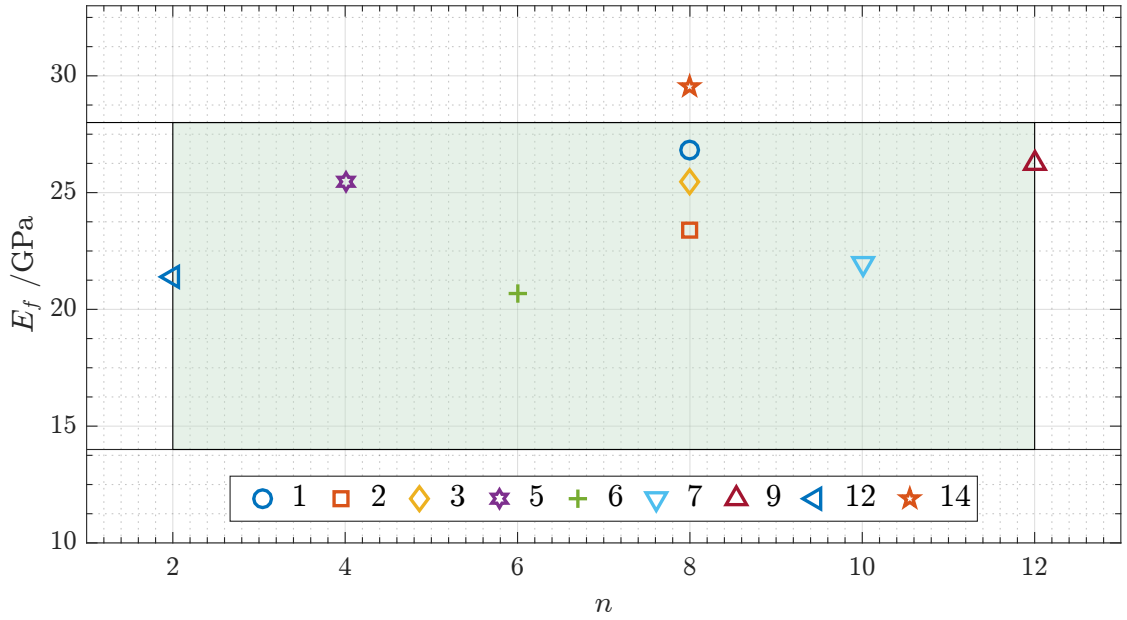
As referred in the previous **Chapter 4**, if a relation between the the flexural stiffness and the number of copper layers of any printed circuit board would be found, a clearer perception of their mechanical properties would be obtained. This E_f versus n relation was analysed for both longitudinal and transversal directions, as illustrated in **Fig. 5.47**.[5]

[4] PCB model 9 specimen would have been the right choice for this test.

[5] The green shaded area contains the $14 - 28$ GPa flexural stiffness window for FR-4, based on [5].



(a) Longitudinal direction

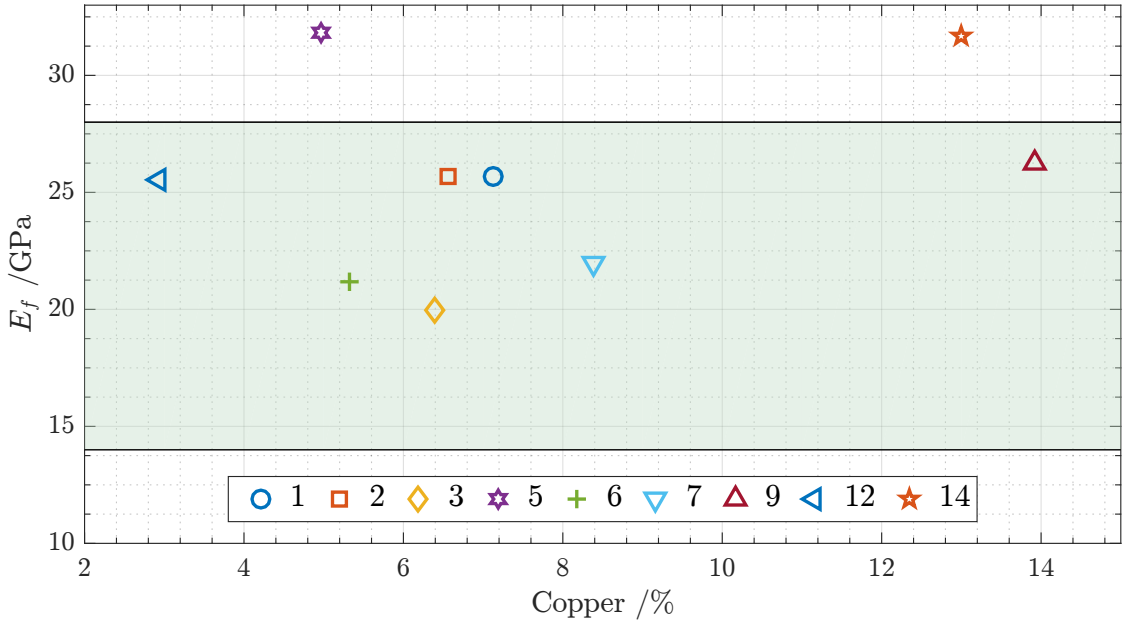


(b) Transversal direction

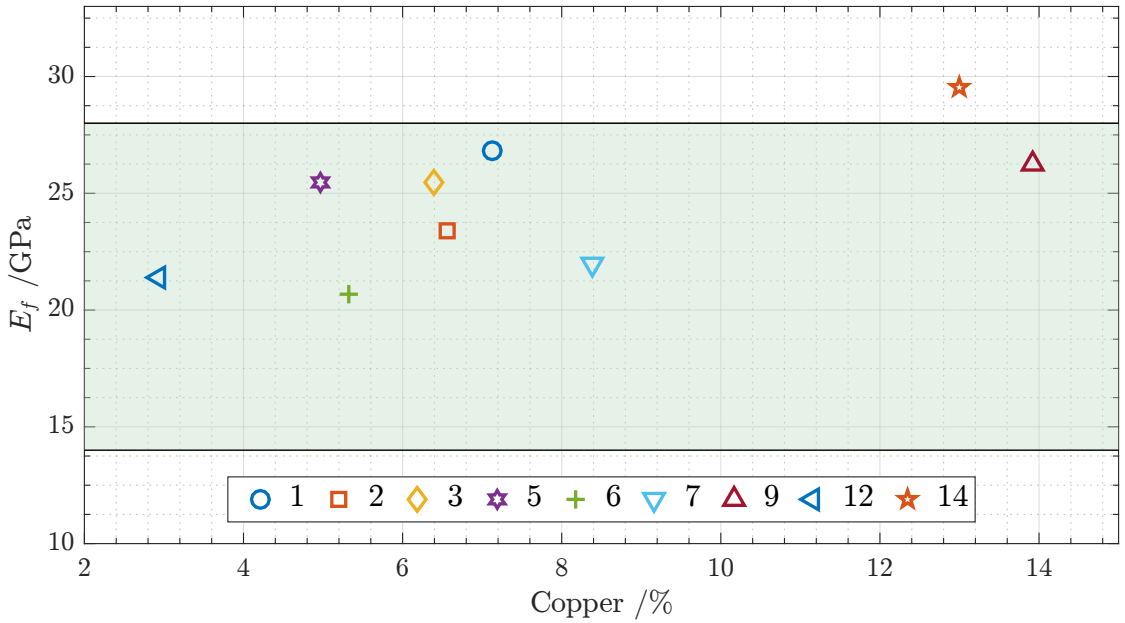
Figure 5.47. Flexural Young modulus in function of the number of copper layers of the selected PCB models, in longitudinal and transversal directions

As perceived from the two previous illustrations, no relation between the mechanical properties of the selected PCB models and their number of copper layers can be established. Furthermore, if now opting for comparing with the copper percentage of each printed circuit board[6], the same conclusion can be drawn (**Fig. 5.48**).

[6] Extracted from the Gerber file of each PCB model.



(a) Longitudinal direction



(b) Transversal direction

Figure 5.48. Flexural Young modulus in function of the copper percentage of the selected PCB models, in longitudinal and transversal directions

These observations confirm what has been referred by Bosch CM – Braga, *i.e.* no direct relation between the number of copper layers and the mechanical properties of a PCB model can be obtained. Additionally, two other factors that may have influence in the mechanical properties of a printed circuit board are the FR-4 layers orientation and the pre-preg used [15].

5.7 Summary

This chapter covered the overview and methodology of the 3PB and 4PB tests. The mechanical properties of every printed circuit board model were determined, and the results obtained were within the expected range. However, no linear relation between the flexural stiffness and the number of copper layers or copper percentage could be identified.

The next step is, through numerical modelling, create material models of the tested specimens, under either 3PB or 4PB test conditions, and validate them. By having a validated material model of every PCB model, other parameters (*e.g.* stress and strain) can be obtained feasibly. Further, by solely modelling the PCB, no extra stiffness – added by modelling the electronic components – is being considered. Therefore, by working with lower stiffness values for every PCB model, a safety margin is being applied.

Chapter 6

Numerical Modelling

This chapter covers the numerical validation of the three and four-point bending tests using finite element models and a parametric evaluation study. For these purposes, the commercial software Abaqus 2017 was used. Depending on the type of experimental test, a material model with the same experimental configuration was created to capture the real conditions under which PCB models specimens were tested. Their geometry was simplified to a rectangular plate. The support and loading noses were initially modelled as rigid cylinders, and then as analytical surfaces, respecting the dimensions of each experimental test. For comparison purposes, the material properties obtained from the experimental results – flexural stiffness, in longitudinal and transversal directions – were inserted in the material model. The numerical outputs (load and displacement values) were compared to the ones obtained experimentally for the longitudinal direction. As previously mentioned, by considering only the PCB, the critical values for the stress and strain values are within a safe margin, since modelling the components leads to stiffness increase. Although no information about the candidate areas of failure in the components, it is guaranteed that this scenario never occurs.

Besides conducting the numerical validation for the three and four-point bending tests, a parametric evaluation was conducted. Seven different scenarios were created and the influence of the variation of certain parameters on the obtained outputs (load-displacement curve) was evaluated. These scenarios include the variation of a PCB model's number of layers, thickness, size and mechanical properties.

6.1 Overview

Firstly, the three-point bending test material models were created and tested. Formerly, the four-point bending test ones were improved, based on the previous registered flaws.

For both three and four-point bending tests, the PCB was modelled as a quasi-isotropic material, not discriminating its alternating copper and FR-4 layers. The only material property obtained from the experimental tests was the flexural stiffness in longitudinal and transversal directions (E_1 and E_2, respectively). The values of the Poisson ratio were arbitrated, set to 0.2. The reason behind this flexible assumption can be justified by the little (or even null) traction influence on the printed circuit boards' mechanical behaviour, since it does not occur in bending cases. In order to validate the material models, load and displacement values at the center location of the specimens, obtained both from experiment and the simulation, were compared carefully [19].

On the other hand, for the parametric evaluation, copper and FR-4 material properties were considered, obtained from [74; 75]. The different selected scenarios consider printed circuit boards with:

1. **Equal number of layers and different copper surface thickness**
2. **Equal size and different number of layers**
3. **Different size and equal number of layers**
4. **Stack-up with FR-4 only**
5. **Different orientations of the FR-4 layers**
6. **Simplified geometry versus exact geometry**
7. **Thickness variation**

6.2 Three-point bending tests

The three-point bending tests numerical modelling considered the three PCB models selected for the respective experimental test, covered in **Section 5.4**. It follows an explanation of the material model set-up, proceeded by the display and discussion of the results.

6.2.1 Set-up

For illustration purposes, the following images correspond to the PCB model 7 material model.

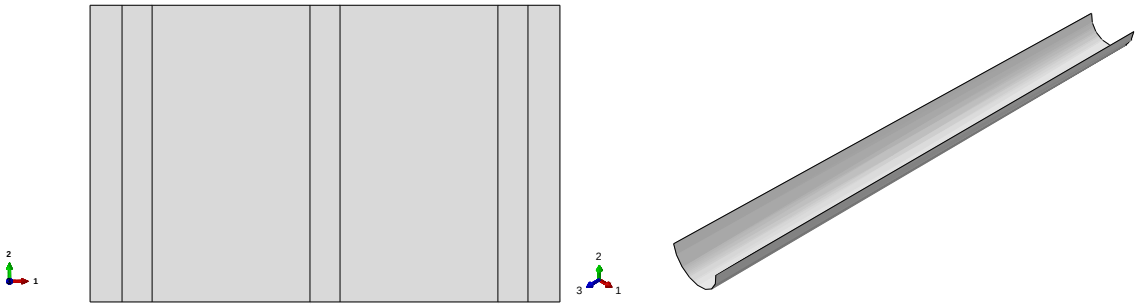
Parts

The material model for every PCB model's geometry resumes with the creation of its parts – a rectangular plate and a half cylinder, corresponding to the loading and support noses. The plate has a defined length and width, depending on the PCB model. The cylinder's depth is limited by the width (in direction 1) or length (in direction 2) of the PCB specimen, guaranteeing that the loaded surface is entirely covered. The diameter of the cylinder is the same as the one used for the experimental tests, equal to 8 mm. The plate was partitioned in three sections, being two for the supports and one for the loading noses. Initially, every cylinder was set as a rigid component.[1]

Every simulation is composed by three cylinders – two supporting the plate and one loading it – and a rectangular plate, which resembles the PCB plate.[2]

[1] Later in this analysis, its type was set as "analytical", as discussed in **Section 6.2.1**.

[2] Not every PCB model geometry is completely rectangular. In **Section 6.4.2**, the accuracy of this simplification is evaluated.



(a) Rectangular plate part

(b) Cylinder part

Figure 6.1. Three-point bending material model parts

Material Properties

The inserted material properties are the flexural stiffness (corresponding to the Young modulus) measured in directions 1 and 2 (E_1 and E_2, respectively). The selected type of properties was "Engineering Constants". Additionally, this requires the values of the flexural stiffness in direction 3 (E_3) and of the Poisson ratio ν and Shear modulus G, in each of the three directions – ν_{12}, ν_{13}, ν_{23} and G_{12}, G_{13}, G_{23}. As previously stated, the latter two parameters have little influence on the outputs of this simulations, once the mechanical behaviour is not affected by traction effects. Therefore, the Poisson ratio values were fixed as 0.2 for every PCB model simulation. To obtain the Shear modulus values, the following formula for isotropic materials was used:

$$G = \frac{E}{2(1+\nu)} \tag{6.1}$$

According to the laminates theory [71], it was assumed that $E_2 = E_3$, $\nu_{12} = \nu_{13}$ and $G_{12} = G_{13}$ (**Fig. 6.2**). The laminate theory is based on some assumptions more. The most important ones are:

- Each layer has a uniform thickness and homogeneous or quasi-homogeneous material properties.
- The material behaviour of each layer is linear elastic in both modes, tension and bending.
- The thickness of the laminate stays constant during the deformation and the deformations are small compared to the thickness [49; 71].

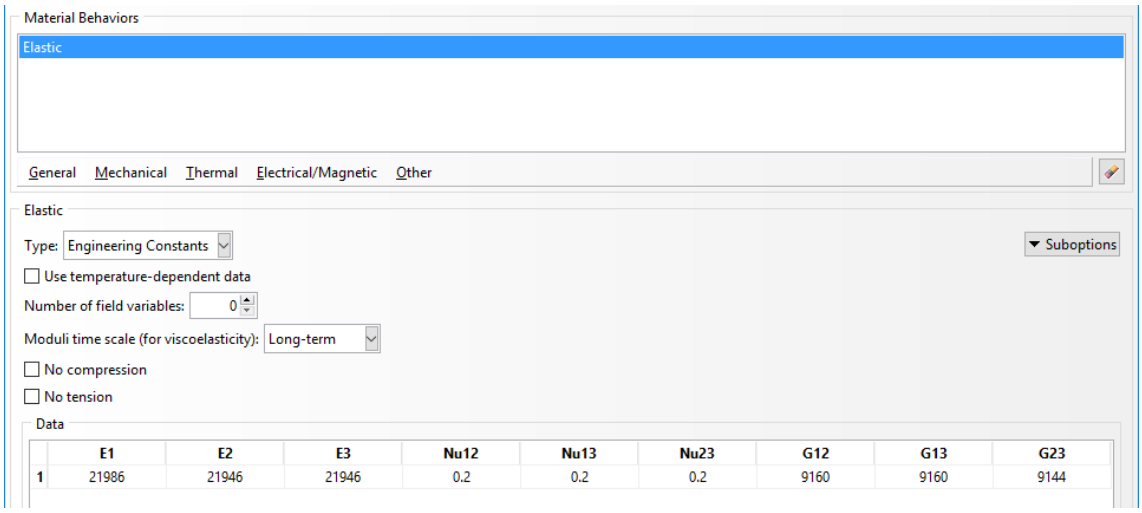


Figure 6.2. Material properties window

Assembly

The assembly consists on gathering the parts and place them in the correct positions, namely aligning the cylinders with the partition lines defined on the plate surface.

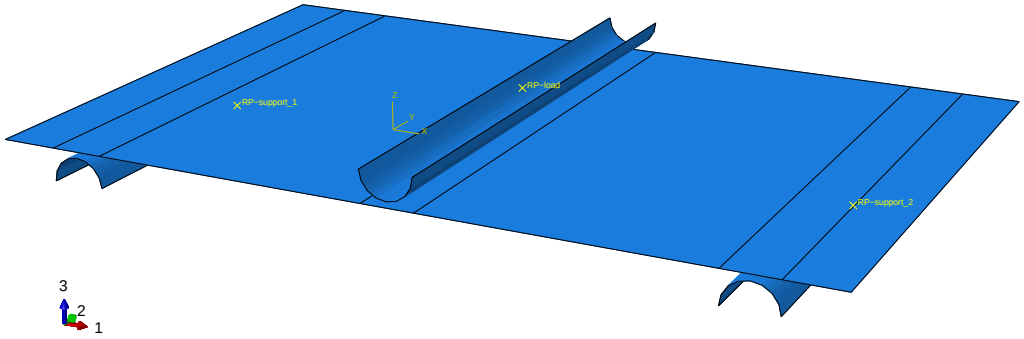


Figure 6.3. Assembly module interface, in Abaqus 2017

Step

Two steps were created:

- **Initial**, in which all the configuration is static.
- **Final**, from the moment the contact is initiated until the final prescribed displacement is reached.

Initially, Abaqus default time-step was being considered, and the obtained load values were not consistent with the experimental results. In order to obtain more accurate values, the number of increments was increased (meaning that the time-step values were reduced), so that the numerical load values better converged to the experimental ones.

Interaction

In this module, the contact between the cylinders and the plate is defined. Therefore, three "surface-to-surface" contact conditions were created, one for each of the cylinders, by

selecting the master and slave surfaces. The former corresponded to the cylinders contact surface with the plate, and the latter always to the plate. A contact interaction property was created, and a residual friction coefficient value was added, in order to improve the model convergence. Lastly, three reference points were defined, each corresponding to the middle point of support and load cylinders.

This interaction sequence was used for the three 3PB material models.

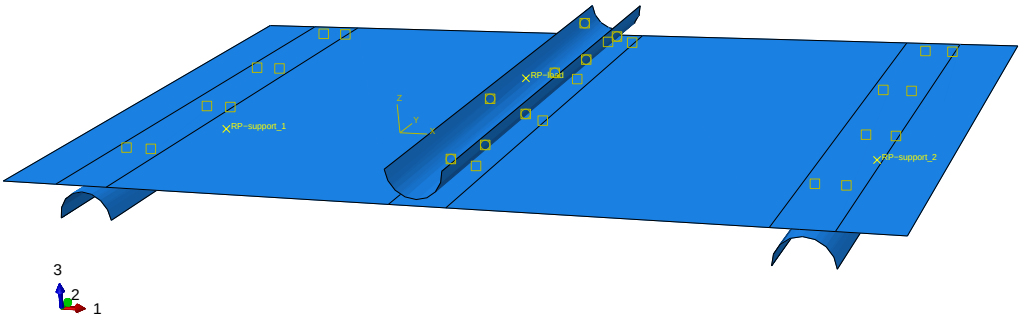


Figure 6.4. Interaction module interface, in Abaqus 2017

Load

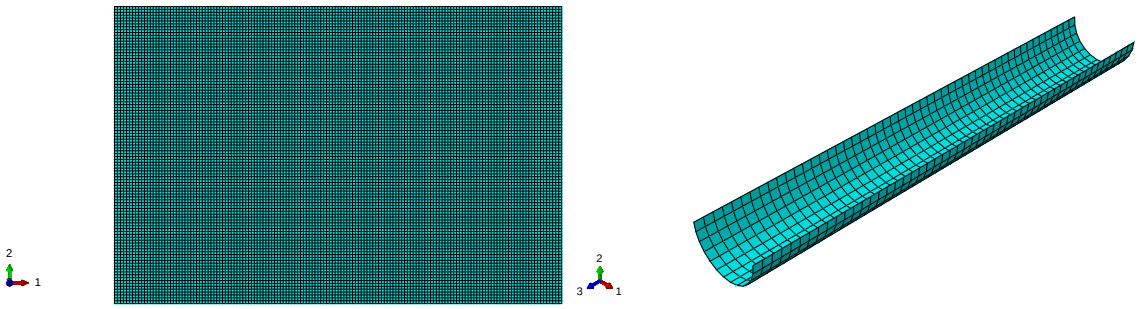
Three boundary conditions were created:

- Null displacement and rotation of the support cylinders.
- Null U_1 and U_2 displacements and rotation of the loading cylinder.
- U_3 displacement of 2 mm applied to the load cylinder.

Similarly, this loading sequence was also used for the three 3PB material models.

Mesh

For the plate, a quadrangular element with reduced integration, a linear geometric order[3] was used and approximate global seed size of 0.5. The use of a finer mesh would bring no improvement to the results (**Fig. 6.5**). On the contrary, the cylinder meshing had to be reformulated several times.



(a) Plate mesh

(b) Cylinder mesh

Figure 6.5. Meshing of the plate and cylinder parts, in Abaqus 2017

[3] The use of a quadratic order would just increase the computational time, with no results improvement in this case.

It was verified that, in the obtained load-displacement curve, a discontinuity would appear, even when trying with sequentially finer meshes – 1.0, 0.5 and 0.25 global seed sizes. This occurrence can be due to the interaction module, in which the contact was unstable. Therefore, one decided to create a new part for the cylinder, defining it as an "analytical rigid" one, *i.e.* it does not need to be meshed, and can instead be described by an analytical function. As seen in **Fig. 6.6**, between the given displacement interval, the slope difference between the different curves is perceived. Although this instability event still occurs once an analytical surface is used, the accuracy of the results is increased.

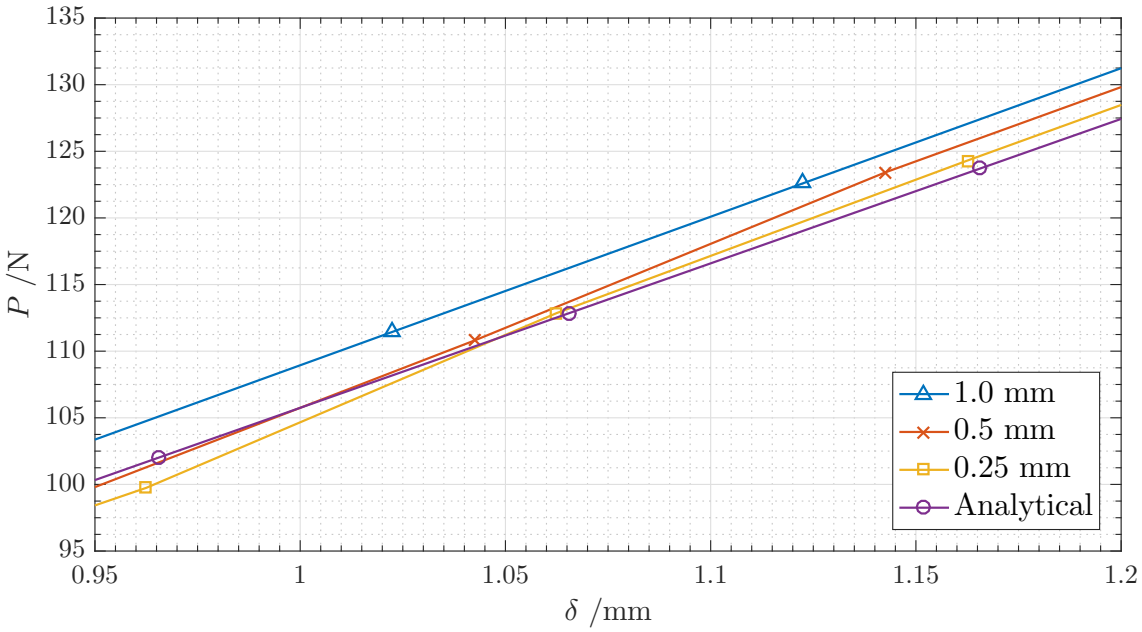


Figure 6.6. Comparison of the cylinders' mesh influence on the load-displacement curve

Since this event was detected, in every following material models, the cylinders were considered as analytical rigid parts.

6.2.2 Results

As previously mentioned, in order to validate each material model, the load and displacement values at the center of the plate were extracted, when the specimen was being loaded along its longitudinal direction. Similarly to the experimental tests, a linear fitting was made to the numerical results. It follows the graphical representation of the displacements' distribution, followed by the comparison between the numerical and experimental load-displacement curves, obtained for the PCB models 3, 7 and 9.

PCB model 3

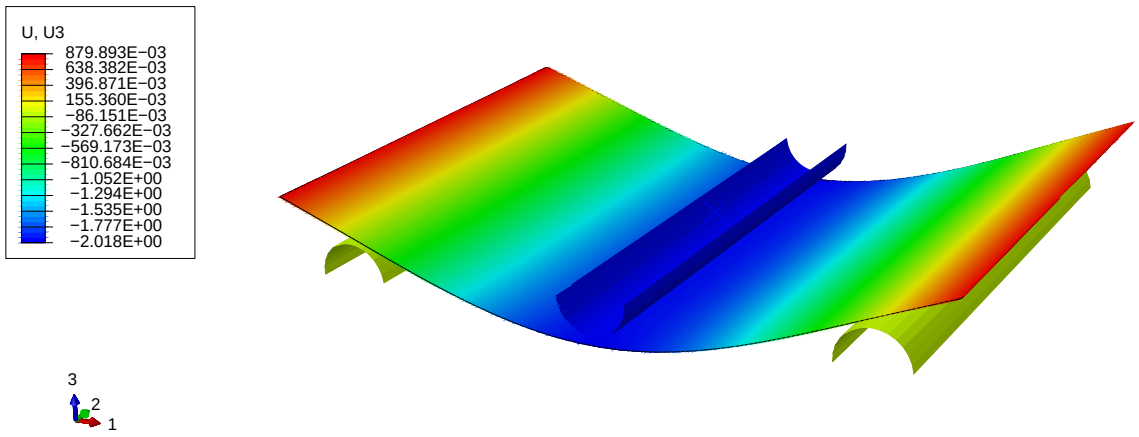


Figure 6.7. Deformed shape with a magnification of U_3 displacement distributions along PCB model 3

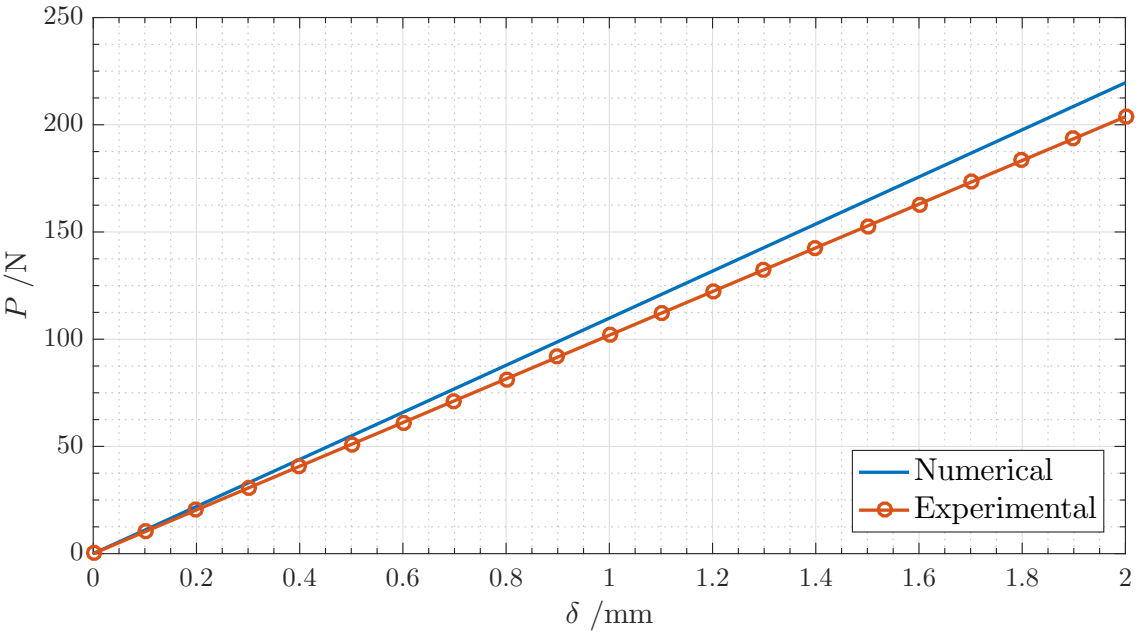


Figure 6.8. Numerical and experimental load-displacement curves comparison, for PCB model 3

PCB model 7

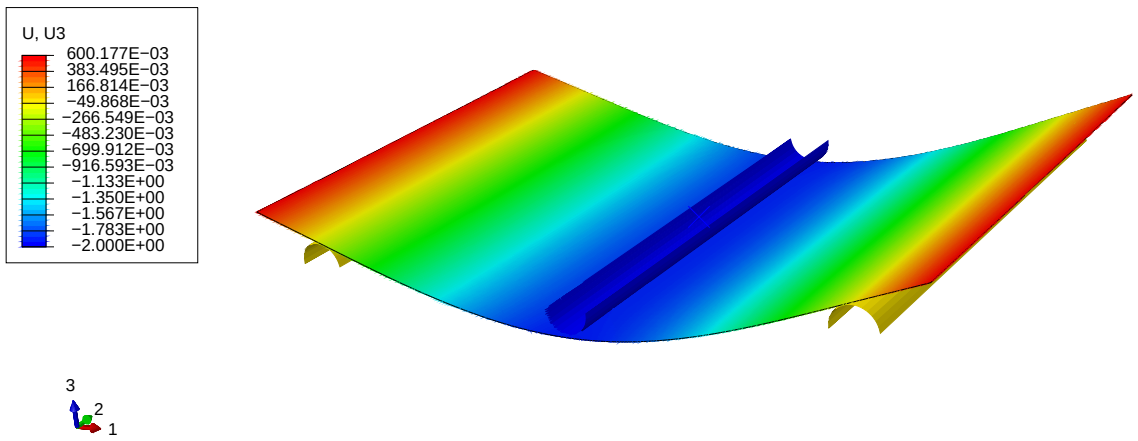


Figure 6.9. Deformed shape with a magnification of U_3 displacement distributions along PCB model 7

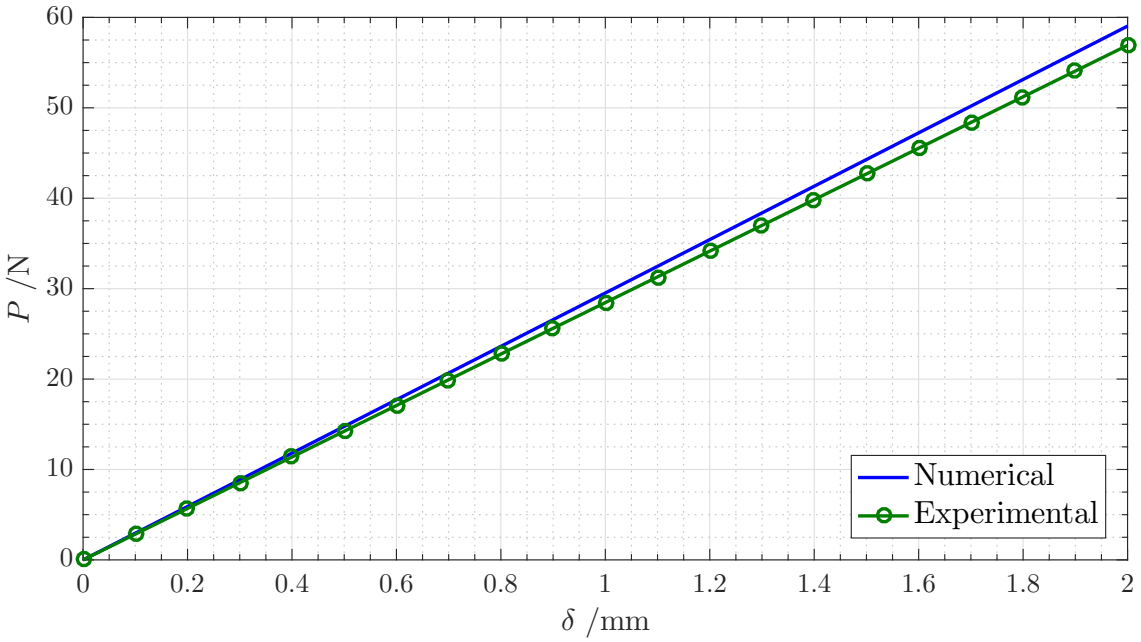


Figure 6.10. Numerical and experimental load-displacement curves comparison, for PCB model 7

PCB model 9

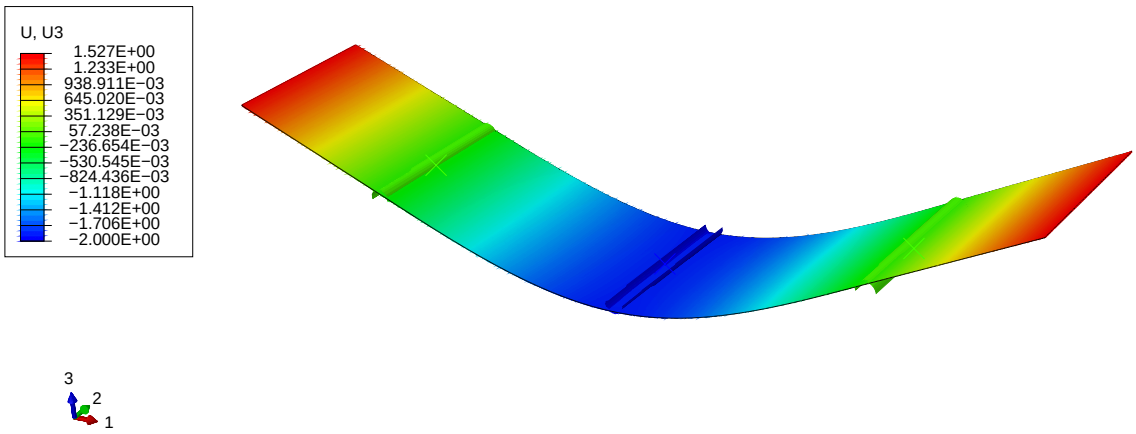


Figure 6.11. Deformed shape with a magnification of U_3 displacement distributions along PCB model 9

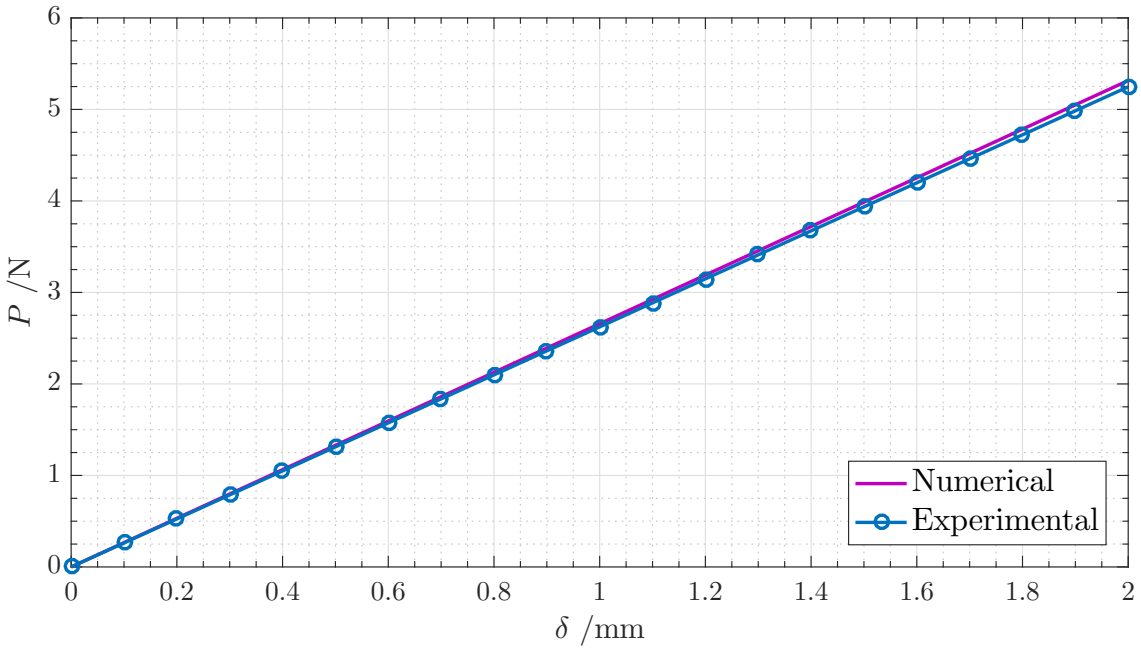


Figure 6.12. Numerical and experimental load-displacement curves comparison, for PCB model 9

6.2.3 Discussion

Based on the previous comparisons, one concludes that, for every PCB model, the numerical slope is always higher than the experimental one. This states that, for a prescribed displacement value, the numerical load is always higher than the experimental one. Therefore, it is reasonable to infer that the printed circuit board specimens may be under-dimensioned.

Although with no clear certainty, the more rectangular the plate, the better the results matching. This is justified by the relative error decrease, as seen in **Tab. 6.1**.

The relative error is equal to:

$$\epsilon_{rel} = \frac{m^{\#x} - m^{def.}}{m^{def.}} \cdot 100 \tag{6.2}$$

A factor N could be introduced, equal to:

$$N = \frac{m_{num}}{m_{exp}} \tag{6.3}$$

Dividing the numerical slope by this factor, the experimental slope to consider in a practical case would be obtained. In other words, once having a material model for a given PCB model, by dividing the correspondent numerical slope by a factor of 1.078[4], the experimental slope can be obtained (**Tab. 6.1**).

Lastly, although experimental errors could have had some influence on the measurements, good matching between the numerical and experimental results was revealed. This means the conceived material models are feasible and reliable.

Table 6.1. Experimental and numerical slopes comparison of the PCB models subjected to the three-point bending tests

PCB model	m_{num}	m_{exp}	ϵ_{rel} /%	N
3	109.8	101.8586	7.80	1.078
7	29.52	28.4573	3.73	1.037
9	2.658	2.6237	1.31	1.013

[4] Value obtained so far. For the four-point bending tests, this value might increase.

6.3 Four-point bending tests

The four-point bending numerical modelling considered the six PCB models selected for the respective experimental test, covered in **Section 5.5**.

6.3.1 Set-up

The set-up is overall similar to the three-point bending material models. However, some new features were added:

- One more cylinder was considered, to serve as the other loading nose, and the diameter was now set to 4 mm.
- Due to the numerical instability of the model (no convergence and horizontal slip of the plate, when the load noses contacted with it), a null U_1 displacement was applied to the middle point of every plate.

6.3.2 Results

This time, the load and displacement values were extracted at the center of each loading cylinder, being the total load equal to the sum of both cylinder loads. Similarly, the specimen was loaded along the longitudinal direction and a linear fitting was made to the obtained load-displacement curves. The graphical representation of the displacement distributions and the comparison between the numerical and experimental load-displacement curves, obtained for the PCB models 1, 2, 5, 6, 12 and 14, is next presented.

PCB model 1

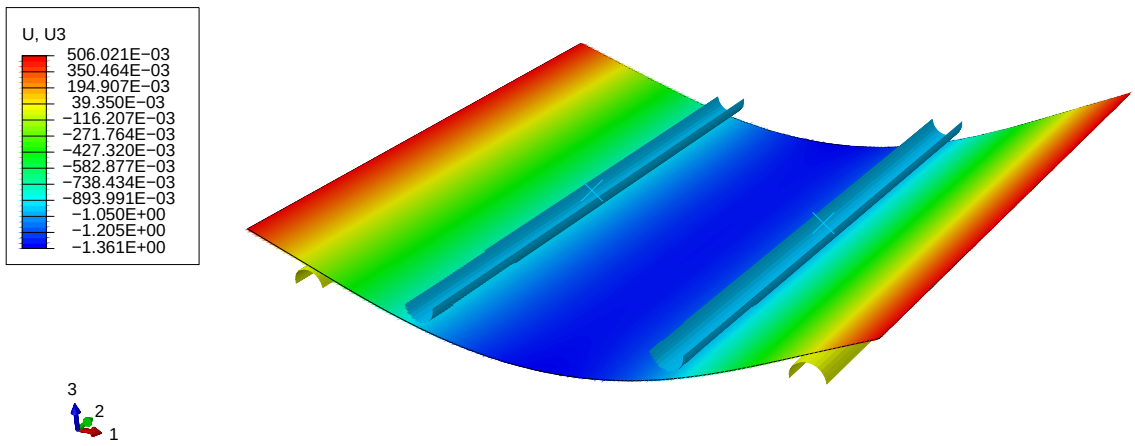


Figure 6.13. Deformed shape with a magnification of U_3 displacement distributions along PCB model 1

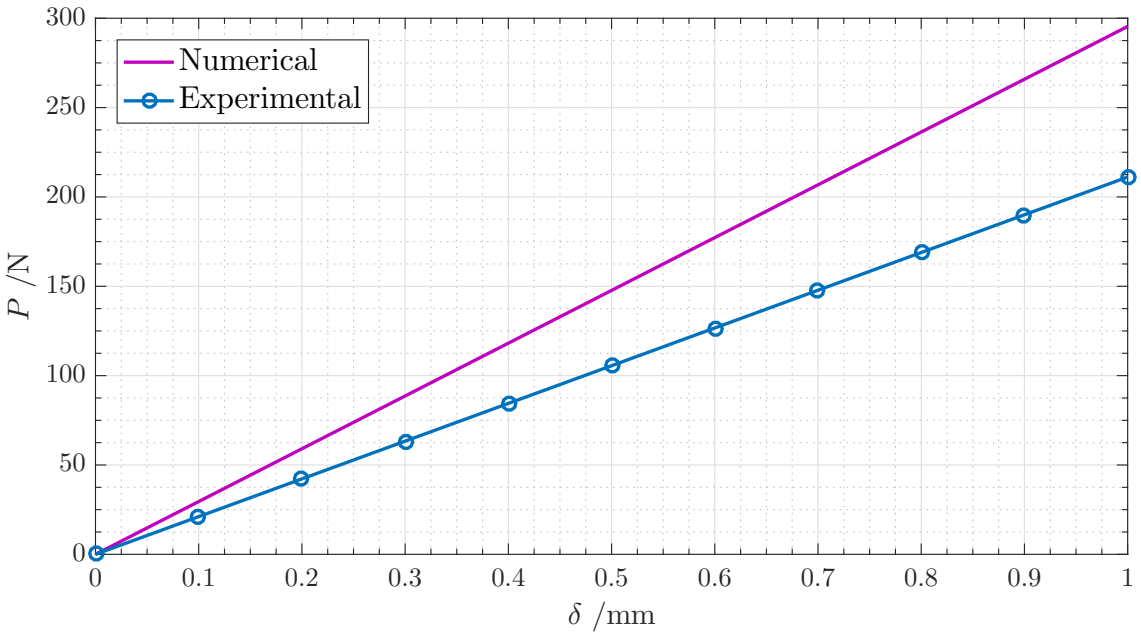


Figure 6.14. Numerical and experimental load-displacement curves comparison, for PCB model 1

PCB model 2

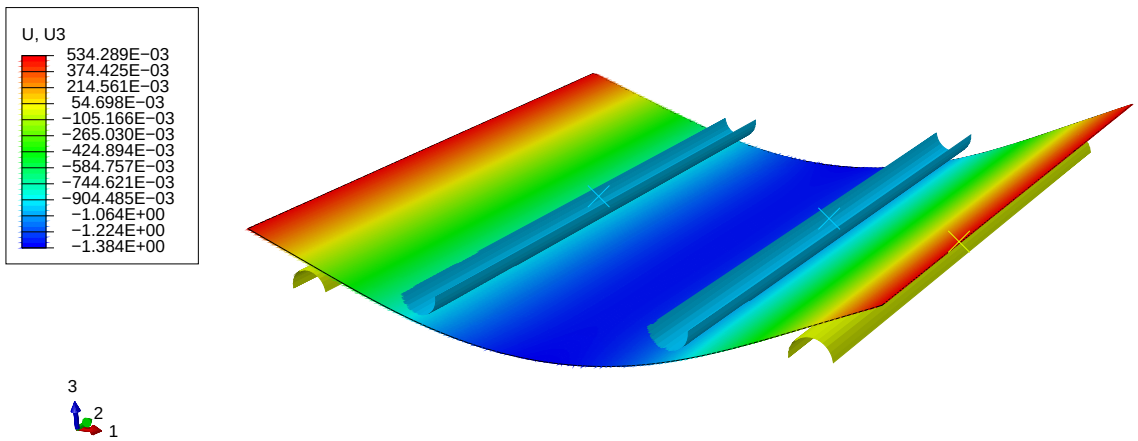


Figure 6.15. Deformed shape with a magnification of U_3 displacement distributions along PCB model 2

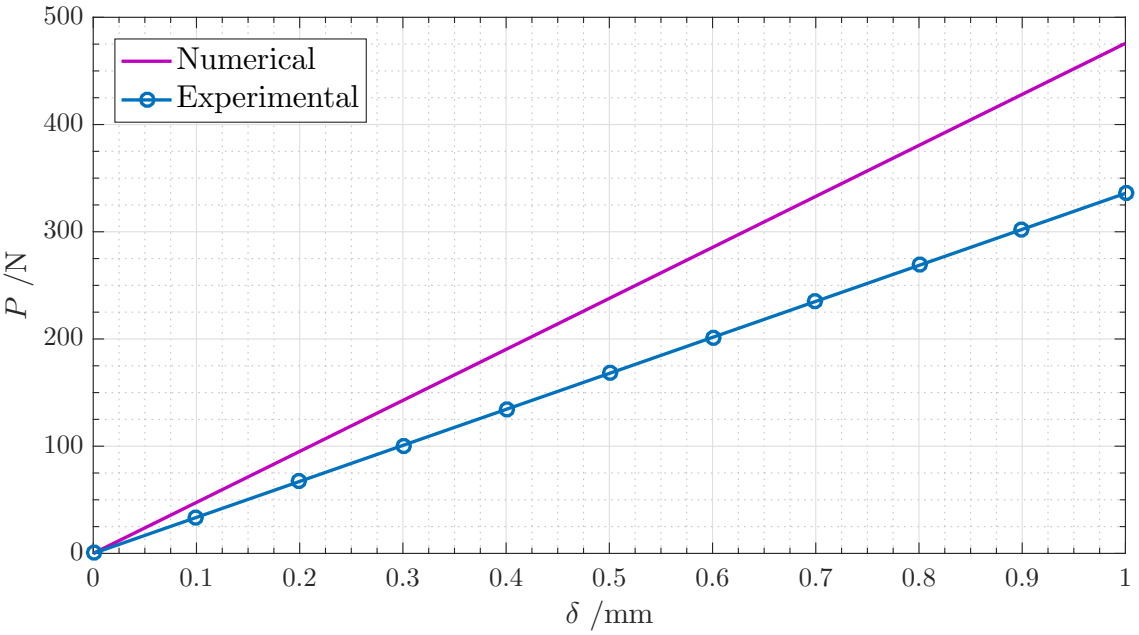


Figure 6.16. Numerical and experimental load-displacement curves comparison, for PCB model 2

PCB model 5

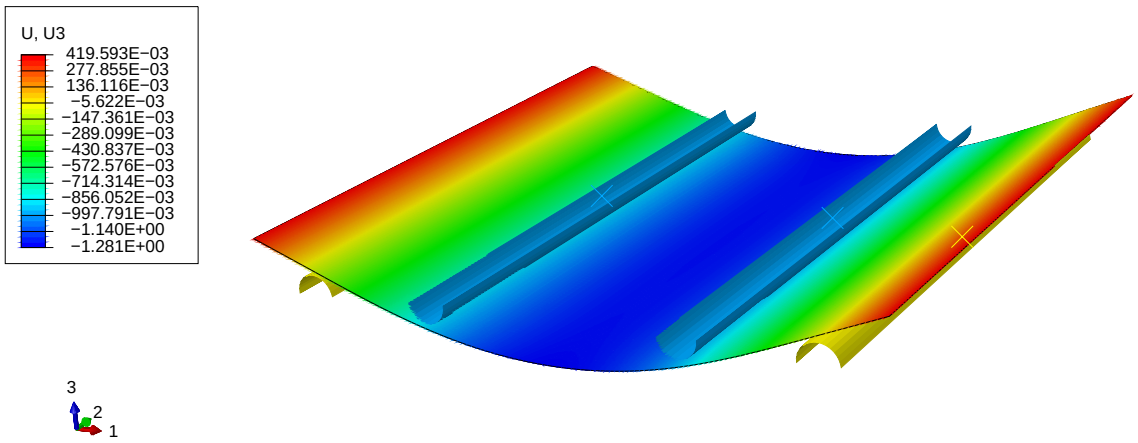


Figure 6.17. Deformed shape with a magnification of U_3 displacement distributions along PCB model 5

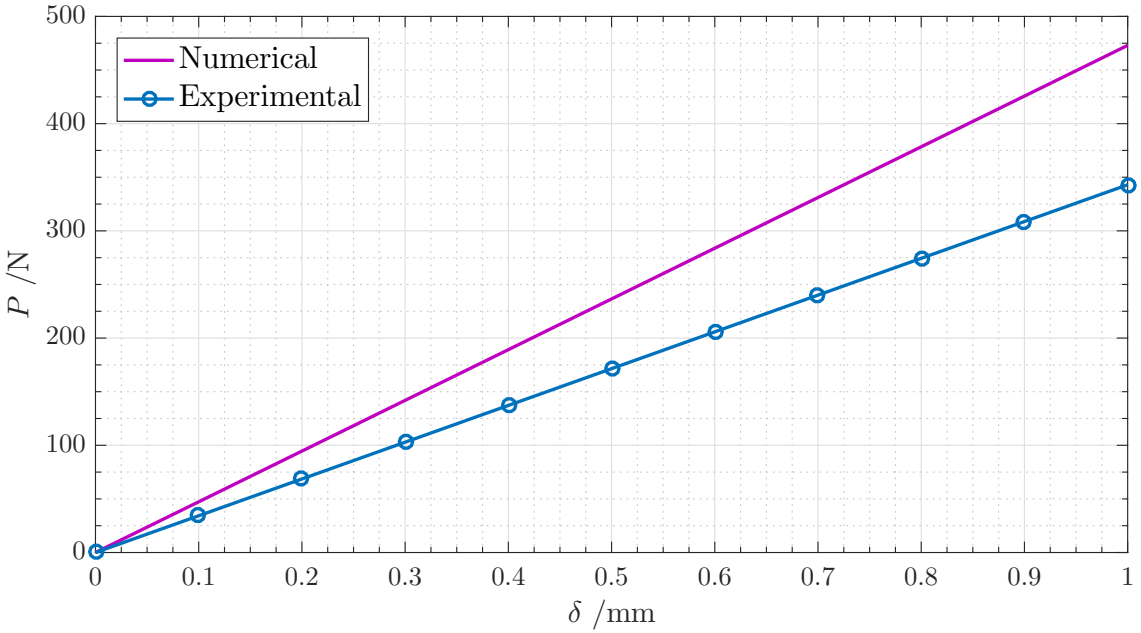


Figure 6.18. Numerical and experimental load-displacement curves comparison, for PCB model 5

PCB model 6

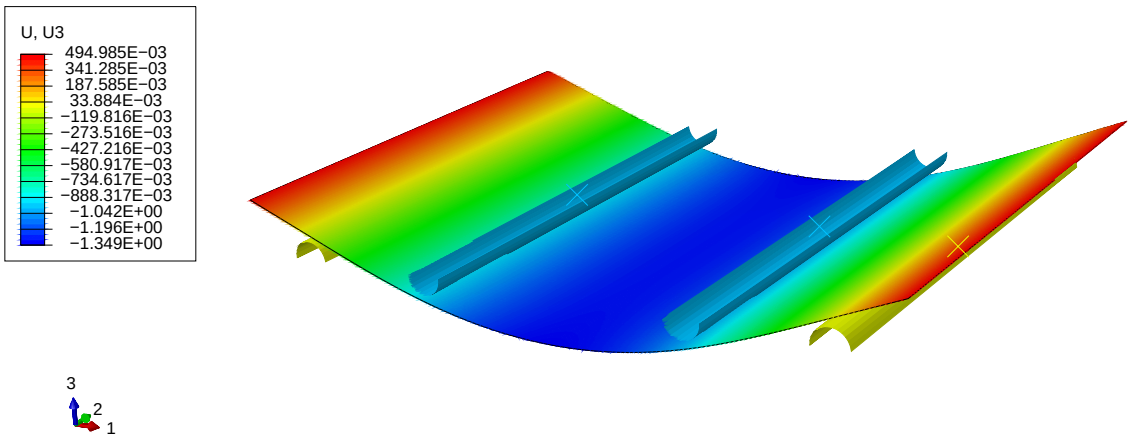


Figure 6.19. Deformed shape with a magnification of U_3 displacement distributions along PCB model 6

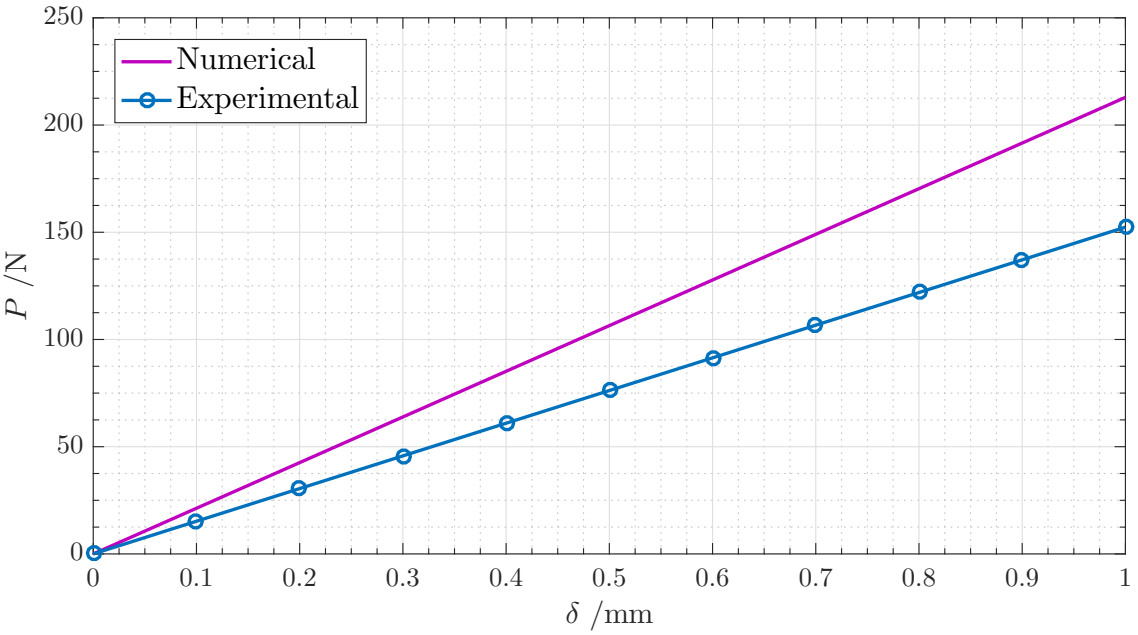


Figure 6.20. Numerical and experimental load-displacement curves comparison, for PCB model 6

PCB model 12

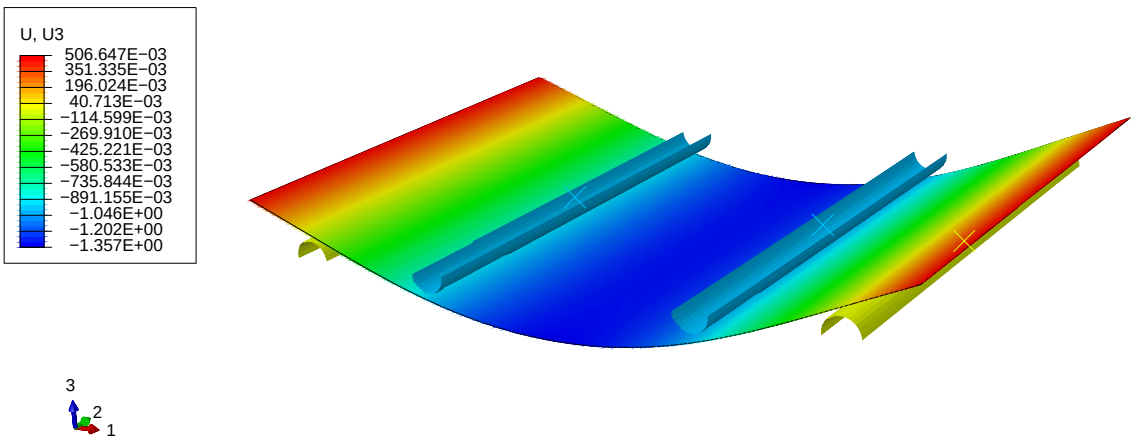


Figure 6.21. Deformed shape with a magnification of U_3 displacement distributions along PCB model 12

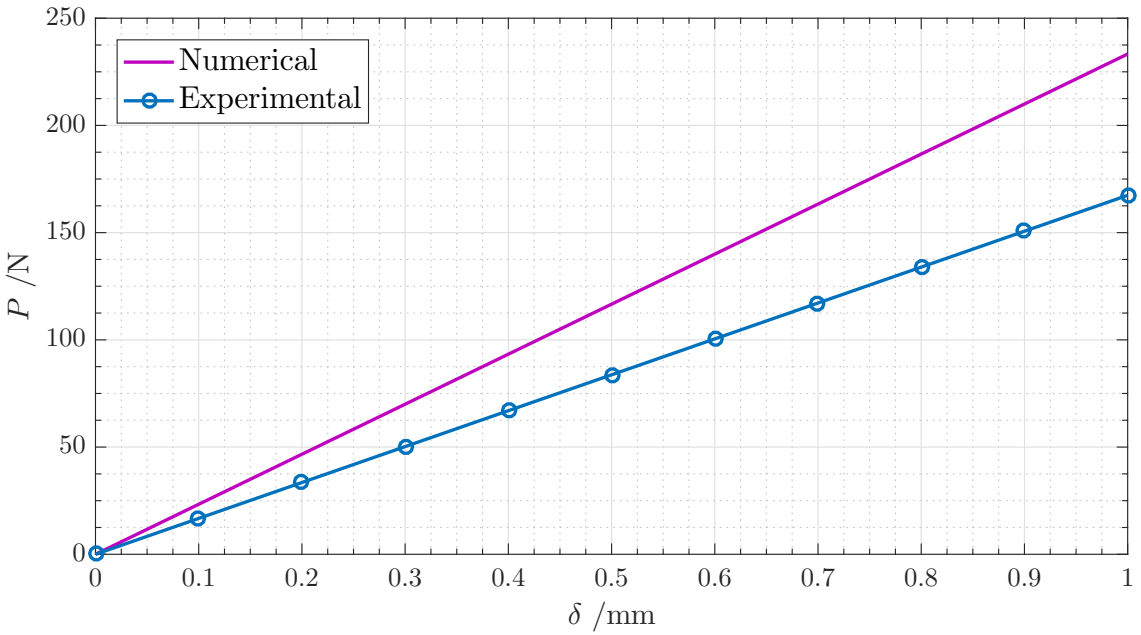


Figure 6.22. Numerical and experimental load-displacement curves comparison, for PCB model 12

PCB model 14

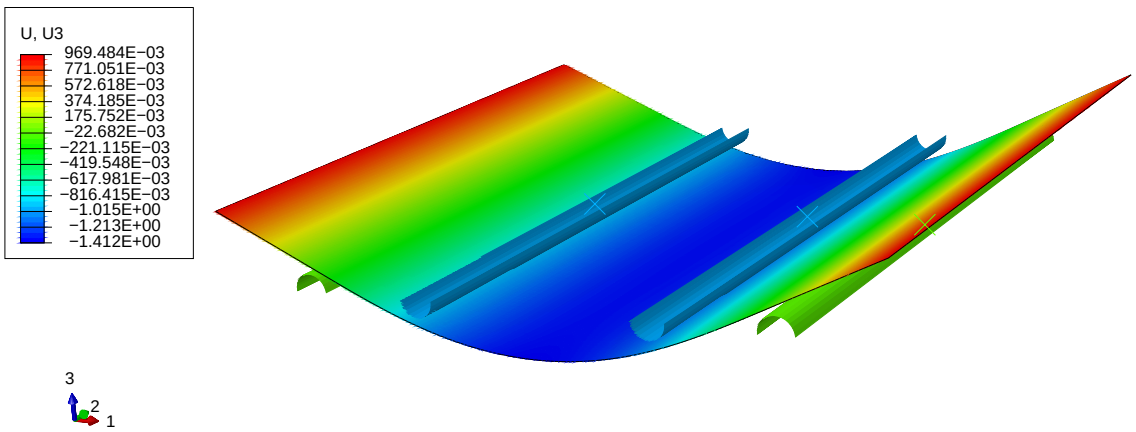


Figure 6.23. Deformed shape with a magnification of U_3 displacement distributions along PCB model 14

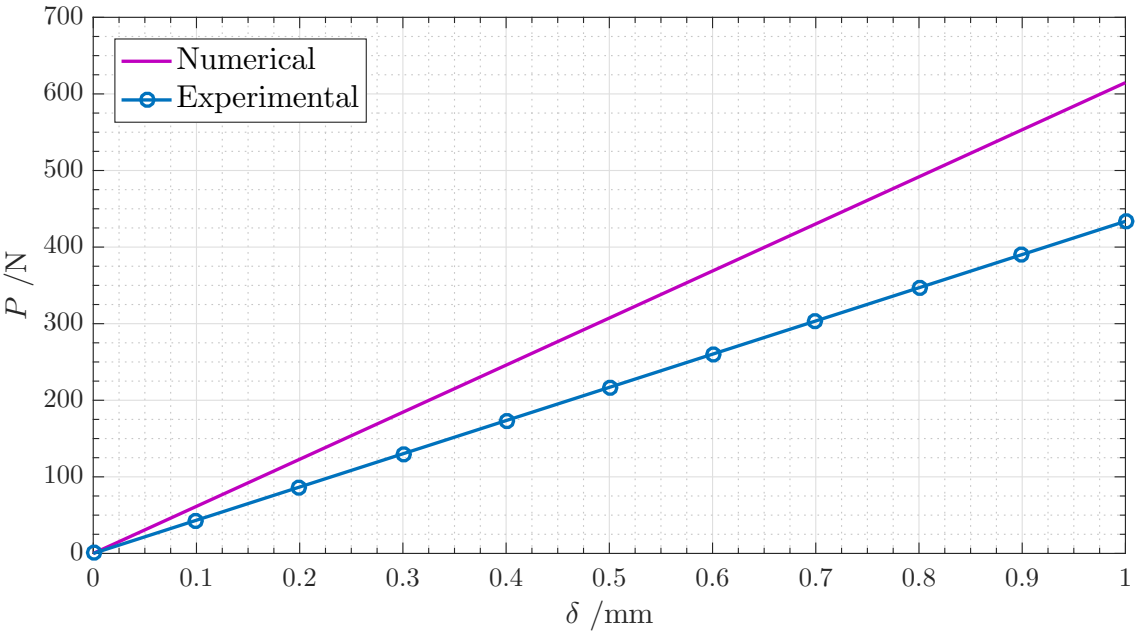


Figure 6.24. Numerical and experimental load-displacement curves comparison, for PCB model 14

6.3.3 Discussion

Although the same tendency was verified for these material models – numerical slope superior to the experimental one – the relative error is now superior. The new maximum value for the factor N, obtained using Eq. (6.3), is now 1.418 (**Tab. 6.2**). A possible explanation for this occurrence may be due to random errors existent in the installation and execution of the 4PB tests. In fact, this configuration is more sensitive to errors, since it requires tighter tolerances. Therefore, not loading the specimens directly in the center or not guaranteeing both load and supports' alignment is sufficient for creating this divergence in the slope values. Additionally, according to [39], the 4PB tests are more appropriate for specimens of bigger dimensions. Therefore, in further experiments, the optimal experimental tests to obtain the mechanical properties of PCB models would be the 3PB ones, since they are less susceptible to errors and easier to conceive numerically.

On the other hand, the outputs of the 4PB test material models have a superior N value, which indicates that this configuration is less conservative than the 3PB one.

Table 6.2. Experimental and numerical slopes comparison of the PCB models subjected to the four-point bending tests

PCB model	m_{num}	m_{exp}	ϵ_{rel} /%	N
1	295.4	211.1295	39.91	1.399
2	475.7	335.8023	41.66	1.417
5	473	342.9780	37.91	1.379
6	212.9	152.3840	39.71	1.397
12	233.3	167.4068	39.36	1.394
14	614.7	433.6378	41.75	1.418

6.4 Parametric Evaluation

To further extend and complement the previous numerical validation, additional scenarios were investigated to assess the quality of the simplified quasi-isotropic model. For this purpose, each PCB stack-up profile with thickness values for each discrete copper and FR-4 layers was required. These stack-ups were obtained from the PCB models' datasheets, of Bosch ST's internal database.

Although Bosch ST – Ovar suppliers provided datasheets containing FR-4 properties, the mandatory ones to create the material model are not provided or even known by the suppliers. Therefore, these were obtained from the literature [74; 75]. A summary of copper and FR-4 properties is presented in **Tabs. 6.3** and **6.4**, respectively.

Table 6.3. Copper properties [74]

ρ /kg·m^{-3}	E /GPa	ν /-	G /GPa	α /μm·(mK)$^{-1}$
8960	110	0.34	48	16.5

Table 6.4. FR-4 properties [75]

ρ /kg·m^{-3}	E_1 /GPa	E_2 /GPa	ν_{12} /-	ν_{21} /-	G_{12} /GPa	G_{21} /GPa
1850	24	21	0.136	0.118	10.56	9.39

For the default and every other scenario, PCB model 6 size and stack-up profile was used (**Fig. 6.25**). The boundary conditions are the same as the ones for the four-point bending tests. Additionally, a comparison between this PCB model 6 discrete layers material model results with the previous experimental and numerical ones is made.

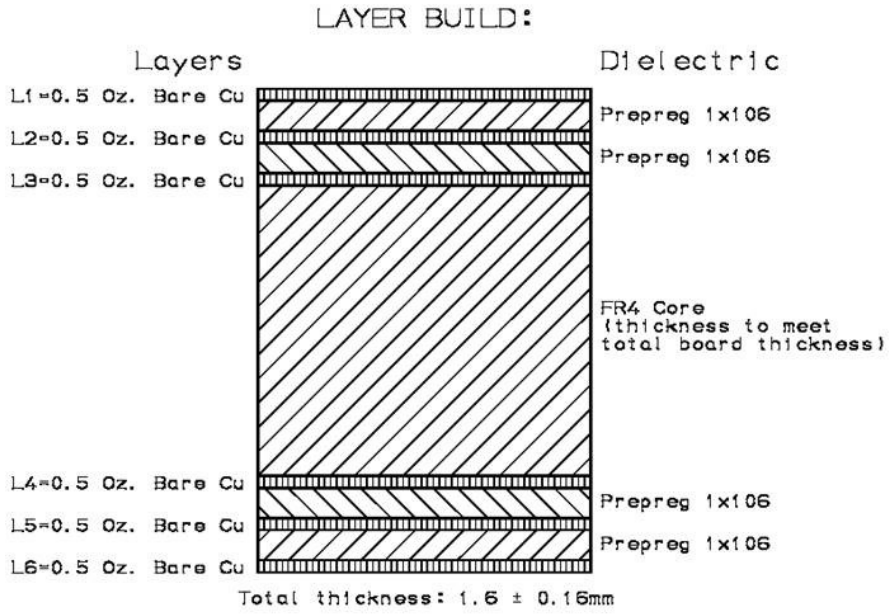


Figure 6.25. PCB model 6 stack-up

6.4.1 Scenarios

A list of the prescribed scenarios is presented below, followed by a brief description of each.

- **Default Scenario** – the default scenario consists of a material model with six copper layers and five FR-4 layers, resulting in a thickness of 1.576 mm, as illustrated in **Fig. 6.25**. The geometric parameters are equal to the ones defined in **Tab. 5.6**.
- **Scenario # 1** – this scenario consists in a material model with an **equal number of layers and different copper surface thickness**, which was increased from 12 μm to 30 μm (total of 1.582). This scenario was considered, given that the outer copper layers, both exposed to the etching process, have a superior thickness than the internal ones, since copper is accumulated at the top and bottom sides of each PCB. Therefore, these outer layers thickness variation influence is investigated.
- **Scenario # 2** – this scenario considers a material model with **equal size and different number of layers**. For this scenario, PCB model 2 stack-up profile, with eight copper layers and with 1.627 mm of thickness, was used.
- **Scenario # 3** – this scenario evaluates the influence of considering **different size and equal number of layers**. For this purpose, the size of PCB model 2 was considered.
- **Scenario # 4** – here, the PCB model 6 has a **stack-up configuration with FR-4 only**. It is intended to evaluate how much the results deviate not only from the default scenario, but also from the experimental results obtained for this PCB model [49].
- **Scenario # 5** – this scenario studies the impact of considering **different orientations of the FR-4 layers**. Four cases were tested:

  (i) **0°/90°/90°/0°/90°**

  (ii) **90°/0°/0°/90°/0°**

  (iii) **45°/-45°/-45°/45°/-45°**

  (iv) **-45°/45°/45°/-45°/45°**

- **Scenario # 6** – this scenario compares the **simplified geometry versus the detailed geometry** of PCB model 6, *i.e.* considering the rounded corners and hole distribution along the plate. The detailed geometry was sketched in the software Solidworks 2017, and then imported to Abaqus. It was expected a considerable variation of the results.
- **Scenario # 7** – lastly, this scenario studies the effect of **thickness variation** of the material model (in this case, an increase). Hence, 5 μm were added to each layer, making the initial thickness from 1.576 mm to 1.631 mm (only 4 μ m of difference from scenario # 2). It is expected that the thickness variation will result in a great deviation on the results, since it is a very sensitive parameter.[5]

[5] The knowledge of thickness exact value is key for good matching between numerical and experimental results.

6.4.2 Discussion

A global comparison between the obtained load-displacement curves of the default and every other scenarios is illustrated in **Fig. 6.26**, and the different slope values for each of the scenarios and the correspondent relative error between a scenario x and the default one – obtained using Eq. (6.2) – are presented in **Tab. 6.5**.

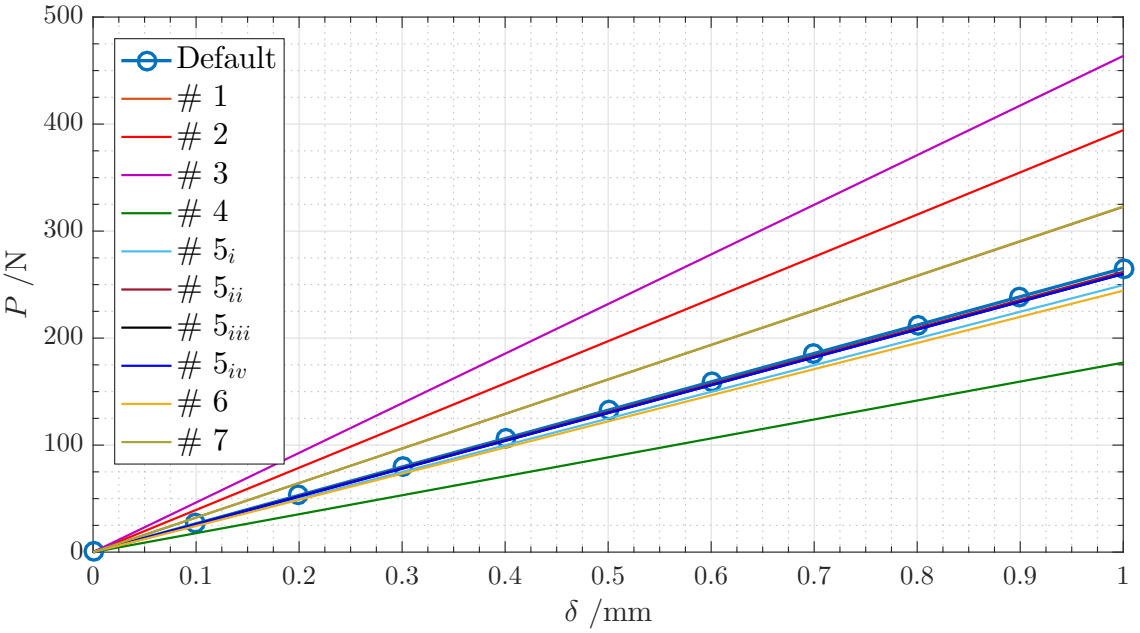


Figure 6.26. Global comparison of numerical model's scenarios

Table 6.5. Slope values for the different scenarios, and relative error calculation

Scenarios	m	ϵ_{rel} /%
Default	265.2	–
# 1	322.6	21.64
# 2	394.3	48.68
# 3	463.7	**74.85**
# 4	177.1	33.22
# 5_i	249.6	5.88
# 5_{ii}	261.9	1.24
# 5_{iii}	259.9	2.00
# 5_{iv}	259.9	2.00
# 6	244.3	7.88
# 7	323	21.78

Slope Comparison

In comparison with the default scenario, for scenario # 1, the influence of adding copper thickness to the PCB surface creates a visible deviation from the default scenario. However, as seen in **Section 5.6** the copper percentage for the complete PCB is very small. Perhaps by inserting the exact copper percentage in the material model, the results would deviate less or even no deviation would exist from the default scenario.

For scenario # 2, varying the number of layers also generates a deviation in the obtained results. This confirms that the number of layers has a considerable impact on the generated results.

Scenario # 3 has the highest slope deviation from every other scenario, and remarks the importance of knowing the geometry parameters' accurate values when creating a material model, either for case analysis or experimental validation.

For scenario # 4, the fact of considering FR-4 as the only material reduces substantially the slope value, lower than the default scenario one.

For every case of scenario # 5, the difference between the default and the four obtained slopes is minimal. This observation is clearly perceived from **Fig. 6.27**. One can conclude that lack of information about the FR-4 layers orientation is not critical when creating a printed circuit board material model.

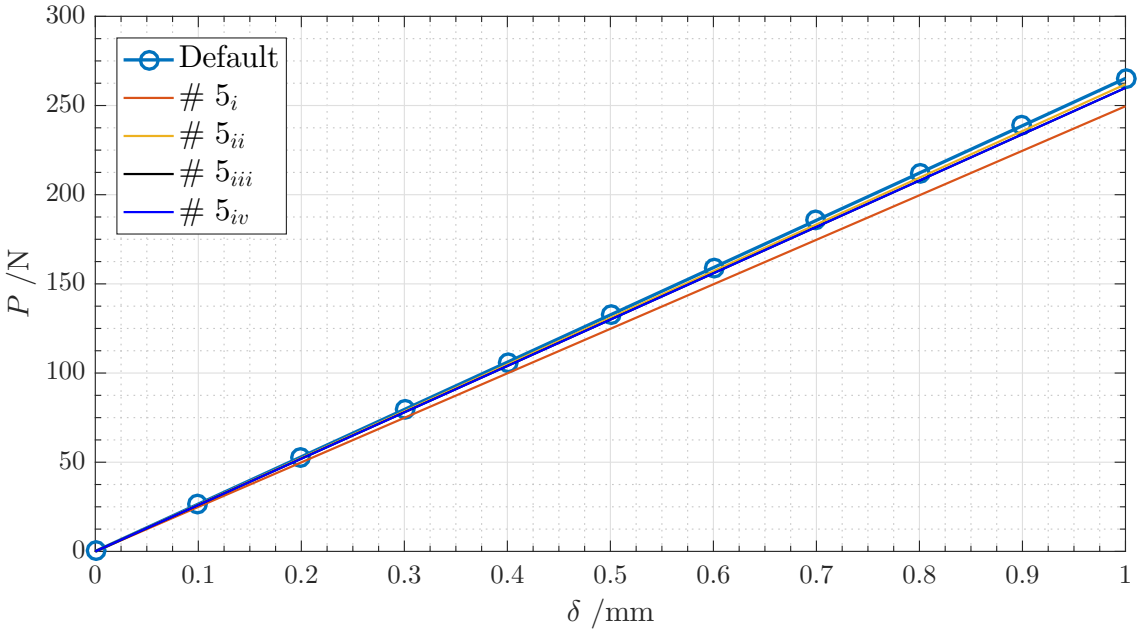


Figure 6.27. Load-displacement curves comparison between the default and # 5 scenarios

Detailing the geometry of the material model in scenario # 6 did not lead to considerable deviations between the slope values. Thus, the additional computational effort for detailed material models does not compensate the difference in the generated results. The number of layers and size of a PCB model are the variables which still have greater impact. **Fig. 6.28** illustrates the von Mises stress distribuition on the detailed geometry material model.[6]

[6] Since in this case the considered holes originate stress concentrations, the highest stress values correspond to these regions, and not along the middle surface of the plate.

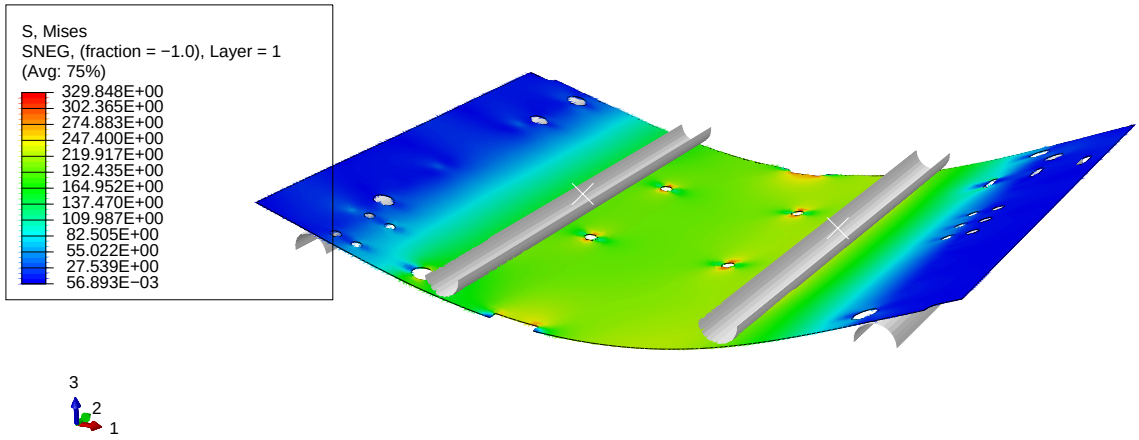


Figure 6.28. Von Mises stress distribution in scenario # 6 detailed geometry material model

Lastly, scenario # 7 confirms that, along with scenario # 2, thickness variations play a sensitive part in printed circuit boards numerical modelling.

Flexural Young Modulus Comparison

The flexural Young moduli of the considered scenarios were calculated using Eq. 5.5, and are presented in **Tab. 6.6**.

Table 6.6. Flexural Young Moduli values for the different scenarios

Scenarios	E_f /GPa
Default	48.705
# 1	58.842
# 2	65.816
# 3	50.014
# 4	**32.525**
# 5_i	45.840
# 5_{ii}	48.099
# 5_{iii}	47.731
# 5_{iv}	47.731
# 6	44.866
# 7	53.519

With the exception of scenario #4, all the other values far exceed the defined $14-28$ GPa range for the flexural Young modulus. If the exact properties of FR-4 would be known, perhaps the difference between the obtained numerical slope value and the experimental one for PCB model 6 would be minimal. This conclusion additionally infers that copper may have a low impact on numerical modelling, which is backed up by its little percentage for each printed circuit board model, as discussed in **Section 5.6**.

6.5 Summary

This chapter aimed to validate the material models conceived for the selected printed circuit boards, and the parametric evaluation allowed to extract useful insights about the parameters which most influence the derived results.

From the numerical validation, the following conclusions were extracted:

- The numerical correlation coefficient (slope) was always superior to the experimental one.
- Therefore, if the experimental results show a higher measured value than the ones obtained from the numerical simulations for the load-displacement slopes, this indicates that the printed circuit board models are under-dimensioned.
- For the 3PB tests, the good matching of results indicates that the numerical models are feasible and reliable, making 3PB the optimal experimental tests to obtain the mechanical properties of PCB models.
- As Bosch CM – Braga stated, each PCB model is unique, and the creation of a generic model always leads to results deviation.

Further, for the numerical scenarios:

- The difference in number of layers accounts for the biggest influence in the obtained results, mainly due to thickness variation.
- The fact of considering inaccurate material properties, *i.e.* copper and FR-4, to model the PCBs also generates erroneous results.
- The knowledge of the exact FR-4 properties and modelling each PCB solely with this material could potentially capture the real physical behaviour of a printed circuit board, since copper influence may be neglected.
- A parametric evaluation is crucial, in the measure that dictates how accurate the numerical results can be while compared to the real scenarios, and explores the inherent difficulties which urge while creating and relying on numerical procedures.

Now that the mechanical properties of the selected PCB models were obtained and their material models were created, the addition of the thermal and vibrational effects would enrich the knowledge about their influence on printed circuit boards' reliability. The following **Chapter 7** explores these two effects, through a set of additional experimental tests.

Chapter 7

Thermal & Vibration Testing

The analysis of the thermal behaviour of a printed circuit board leads to better understanding about its functional life. Thermal effects are reliable indicators, since their study may predict the failure of a critical components (namely, the BGAs), mainly due to thermal fatigue.

A first attempt to face this issue was to gather knowledge about the temperature profile along the board's top and bottom surfaces, while the PCBA model 13 is powered up.

Additionally, this analysis was extended by incorporating digital shearography to measure the displacement gradients on the PCBA connected to its housing.

Finally, a thermo-vibrational analysis was carried out, by submitting the housing with the PCBA to a given number of cycles of vibration, also while powered up. This test aimed to verify if under severe conditions – close to the system's resonance frequencies – the PCBA still remains functional.

Hence, this chapter covers the three aforementioned experimental tests, starting with an overview about the selected PCBA product, followed by the description of the experimental set-up and procedure of each test, culminating with the analysis and discussion of the results. The former two tests were perfomed at LOME and the latter at LVMS.

7.1 Thermography

7.1.1 Overview

For this approach, the PCB model 13 was selected. Originally, it belongs to the DCN-WAP (Wireless Access Point) product (**Fig. 7.1**). Briefly, it consists of an access point which links a central control unit (CCU) to the wireless conference units by means of a secure wireless communication. Its main application is mostly in meeting rooms and conference venues.

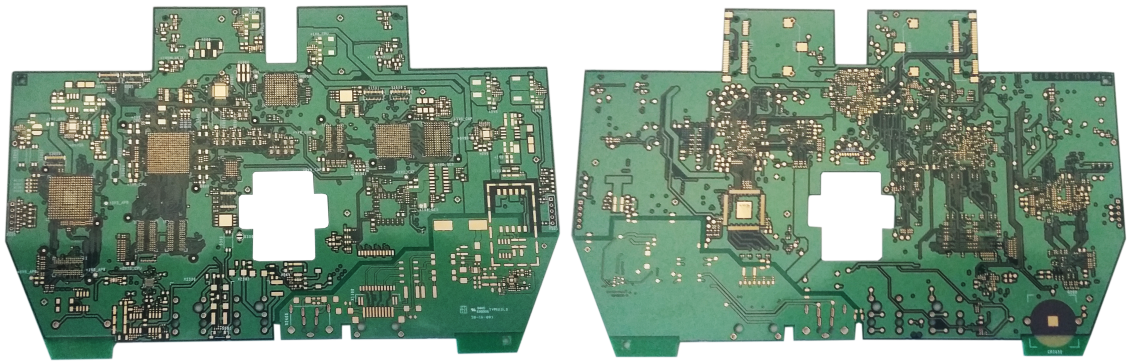


(a) Conference units **(b)** Housing

Figure 7.1. Bosch DCN-WAP [1]

The reason behind choosing this PCBA product for analysis relies on previous claims from customers about its overheating issues while operating, especially if the area where it is placed is not properly isolated from external heat sources, such as artificial light or heating devices. These heating problems suggest placing a gap pad against the critical components – the ones which reach the highest temperature – so that heat dissipation can be more efficient. Hence, this PCBA is the right choice for studying the thermal effects during its normal functioning. Its main electronic components are discriminated in **Fig. 7.3**.

The focus of this approach is to measure the maximum achieved temperatures on the PCBA top and bottom surfaces and indicate the correspondent electronic component which heats up the most. In the end, the extracted data is plotted to obtain the temperature evolution with time during the tests execution.



(a) Top view **(b)** Bottom view

Figure 7.2. PCB model 13

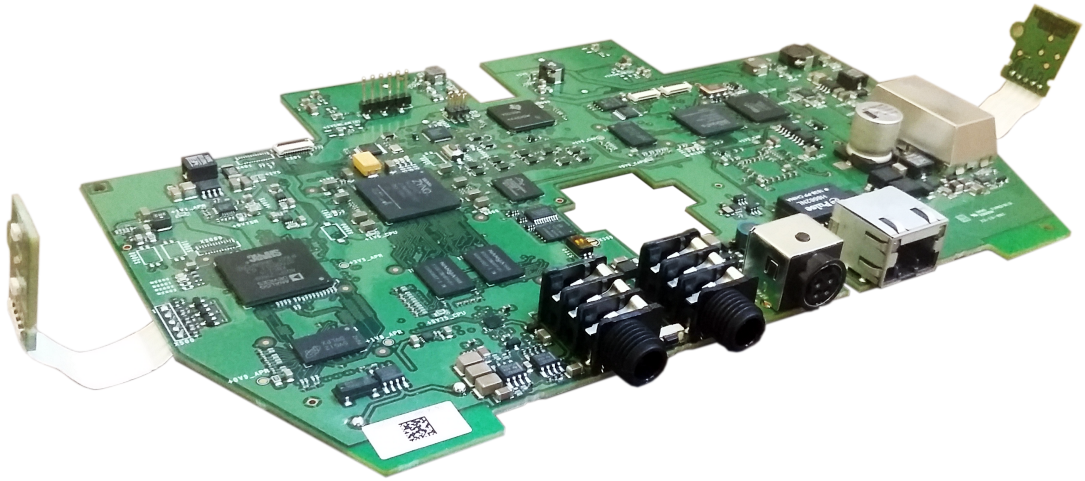


Figure 7.3. PCBA of the DCN-WAP product

7.1.2 Experimental Set-up

The set-up of the thermography test is shown in **Fig. 7.4**. In the test, the PCBA was stabilized using two metal supports, so that it could remain stationary and, simultaneously, was elevated enough so that the thermal camera could capture it entirely in its lens. The infrared camera used was a FLIR SC7500, of the SC7000 series, from the FLIR company, with high sensitivity, accuracy, spatial resolution and speed [76]. It is capable of measuring

temperature within a range of $5 - 300$ °C, and image capturing is done at 323 Hz. Also from the same company, the companion radiometric software for data acquisition was Altair, with a flexible layout, real time storage and camera control [77]. Although not perceptible in **Fig. 7.4**, the PCBA was placed at a sufficient distance from the back wall, so that no light would be reflected to the camera, as it is highly sensitive to these small variations. Further, to avoid the aforementioned situation, two wall panels were placed to restrict the test area (not shown in the figure below).

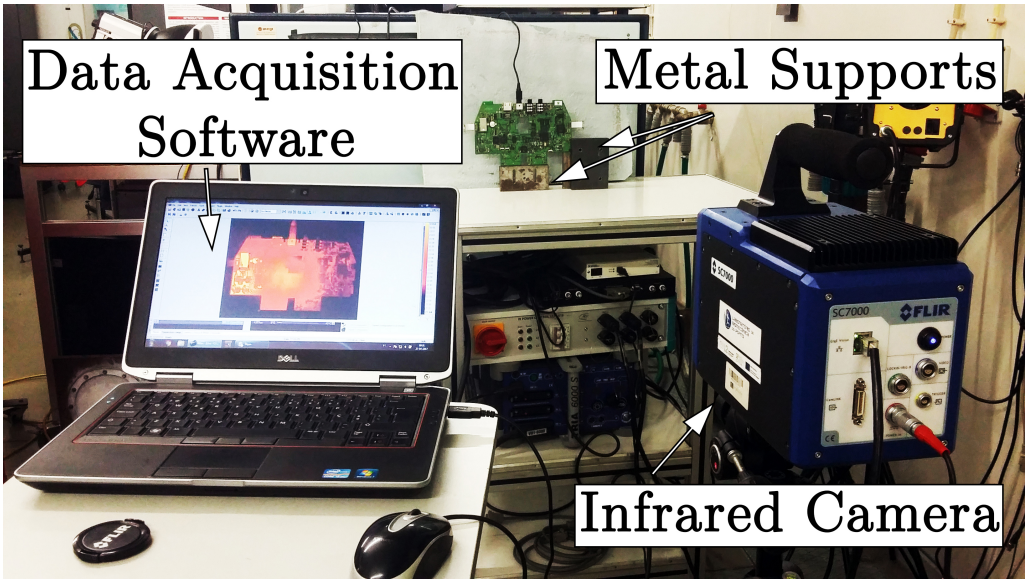


Figure 7.4. Experimental set-up for the thermography tests

Prior to the tests execution, the room temperature was measured using a thermometer. Upon initialization of the FLIR SC7500 camera, ten minutes were necessary to load its capacitors.[1] The Altair software captured the temperature distribution along the PCBA, and indicated the minimum and maximum temperature, in degrees Celsius, registered along a sketched line. Its behaviour can be compared to a thermometer – it measures the temperature resultant from the heat dissipation of the PCBA, which is what matters in these experimental tests. More detailed procedures, such as temperature measurement coming from the application of external heat sources, require additional software for these purposes.

Initially, the tests duration was set differently for the top and bottom surfaces:

- **Top surface** – 30 seconds at room temperature, followed by 15 minutes heating (power up) and 15 minutes cooling (power down), both at room temperature.
- **Bottom surface** – 30 seconds at room temperature, followed by 20 minutes heating (power up) and 20 minutes cooling (power down), also both at room temperature.

The reason behind increasing the test duration for the bottom surface is the longer time for the components to achieve their peak temperature, since they were also dissipating heat through the top surface by convection and radiation. Thus, instead of a test duration of thirty minutes, forty minutes where fixed for the bottom surface test.

The fact that the room temperature was not kept under control was a limitation of both tests.

[1] As a result of experimental use, the capacitors reach a final wear point. Therefore, equipment maintenance has to be done, by replacing the old capacitors.

7.1.3 Analysis & Discussion

The following results gather the temperature profiles along the sketched lines – which include the critical components – on Altair software.

A first trial attempted to position the lines correctly on the display. To do so, the brightest components were observed, which means they indicated higher temperatures. Therefore, the sketched lines tried to reach those components, so that their maximum temperature would be registered. A more precise temperature measurement could also have been done, by sketching a point on the center of each component. Nevertheless, extracting the temperature values along a line or a point resulted in smaller deviations in the collected data. Hence, the sketched lines approach was the one considered for both tests.

The value of the minimum temperature had no utility for this analysis, since it corresponds to the minimum temperature measured within the FLIR SC7000 camera lens domain, including the surroundings, and not just necessarily on the PCBA surface.

Top surface

The initial room temperature registered for the top surface test was about 21 °C, corresponding to the maximum value in line 3 (**Fig. 7.5**). Although higher and lower values were registered along the other three lines, they are affected by the camera's noise, the reason behind the values fluctuation. Therefore, a mean value of 21 °C was fixed.

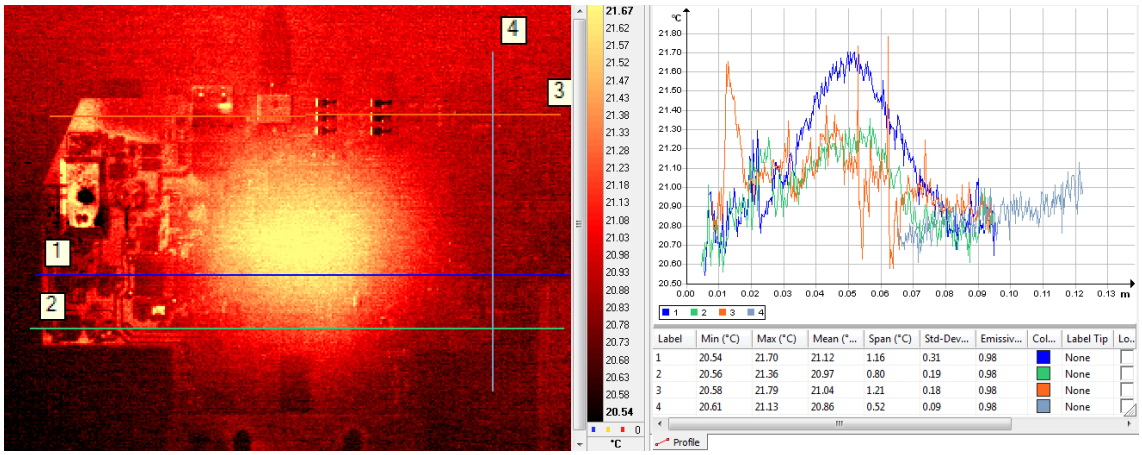


Figure 7.5. Temperature profile along the sketched lines on PCBA model 13 top surface, at room temperature

From the first five minutes until ten minutes, the temperature range in line 2 was between 50 and 55 °C. After approximately twelve minutes, the maximum temperature registered was 55.17 °C, on the second line. One can observe that the heating of the PCBA was not uniform, being the temperature peaks only registered for the components.

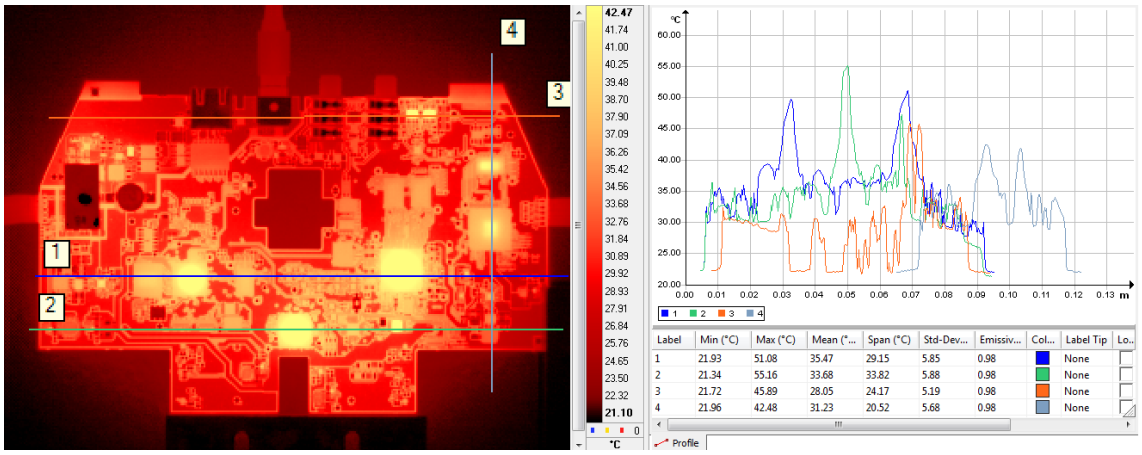


Figure 7.6. Temperature profile along the sketched lines on PCBA model 13 top surface, at the maximum temperature time instant

On the contrary, the PCBA cooling revealed a more uniform temperature distribution along the plate, illustrated by the brighter colours in **Fig. 7.7**, which represent the copper paths. As happened previously, after sensibly twelve minutes, the maximum temperature registered in the four lines stabilized around 22 °C.

Note that the middle area temperature of the critical components is lower than the one on its corners. This may be due to the the non-existence of solder joints on this middle area, which makes the temperature higher in the corners' solder joints, where heat flows through them.

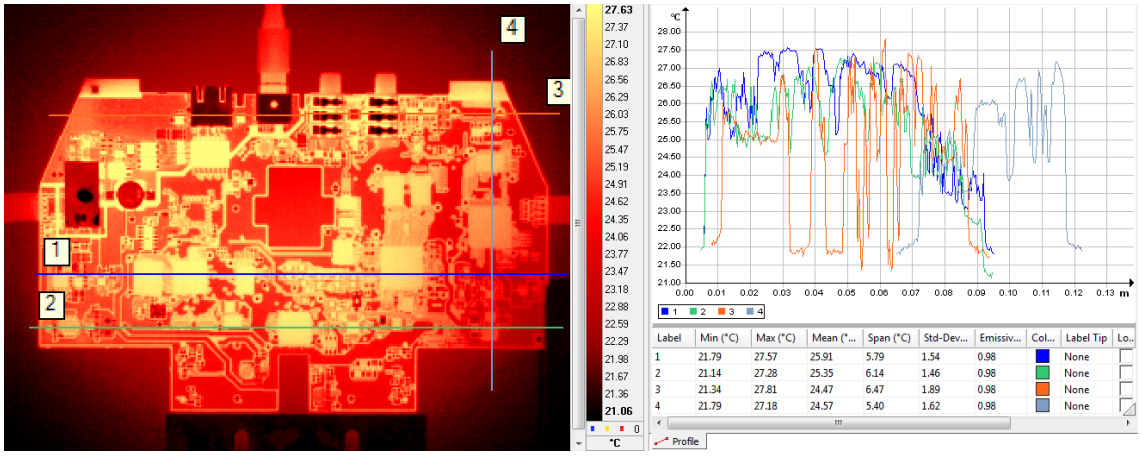


Figure 7.7. Temperature profile along the sketched lines on PCBA model 13 top surface, during cooling

In order to improve the perception of the temperature evolution during the top surface test, the maximum temperatures along the lines 1 to 4 were extracted, and the time instant was registered. The temperature evolution with time is illustrated in **Fig. 7.8**.

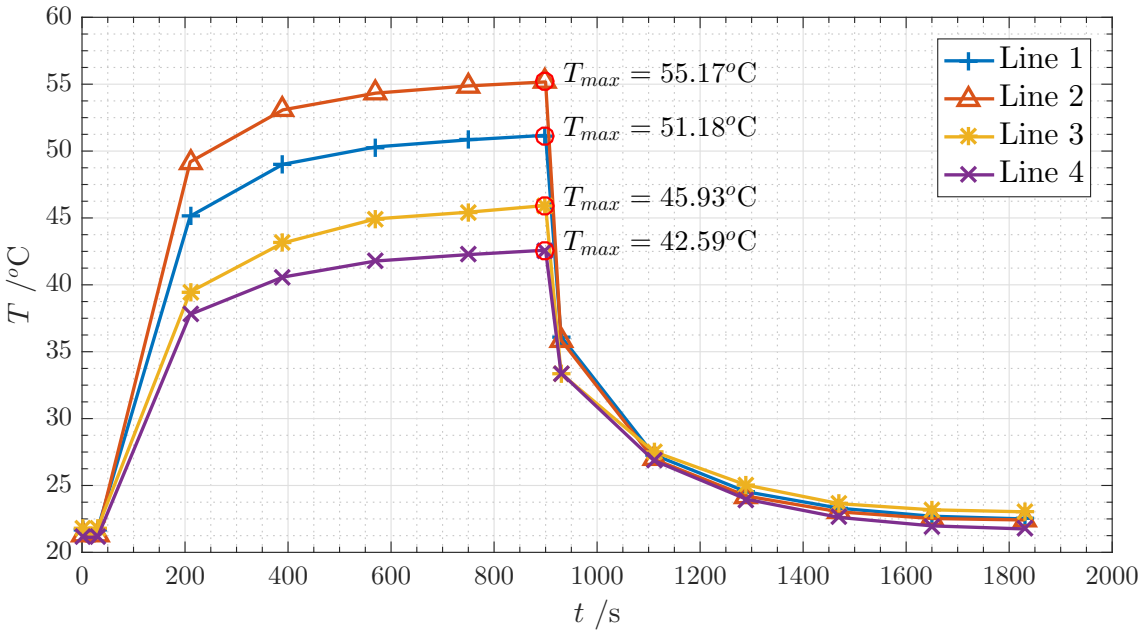


Figure 7.8. Temperature evolution with time along the sketched lines of the top surface of PCBA model 13

In the first 200 seconds, the temperature rises rapidly until a value closer to the maximum registered temperature, for each component. From 200 seconds until the instant the PCBA is powered down (900 seconds), the temperature evolves very slowly, approximately reaching a steady-state from 700 seconds until the electric current is cut. Until then, there are four different maximum temperatures values measured, each corresponding to different components. From there on, the cooling temperatures registered values are more uniform for every of the four lines, which almost match until the end of the test. At 1650 seconds, the temperature values are almost stable for every line. The small deviation from the final temperature values to the initial room temperature is normal, since the surrounding atmosphere was not controlled.

The maximum temperature difference registered was:

$$\Delta T_{max} = 55.17 - 21 = 34.17\ ^\circ\text{C} \tag{7.1}$$

Bottom surface

Similarly, the initial room temperature was measured, and its value was about 21 °C, one more degree than the previous test, according to **Fig. 7.9**. This time, more points were collected to plot the temperature evolution with time graph, so the resultant curve was more accurate.

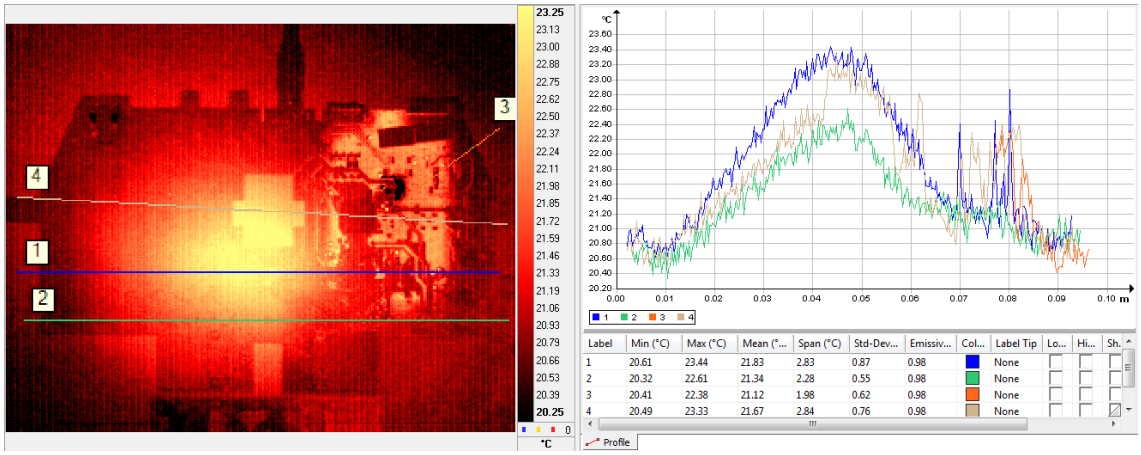


Figure 7.9. Temperature profile along the sketched lines on PCBA model 13 bottom surface, at room temperature

The heating phase, this time, took longer to stabilize, approximately 17 minutes.

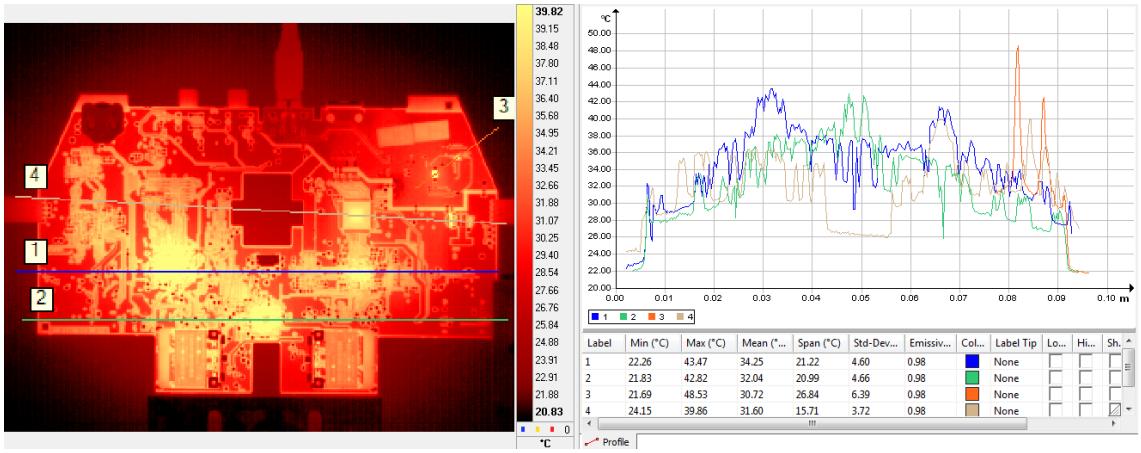


Figure 7.10. Temperature profile along the sketched lines on PCBA model 13 bottom surface, at the maximum temperature time instant

From **Fig. 7.11**, it can be concluded that the cooling is even more uniform than the previous test for the top surface, since they almost overlap.

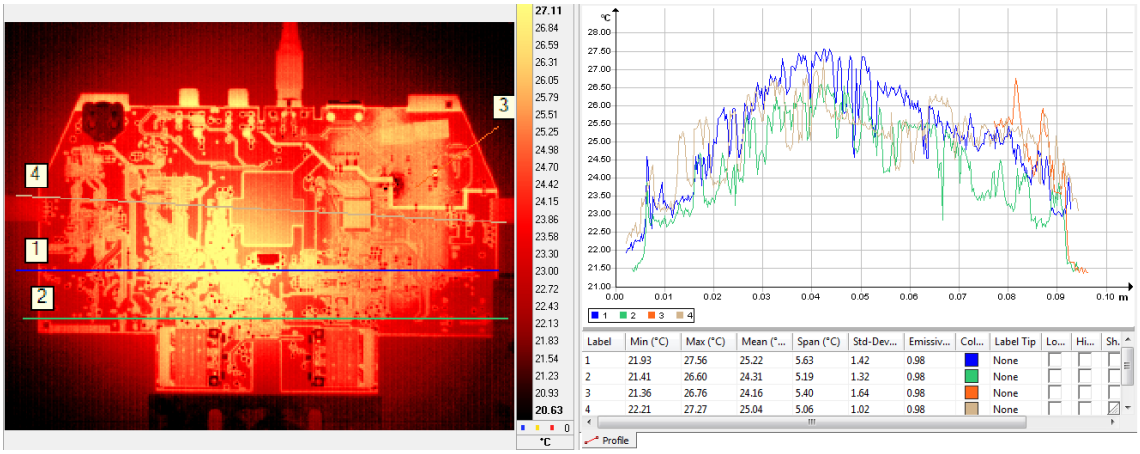


Figure 7.11. Temperature profile along the sketched lines on PCB model 13 bottom surface, during cooling

The temperature evolution with time is illustrated in **Fig. 7.12**. In the first 150 seconds, the temperature rises rapidly, as in the previous case. The steady-state is reached more or less at 900 seconds, as in the previous test. However, the peak temperatures registered values are smaller, with a maximum of 48.56 °C, for line 3. Again, the cooling temperature profiles were more uniform, independently of the maximum temperature reached previously during the heating phase, and it also took longer to occur. Moreover, the final temperatures slightly deviate from the initial room temperature, due to the same reasons mentioned before.

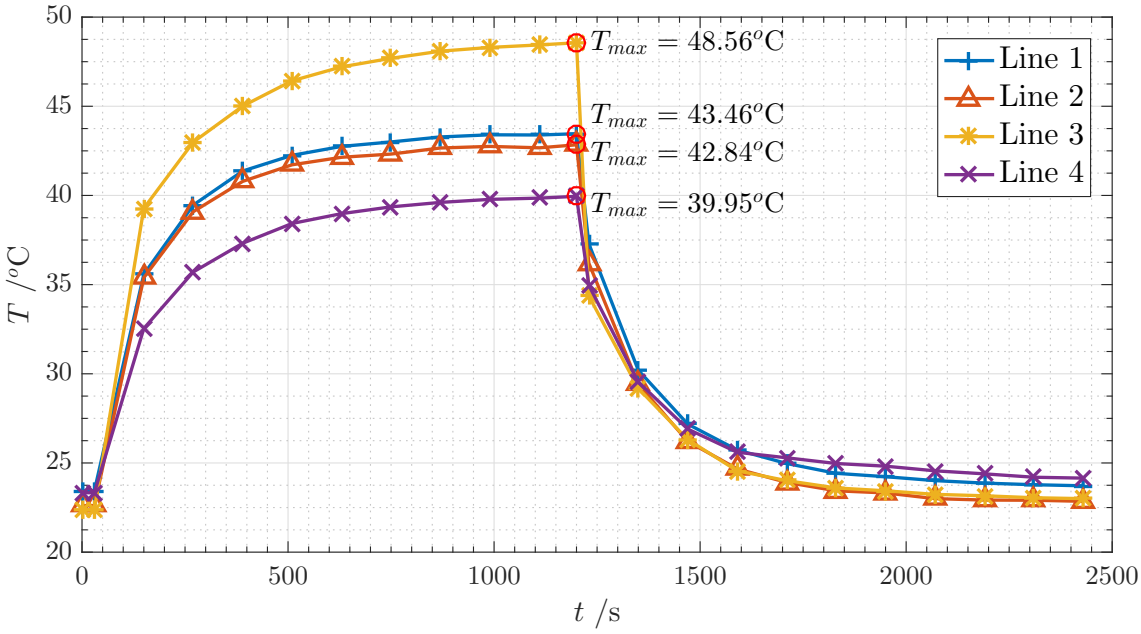


Figure 7.12. Temperature evolution with time along the sketched lines of the bottom surface of PCBA model 13

The maximum temperature difference observed was:

$$\Delta T_{max} = 48.56 - 22 = 26.56 \text{ °C} \tag{7.2}$$

7.2 Digital Shearography

Although it was initially intended to use ESPI to visualize the static displacements on the selected PCBA placed in its housing, resultant from its thermal behaviour, it was decided to use Digital Shearography instead.

Digital Shearography is a full-field, non-contact, coherent optical measurement method which has become an important diagnostic tool that is primarily used for qualitative inspection (**Fig. 7.13**). The possibility of damage identification has high importance for one to be able to schedule a repair or to make a precise estimation of the useful life of products [78]. In fact, it provides several other advantages over traditional contact measurement methods [79; 80]. Contrary to the ESPI technique, the sensitivity of measurements can be controlled [81].

A review of this measurement method is next presented.

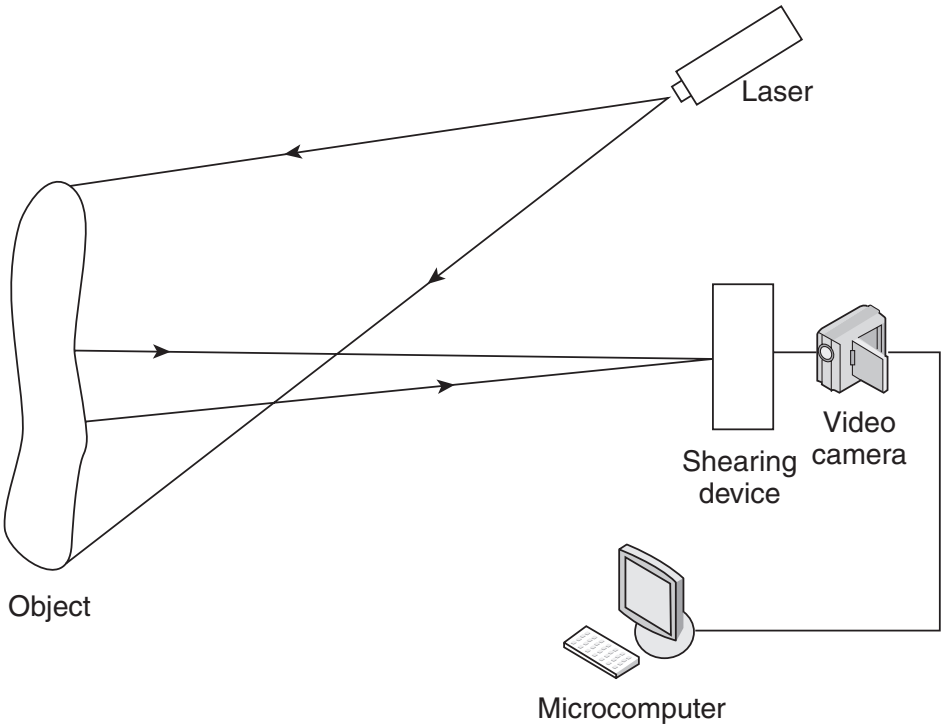


Figure 7.13. Schematic diagram of digital shearography [82]

7.2.1 Review

The sensitivity of measurements using Digital Shearography can be adjusted by controlling the amount of shearing. The shearing can be made in the x-direction, as well as in the y- or other angular directions. Also, radial shearing, rotational shearing, inversion shear or reversal shear can be performed with related optical arrangements [81]. The amount of shearing is given by the shift between the two wave-fronts, captured by the charge-coupled device (CCD) camera, both being reflected from the object. This explains why one can visualize two objects when looking at the reference image (**Fig. 7.14**). Since both wave-fronts come from the object's reflection, the sum of speckle noise is added, making this technique noisier than ESPI [81; 83].

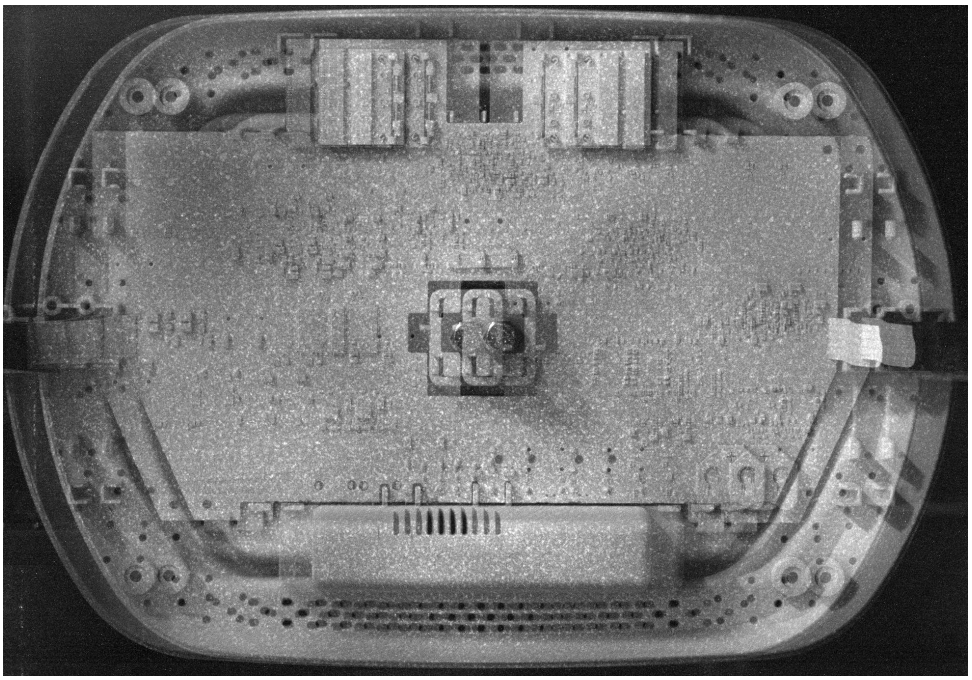


Figure 7.14. Reference image of PCBA model 13 for the digital shearography measurements

The basic concept is that this shift, given by the superposition of the two wave-fronts, allows to extract information about the out-of-plane displacement gradients fields – the so called "rotations" of the object. Basically, the outputs simply correspond to the numerical differentiation of the out-of-plane displacements obtained optically, and not numerically [83].

The illumination of the object's surface is made using a coherent light source coming from a LASER with specified wavelength and power output.

The speckles transport information to the CCD camera, but it is only capable of capturing the intensity of the incident light. Therefore, in order to extract the phase information, several algorithms can be used. The most common ones are Temporal Phase Modulation (TPM) – appropriate for static measurements – or Spacial Phase Modulation (SPM) [81].

The speckle comes from the diffraction effect of the roughness of the surface. The object's surface consists of a given roughness profile, and measurements can only be made if the surface roughness level is below the wavelength of the LASER. Microscopically, the surface roughness is formed by peaks, valleys and multiple random surfaces. The reflection of those micro-surfaces causes a beat, forming the speckle grains. The speckle grains are repeated periodically along a path. The ones which do not contain information about the phase are responsible for noise generation in the wave-front [81].

To resolve speckle, which consists in adjusting the size of the speckles to the size of the pixels, one must adjust the intensity of the light source and the aperture of the image formation system, which includes the lens and the iris. The perception of the results can be clearer and the computational effort can be reduced by adjusting, in the software, the display window so that it fits the size of the object [81; 83].

Beyond the aforementioned concepts, some additional considerations about this measurement technique are presented throughout the experimental set-up & procedure description that follows.

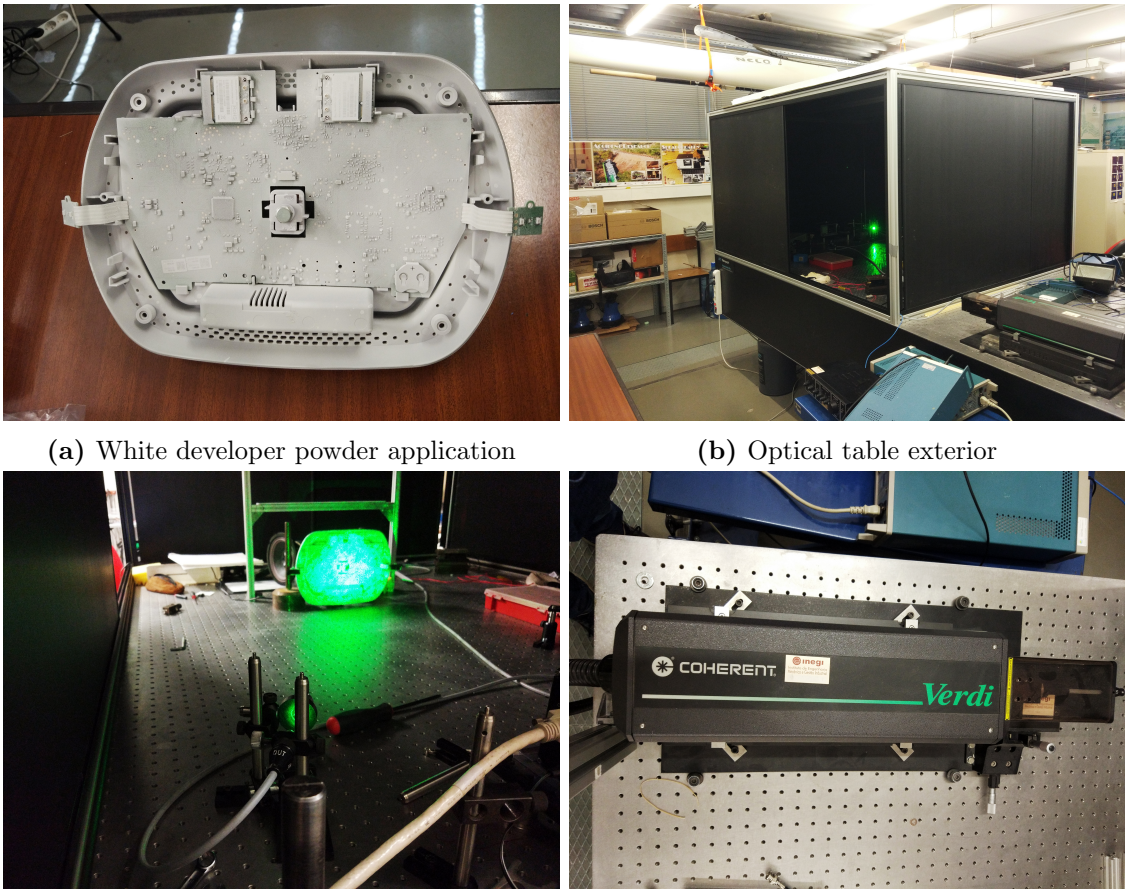
7.2.2 Experimental Set-up & Procedure

The experimental set-up was prepared under the guidance of a professor from ISEP.[2]

The first step for performing the Digital Shearography tests was preparing the object's surface. Thus, it was pulverized with lacquer before applying white developer powder on it, so that the powder would adhere easier (**Fig. 7.15a**). The developer powder uniforms the LASER light reflectivity. All the experimental set-up was made on top of an optical table (**Fig. 7.15b**), in order to prevent the perturbation of external vibrations on the measurement's quality. Additionally, every object was fixed on the optical table and the PCBA's peripheral lights were covered with black tape, in order to reduce light's reflectivity (**Fig. 7.15c**).

Since the PCBA was to be kept quasi-static, the phase information was extracted using the TPM technique, with a shift of $\pi/2$, which means recording five images for each of the states (reference and measurement).

For every measurement, a camera with four megapixels of resolution – equal to a spatial resolution of 4 million speckles – and a Coherent Verdi LASER (**Fig. 7.15d**), with a power output of 2 W and a wavelength of 532 nm was used. The amount of shearing was set to 10 mm.[3]



(a) White developer powder application

(b) Optical table exterior

(c) Optical table interior

(d) Coherent Verdi LASER

Figure 7.15. Experimental set-up of the digital shearography tests

[2] Hernâni Lopes (Adjunct Professor).

[3] For shearing amounts of 50 mm, even the human breathing has implications in the measurements' quality.

Three measurements were made:

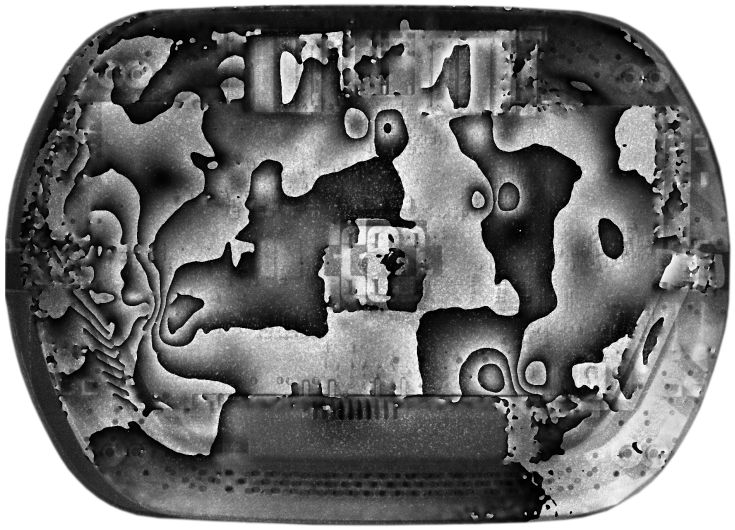
- The 1^{st} measurement was made 15 seconds right after the PCBA was powered up.
- The 2^{nd} one was made 60 seconds also after the PCBA was powered up, having been turned off between the first and this measurement.
- The 3^{rd} and final measurement was made 60 seconds after the previous measurement, not turning off the electrical current between measurements, and letting the PCBA cooling (from natural convection) for approximately 120 seconds.

7.2.3 Results & Discussion

The obtained shearographic patterns – obtained results of Digital Shearography – of each of the measurements are presented in **Fig. 7.16** and the correspondent displacement gradients fields – the rotation values – are presented in **Figs. 7.17**, **7.18** and **7.19**, generated after post-processing the shearographic patterns images.

A fringe pattern directly represents the deformation derivative. If a defect on the surface or subsurface produces a deformation anomaly during a loading (in this case, thermal loading), the defect will be revealed by an anomaly in the fringe pattern, as seen from **Fig. 7.16** for the three different measurements [84].

The results indicate different displacement gradients for every measurement. The areas populated with a great number of fringes indicate the presence of strong displacement gradients, *i.e.* considerable deformations occur on those areas, resultant from the thermal behaviour of the PCBA model 13. The perception of this phenomena reveals the potential of this measurement method in qualitative inspection of any desired printed circuit board model.



(a) 1^{st} measurement

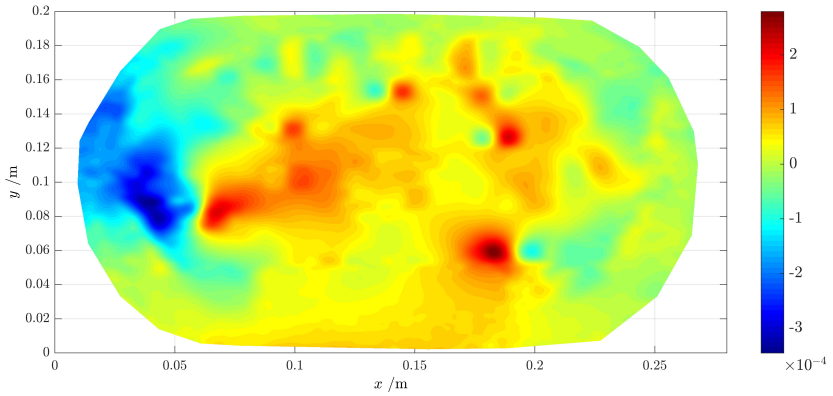


(b) 2^{nd} measurement

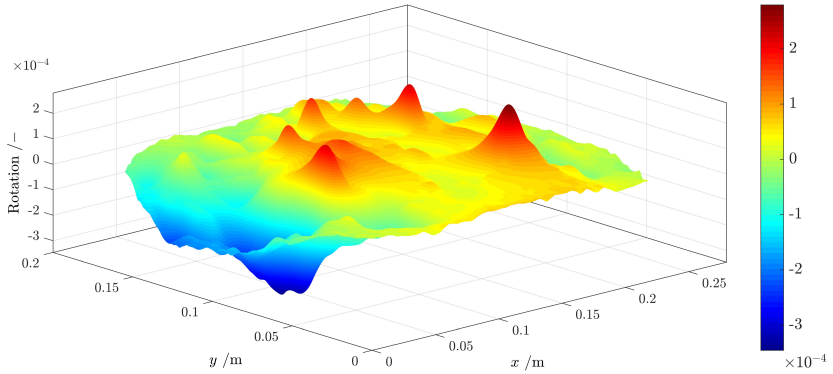


(c) 3^{rd} measurement

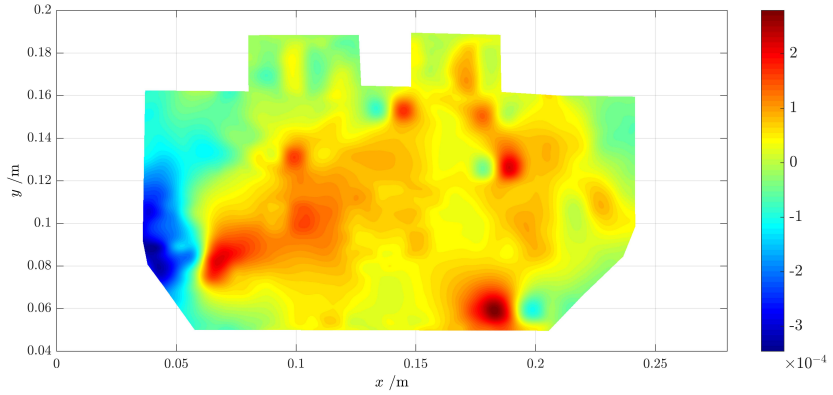
Figure 7.16. Shearographic patterns obtained for the different measurements



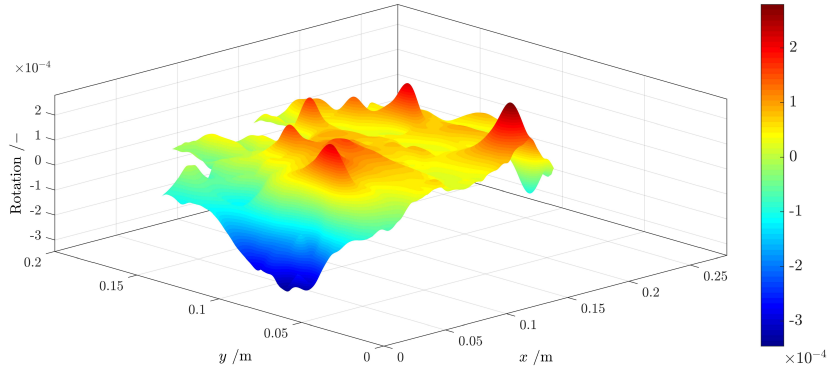
(a) PCBA + housing – 2D view



(b) PCBA + housing – 3D view

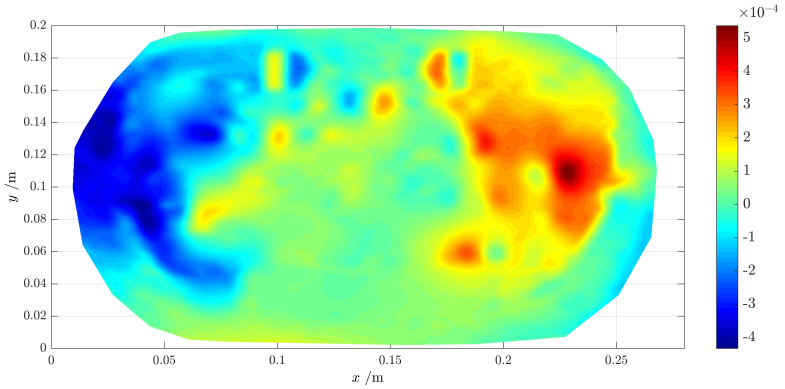


(c) PCBA – 2D view

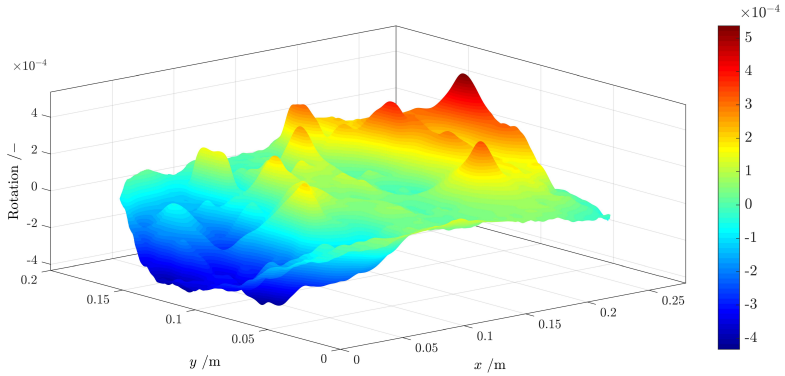


(d) PCBA – 3D view

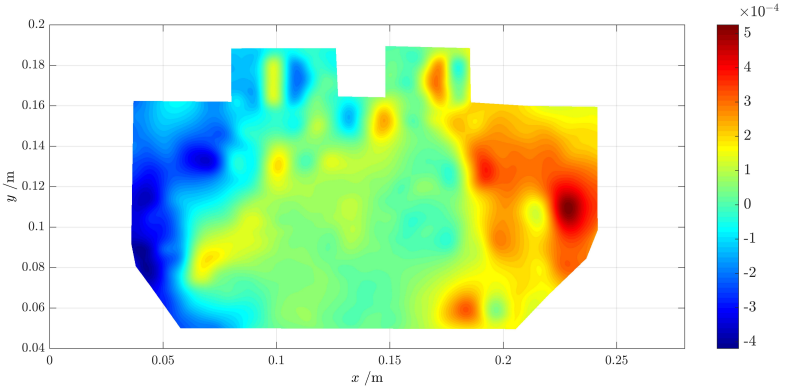
Figure 7.17. Rotation values obtained for the 1^{st} measurement in digital shearography



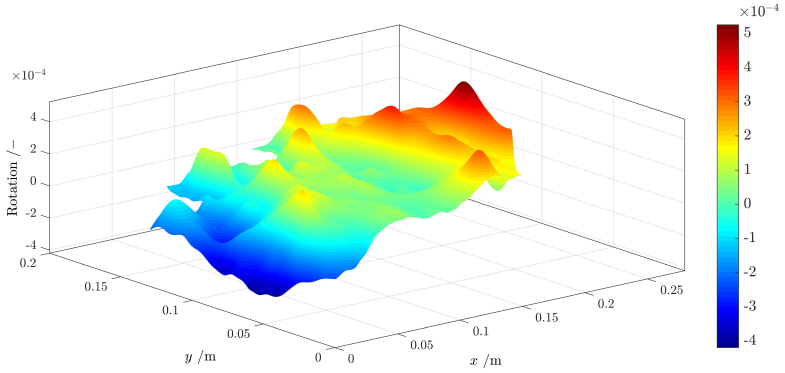
(a) PCBA + housing – 2D view



(b) PCBA + housing – 3D view

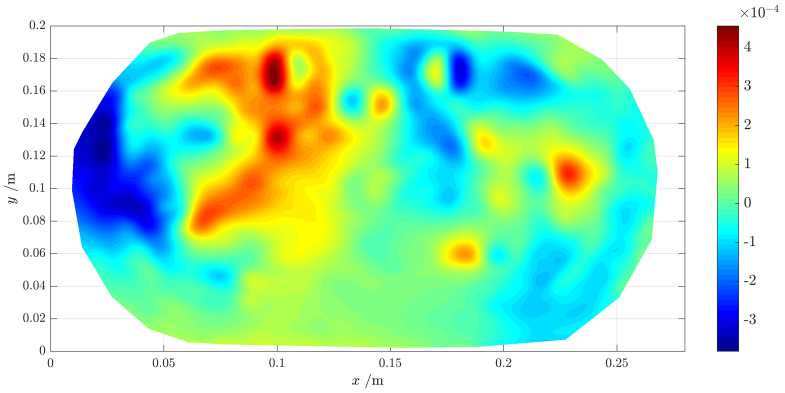


(c) PCBA – 2D view

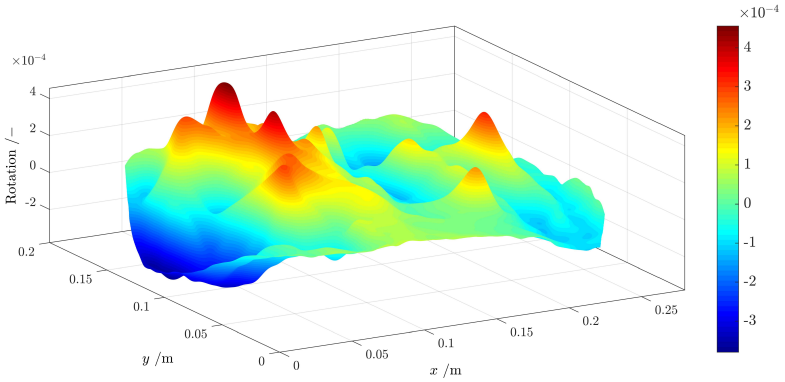


(d) PCBA – 3D view

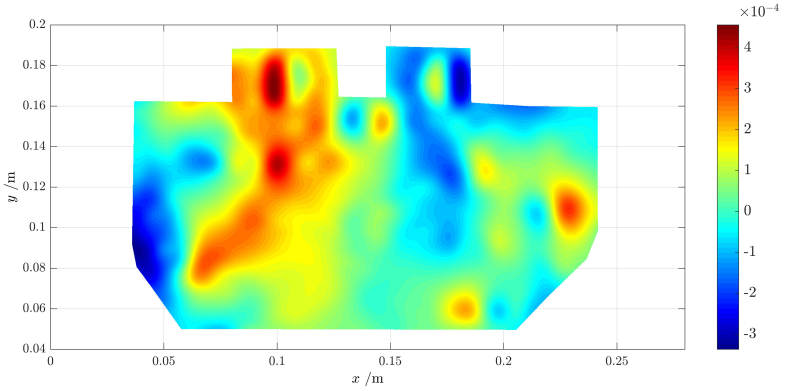
Figure 7.18. Rotation values obtained for the 2^{nd} measurement in digital shearography



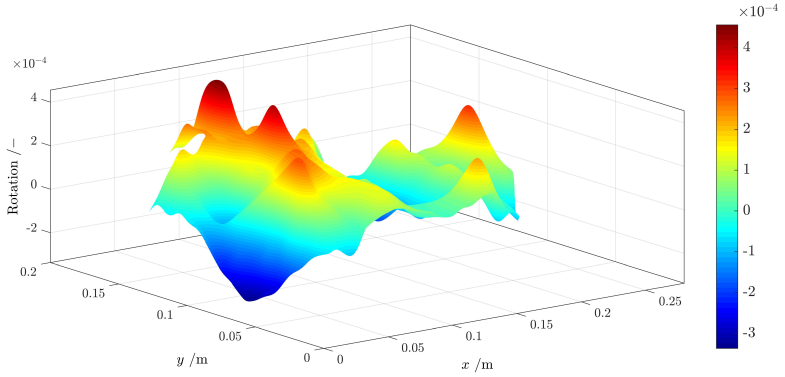
(a) PCBA + housing – 2D view



(b) PCBA + housing – 3D view



(c) PCBA – 2D view



(d) PCBA – 3D view

Figure 7.19. Rotation values obtained for the 3^{rd} measurement in digital shearography

7.3 Thermo-Vibration

The characterization of a printed circuit board would not be complete without vibration fatigue analysis. Throughout their operating life, PCBAs work under the influence of mechanical and thermal loads. Pre-loads, bending of components and impact are some of the main mechanical loads, while heat generation of the electronic components, resultant from the power-up of the electrical circuit, is the main source of thermal loads.[4] Summed to the mechanical ones, the latter account for a bigger effect on printed circuit boards durability.

From a mechanical point of view, it is interesting to study the PCB behaviour and evaluate from which number of vibration cycles a crack is generated.

From an electrical point of view, the vibration tests are very beneficial, to the extent that the number of cycles until the electrical current of the circuit stops flowing is obtained, meaning the PCBA is no longer functional. For the selected model, this corresponds to not observing anymore the intermittent LED blinking while it is turned on.

As mentioned before, the crack of the solder joints of the critical components (mainly BGAs) are the root of this problem. Although the number of cycles until this happens can be measured, the critical components solder joints failure have started to continuously crack way before the failure of the PCBA is detected. Therefore, until none of these solder joints crack compromises the circuit functioning, the PCBA continues to function normally. This scenario captures what happens in real cases of electronic packaging, and stands as the main cause of reduction of products' operating life, not due to mechanical integrity, but to electrical integrity.

The preparation of an experimental set-up raises some difficulties. The high density of components makes it difficult to clamp the PCBA specimen without damaging any of them, compromising the circuit integrity from the start. Thus, the ideal set-up would consider submitting the PCBA, inserted in its housing, to a given vibration frequency. For this purpose, the PCBA + housing set would need to be attached to an electromagnetic shaker.

The tailored experimental set-up and procedure for this study comes next, followed by the discussion of the observed behaviour of the dynamic system (PCBA + housing set).

7.3.1 Experimental Set-Up

As mentioned before, this set-up was created for this specific case, with the support and guidance of a FEUP professor[5] at the Laboratory of Vibrations of Mechanical Systems (LVMS), and did not follow any existing industry standard. Literature on this issue was consulted beforehand, and a set of analytical approaches to obtain some parameters (first natural frequency, stiffness, maximum displacement...) were found [85]. However, these were only suitable for the correspondent boundary conditions of the printed circuit board. As none could resemble the ones of this case, it was decided to tailor both the experimental set-up and procedure to it.

The setting of the PCBA + housing set and experimental set-up is illustrated in **Figs. 7.20** and **7.21**, and its correspondent schematic diagram in **Fig. 7.22**.

[4] Nonetheless, the environmental effects should also be taken into account.
[5] José Dias Rodrigues (Associate Professor).

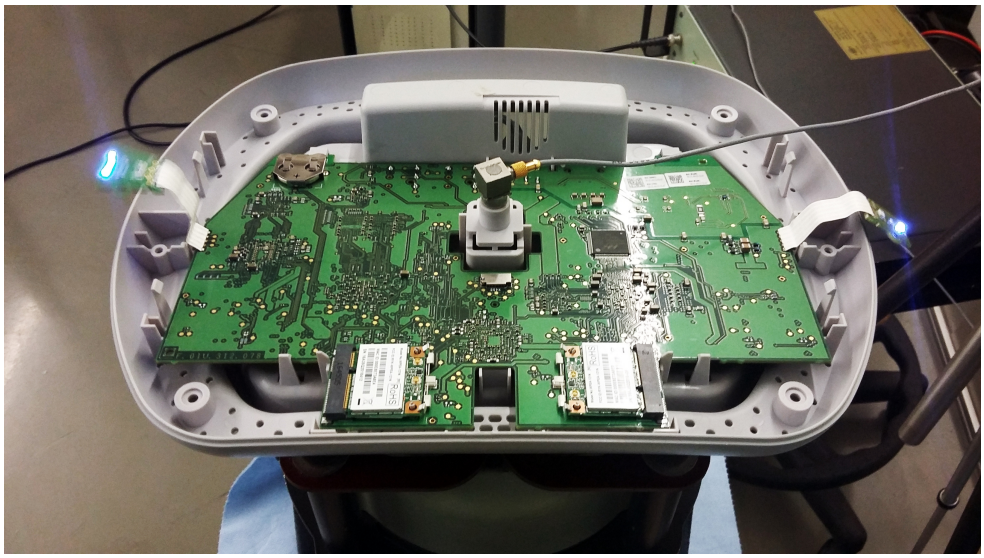


Figure 7.20. Setting of the PCBA and housing on the electromagnetic shaker

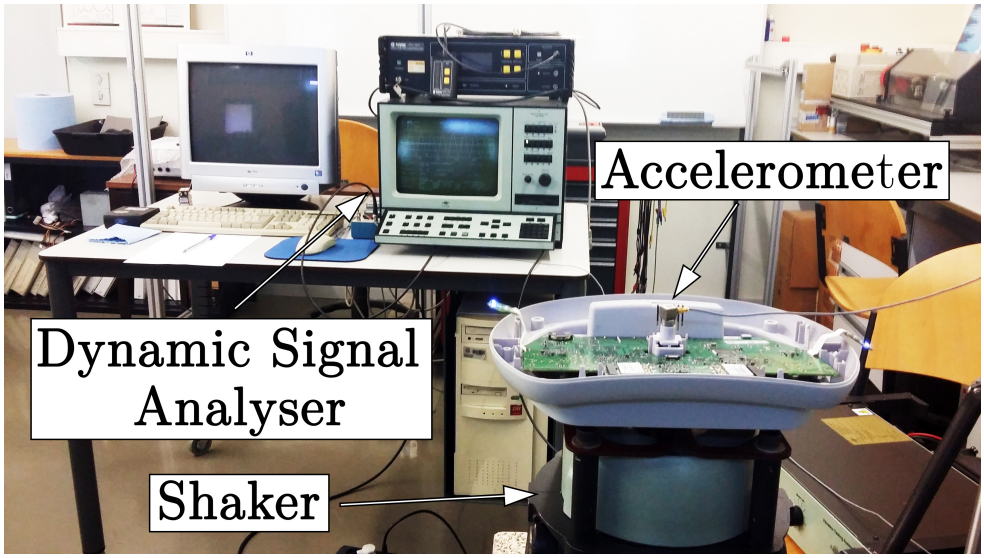


Figure 7.21. Experimental set-up of the vibration tests

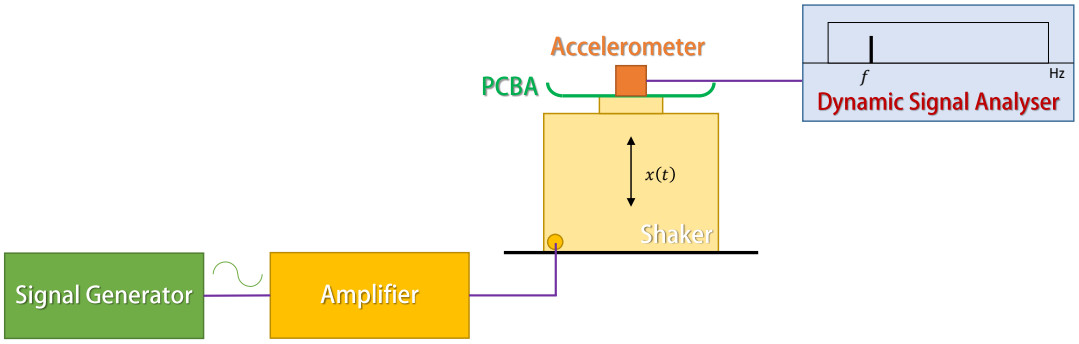


Figure 7.22. Schematic diagram of the vibration tests experimental set-up

The instrumentation for this test is presented below:[6]

- Signal generator
- Amplifier
- Electromagnetic shaker (or simply, “shaker”)
- Accelerometer
- Dynamic signal analyser

7.3.2 Experimental Procedure

Prior to conduct a series of measurements for different excitation frequencies, the first natural frequency (or resonance frequency) was found, through trial and error measurements.[7] It was verified that its value would lie within the range of $42 - 44$ Hz. It was considered that the resonance frequency would be equal to 44 Hz.[8]

Afterwards, a series of four measurements were conducted. The system (PCBA + housing) was submitted to an harmonic excitation – defined by a sine wave – for every test (**Fig. 7.23**), with a given amplitude $x(t)$ /m, obtained using Eq. (7.3), acceleration a /m·s^{-2} and frequency f /Hz, whose chosen values lied within the previous specified range. Every test duration was set to thirty minutes. **Tab. 7.1** summarizes the aforementioned parameters for every measurement.[9]

Although it would not have great influence on the tests, the room temperature was not controlled.

$$x(t) = \frac{a}{(2 \cdot \pi \cdot f)^2} \tag{7.3}$$

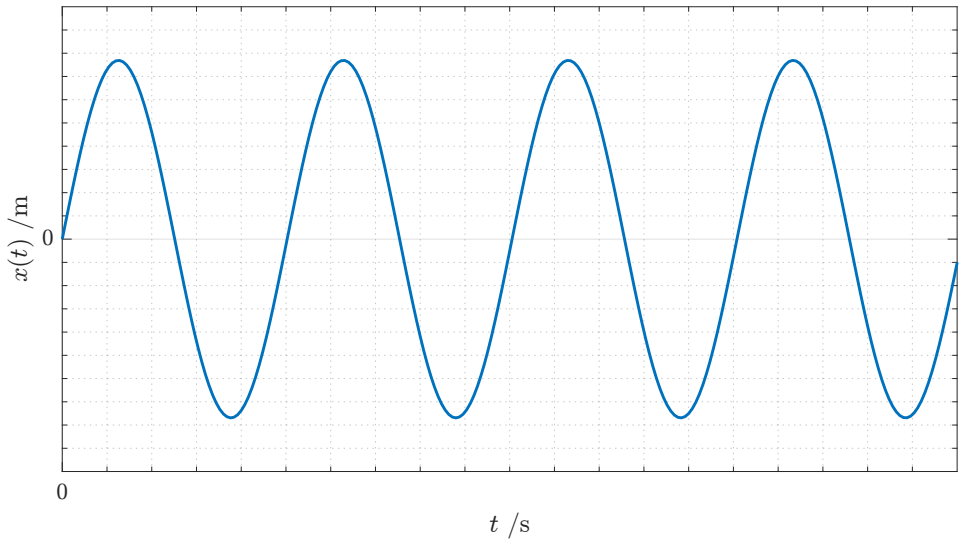


Figure 7.23. Harmonic excitation, defined by a sine wave

[6] The former two instruments are not displayed in **Figs. 7.20** and **7.21**.
[7] Done by seeking for the highest pitch of that interval of frequencies.
[8] Note that the dynamic system is the PCBA + housing, and not solely either the PCBA or housing.
[9] The fourth and last measurement simulates more severe conditions than the previous three ones.

Table 7.1. Values of the parameters for the vibration measurements

Measurement	a /m·s^{-2}	f /Hz	$x(t)$ /mm	t /min
1	10	34	0.220	30
2	11	44	0.144	30
3	11	54	0.096	30
4	55	42.5	0.771	30

7.3.3 Discussion

From the performed measurements, some remarks can be highlighted:

- The boundary conditions have a strong influence on the dynamic response of the PCBA + housing system [85].
- Every measurement was not performed in ideal conditions. Therefore, the best would have been excite the system for a longer period, between two and four hours.
- The HALT tests (stated in **Chapter 4** are confirmed to be reliable, since the PCBA still remained functional after the conducted measurements.

Therefore, in further experiments, the measurements should be made in a cleanroom and repeated for a wider range of frequencies, containing the first natural frequency, and for longer durations. Based on standards of similar tests applied in the automotive industry [86], the dynamic system should be excited on the three axes. For the axis with lower dynamic stiffness, set the duration up to four hours, and for the other two, up to two hours. Moreover, instead of relying on the tests duration for evaluating the reliability of a printed circuit board, the assessment of the number of cycles until electrical failure would be a more consistent indicator.

7.4 Summary

The three additional experimental tests provided value to printed circuit boards characterization was massive.

The thermography tests allowed to clearly understand the critical temperature areas on a PCBA while turned on. The main points to highlight are the following:

- The top surface reaches the equilibrium/steady-state condition more rapidly than the bottom surface.
- The maximum temperature measured was 55.17 °C, for the top surface, and 48.56 °C, for the bottom surface. Also, the components to which these maximum temperatures correspond are different ones.
- The higher the components processing, the higher the final reached temperature.
- For both tests, the middle area temperature of the critical components is lower than the one on its corners, due to the non-existence of solder-joints on this middle area. In contrast, the temperature is higher in the corners, where heat flows through these joints.
- In further works, the maximum temperature difference registered value can be used to obtain the thermal parameters stated in **Chapter 3**.

Allied to the thermography tests, Digital Shearography revealed to be a powerful measurement technique, to the extent that the surface areas most affected by the thermal loads can be clearly identified, making qualitative inspection of printed circuit boards more accessible and better perceived.

Lastly, the vibration tests enabled to acknowledge the difficulty in finding the natural frequencies of the dynamic system (PCBA + housing), since they are strongly dependent on the boundary conditions, and to confirm the reliability of the HALT tests performed on every printed circuit board model, although still for a reduced number of vibration cycles.

Chapter 8

Conclusions & Further Work

This chapter states the key conclusions of this work and suggests future topics to be explored.

8.1 Conclusions

This work aimed to give answer to the fundamental issues regarding printed circuit boards characterization. Throughout a research about their morphology, manufacturing process, reliability concerns (mechanical, thermal and vibration loads) and numerical modelling, a straightforward approach for a clearer understanding of printed circuit boards' material properties and prevention of electrical failure of their components was outlined. No matter how many hypotheses are drawn up and tested, without failure analysis there is never certainty concerning the root causes of printed circuit board's failure. Nevertheless, the fact that one or more flaws are detected does not necessarily mean those are the root causes.

The complexity of this topic required starting out with an accurate notion of the material properties – namely, the flexural stiffness – of a population of printed circuit board models. Further, prediction of their behaviour was attempted with the creation of material models and of a parametric evaluation. Although not incorporated in numerical modelling (due to complexity arise of the material models), an additional test campaign aimed to provide insights about the thermal and vibration influences on printed circuit boards' reliability.

The main conclusions derived from this work are now presented:

- Gap pads are the most feasible TIMs for efficient heat dissipation through printed circuit board components.

- For both experimental and numerical testing, it is crucial to have accurate knowledge of the material properties of a given printed circuit board to be analysed.

- The material properties obtained for the selected printed circuit board models based on the ASTM D7264/7264M – 15 standard, for the 3PB and 4PB tests, were within the expected range of values found in literature, yet still with a few exceptions.

- It is important to measure specimen geometric variability, so that more uniform values for the geometric parameters – and for the derived material properties as well – can be known, and flawed specimens can be discarded.

- The thickness is the geometric parameter with the biggest influence on the obtained material properties and correspondent material models' results. Therefore, the knowledge of its exact value is of great importance.

- No thickness tendency was found for the selected PCB models, for either shape and size. The same can be said for the relation between their flexural stiffness and number of copper layers or copper percentage.

- From the numerical validation, the numerical results were always superior to the experimental ones. This could mean that the printed circuit boards specimens were under-dimensioned. By assuming this, every printed circuit board experimental values could be derived from the correspondent material models by the introduction of a factor N with a maximum value of 1.5.
  The 3PB configuration revealed a better matching between the numerical and experimental results than the 4PB configuration. Therefore, in future experimental tests, the 3PB configuration should be used for obtaining the flexural properties of any desired printed circuit board models. On the other hand, the 4PB configuration revealed to be, experimentally, more susceptible to measurement errors. Numerically, they were less conservative, since the numerical results deviated more from the experimental ones.

- From the parametric evaluation, copper thickness variation led to a non negligible difference of the obtained results, by the fact of considering a full layer of it, and not by considering its exact volume percentage for the material models. Since its volume percentage is considerably small, copper may be neglected from printed circuit boards orthotropic material models, considering solely FR-4 for every layer.

- The thermography, digital shearography and vibration tests greatly contributed to printed circuit boards thermal and vibration characterization, namely the knowledge of the maximum temperature differences (required for gap pad's dimensioning), displacement gradients fields and number of vibration cycles until electrical failure, respectively.

8.2 Further Work

- For future experimental tests, ensure that specimen geometric variability is measured and that the 3PB or 4PB tests would now consider a PCBA, so that one could evaluate how much the stiffness of the board increases when the electronic components are present.

- For future numerical simulations, when modelling the solder joints, the material models should describe their strain rate effect, so that an accurate prediction of the stress and strain values can be made. Moreover, in order to understand the risk due to fatigue failure of a solder joints, the Coffin-Manson relation should be used.
  If thermal considerations would also be added, material models should reproduce cyclic thermal loading cases, as well as damage evolution. This would greatly improve the data quality obtained from the thermo-mechanical behaviour of a given printed circuit board, capturing real life operating conditions.

- Further explore the application of Thermography and Digital Shearography in printed circuit boards thermal behaviour analysis.

- For crack monitoring in printed circuit board assemblies, explore the use of automated X-ray inspection, combined with Digital Shearography.
- Proceed with the creation of the artificial neural network, gathering the results from the conceived material models of the selected printed circuit boards and, further, improve those material models – add new boundary conditions, insert components on the board (*e.g.* BGA's), etc. – including the thermo-mechanical and fatigue behaviour prediction, and generate a new collection of results, broader with new practical cases.
- Create the GUI software in Matlab, having the algorithm presented in **Appx. D** as a basis, and gradually improve it by optimizing the associated artificial neural networks.

References

[1] "Bosch global," last accessed on 22.06.2017. [Online]. Available: https://www.bosch.com/

[2] R. Khandpur, *Printed Circuit Boards: Design, Fabrication and Assembly.* New Delhi: MCGraw-Hill, 2008.

[3] "Printed circuit board (PCB)," Sep. 2013, last accessed on 22.06.2017. [Online]. Available: http://whatis.techtarget.com/definition/printed-circuit-board-PCB

[4] "PCB – printed circuit board," last accessed on 22.06.2017. [Online]. Available: http://www.eurocircuits.com/PCB-Printed-Circuit-Board/

[5] T.-I. Lee, C. Kim, M. S. Kim, and T.-S. Kim, "Flexural and tensile moduli of flexible fr4 substrates," *Polymer Testing*, vol. 53, pp. 70–76, 2016.

[6] (image), last accessed on 22.06.2017. [Online]. Available: http://www.epectec.com/images/pcb-electrical-engineering.jpg

[7] (image), last accessed on 22.06.2017. [Online]. Available: http://www.epectec.com/images/microwave-rf-circuit-board.jpg

[8] "PCB – Wikipedia," last accessed on 22.06.2017. [Online]. Available: http://en.wikipedia.org/wiki/Printed_circuit_board

[9] "PCB – MadeHow," last accessed on 22.06.2017. [Online]. Available: http://www.madehow.com/Volume-2/Printed-Circuit-Board.html

[10] (image), last accessed on 22.06.2017. [Online]. Available: http://jing-chao.com/uploadfile/2015101982149795.jpg

[11] P. D. O'Connor, *Practical Reliability Engineering.* John Wiley & Sons, 2012.

[12] A. Salahouelhadj, M. Martiny, S. Mercier, L. Bodin, D. Manteigas, and B. Stephan, "Reliability of thermally stressed rigid–flex printed circuit boards for high density interconnect applications," *Microelectronics Reliability*, vol. 54, no. 1, pp. 204–213, 2014.

[13] W. Kpobie, M. Martiny, S. Mercier, F. Lechleiter, L. Bodin, A. L. des Etangs-Levallois, and M. Brizoux, "Thermo-mechanical simulation of PCB with embedded components," *Microelectronics Reliability*, vol. 65, pp. 108–130, 2016.

[14] M. Brizoux, A. Grivon, W. Maia Filho *et al.*, "Development of a design & manufacturing environment for reliable and cost-effective PCB embedding technology," in *IPC Apex Expo conference*, 2011.

[15] P. Fuchs, G. Pinter, and M. Tonjec, "Determination of the orthotropic material properties of individual layers of printed circuit boards," *Microelectronics Reliability*, vol. 52, no. 11, pp. 2723–2730, 2012.

[16] F. Liu, Y. Lu, Z. Wang, and Z. Zhang, "Numerical simulation and fatigue life estimation of BGA packages under random vibration loading," *Microelectronics Reliability*, vol. 55, no. 12, pp. 2777–2785, 2015.

[17] J. H. L. Pang, *Lead Free Solder: Mechanics and Reliability.* Springer Science & Business Media, 2011.

[18] Y. Yao and L. M. Keer, "Cohesive fracture mechanics based numerical analysis to BGA packaging and lead free solders under drop impact," *Microelectronics Reliability*, vol. 53, no. 4, pp. 629–637, 2013.

[19] T. An, F. Qin, and J. Li, "Mechanical behavior of solder joints under dynamic four-point impact bending," *Microelectronics Reliability*, vol. 51, no. 5, pp. 1011–1019, 2011.

[20] K. Fellner, T. Antretter, P. F. Fuchs, and Q. Tao, "Numerical simulation of the electrical performance of printed circuit boards under cyclic thermal loads," *Microelectronics Reliability*, vol. 62, pp. 148–155, 2016.

[21] M. Bajaj, R. Peak, D. Zwemer, T. Thurman, L. Klein, G. Liutkus, K. Brady, J. Messina, and M. Dickerson, "Automating thermo-mechanical warpage estimation of PCBs/PCAs using a design-analysis integration framework," in *User2User-Mentor Graphics Intl. User Conference*, 2006.

[22] P. Denis Barbini, "Pad cratering: Assessing long term reliability risks," Universal Instruments.

[23] D. Xie, D. Shangguan, and H. Kroener, "Pad cratering evaluation of PCB," *APEX*, 2010.

[24] C. Basaran and H. Tang, "A damage mechanics based fatigue life prediction model for solder joints," *Journal of Electronic Packaging*, vol. 125, pp. 120–125, 2003.

[25] R. A. Amy, G. S. Aglietti, and G. Richardson, "Sensitivity analysis of simplified printed circuit board finite element models," *Microelectronics Reliability*, vol. 49, no. 7, pp. 791–799, 2009.

[26] H. Zhang, Y. Liu, J. Wang, and F. Sun, "Effect of elevated temperature on PCB responses and solder interconnect reliability under vibration loading," *Microelectronics Reliability*, vol. 55, no. 11, pp. 2391–2395, 2015.

[27] F. Yang and S. A. Meguid, "Efficient multi-level modeling technique for determining effective board drop reliability of PCB assembly," *Microelectronics Reliability*, vol. 53, no. 7, pp. 975–984, 2013.

[28] "Rohs directive," last accessed on 22.06.2017. [Online]. Available: http://ec.europa.eu/environment/waste/rohs_eee/index_en.htm

[29] C. Handwerker, U. Kattner, and K.-W. Moon, "Fundamental properties of Pb-free solder alloys," *chapter 207, Lead-Free Soldering*, pp. 21–74, 2007.

[30] "WEEE directive," last accessed on 22.06.2017. [Online]. Available: http://ec.europa.eu/environment/waste/weee/index_en.htm

[31] T. Sawamura, T. Igarashi, and A. Ltd., "Difference between various sn/ag/cu solder compositions," *Almit Ltd Technical Paper*, 2005.

[32] (image), last accessed on 22.06.2017. [Online]. Available: https://www.linkedin.com/pulse/through-hole-vs-surface-mount-solder-fatigue-gil-sharon

[33] H. Xiao, D. Luo, and Q. Wang, "Study on application of strain measuring technology in pcba reliability evaluation," in *Electronic Packaging Technology (ICEPT), 2015 16th International Conference on*. IEEE, 2015, pp. 338–342.

[34] (image), last accessed on 22.06.2017. [Online]. Available: https://www.johansondielectrics.com/images/polymer-complete-seperation-of-capacitor-flex-test.jpg

[35] E. Wong and C. Wong, "Approximate solutions for the stresses in the solder joints of a printed circuit board subjected to mechanical bending," *International Journal of Mechanical Sciences*, vol. 51, no. 2, pp. 152–158, 2009.

[36] E.-H. Wong and Y.-W. Mai, *Robust Design of Microelectronics Assemblies Against Mechanical Shock, Temperature and Moisture*. Woodhead Publishing, 2015.

[37] E. Moltz, "Use and handling of semiconductor packages with enig pad finishes," *Texas Instruments, Austin, TX, USA, Appl. Rep. SPRAA55*, 2004.

[38] L. Li, S. Kim, S. Song, T. Ku, W. Song, J. Kim, M. Chong, J. Park, and B. Kang, "Finite element modeling and simulation for bending analysis of multi-layer printed circuit boards using woven fiber composite," *Journal of Materials Processing Technology*, vol. 201, no. 1, pp. 746–750, 2008.

[39] S. Shetty and T. Reinikainen, "Three-and four-point bend testing for electronic packages," *Americal Society of Mechanical Engineers Transactions, Journal of Electronic Packaging*, vol. 125, no. 4, pp. 556–561, 2003.

[40] R. A. Amy, G. S. Aglietti, and G. Richardson, "Accuracy of simplified printed circuit board finite element models," *Microelectronics Reliability*, vol. 50, no. 1, pp. 86–97, 2010.

[41] F. Liu, G. Meng, M. Zhao, and J. feng Zhao, "Experimental and numerical analysis of BGA lead-free solder joint reliability under board-level drop impact," *Microelectronics Reliability*, vol. 49, no. 1, pp. 79–85, 2009.

[42] B. Yegnanarayana, *Artificial neural networks*. PHI Learning Pvt. Ltd., 2009.

[43] V. K. Ojha, A. Abraham, and V. Snášel, "Metaheuristic design of feedforward neural networks: A review of two decades of research," *Engineering Applications of Artificial Intelligence*, vol. 60, pp. 97–116, 2017.

[44] D. Borza and I. Nistea, "Experimental investigation by speckle interferometry of solder joint failure under thermomechanical load aggravated by boundary conditions at board level," *Journal of Electronic Packaging*, vol. 134, no. 4, p. 041007, 2012.

[45] W. Van Driel, G. Zhang, and X. Fan, "Thermo-mechanics of integrated circuits and packages," in *Mechanics of Microelectronics*. Springer, 2006, pp. 169–279.

[46] Y. J. Lee, "Thermo-mechanical properties of high performance thermal interface gap filler pads," in *Thermal and Thermomechanical Phenomena in Electronic Systems (ITherm), 2010 12th IEEE Intersociety Conference on*. IEEE, 2010, pp. 1–8.

[47] Y.-C. Lee, B.-T. Wang, Y.-S. Lai, C.-L. Yeh, and R.-S. Chen, "Finite element model verification for packaged printed circuit board by experimental modal analysis," *Microelectronics Reliability*, vol. 48, no. 11, pp. 1837–1846, 2008.

[48] S. Akbari, A. Nourani, and J. K. Spelt, "Bending strength of adhesive joints in microelectronic components: Comparison of edge-bonding and underfilling," *Composites Part A: Applied Science and Manufacturing*, vol. 88, pp. 178–189, 2016.

[49] S. Rzepka, F. Kramer, O. Grassmé, and J. Lienig, "A multilayer PCB material modeling approach based on laminate theory," in *Thermal, Mechanical and Multi-Physics Simulation and Experiments in Microelectronics and Micro-Systems, 2008. EuroSimE 2008. International Conference on*. IEEE, 2008, pp. 1–10.

[50] J. M. Lloyd, *Thermal imaging systems*. Springer Science & Business Media, 2013.

[51] "Wien's law," last accessed on 22.06.2017. [Online]. Available: https://en.wikipedia.org/wiki/Wien%27s_displacement_law

[52] (image), last accessed on 22.06.2017. [Online]. Available: http://www.allmaxhome.ca/wp-content/uploads/2013/05/trm_img_house.jpg

[53] (image), last accessed on 22.06.2017. [Online]. Available: https://static1.squarespace.com/static/5015d59ce4b006ef411bc8d9/t/53997e29e4b08b1a1a8405b2/1402568274788/1344x784-Cooled-InSb-14um-Pitch-SC8300-pcb.jpg?format=1000w

[54] "Thermal interface material," last accessed on 22.06.2017. [Online]. Available: https://en.wikipedia.org/wiki/Thermal_interface_material

[55] K. Bruzda, "Stress minimization during deflection of thermally conductive gap pads," in *Semiconductor Thermal Measurement and Management Symposium, 2007. SEMI-THERM 2007. Twenty Third Annual IEEE*. IEEE, 2007, pp. 136–143.

[56] "Bergquist company," last accessed on 22.06.2017. [Online]. Available: http://www.bergquistcompany.com/thermal_materials/gap-pad.htm

[57] "Modus advanced," last accessed on 22.06.2017. [Online]. Available: https://www.modusadvanced.com/resources/blog/thermal-pads-or-thermal-form-in-place

[58] "Thermal management materials," last accessed on 22.06.2017. [Online]. Available: http://www.timtelthermal.com/siltelpads.html

[59] "Universal science," last accessed on 22.06.2017. [Online]. Available: http://www.universal-science.com/thermal-products/thermal-gap-filling-pads/

[60] "Thermally conductive pad," last accessed on 22.06.2017. [Online]. Available: https://en.wikipedia.org/wiki/Thermally_conductive_pad

[61] "Stockwell elastomerics," last accessed on 22.06.2017. [Online]. Available: http://www.stockwell.com/thermal-gap-filler-pads.php

[62] T. Wong, C. Koontz, C. Chu, and C. Sumner, "Adaptive thermal gap pad," Jun. 21 2012, uS Patent App. 12/973,699. [Online]. Available: https://www.google.com/patents/US20120155029

[63] "Standard test method for thermal transmission properties of thermally conductive electrical insulation materials," American Society for Testing Materials (ASTM), D 5470 - 12, 2012.

[64] L. Fältström, "Graphite sheets and graphite gap pads used as thermal interface materials: A thermal and mechanical evaluation," MSc Thesis, 2014.

[65] "JEDEC: Global Standards for the Microelectronics Industry," last accessed on 22.06.2017. [Online]. Available: https://www.jedec.org/

[66] M. Tkáč and R. Verner, "Artificial neural networks in business: Two decades of research," *Applied Soft Computing*, vol. 38, pp. 788–804, 2016.

[67] M. S. Hossain, O. Z. Chao, Z. Ismail, S. Noroozi, and K. S. Yee, "Artificial neural networks for vibration based inverse parametric identifications: A review," *Applied Soft Computing*, 2016.

[68] J. E. Shigley, C. R. Mischke, and R. G. Budynas, *Mechanical engineering design*. McGraw-Hill,, 2004.

[69] W. C. Young and R. G. Budynas, *Roark's formulas for stress and strain*. McGraw-Hill New York, 2002, vol. 7.

[70] S. Timoshenko and S. Woinowsky-Krieger, *Theory of plates and shells*. McGraw-Hill, Incorporated, 1959.

[71] J. N. Reddy, *Mechanics of laminated composite plates and shells: theory and analysis*. CRC press, 2004.

[72] "Standard test method for flexural properties of polymer matrix composite materials," American Society for Testing Materials (ASTM), D 7264/D 7264M - 15, 2015.

[73] P. Bastardo, "Rosen - PCBA Bending," Bosch ST - Ovar report, May 2014.

[74] Matweb, "Copper properties," last accessed on 22.06.2017. [Online]. Available: http://www.matweb.com/search/DataSheet.aspx?MatGUID=9aebe83845c04c1db5126fada6f76f7e

[75] ——, "FR-4 properties," last accessed on 22.06.2017. [Online]. Available: http://www.matweb.com/search/DataSheet.aspx?MatGUID=e6e0c2f989084541b99868893e3d6ee2

[76] "FLIR SC7000," last accessed on 22.06.2017. [Online]. Available: FLIRSC7000http://www.flir.com/science/display/?id=50093

[77] "Altair software," last accessed on 22.06.2017. [Online]. Available: http://www.flir.co.uk/cs/display/?id=42413

[78] M. Mininni, S. Gabriele, H. Lopes, and J. A. dos Santos, "Damage identification in beams using speckle shearography and an optimal spatial sampling," *Mechanical Systems and Signal Processing*, vol. 79, pp. 47–64, 2016.

[79] P. Bai, F. Zhu, and X. He, "Out-of-plane displacement field measurement by shearography," *Optics & Laser Technology*, vol. 73, pp. 29–38, 2015.

[80] X. Xie, N. Xu, J. Sun, Y. Wang, and L. Yang, "Simultaneous measurement of deformation and the first derivative with spatial phase-shift digital shearography," *Optics Communications*, vol. 286, pp. 277–281, 2013.

[81] T. Kreis, *Handbook of holographic interferometry: optical and digital methods.* John Wiley & Sons, 2006.

[82] Y. Hung, L. Yang, and Y. Huang, "5-non-destructive evaluation (nde) of composites: digital shearography," *Non-Destructive Evaluation (NDE) of Polymer Matrix Composites, Woodhead Publishing*, pp. 84–115, 2013.

[83] W. Steinchen and L. Yang, *Digital shearography: theory and application of digital speckle pattern shearing interferometry.* SPIE Press, 2003.

[84] Y. Wang, X. Gao, X. Xie, S. Wu, Y. Liu, and L. Yang, "Simultaneous dual directional strain measurement using spatial phase-shift digital shearography," *Optics and Lasers in Engineering*, vol. 87, pp. 197–203, 2016.

[85] D. S. Steinberg, *Vibration analysis for electronic equipment.* John Wiley & Sons, 2000.

[86] "Vibration testing methods for automobile parts," Japanese Industrial Standard (JIS), D 1601, 1995.

[87] O. T. Holland and P. Marchand, *Graphics and GUIs with MATLAB.* CRC Press, 2002.

[88] D. Lau, M. Tsang, S. R. Lee, J. Lo, L. Fu, J. Jin, and S. Liu, "Experimental testing and computational stress analysis of printed circuit board for the failure prediction of passive components under the depaneling load condition," in *Electronic Components and Technology Conference, 2005.* IEEE, 2005, pp. 1783–1791.

[89] D. C. Hanselman and B. Littlefield, *Mastering MATLAB 7.* Pearson/Prentice Hall, 2005.

[90] R. C. Juvinall and K. M. Marshek, *Fundamentals of machine component design.* John Wiley & Sons New York, 2006.

[91] T. L. Bergman, F. P. Incropera, D. P. DeWitt, and A. S. Lavine, *Fundamentals of heat and mass transfer.* John Wiley & Sons, 2011.

[92] T. Tinga, *Principles of loads and failure mechanisms.* Springer, 2013.

[93] T.-K. Lee, T. R. Bieler, C.-U. Kim, and H. Ma, *Fundamentals of lead-free solder interconnect technology.* Springer, 2015.

[94] A. V. Vasilakos, Y. Tang, Y. Yao *et al.*, "Neural networks for computer-aided diagnosis in medicine: A review," *Neurocomputing*, vol. 216, pp. 700–708, 2016.

[95] A.-D. Almási, S. Woźniak, V. Cristea, Y. Leblebici, and T. Engbersen, "Review of advances in neural networks: Neural design technology stack," *Neurocomputing*, vol. 174, pp. 31–41, 2016.

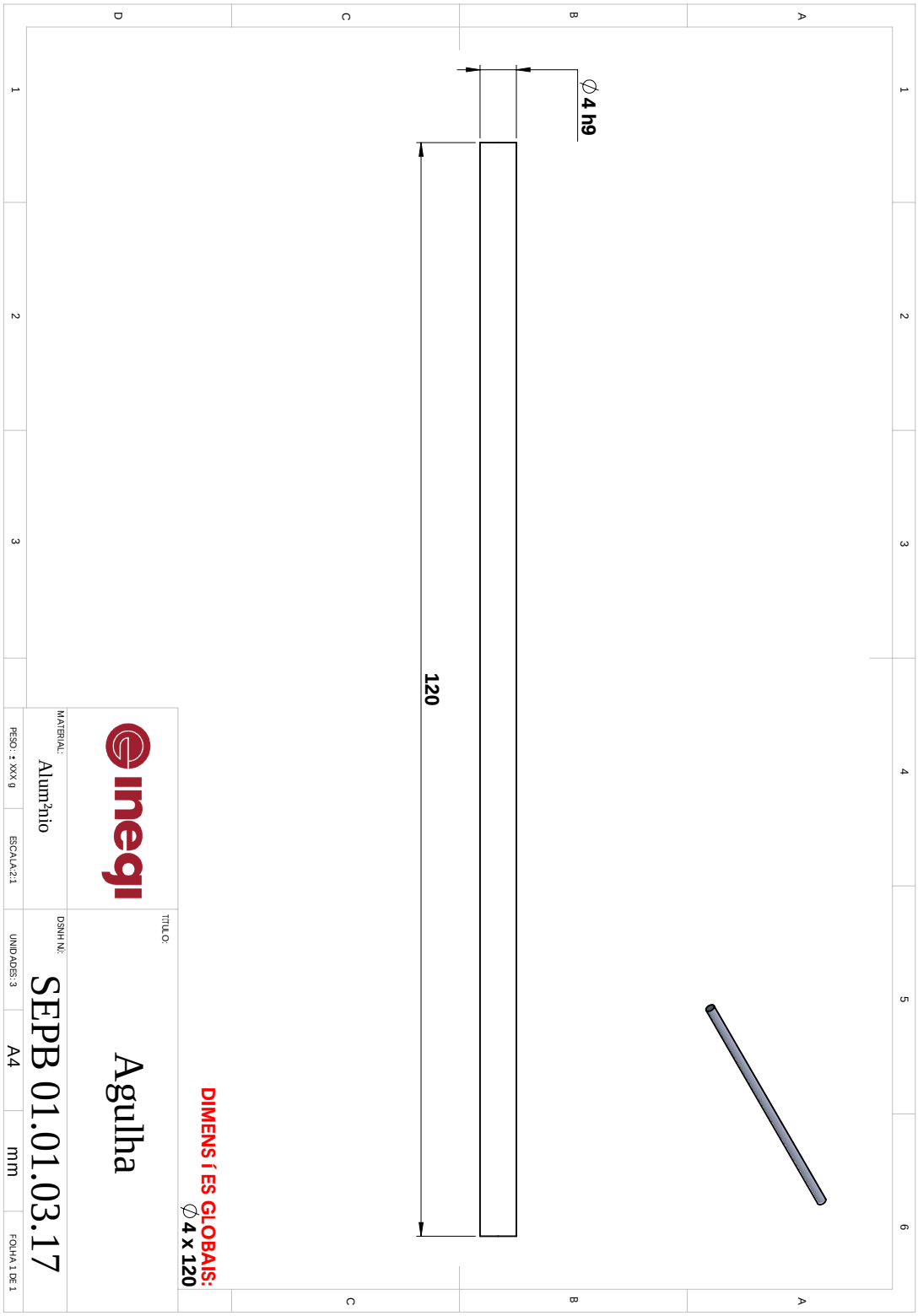
[96] A. Bansal, S. Yoon, and V. Mahadev, "Flexural strength of bga solder joints with enig substrate finish using 4-point bend test," in *Proceedings of the SMTA Pan Pacific Microelectronics Symposium*, 2005, pp. 1–8.

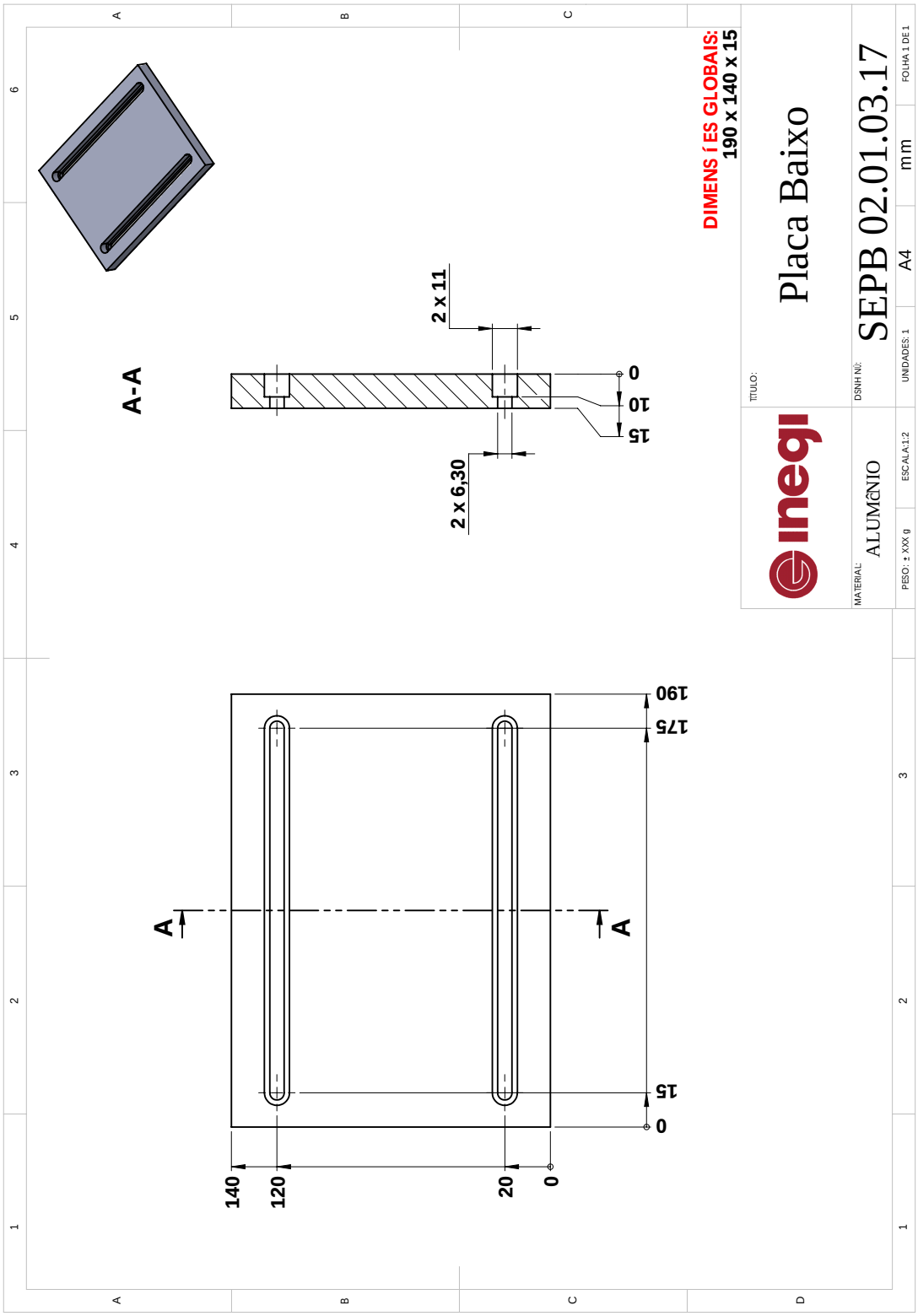
[97] T.-K. Lee, T. R. Bieler, C.-U. Kim, and H. Ma, "Interconnection: The joint," in *Fundamentals of Lead-Free Solder Interconnect Technology.* Springer, 2015, pp. 21–50.

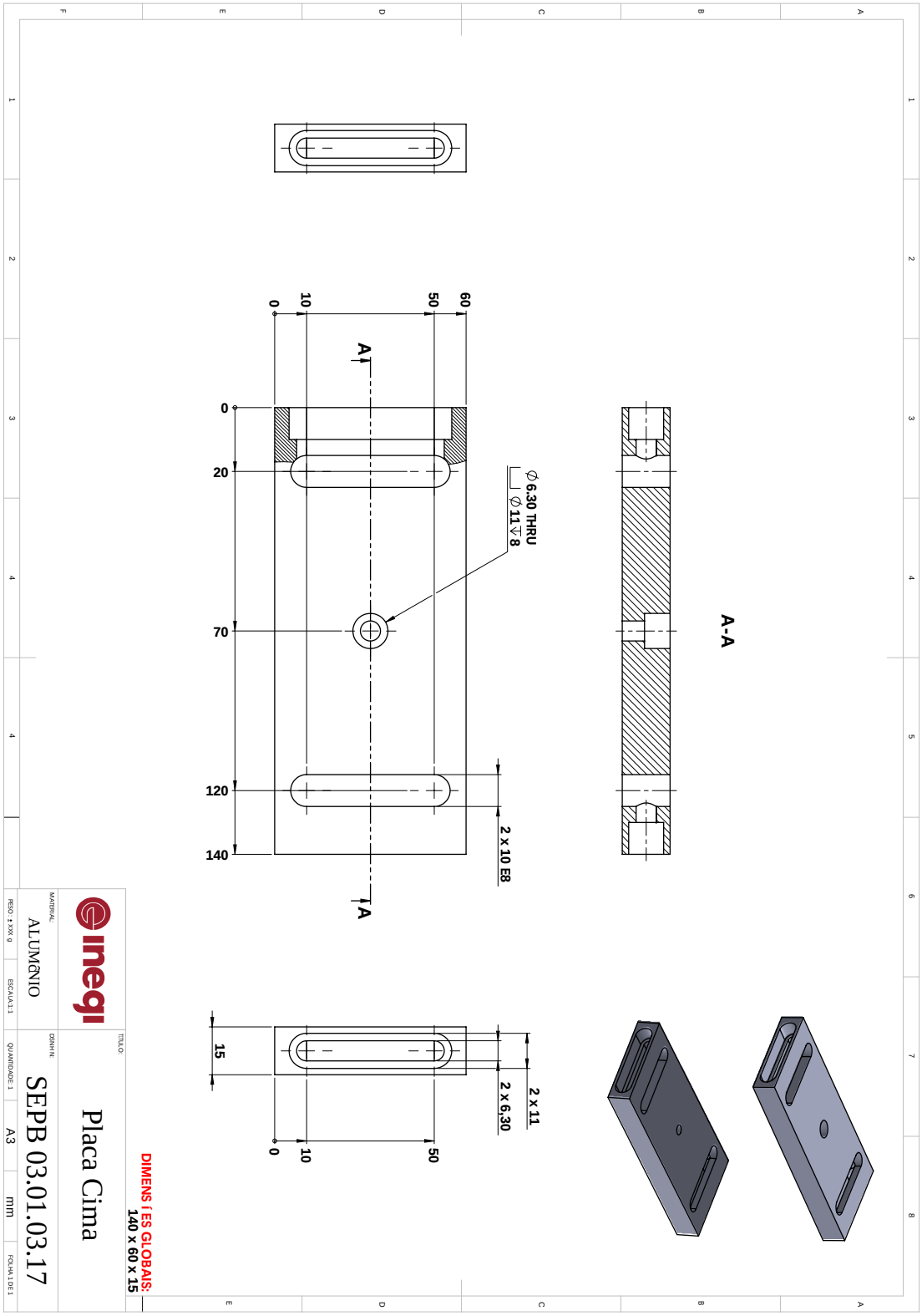
[98] B. Roggeman, P. Borgesen, J. Li, G. Godbole, P. Tumne, K. Srihari, T. Levo, and J. Pitarresi, "Assessment of pcb pad cratering resistance by joint level testing," in *Electronic Components and Technology Conference, 2008. ECTC 2008. 58th.* IEEE, 2008, pp. 884–892.

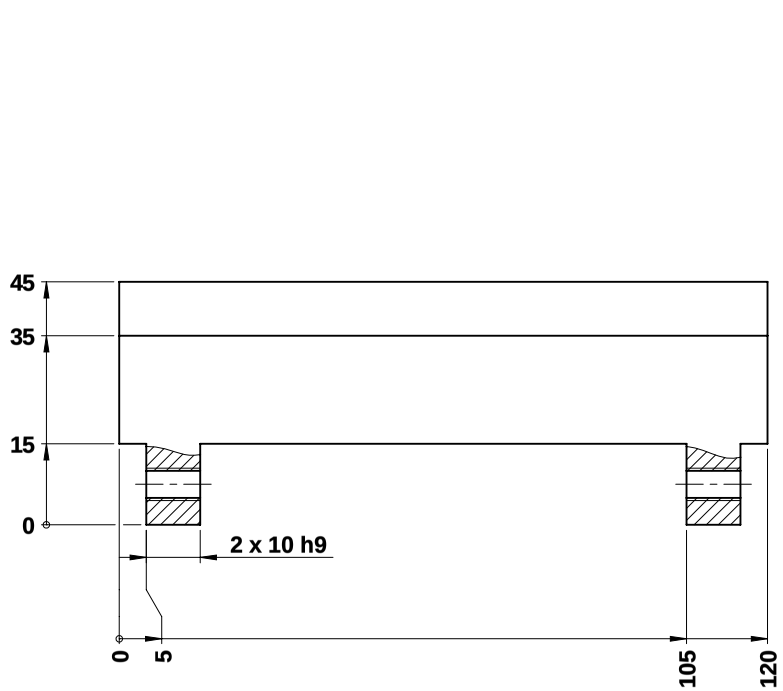
Appendix A

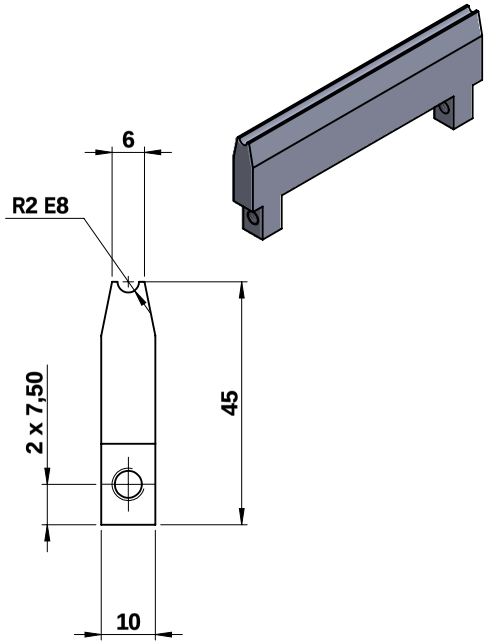
4PB CAD Drawings


∅4 h9
120
DIMENSÕES GLOBAIS:
∅4 x 120
TÍTULO:
Agulha
DSNH Nº:
SEPB 01.01.03.17
MATERIAL:
Alum²nio
PESO: ≈ XXX g
ESCALA:2:1
UNIDADES: 3
A4
mm
FOLHA 1 DE 1
inegi


DIMENSÍES GLOBAIS:
190 x 140 x 15
Placa Baixo
SEPB 02.01.03.17
inegi
ALUMÍNIO
A4
mm
A-A
2 x 11
2 x 6,30
0
10
15
190
175
15
0
140
120
20
0
A
A

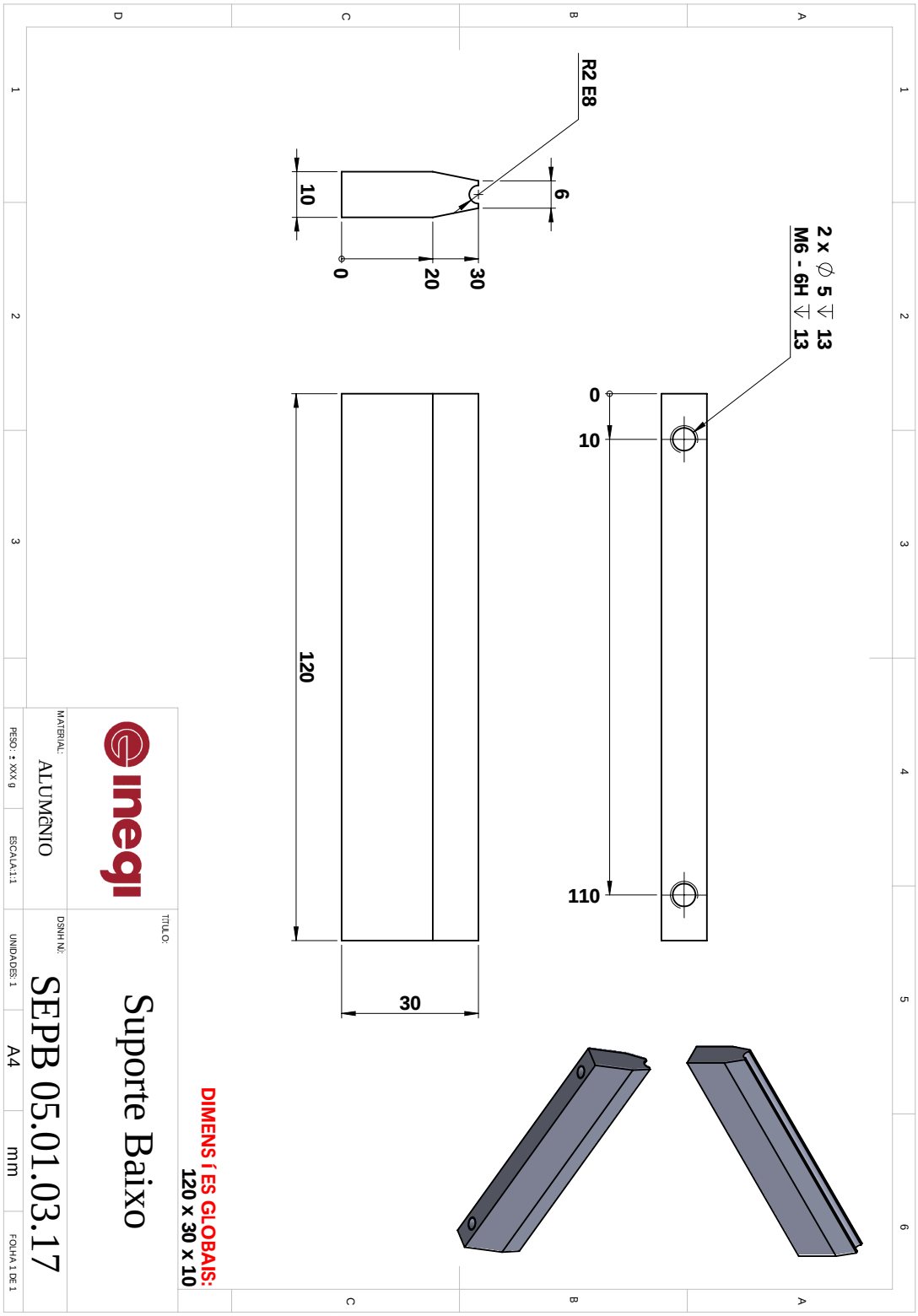

A-A
Ø 6.30 THRU
Ø 11 ↧ 8
2 x 10 EB
2 x 11
2 x 6.30
DIMENSÕES GLOBAIS:
140 x 60 x 15
inegi
MATERIAL:
ALUMÍNIO
DESENHO N.
SEPB 03.01.03.17
TÍTULO:
Placa Cima
ESCALA 1:1
QUANTIDADE 1
A3
mm
FOLHA 1 DE 1





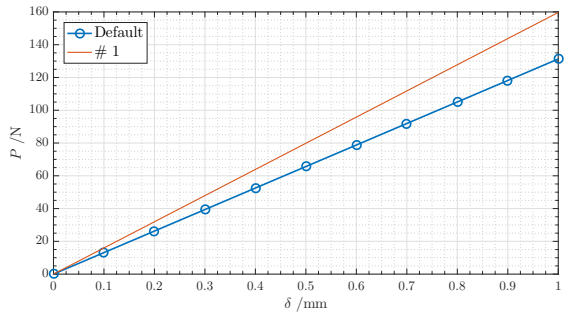
DIMENSÕES GLOBAIS:
120 x 45 x 10

inegi		TÍTULO: Suporte Cima			
MATERIAL: ALUMÍNIO		DESENHO Nº: SEPB 04.01.03.17			
PESO: ± XXX g	ESCALA:1:1	UNIDADES: 1	A4	mm	FOLHA 1 DE 1

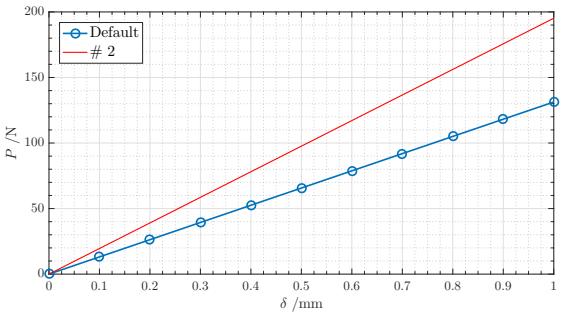

R2 E8
6
10
0
20
30
2 x ∅ 5 ↧ 13
M6 - 6H ↧ 13
0
10
110
120
30
DIMENSÕES GLOBAIS:
120 x 30 x 10
inegi
TÍTULO:
Suporte Baixo
DSNH Nº:
SEPB 05.01.03.17
MATERIAL:
ALUMÍNIO
PESO: ≈ XXX g
ESCALA:1:1
UNIDADES: 1
A4
mm
FOLHA 1 DE 1

Appendix B

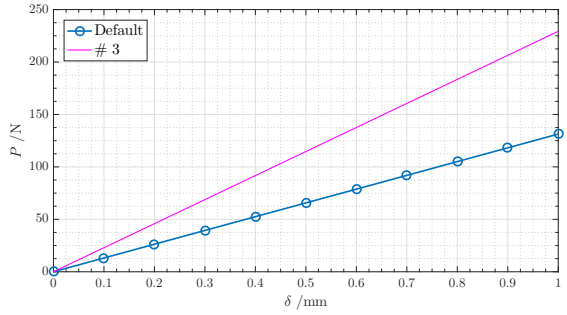
Numerical Scenarios Comparison



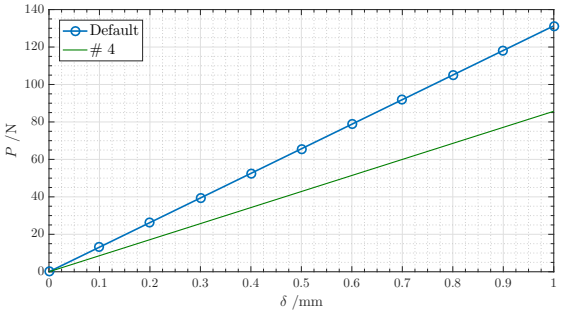
(a) Default versus scenario # 1



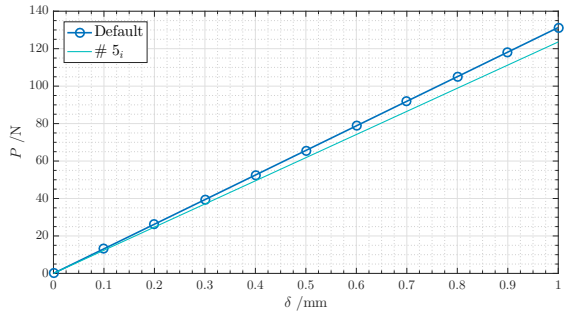
(b) Default versus scenario # 2



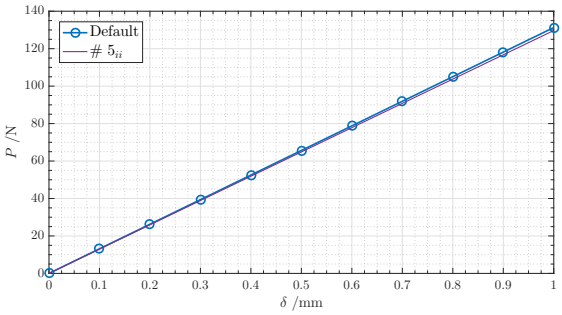
(c) Default versus scenario # 3



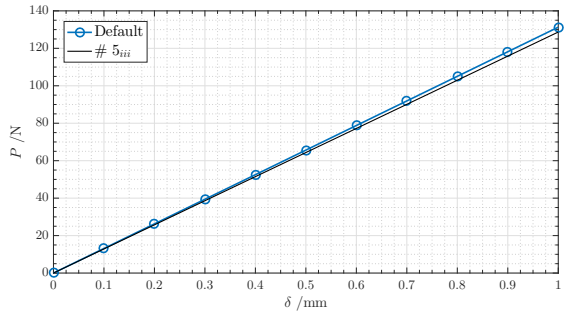
(d) Default versus scenario # 4



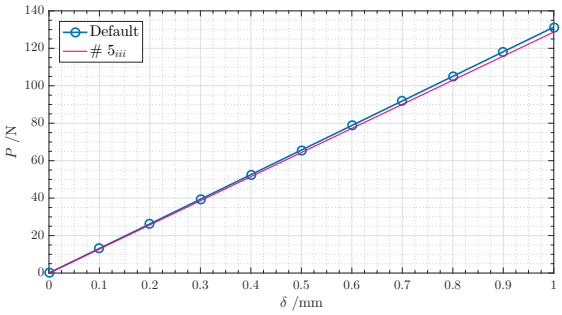
(e) Default versus scenario # 5_i



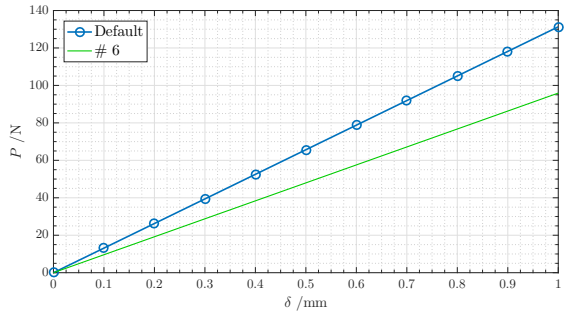
(f) Default versus scenario # 5_{ii}



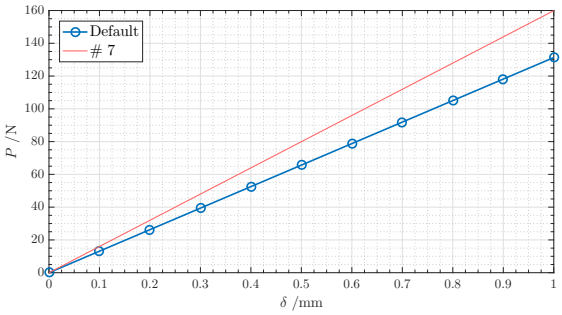
(g) Default versus scenario # 5_{iii}



(h) Default versus scenario # 5_{iv}



(i) Default versus scenario # 6



(j) Default versus scenario # 7

Appendix C

Matlab Codes

C.1 Gap Pads Data Analysis

```
%% Initialization
clearvars
close all
clc

%% T-Global Gap-Pads
% 1. L37-3
TG_P_psi_1=[10 20 30 40 50]';
TG_P_MPa_1=TG_P_psi_1*6894.75729e-6;
TG_def_1=[5 9 14 19 24]';
TG_imped_1=[15.639 15.464 15.335 15.252 15.206]';

% 2. L37-3S
TG_P_psi_2=TG_P_psi_1;
TG_P_MPa_2=TG_P_MPa_1;
TG_def_2=[5 15 25 35 46]';
TG_imped_2=[9.161 8.103 7.232 6.548 5.910]';

% 3. TGX
TG_P_psi_3=TG_P_psi_2;
TG_P_MPa_3=TG_P_MPa_2;
TG_def_3=[6 22 32 39 41]';
TG_imped_3=[2.006 1.845 1.639 1.432 1.187]';

% Plotting
figure1=figure('Name','T-Global Gap-Pads','Position',[60 60 800 400]);
axes1 = axes('Parent',figure1);
hold(axes1,'on');
set(axes1,'FontSize',12,'XMinorTick','on','YMinorTick','on',...
    'defaulttextinterpreter','latex');

%L37-3
subplot(3,2,1)
plot(TG_imped_1,TG_P_MPa_1,...
    'MarkerEdgeColor',[0 0.447058826684952 0.74117648601532],...
    'Marker','o',...
    'LineWidth',1.5)
ylabel('Pressure /MPa')
xlabel('Thermal Resistance /K-cm$^2$W$^{-1}$')
box on
grid on
grid minor
set(gca,'TickLabelInterpreter','latex')

subplot(3,2,2)
plot(TG_def_1,TG_P_MPa_1,...
    'Marker','*',...
    'LineWidth',1.5,...
    'Color',[0.850980401039124 0.325490206480026 0.0980392172932625])
ylabel('Pressure /MPa')
xlabel('Deflection /\%')
box on
grid on
grid minor
set(gca,'TickLabelInterpreter','latex')

%L37-3S
```

```
subplot(3,2,3)
plot(TG_imped_2,TG_P_MPa_2,...
    'Marker','o',...
    'LineWidth',1.5,...
    'Color',[0.749019622802734 0 0.749019622802734])
ylabel('Pressure /MPa')
xlabel('Thermal Resistance /K-cm$^2$W$^{-1}$')
box on
grid on
grid minor
set(gca,'TickLabelInterpreter','latex')

subplot(3,2,4)
plot(TG_def_2,TG_P_MPa_2,...
    'Marker','*',...
    'LineWidth',1.5,...
    'Color',[0.635294139385223 0.0784313753247261 0.184313729405403])
title('L37-3S | Pressure vs. Deflection')
ylabel('Pressure /MPa')
xlabel('Deflection /\%')
box on
grid on
grid minor
set(gca,'TickLabelInterpreter','latex')

%TGX
subplot(3,2,5)
plot(TG_imped_3,TG_P_MPa_3,...
    'Marker','o',...
    'LineWidth',1.5,...
    'Color',[0 0 1])
ylabel('Pressure /MPa')
xlabel('Thermal Resistance /K-cm$^2$W$^{-1}$')
box on
grid on
grid minor
set(gca,'TickLabelInterpreter','latex')

subplot(3,2,6)
plot(TG_def_3,TG_P_MPa_3,...
    'Marker','*',...
    'LineWidth',1.5,...
    'Color',[0 0.498039215803146 0])
ylabel('Pressure /MPa')
xlabel('Deflection /\%')
box on
grid on
grid minor
set(gca,'TickLabelInterpreter','latex')

%% Bergquist Gap-Pads | Continuous Strain
% GP VO
BQ_CS_def_1=[0 10 20 30 40 50]';
BQ_CS_P_psi_1=[0 20 47 87 167 295]';
BQ_CS_P_MPa_1=BQ_CS_P_psi_1*6894.75729e-6;

% GP Soft
BQ_CS_def_2=BQ_CS_def_1;
BQ_CS_P_psi_2=[0 10 20 40 75 151]';
BQ_CS_P_MPa_2=BQ_CS_P_psi_2*6894.75729e-6;
```

```
% GP Ultra S.
BQ_CS_def_3=BQ_CS_def_2;
BQ_CS_P_psi_3=[0 2 5 18 42 80]';
BQ_CS_P_MPa_3=BQ_CS_P_psi_3*6894.75729e-6;

% HC 1000
BQ_CS_def_4=BQ_CS_def_3;
BQ_CS_P_psi_4=[0 5 20 47 82 143]';
BQ_CS_P_MPa_4=BQ_CS_P_psi_4*6894.75729e-6;

% GP 1500
BQ_CS_def_5=BQ_CS_def_4;
BQ_CS_P_psi_5=[0 15 28 53 104 210]';
BQ_CS_P_MPa_5=BQ_CS_P_psi_5*6894.75729e-6;

% GP 2000
BQ_CS_def_6=BQ_CS_def_5;
BQ_CS_P_psi_6=[0 30 69 110 167 265]';
BQ_CS_P_MPa_6=BQ_CS_P_psi_6*6894.75729e-6;

% GP 3000
BQ_CS_def_7=BQ_CS_def_6;
BQ_CS_P_psi_7=[0 22 55 87 138 202]';
BQ_CS_P_MPa_7=BQ_CS_P_psi_7*6894.75729e-6;

% Plotting
figure2=figure('Name','Bergquist Company Gap-Pads | Continuous Strain',...
    'Position',[60 60 800 400]);
axes2 = axes('Parent',figure2);
hold(axes2,'on');
set(axes2,'FontSize',12,'XMinorTick','on','YMinorTick','on',...
    'defaulttextinterpreter','latex');

plot(BQ_CS_def_1,BQ_CS_P_MPa_1,...
    'Marker','+',...
    'MarkerSize',8,...
    'LineWidth',1.5)
hold on
plot(BQ_CS_def_2,BQ_CS_P_MPa_2,...
    'Marker','o',...
    'MarkerSize',8,...
    'LineWidth',1.5)
hold on
plot(BQ_CS_def_3,BQ_CS_P_MPa_3,...
    'Marker','*',...
    'MarkerSize',8,...
    'LineWidth',1.5)
hold on
plot(BQ_CS_def_4,BQ_CS_P_MPa_4,...
    'Marker','x',...
    'MarkerSize',8,...
    'LineWidth',1.5)
hold on
plot(BQ_CS_def_5,BQ_CS_P_MPa_5,...
    'Marker','square',...
    'MarkerSize',8,...
    'LineWidth',1.5)
hold on
plot(BQ_CS_def_6,BQ_CS_P_MPa_6,...
    'Marker','^',...
    'MarkerSize',8,...
```

```
    'LineWidth',1.5)
hold on
plot(BQ_CS_def_7,BQ_CS_P_MPa_7,...
    'Marker','pentagram',...
    'MarkerSize',8,...
    'LineWidth',1.5)
xlabel('Deflection /\%')
ylabel('Pressure /MPa')
a=legend({'GP VO','GP Soft','GP Ultra S.','HC 1000','GP 1500',...
    'GP 2000','GP 3000'});
box on
grid on
grid minor
set(gca,'TickLabelInterpreter','latex')
set(a,'Location','northwest','interpreter','latex','FontSize',12)

%% Print
print -depsc2 gapPads_Bergquist_continuousStrain.eps

%% Bergquist Gap-Pads | Step Strain
% GP VO
BQ_SS_def_1=BQ_CS_def_7;
BQ_SS_P_psi_1=[0 15 35 62 130 200]';
BQ_SS_P_MPa_1=BQ_SS_P_psi_1*6894.75729e-6;

% GP Soft
BQ_SS_def_2=BQ_SS_def_1;
BQ_SS_P_psi_2=[0 8 15 25 51 100]';
BQ_SS_P_MPa_2=BQ_SS_P_psi_2*6894.75729e-6;

% GP Ultra S.
BQ_SS_def_3=BQ_SS_def_2;
BQ_SS_P_psi_3=[0 1 5 10 20 60]';
BQ_SS_P_MPa_3=BQ_SS_P_psi_3*6894.75729e-6;

% HC 1000
BQ_SS_def_4=BQ_SS_def_3;
BQ_SS_P_psi_4=[0 3 10 23 48 95]';
BQ_SS_P_MPa_4=BQ_SS_P_psi_4*6894.75729e-6;

% GP 1500
BQ_SS_def_5=BQ_SS_def_4;
BQ_SS_P_psi_5=[0 8 15 25 58 128]';
BQ_SS_P_MPa_5=BQ_SS_P_psi_5*6894.75729e-6;

% GP 2000
BQ_SS_def_6=BQ_SS_def_5;
BQ_SS_P_psi_6=[0 11 30 51 82 135]';
BQ_SS_P_MPa_6=BQ_SS_P_psi_6*6894.75729e-6;

% GP 3000
BQ_SS_def_7=BQ_SS_def_6;
BQ_SS_P_psi_7=[0 14 30 48 78 118]';
BQ_SS_P_MPa_7=BQ_SS_P_psi_7*6894.75729e-6;

% Plotting
figure3=figure('Name','Bergquist Company Gap-Pads | Step Strain',...
    'Position',[60 60 800 400]);
axes3 = axes('Parent',figure3);
hold(axes3,'on');
set(axes3,'FontSize',12,'XMinorTick','on','YMinorTick','on',...
```

```
    'defaulttextinterpreter','latex');

plot(BQ_SS_def_1,BQ_SS_P_MPa_1,...
    'Marker','+',...
    'MarkerSize',8,...
    'LineWidth',1.5)
hold on
plot(BQ_SS_def_2,BQ_SS_P_MPa_2,...
    'Marker','o',...
    'MarkerSize',8,...
    'LineWidth',1.5)
hold on
plot(BQ_SS_def_3,BQ_SS_P_MPa_3,...
    'Marker','*',...
    'MarkerSize',8,...
    'LineWidth',1.5)
hold on
plot(BQ_SS_def_4,BQ_SS_P_MPa_4,...
    'Marker','x',...
    'MarkerSize',8,...
    'LineWidth',1.5)
hold on
plot(BQ_SS_def_5,BQ_SS_P_MPa_5,...
    'Marker','square',...
    'MarkerSize',8,...
    'LineWidth',1.5)
hold on
plot(BQ_SS_def_6,BQ_SS_P_MPa_6,...
    'Marker','^',...
    'MarkerSize',8,...
    'LineWidth',1.5)
hold on
plot(BQ_SS_def_7,BQ_SS_P_MPa_7,...
    'Marker','pentagram',...
    'MarkerSize',8,...
    'LineWidth',1.5)
xlabel('Deflection /\%')
ylabel('Pressure /MPa')
a=legend({'GP VO','GP Soft','GP Ultra S.','HC 1000','GP 1500',...
    'GP 2000','GP 3000'});
box on
grid on
grid minor
set(gca,'TickLabelInterpreter','latex')
set(a,'Location','northwest','interpreter','latex','FontSize',12)

%% Print
print -depsc2 gapPads_Bergquist_stepStrain.eps
```

C.2 3PB & 4PB Tests Data Import

```
%% Initialization
clearvars
close all
clc

%% PCB Description
pcb_name='PCB 06 | F.01U.127.336'; % PCB reference
exp_test='4PB'; % choose '3PB' or '4PB'

%% Variables
SS=100; % support span /mm
b=79;   % width of the plate /mm
t=1.60; % thickness of the plate /mm

%% Import Data
A=importdata('edited_data\pcb_07_E1_02_edit.dat');
delta_imp=abs(A(:,1)-A(1,1)); % mid-span deflection /mm
P_imp=abs(A(:,2));            % applied force /mm
delta=max(delta_imp);         % Maximum mid-span deflection /mm
P=max(P_imp);                 % Maximum applied force /N

%% Curve Fitting
[xData,yData]=prepareCurveData(delta_imp,P_imp);
ft=fittype('poly1');
[fitresult,gof]=fit(xData,yData,ft);
coeffs=coeffvalues(fitresult);
m=coeffs(1); % slope of the secant of the force-deflection curve
ord=coeffs(2);

%% Plotting
figure1=figure('Name','P vs. Delta','Position',[60 60 800 400]);
axes1=axes('Parent',figure1);
hold(axes1,'on');
set(axes1,'FontSize',12,'XMinorTick','on','YMinorTick','on',...
    'defaulttextinterpreter','latex');

plot(xData,yData,...
    'MarkerSize',10,'Marker','.',...
    'LineStyle','none',...
    'Color',[0 0 0])
hold on
n=plot(fitresult);
set(n,'LineWidth',1.5,'Color',[0 0 1])
hold all
xlabel('$\delta$ /mm')
ylabel('$P$ /N')
a=legend({'Data','$y = 28.4573x + 15.2736$'});
set(gca,'TickLabelInterpreter','latex')
set(a,'Location','southeast','interpreter','latex','FontSize',14)
box on
grid on
grid minor

%% Print
print -depsc2 pcb_07_E2_03.eps

%% Type of Experimental Test
```

```
switch exp_test
    case '3PB'
        sigma_max_3PB=3*P*SS/(4*b*t^2);    % Maximum Flexural Stress
        epsilon_max_3PB=6*delta*t/(SS^2); % Maximum Strain
        E_3PB=SS^3*m/(4*b*t^3);           % Flexural Young Modulus

        %% Display Results
        disp(pcb_name)
        disp(exp_test)
        disp('Sigma_Max [MPa]')
        disp(sigma_max_3PB)
        disp('Epsilon_Max [-]')
        disp(epsilon_max_3PB)
        disp('E [MPa]')
        disp(E_3PB)

    case '4PB'
        sigma_max_4PB=3*P*SS/(4*b*t^2);      % Maximum Flexural Stress
        epsilon_max_4PB=4.36*delta*t/(SS^2); % Maximum Strain
        E_4PB=0.17*SS^3*m/(b*t^3);           % Flexural Young Modulus

        %% Display Results
        disp(pcb_name)
        disp(exp_test)
        disp('Sigma_Max [MPa]')
        disp(sigma_max_4PB)
        disp('Epsilon_Max [-]')
        disp(epsilon_max_4PB)
        disp('E [MPa]')
        disp(E_4PB)
end
```

C.3 3PB & 4PB Tests Distances

```
%% Initialization
format short
clearvars
close all
clc

%% PCB Description
pcb_name=('PCB 06 | F.01U.127.336'); % PCB references
exp_test=('4PB'); % choose '4PB' or '3PB'

%% Type of Experimental Test
switch exp_test
    case '4PB'
        %% Calculation
        L=75.4;     % size of specimen [mm]
        SS=4/5*L;   % support span [mm]
        LS=SS/2;    % load span [mm]
        C_L_R=SS/4; % corner distances [mm]

        %% Display
        disp(exp_test)
        disp(pcb_name)
        disp('-----------------------------')
        disp('Support Span | SS [mm]')
        disp(SS)
        disp('Loading Span | LS [mm]')
        disp(LS)
        disp('Corners distance | C_L_R [mm]')
        disp(C_L_R)

    case '3PB'
        %% Calculation
        L=50;       % size of specimen [mm]
        SS=4/5*L;   % support span [mm]
        C_L_R=SS/2; % corner distances [mm]

        %% Display
        disp(exp_test)
        disp(pcb_name)
        disp('-----------------------------')
        disp('Support Span | SS [mm]')
        disp(SS)
        disp('Corners distance | C_L_R [mm]')
        disp(C_L_R)
end
```

Appendix D

Software Algorithm

1. For the PCB, insert its:
   - Length (L_{pcb})
   - Width (b_{pcb})
   - Thickness (h_{pcb})
2. Calculate the PCB's area ($A_{pcb} = L_{pcb} \cdot b_{pcb}$)
3. For the BGA, insert its:
   - Length (L_{bga})
   - Width (b_{bga})
   - Thickness (h_{bga})
4. Calculate the BGA's area ($A_{bga} = L_{bga} \cdot b_{bga} = A_{GapPad}$)
5. Insert the heat flux P_D and temperature difference ΔT values
6. Calculate the thermal impedance $\left(R_T = \frac{\Delta T}{P_D}\right)$
7. Look up in the gap pad's catalogue, and from a gap pad model, choose its desired final thickness (h_f)
8. Insert the final thickness value (h_f) in the program
9. Calculate the strain value $\left(\varepsilon = \frac{h_f - h_i}{h_i}\right)$
10. In the stress-strain curve for the gap pad model, obtain the stress value, by ($\sigma = E \cdot \varepsilon$)
11. Calculate the load value ($F = \sigma \cdot A_{GapPad}$)
12. Calculate the tightening torque value ($T = f(F, h_f, \ldots)$)
13. Load the neural network and, based on the inputs, provide the maximum allowable stress (σ_{max}), strain (ε_{max}) and displacement (δ_{max}) values.